The University of Nottingham

Prediction of elastic behaviour and initial failure of textile composites

by

Jonathan Josiah Crookston

MEng.(Hons.)

Thesis submitted to The University of Nottingham for the degree of Doctor of Philosophy

May 2004

CONTENTS

ABSTRACT

When a component is produced from textile reinforcement, it is well known that the reinforcement conforms to the shape of the tooling, predominantly by in-plane shear deformation. Current structural analysis techniques for composite components frequently neglect the effects of this deformation on subsequent mechanical properties. In this thesis the effects of shear deformation in the reinforcement on mechanical properties of the composite are shown to be significant, both for flat laminates with uniform reinforcement deformation, and for a component where deformation changes over the geometry.

Methods are developed to predict the elastic behaviour and initial failure of components manufactured from textile reinforced composites, giving consideration to reinforcement deformation. One of the main objectives is to employ techniques which are purely predictive wherever possible, such that experimental test data are required principally for validation, rather than as input to the models. Implementation is performed in a modular fashion such that alternative models may be substituted at any stage in the procedure without affecting subsequent stages.

Micromechanics models are employed to predict the properties of unidirectional composites from fibre and matrix properties and experimental validation is performed. A failure criterion is employed to determine lamina failure under biaxial loading. A simple model for woven fabric stiffness is implemented and extended to predict failure. Classical laminate theory is used to predict elastic and failure behaviour of angle-ply laminates; predictions are subsequently validated against experimental data. Material property and compaction models are incorporated into a draping simulation software tool which is used to create input files for structural analysis of components using layered shell finite elements, thought to be the most rigorous technique for textile composite components published to date. Results are shown to agree well with experimental data.

To give full consideration of reinforcement geometry, initial studies of finite element modelling of the repeating unit cell are performed, whereupon the benefits and disadvantages of this technique are highlighted.

ACKNOWLEDGEMENTS

The author wishes to thank his academic supervisors, Professor Andrew Long and Dr. Arthur Jones for their outstanding support during the course of this work, as well as Dr. Phil Shipway and Professor Graham McCartney for explaining the concepts of 'good science' during his undergraduate studies. Professor Tom Hyde, head of the School of Mechanical, Materials and Manufacturing Engineering, is also thanked for the use of the University facilities.

The financial support of the Engineering and Physical Sciences Research Council (EPSRC) and the collaborative support of the Ford Motor Company, Dowty Propellers, Formax UK and ESI Group are gratefully acknowledged.

Appreciation for the technical support of Roger Smith, Paul Johns, Dave Smith and Geoff Tomlinson is also expressed.

The help, guidance and opportunities for late night discussion provided by Dr. François Robitaille and Nuno Correia, together with the unfailing friendships of Brendon Weager and Agnes Ragondet are sincerely acknowledged. Thanks are also expressed for the assistance given and contributions to the working environment made by Dr. Rafael Garcia Gil, Dr. Martin Wilson, Dr. Phil Harrison, Tom Turner, Lee Harper, Joul Way Ooi, Chee Chiew Wong, Sophie Cozien-Cazuc, Martin Sherburn, Peter Schubel, Graham Aitchison and Martin Dunmore, amongst others.

The assistance of Tim Baillie, Joel Hughes-Thomas and Alastair Pickburn are also gratefully acknowledged.

Most importantly, the unconditional love, support and care of my wife, Rachel, has been unsurpassed at all times; for this I am eternally indebted.

GLOSSARY

Angle-ply laminate	A laminate having equal amounts of fibre reinforcement orientated at angles $+\phi$ and $-\phi$ to the reference direction (e.g. a ±45° laminate).
Blankholder	A device used to maintain tension around the edge of a sheet (blank) being formed by drawing or stamping.
Braiding	A process where reinforcement tows are interlaced around a tool (which is often axisymmetric), providing a continuous 'stocking' of interwoven reinforcement.
Continuous filament random mat (CFRM)	Reinforcement made from swirls of reinforcing fibres, notionally placed at random to give quasi-isotropic in-plane mechanical properties.
Convergence study	A technique to determine the size of discretisations required in numerical methods (e.g. finite element analysis), usually performed by reducing the discretisation size until results tend to a constant value.
Cross-ply laminate	A laminate with orthogonal fibres orientated such that one set of tows is parallel to the reference direction (e.g. a 0°/90° laminate).
Darting	The practice of introducing a cut, or dart, into fibre reinforcement material to facilitate the draping process.
Draping	Deforming a dry textile reinforcement material to the shape of a tool or component.
Fill	See 'weft'.
Homogenisation	The practice of assuming that heterogeneous materials can be considered as a single homogeneous material and the calculation of the equivalent properties.
Isotropic	Having the same properties in all directions.
MDF	Medium density fibreboard, a wood-fibre based manufactured board.
Non-crimp fabric (NCF)	A fabric manufactured from discrete layers of tows by stitching through the thickness.

Orthotropic	Having material properties which are symmetric about three mutually perpendicular planes within the material. A special case of orthotropy is that when a plane exists in which mechanical properties are the same in all directions such that, for example, $E_2 = E_3$ and $G_{12} = G_{13}$; this is known as transverse isotropy.
Ply	A single lamina within a laminated composite structure.
Prepreg	Aligned fibre reinforcement material impregnated with a partially cured thermosetting resin in order that it may be formed in a viscous manner until the resin is fully cured by increasing the temperature.
Resin transfer moulding (RTM)	A manufacturing process using rigid tooling which provides a cavity into which dry reinforcement is placed prior to injection of liquid thermosetting resin under an applied pressure.
Specific stiffness/strength	Stiffness or strength of a material with respect to its density.
Thermoplastic	A polymer which can be heated and formed plastically; this process can be repeated many times.
Thermosetting resin	A polymer produced by a chemical reaction which causes a resin to set such that it does not melt on heating.
Tow	A combination or bundle of filaments in an untwisted configuration.
Warp	The tows in a woven fabric lying parallel to the machine direction (the 0° direction), between which the weft tows are interwoven.
Weft	The tows in a woven fabric perpendicular to the machine direction, i.e. in the 90° direction; also known as fill tows.
Woven fabric	A fabric made using a traditional interlaced weaving technique.

NOMENCLATURE

Symbols

A	area (mm^2)
E	Young's modulus (MPa)
F	force (N)
G	shear modulus (MPa)
RF	reaction force (N)
V_f	volume fraction of reinforcement (dimensionless)
a	aspect ratio (dimensionless)
b	amplitude of tow undulation in wavy reinforcement (mm)
h	height or thickness (mm)
k_σ	stress concentration factor (dimensionless)
l	length (mm)
l_s	length of stitches in a non-crimp fabric (mm)
m	mass (kg)
n	tow shape geometric parameter (dimensionless)
r_f	radius of a single glass filament (mm)
r_a	area ratio (ratio of tow cross-sectional area to area of bounding rectangle) (dimensionless)
s_f	spacing between glass filaments within a tow (between centres) (mm)
s_s	spacing between stitches in a non-crimp fabric (mm)
w	width (mm)
α	out-of-plane angle of wavy reinforcement (angular units)
λ	wavelength of tow undulation in wavy reinforcement (mm)
ϕ	ply angle (angle between tows and loading direction) (angular units)
ν	Poisson's ratio (dimensionless)
ρ	density ($kg\ m^{-3}$)
ρ_t	tow linear density (tex)
σ	stress (MPa)
$\sigma_{0.2ps}$	0.2% proof (offset) stress (MPa)
τ	shear stress (MPa)
ε	strain (dimensionless)
γ	engineering shear strain (dimensionless)

Matrices

[C]	stiffness matrix
[S]	compliance matrix
[T]	transformation matrix
$[\overline{C}], [\overline{S}]$	transformed stiffness and compliance matrices
$[A]^T$	matrix transpose of [A]
$[A]^{-1}$	matrix inverse of [A]

Subscripts

c	compressive property (in Chapter 6 only: parameter relating to a unit cell)
f	property of fibre
m	property of matrix
t	tensile property (in Chapter 6 only: parameter relating to a tow)
u	ultimate stress
θ	dimension after shearing reinforcement through angle, θ
1	primary axis of a unidirectional lamina (parallel to fibre direction)
2	transverse axis of a unidirectional lamina (perpendicular to the fibre direction, in the plane of the lamina)
3	through-thickness axis of a unidirectional lamina
x,y,z	global Cartesian coordinates
x',y',z'	local directions of a tow with out-of-plane waviness

1 INTRODUCTION

1.1 The nature of composite materials and their applications

Due to their high specific stiffness and strength, fibre reinforced polymer composite materials have long been used in the aerospace industry and, with the increasing focus on lightweight vehicle manufacture due to environmental legislation, automotive applications are becoming more widespread. Other notable engineering applications include pressure vessels and waste water pipes and fittings. The need to utilise the mechanical performance of materials and to avoid unreasonable overspecification for aerospace applications was highlighted by Boeing, who estimated that it cost $10,000 per pound (approximately £12,500/kg) to launch a satellite into orbit [1]. Also of significance, when considered in terms of the levels of production and use, is that up to 40% of the fuel consumption of a road vehicle is considered to be attributable to its inertia; the effects of inertia are particularly significant on the urban test cycle [2]. With increasing environmental pressure, some vehicle manufacturers look towards an increased use of polymer composite materials for weight savings. Another driving force for efficient design with composites in high volume production industries is the cost of the basic material; fibre and resin materials are approximately three times the price of steel per unit mass [3]. Although design optimisation techniques are well established for metals, the heterogeneity and anisotropy of fibre reinforced composite materials make the application of standard structural analysis methods unsuitable.

While composite stress analysis has become well developed in more recent years, prediction of mechanical performance of composites manufactured using textile reinforcements is an area of ongoing research, and failure analysis of composites has recently been shown to be an area of relative immaturity [4]. In order to facilitate further discussion of the aims of the work contained in this thesis, it is appropriate to introduce reinforcement types and manufacturing methods in current use. This is fulfilled by Sections 1.2 and 1.3, whereafter the project framework within which this work was undertaken and the aims of this thesis are described in Sections 1.4 and 1.5 respectively.

1.2 Types of textile reinforcement

When considering the architecture of fibre reinforced polymer composites, two fundamental categories can be identified: those with randomly orientated fibres and those with aligned fibres. Although consideration was given to one specific randomly orientated reinforcement used during the course of the experimental work in this thesis, the principal area of investigation is of reinforcements consisting of long aligned fibres. This section provides a brief overview of different forms of aligned fibre reinforced polymer composites in order to provide a background to the approaches required to characterise the mechanical behaviour of each type.

The focus of the present work is on textile reinforcements which are, in general, easy to handle, able to conform to the shape of a mould with minimal tailoring and offer the potential for excellent mechanical properties when the fibres lie parallel to the loading directions. Textile reinforced composite components may be produced using a number of manufacturing processes, which are discussed in Section 1.3. This section provides an overview of the different textile architectures in common use.

Woven textiles are produced with various weave styles, examples of which are shown in Figure 1.1. Woven fabrics are supplied on a roll, and can be formed to a three dimensional shape with relative ease, provided that the deformation required is not too great. The fibre bundles, or tows, exhibit crimp, i.e. they follow an undulating path. It is generally accepted that the presence of crimp reduces mechanical performance. Different weave styles exhibit different characteristics; for example, plain woven reinforcements are the easiest to handle but also exhibit the highest level of crimp and are the least conformable. In contrast, an eight harness satin weave requires more careful handling due to the lower level of interlacing, but permits high deformation during forming (draping) and exhibits very low crimp.

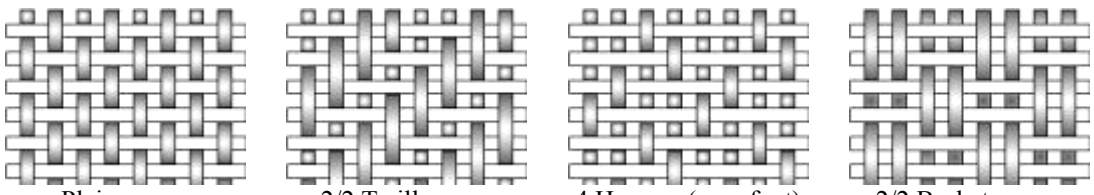

Figure 1.1 Different styles of woven textile reinforcement. Reproduced from [5].

For structures which are nearly axisymmetric, 2D braided reinforcements can be used to provide seamless reinforcement around the geometry. These are produced by winding tows around a mandrel or former in an interlacing pattern, rather like that produced by a Maypole dance. In the case of cylindrical braiding, the resultant angle between the fibres and the component axis is a function of the mandrel feed rate, braid carrier rotational speed and the mandrel diameter [6]. The triaxial braiding process introduces a third set of tows which remain parallel to the component axis. A photograph of the braiding process and a diagram of the resulting fibre architecture are shown in Figure 1.2.

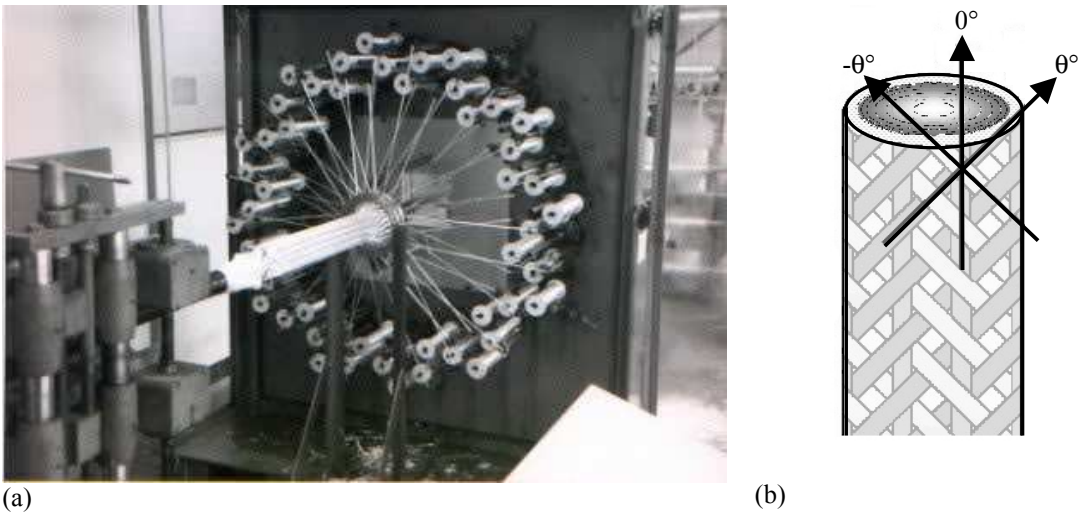

Figure 1.2 (a) Photograph of the braiding process (reproduced from [7]) and (b) triaxial braided fibre architecture (adapted from [8]).

Weft-knitted fabric reinforcements consist of tows which are looped together as illustrated in Figure 1.3. Weft knitting has the advantages that it can be used to make near net-shape preforms, and significantly improves component impact resistance and damage tolerance [9], but in the as-moulded condition the mechanical properties are poor since the loops do not provide continuous aligned reinforcement and give rise to stress concentrations [10]. Rudd et al [11] concluded that the mechanical properties, and in particular strength, achieved using weft knit reinforcements were lower than those using a continuous filament random mat reinforcement at the same fibre volume fraction. Similarly, Pandita and Verpoest [12] found that while tension-tension fatigue performance of weft knitted composites was comparable to that in the off-axis directions of woven fabrics, it was lower than that of woven fabrics loaded in the principal fibre directions.

Figure 1.3 Schematic illustration of a weft-knitted textile (reproduced from [9])

Non-crimp fabric (NCF) reinforcements are manufactured by placing tows at the required orientations in discrete layers and stitching them together using a lightweight textured polyester thread. A schematic illustration of an NCF is shown in Figure 1.4. The term warp-knitted refers to the method of stitching; hence, a warp-knit with inserted tows describes the architecture of the textile as a whole. These reinforcements are generally considered to offer mechanical properties superior to those available from woven reinforcements since the tows remain straight, not having to interlace with the crossing tows [13]. Fibre waviness is universally related to a reduction in both in-plane stiffness and strength [13-18].

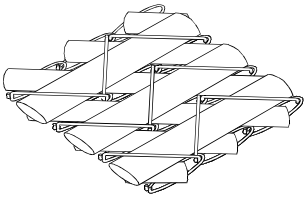

Figure 1.4 Schematic illustration of a warp-knitted textile with inserted tows (reproduced from [19]).

Other, more exotic, textile reinforcements exist, including 3D weaves and 3D braided structures, some examples of which are illustrated in Figure 1.5. Notably, the 3D braiding process can be used to produce near net-shape preforms for thick composite structures [20]. These reinforcements lie beyond the scope of the present work, which addresses traditional 2D woven and non-crimp fabrics; however, many of the techniques could be extended to 3D reinforcements provided appropriate consideration is given to the reinforcement architecture and to the effects of process-induced stress on thick sections.

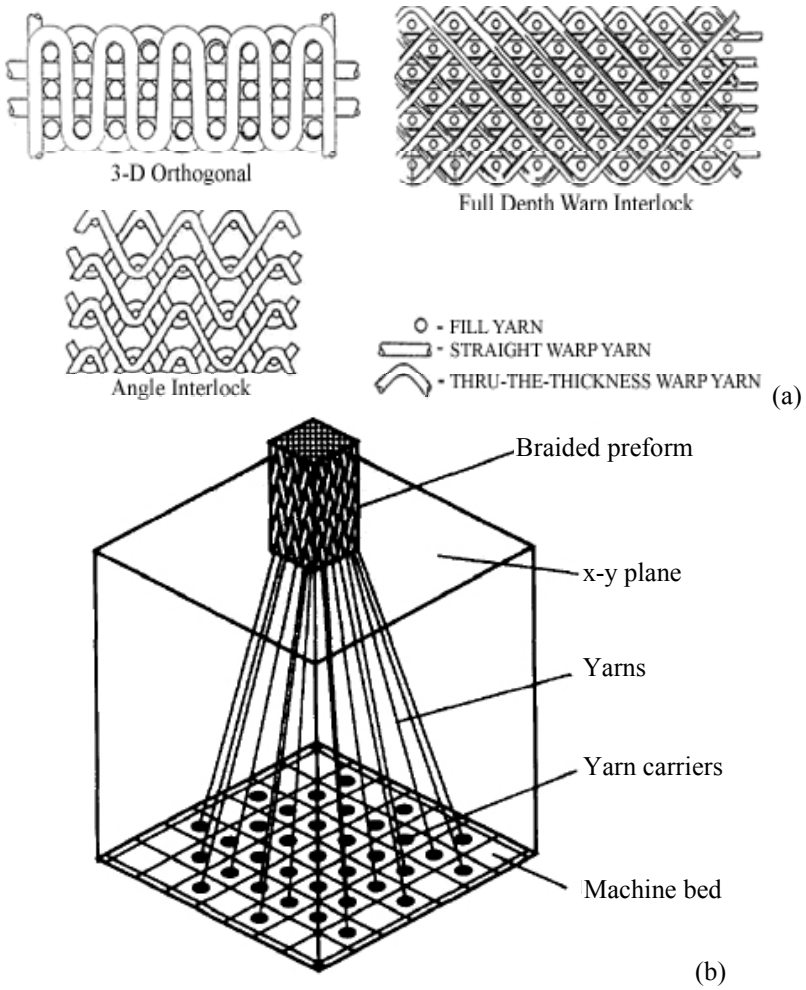

Figure 1.5 Schematic illustration of (a) 3D woven textiles (reproduced from [21]) and (b) the 3D braiding process (reproduced from [20]).

1.3 Manufacturing routes

Pre-impregnated composites (prepregs)

Perhaps the most established use of fibre reinforced polymer composites is that of unidirectional carbon fibre prepreg in the aerospace industry. This material consists of unidirectional carbon fibres which are pre-impregnated with partially cured thermosetting resin. It is supplied on a roll with a backing film which separates each layer and improves handling characteristics. It is stored at temperatures below 5°C in order to delay the curing of the resin. After cutting pieces of the material out to the required pattern, the backing film is peeled off and the prepreg is layed at the required orientation, usually by hand, into a female metal mould. Layers are built up

in this way and a polymer film (vacuum bag) is layed over the assembly and the edges are sealed. A vacuum is applied such that entrapped air is removed, and heat is applied in order to complete the curing process. This is often undertaken in an autoclave such that a higher compaction pressure is achieved. After the curing cycle is complete the vacuum bag is removed and the part is demoulded. A schematic illustration of this process is shown in Figure 1.6. High quality parts with excellent mechanical properties can be produced by this method, but the material cost is high and the process is labour intensive. Other reinforcement types and configurations are also available in this pre-impregnated form, e.g. glass unidirectional fibres and glass or carbon fibre textiles.

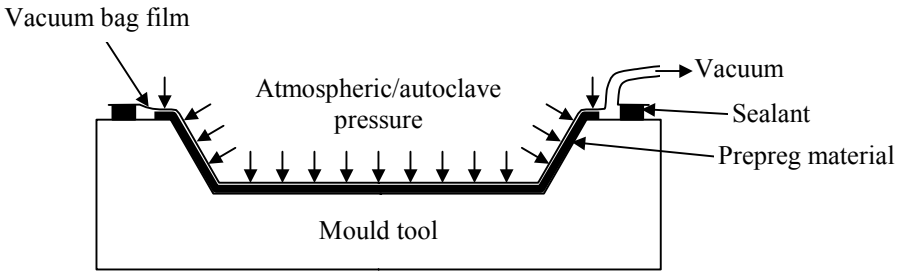

Figure 1.6 Schematic illustration of the prepreg moulding process.

Thermoforming of thermoplastic composites

For high volume applications, the use of thermoplastic composites is popular since no curing time is required. For structural parts, textile reinforced thermoplastic composites, consisting of a consolidated sheet of textile reinforcement in a thermoplastic matrix, are often used. The material is heated in an oven before being press formed between matching tools, or with a male tool and blankholder. The most notable example of such a material is Twintex, made by Saint-Gobain Vetrotex, which has a polypropylene matrix reinforced with woven glass fabric. This material is popular with the automotive industry for production of structural parts, having been used in various applications including the Peugeot 806 bumper beam and a load floor used by the Nissan motor company. Twintex is also available in an unconsolidated form, consisting of commingled glass and polypropylene fibres, which can be formed to shape by draping and consolidated under heat and pressure.

Hand lay-up

For applications requiring lower cost manufacturing, liquid moulding techniques offer lower material costs and, in many cases, require less expensive tooling. It is also possible to reduce labour costs compared with traditional lamination of unidirectional prepreg since a relatively large amount of fibre can be placed in the mould in a single operation by using a heavy fabric reinforcement. The traditional method is that known as hand lay-up, in which dry reinforcement (either textile or random mat) is cut from a roll to the desired shape. Liquid thermosetting resin is mixed with a catalyst and applied, whilst still in liquid form, to the reinforcement using a paintbrush, and placed onto a tool. Layers are built up and compacted using a roller, and the resin is allowed to cure in an oven or at room temperature before the part is demoulded. Although this process can employ very low cost tooling, which is frequently made from timber, part quality is variable due to void entrapment and the operator is subjected to emission of harmful aromatic compounds (most notably styrene in the case of polyester resin systems). As a result of this, legislation, e.g. [22], has caused this technique to become significantly less popular. This problem can be overcome by the use of closed mould processes, such as vacuum infusion and resin transfer moulding, which can reduce styrene emissions by up to 95% [23].

Vacuum Infusion (VI)

In the vacuum infusion (VI) method, dry reinforcement is assembled in a female mould and sealed under a vacuum bag similar to that used for consolidation of prepreg. A highly permeable distribution medium is placed between the reinforcement and the vacuum bag to ensure that the vacuum pressure is well distributed. Resin is allowed to enter the system at atmospheric pressure through an inlet and flows through the reinforcement to the vent, as illustrated in Figure 1.7. This process is becoming popular due to the environmental issues mentioned above, the ability to make high quality parts with low void content and the ability to use low cost tooling. Notable applications of VI include large structures such as boat hulls and lorry trailers. The main difficulty associated with this process is that found in ensuring complete infiltration of the reinforcement by the resin; this problem is the subject of considerable research, e.g. [24].

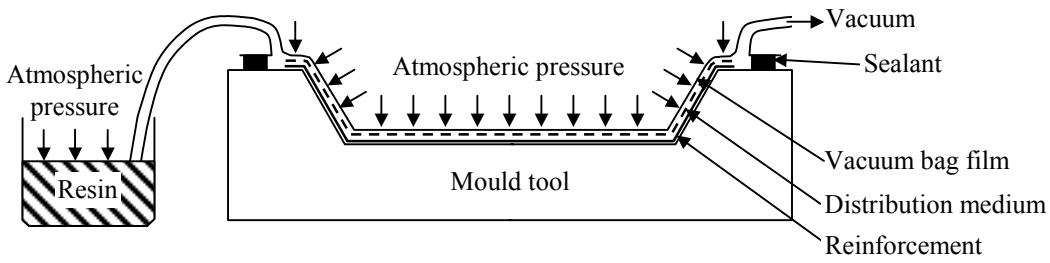

Figure 1.7 Schematic illustration of the vacuum infusion (VI) process.

Resin transfer moulding (RTM)

The liquid moulding techniques discussed above can be used to produce parts with a single smooth surface; the surface which is not adjacent to the mould has an irregular surface finish. Similarly, the part thickness and fibre volume fraction cannot be controlled accurately. For applications where these factors are significant, the resin transfer moulding (RTM) process may be used. In the RTM process, a matched pair of moulds (usually metal) is used, with dry reinforcement (textile or random mat) being placed in the cavity between them, as shown in Figure 1.8. Liquid resin is injected under positive pressure, typically below 10 bar, and flows through the cavity, infiltrating the reinforcement, towards a vent which is maintained at atmospheric or lower pressure. Although tooling costs are higher than for the liquid moulding processes outlined above, parts produced using this technique have excellent dimensional accuracy, surface finish and mechanical properties. The RTM process has been used extensively in commercial environments, for example by Aston Martin (Vanquish 'A' pillar and transmission tunnel), Ford (Escort Cosworth undershield, Transit van extra high roof) and Dowty Propellers (various aircraft and hovercraft propellers).

Although the components examined in this thesis were produced using RTM from glass fibre reinforcement within a polyester resin matrix, many of the techniques developed could be used for other materials and processes with little modification.

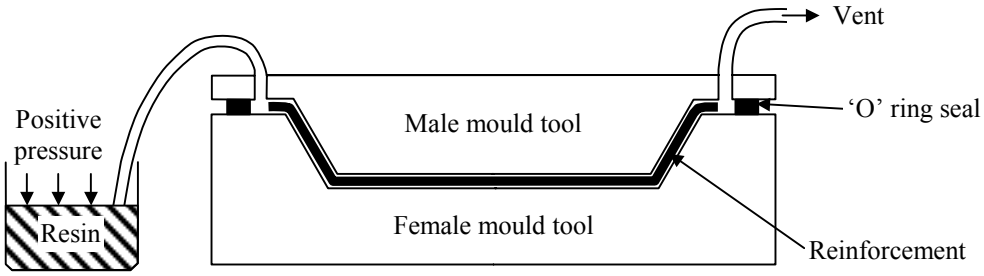

Figure 1.8 Schematic illustration of the resin transfer moulding (RTM) process.

1.4 Project framework

This work was undertaken in the School of Mechanical, Materials, Manufacturing Engineering and Management at the University of Nottingham, within the framework of a project entitled 'The effects of manufacturing on the design and performance of textile composites (ManTex)'. The project, which is still active, is funded by the UK Engineering and Physical Sciences Research Council (EPSRC) through a locally administered research centre at the University, the Innovative Manufacturing Research Centre (IMRC). Overall, the project is concerned with the development of mechanical models for textile composites, and of analysis techniques for components made from these materials. Particular attention is given to the effects of reinforcement architecture on both elastic and failure behaviour, considering the effects of changes in architecture when reinforcement is formed into a three-dimensional shape. A number of technical papers have been published as a result of work conducted within this project framework; these are listed in Appendix A.

1.5 Summary of objectives and overview of thesis

The aim of this thesis is to explore methods for the prediction of elastic and initial failure behaviour of components manufactured from textile composites. Chapter 2 contains a review of the technical literature in this field, which highlights the need for an integrated, predictive approach to this problem which is suitable for use at the design stage.

In order to examine the effects of reinforcement reorientation during forming (draping), in-plane shear deformation was induced into textile reinforcements which were subsequently used to manufacture laminates for characterisation and mechanical testing. A component was also manufactured from draped textile reinforcement and tested in order to investigate these effects further. The experimental work conducted and the materials used are described in Chapter 3, while the results of the testing are reported in Chapter 4.

To develop an approach which is sufficiently integrated to be used in the design environment, various predictive techniques were required. Models for the micromechanical behaviour, at the fibre/matrix scale, were employed to determine properties of the unidirectional composite, which is used as a building block for mechanical properties prediction. Subsequently, models for the behaviour of multi-layered, textile reinforced, laminated composites were implemented and extended where necessary. These were used in conjunction with an existing computer based draping simulation, which was used to predict the local fibre orientations and reinforcement thickness, to generate input files for structural finite element (FE) analysis of composite components using the Abaqus FE package. Results of the models were compared with experimental data at each stage. These comparisons can be found in Chapter 5, together with descriptions of the models used and their implementation.

Finite element analysis of the repeating unit cell is one method proposed in the literature to give full consideration of the true stress field in textile composites. Although the concept itself has been explored by other researchers, one of the missing elements was found to be a parametric study to evaluate the model sensitivity to material and geometric parameters. Such a study is presented in Chapter 6, based on analysis of two-dimensional cross sections under generalised plane strain conditions. Initial studies of three-dimensional unit cells are presented and some of the challenges present in this approach to modelling are discussed.

Final conclusions of the work and recommendations for future investigation are made in Chapter 7.

2 LITERATURE REVIEW

2.1 Introduction

In this chapter, the literature pertaining to components manufactured from textile reinforced composites, and particularly prediction of their mechanical properties, is reviewed in order to identify weaknesses in current approaches and to explore potential routes for mechanical simulation of such components overcoming some of the limitations discovered. Current methods for predicting the elastic properties and failure stress of unidirectional composites are discussed, since these form the basis of any homogenisation method applied to textile composites. Methods to determine properties of multi-directional laminates are reviewed, in addition to treatments used to provide a better representation of the behaviour of textile reinforced materials. Since the work in this thesis relates to three dimensional components, a review of methods to predict the deformation of the textile reinforcement during forming in the manufacturing process, and its significance to mechanical performance of the composite are presented. A review of commercially-available software tools for structural analysis of composite components is also presented. The most significant area which is found to be unresolved is that of the incorporation of post-forming fibre architecture into structural analysis in a way which is integrated and predictive; this is the primary focus of the work in this thesis.

2.2 Micromechanics models for unidirectional composites

2.2.1 Introduction

In almost all approaches to modelling the mechanical behaviour of composite components, the basic 'building block' consists of matrix reinforced with unidirectional fibres, i.e. unidirectional composite. In order to proceed with any modelling technique it is first necessary to determine the mechanical properties of unidirectional composite at the appropriate fibre volume fraction. The behaviour of orthotropic unidirectional materials requires a convention to describe the material axes; this is presented in Figure 2.1, and this convention will be used throughout this thesis.

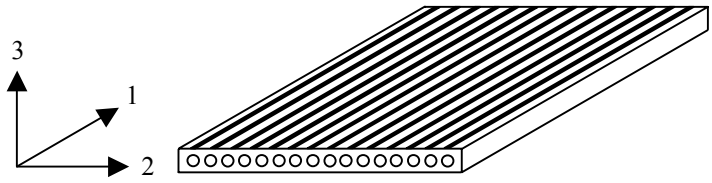

Figure 2.1 Axis system used for unidirectional laminae

2.2.2 Elastic behaviour of the lamina

For thin laminae, if plane stress is assumed (i.e. $\sigma_3 = 0$), the elastic behaviour can be characterised from four parameters, Young's moduli, E_1 and E_2, Poisson's ratio, ν_{12}, and shear modulus, G_{12}.

Provided that the fibres are continuous and well bonded to the matrix phase, when a load is applied in the lamina 1 direction, the axial strain in the fibres and matrix will be equal. This assumption can be used to derive the well known rule of mixtures, which provides a close approximation for the modulus of elasticity of a lamina in its 1 direction, as a function of the moduli of the constituents and their volumetric proportions. This expression is presented in Equation 2.1. The same technique may also be used to determine the in-plane Poisson's ratio of a lamina from the Poisson's ratios of the fibre and matrix, according to Equation 2.2. Note that Equations 2.1 and 2.2 assume that the fibre phase is isotropic, which is the case for glass fibre; in the case of carbon fibre, which is itself orthotropic, it becomes necessary to specify the use of E_{1f} in place of E_f in Equation 2.1, and ν_{12f} in place of ν_f in Equation 2.2.

$$E_1 = (V_f\ E_f\ ) + (1 - V_f\ )E_m \tag{2.1}$$

where V_f is the fibre volume fraction, E_f is the Young's modulus of the fibre and E_m is that of the matrix.

$$\nu_{12} = (V_f\ \nu_f\ ) + (1 - V_f\ )\nu_m \tag{2.2}$$

where ν_f is the Poisson's ratio of the fibre and ν_m is that of the matrix.

Whilst for a load applied in the lamina 1 direction strain in the fibres and matrix is constant, this is not the case for a transverse load, i.e. one applied in the 2 direction. The first approximation for the transverse case is to assume that the stress is the same

in the fibres and matrix. This assumption can be used to derive the expression for transverse modulus of the lamina given in Equation 2.3.

$$E_2 = \left[\frac{V_f}{E_f} + \frac{\left(1 - V_f\right)}{E_m} \right]^{-1} \tag{2.3}$$

The equal stress assumption giving rise to Equation 2.3 is a simplification of the true stress distribution within a unidirectional lamina under a transverse load, since it describes the stress distribution in rectangular blocks of equal thickness and does not consider the effects of bridging. Consequently, it is considered to be rather inaccurate. Better agreement with experiment is noted [25] for the semi-empirical Halpin-Tsai equations [26] which, being an approximation to more exact (and complicated) elasticity solutions [27], give consideration to the inhomogeneous nature of the stress field, requiring the determination of a single parameter for characterisation of a material at all fibre volume fractions. This model is described by Equation 2.4.

$$E_2 = \frac{E_m(1+\xi\eta V_f)}{(1-\eta V_f)} \qquad \text{where} \quad \eta = \frac{\left(\frac{E_f}{E_m} - 1\right)}{\left(\frac{E_f}{E_m} + \xi\right)} \tag{2.4}$$

Where ξ is a parameter related to the fibre geometry, usually taking the value of 2 when calculating the transverse modulus of a composite with cylindrical fibres when $E_f >> E_m$ [28,29]. The value of ξ must be in the range $0 \leq \xi \leq \infty$; when $\xi = 0$, Equation 2.4 becomes the series model described by Equation 2.3, while for $\xi = \infty$, the parallel model described by Equation 2.1 (rule of mixtures) is replicated.

The Halpin-Tsai equations may also be applied to determine the in-plane shear modulus of a unidirectional composite, using the relationship given in Equation 2.5, with $\xi = 1$ [29].

$$G_{12} = \frac{G_m(1+\xi\eta V_f)}{(1-\eta V_f)} \qquad \text{where} \quad \eta = \frac{\left(\frac{G_f}{G_m}-1\right)}{\left(\frac{G_f}{G_m}+\xi\right)} \tag{2.5}$$

Other methods are available to calculate transverse and shear elastic behaviour, most notably the Eshelby method [30], which is used to determine the elastic response of a matrix containing an inclusion with a dissimilar Young's modulus. Although accurate results may be determined using this method, it is a relatively complicated mathematical solution, which is best solved using a computer program. Numerical methods were also employed by Adams and Doner, providing some benchmark theoretical results for E_2 [31] and G_{12} [32] for composites with different ratios of E_f/E_m and G_f/G_m, with which other calculations are often compared. Other computational techniques, such as the finite element method, have also been used [33,34] for micromechanical analysis of transverse loading, however such models are more suited to fundamental investigations than to use by the design engineer due to the time-consuming nature of their application. The Halpin-Tsai equations were shown to agree with Adams and Doner's results both for E_2 and G_{12} for a range of ratios of E_f/E_m and G_f/G_m respectively for V_f=55% [26], and can be evaluated quickly and simply, making this the preferred calculation method when the arrangement of individual fibres is not being investigated.

2.2.3 Failure of the lamina under a uniaxial load

Since the strength of the reinforcement fibres is much greater than that of the matrix phase, i.e. $\sigma_{fu} >> \sigma_{mu}$, it can be assumed that the lamina can carry a tensile load in the fibre direction until the fibres themselves break. Hence, ultimate strength of the lamina is considered to be fibre dominated according to Equation 2.6.

$$\sigma_{1u} = V_f \sigma_{fu} \tag{2.6}$$

In order to find the onset of failure, however, various expressions may be used depending on the ratio of the failure strains of the constituents ($\varepsilon_{fu}/\varepsilon_{mu}$). Hull and Clyne [35] presented notional stress-strain diagrams indicating how load is

transferred between the constituents during failure, assuming linear elasticity and brittle fracture. These diagrams are reproduced in Figure 2.2.

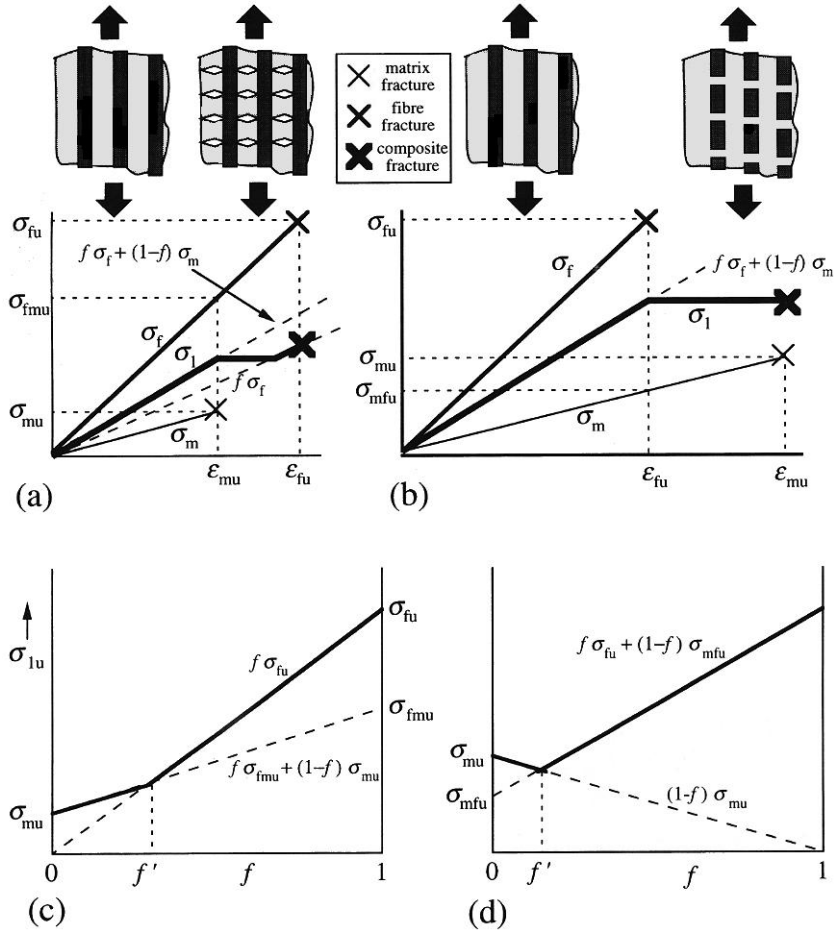

Figure 2.2 Schematic plots for idealised long-fibre composites with both components behaving in a brittle manner. (a) and (c) refer to a system in which the fibre has a higher strain to failure than the matrix and show respectively stress-strain relationships (of fibre, matrix and composite) and dependence of composite failure stress on volume fraction of fibre. (b) and (d) show the same plots for the case where the matrix has the higher strain to failure. Reproduced from [35], fig 8.2, p.160. Note that fibre volume fraction is represented using the symbol, *f*.

Since glass fibres have a higher strain to failure than typical polyester resins, it can be observed from Figure 2.2a that for these composites the onset of failure occurs at the stress given by Equation 2.7, while final failure occurs at the stress level given by Equation 2.6.

$$\sigma_{1u} = V_f \sigma_{fmu} + (1 - V_f)\sigma_{mu} \tag{2.7}$$

where σ_{fmu} is the stress in the fibre at the onset of matrix cracking and σ_{mu} is the failure stress of the matrix.

Transverse tensile strength within a lamina is considerably lower than the strength of the resin alone. One of the simplest models for this behaviour treats the fibres as holes in the resin and evaluates the minimum remaining load bearing cross section, as indicated schematically in Figure 2.3. This purely geometric model is evaluated using Equation 2.8 [35], and can be found to give unrealistically low strength predictions, particularly at high fibre volume fractions (note that since square packing is assumed, when $V_f = 0.785$, $\sigma_{2u} = 0$).

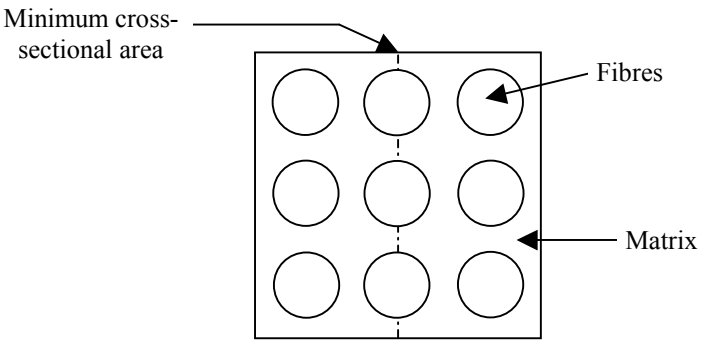

Figure 2.3 Schematic illustration of minimum cross section calculation for transverse tensile strength as calculated using Equation 2.8.

$$\sigma_{2u} = \sigma_{mu}\left[1 - 2\left(\frac{V_f}{\pi}\right)^{\frac{1}{2}}\right] \tag{2.8}$$

As for transverse modulus, numerous methods and arguments exist to determine the transverse strength; a much improved estimate compared with that obtained using Equation 2.8 is predicted using a micromechanics model which evaluates stress concentration induced by the presence of stiff cylindrical fibres within the matrix [36]. Consequently, the transverse failure stress is given by Equation 2.9.

$$\sigma_{2u} = \frac{\sigma_{mu}}{k_{\sigma 2}} \tag{2.9}$$

where σ_{mu} is the matrix failure stress and $k_{\sigma 2}$ is the stress concentration factor for transverse stress, which is given by Equation 2.10, after [36].

$$k_{\sigma 2} = \frac{E_m}{E_{2t}\left(\frac{2r_f}{s_f}\left[\frac{E_m}{E_f}-1\right]+1\right)} \tag{2.10}$$

where r_f is the fibre radius, s_f is the spacing between the fibres (assuming square packing) and E_{2t} is the effective modulus of the lamina in the direction transverse to the fibres.

This method provides a relatively simple relationship between fibre volume fraction and transverse strength, provided that the fibre radius is known. The fibre spacing may be calculated using standard geometric analysis, which is detailed in Chapter 5. Although more rigorous models exist, such as that suggested by King et al [37], these often require a knowledge of the fibre/matrix interfacial bond strength and of the residual stress introduced during the manufacturing process. The use of such parameters dictates further experimental measurement and makes the techniques less suitable for purely predictive modelling, which is the focus of this thesis. Micromechanical finite element analysis was used by Asp et al [38] to predict transverse strength due to matrix failure, neglecting interfacial effects and the presence of voids. Although such work is valuable to the research community, this type of analysis is not suited to design approaches since different FE meshes are required for each fibre volume fraction.

In-plane shear strength of the lamina is a parameter for which there is no widely accepted micromechanics model. Results from the finite difference calculations for shear stress concentration factor, k_τ, performed by Adams and Doner [32] may be used to give an estimate of lamina shear strength, τ_{12u}, as a function of the resin shear strength, τ_{mu}, but this is not a flexible method suitable for design calculations, particularly if a range of materials and fibre volume fractions are to be compared. Kies [36] derived an expression for transverse shear stress concentration factor, $k_{\tau 23}$, having the same form as Equation 2.10. The lamina failure stress in transverse shear may be determined according to this treatment using Equations 2.11 and 2.12. Although he stated that the same equation could also be used for in-plane shear strength, it is expected that $\tau_{12u} \neq \tau_{23u}$, and published data (e.g. [39]) indicates that in-plane shear strength is typically higher than the matrix shear strength, suggesting that this model is not suitable for determination of τ_{12u}.

$$\tau_{23\,u} = \frac{\tau_{mu}}{k_{\tau\,23}} \tag{2.11}$$

where $k_{\tau 23}$ is the shear stress concentration factor, defined in Equation 2.12.

$$k_{\tau\,23} = \frac{G_m}{G_{23\,t}\left(\frac{2r_f}{s_f}\left[\frac{G_m}{G_f}-1\right]+1\right)} \tag{2.12}$$

where G_{23t} is the in-plane shear modulus of the lamina.

Various published models exist to describe the failure of the lamina in compression [35,40]. In longitudinal compression, models pertain to buckling of the fibres, which is the dominant failure mechanism; this failure mechanism is highly dependent on the mechanical properties of the resin, since the matrix inhibits buckling by giving lateral support to the fibres. Under transverse compressive loads, shear failure of the matrix is dominant. Although compressive material behaviour can be significant in real components, failure under compressive loads is frequently caused by macroscopic structural (Euler) buckling, or by defects, such as local wrinkles, in the reinforcement. Note also that out-of-plane fibre waviness, such as that present in woven fabric reinforcements, has a significant effect on compressive strength. To avoid the complexities associated with compressive behaviour, the work in this thesis is presently restricted to tensile and shear loads. Where compressive failure stresses are required as fitting parameters for failure criteria, simple 'rules of thumb' are employed based on approximations to experimental findings; these are described in Chapter 5 as appropriate. Investigation and incorporation of appropriate failure models for compressive behaviour is an area where future work should be performed.

2.2.4 Summary

A number of theoretical treatments exist to determine the mechanical behaviour of a unidirectional lamina. Some approaches, such as that of Adams and Doner [31,32], are considered to give high accuracy but are not easily implemented into the design process. For composites containing ductile phases, e.g. aramid fibres or some thermoplastic matrices, alternative treatments must be applied, but the equations

described above are frequently employed for the materials used within the scope of this thesis. The choice of models for the purposes of the present work must involve some compromise between accuracy and ease of application. The approaches adopted in Chapter 5 have been selected such that they may be expected to give suitably accurate results, and may be incorporated into simple computer-based calculation methods, such as a spreadsheet or an analysis preprocessor written in the C++ programming language. Further assessment of their validity is made in Chapter 5 using results of experimental investigations described in Chapter 4.

2.3 Failure of the lamina under a biaxial load (failure criteria)

2.3.1 Introduction

Failure prediction for composite laminates in a state of biaxial stress has received a great deal of attention in the scientific literature in recent years. The most notable study in this area is a round-robin exercise to compare existing failure theories both with one another and with experimental biaxial test data; this is known as the world-wide failure exercise (WWFE), and the summary of its findings was published recently [4]. The WWFE, which was published in three stages [41-43], represents the most comprehensive selection of failure theories published in a single study, and is strongly recommended for further reading on failure prediction. For the discussion in this chapter, different approaches to failure prediction are considered, encompassing the major failure theories. This is not intended to be a comprehensive review of all available techniques, but rather an exposition of the basic themes. Moreover, this review is focussed on the prediction of initial failure, while a significant amount of effort was directed towards post-failure behaviour and damage development by the participants in the exercise.

There are two main classifications of failure theories: those which identify all modes of failure individually and provide a series of criteria for each one which are superimposed to determine the biaxial failure envelope (here termed independent failure theories), and those which use a single criterion calculated using some function of the strength values for each failure mode (interactive failure theories). In Section 2.3.2 some of the more prominent failure theories from the former category

are discussed, while those from the latter are considered in Section 2.3.3. Plane stress conditions are assumed throughout these sections. For comparison of different theories, predicted failure envelopes of a 0° unidirectional glass/epoxy lamina ($V_f = 60\%$) are presented in many cases. This represents test case 3 in the WWFE. Note that, due to the lamina orientation, $\sigma_x = \sigma_1$.

2.3.2 Independent failure theories

Maximum stress criterion

The maximum stress criterion for composites was developed by Jenkins [44] from the maximum principal stress criterion used for metals. Since the orthotropic nature of composites makes the use of principal stresses inappropriate, the criterion was formulated in terms of stresses in the material directions (1 and 2 in Figure 2.1), and shear stresses were incorporated. The criterion simply states that if any of the stresses in the material axes reaches the value of the corresponding strength, failure occurs. Mathematically it is expressed according to Equation 2.13. Note that no interaction between stresses is considered, i.e. that a lamina subjected to 99% of its maximum transverse tensile stress would also be expected to support 99% of its maximum in-plane shear stress without failing.

$$\begin{aligned} \sigma_1 &= \sigma_{1ut} \quad (\sigma_1 > 0) \\ \sigma_1 &= -\sigma_{1uc} \quad (\sigma_1 < 0) \\ \sigma_2 &= \sigma_{2ut} \quad (\sigma_2 > 0) \\ \sigma_2 &= -\sigma_{2uc} \quad (\sigma_2 < 0) \\ |\tau_{12}| &= \tau_{12u} \end{aligned} \tag{2.13}$$

where σ and τ are normal and shear stresses; σ_u and τ_u are the corresponding strengths; subscripts t and c indicate tension and compression respectively.

In the WWFE, Zinoviev et al [45] adopted the maximum stress criterion for their predictions of the onset of failure. They also accounted for geometric non-linearity due to fibre reorientation under off-axis loading, and for reductions in stiffness caused by the onset of cracking in the matrix phase. The failure envelope predicted by Zinoviev et al for a unidirectional glass/epoxy lamina is shown in Figure 2.4. It

can be observed that the rectangular envelope is constructed from the intersection of four straight lines, each indicative of a failure mode. The failure modes are also listed.

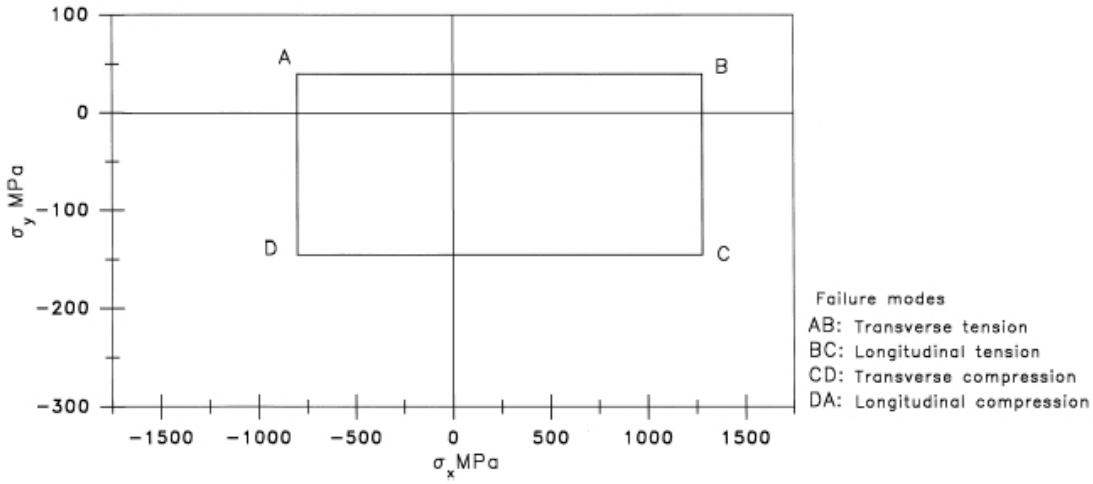

Figure 2.4 Predicted failure envelope for a glass/epoxy unidirectional lamina (V_f = 60%) using the maximum stress failure criterion. After Zinoviev et al [45].

Edge criterion

Edge [46] reported failure predictions using a code developed at British Aerospace Defence Ltd., based primarily on the maximum stress criterion. Additional criteria were superimposed to describe failure under combined shear and transverse tension, and under combined longitudinal compression and shear loading. A simple delamination criterion was also included. For the unidirectional lamina, the biaxial (σ_1-σ_2) failure envelope exhibited the classical rectangular shape associated with the maximum stress theory. The author also considered stiffness reduction after the onset of failure, reducing stiffness terms gradually according to the magnitude of the strain in the direction in which failure has occurred.

Puck criterion

Advocating the use of separate criteria for each possible failure mode, Puck and Schürmann [47] presented separate equations to define failure by fibre tension, fibre compression, and three modes of inter-fibre fracture for brittle matrix materials (denoted A, B and C by the authors). Fibre tension and compression can be understood intuitively; the inter-fibre fracture (IFF) modes result from:

Mode A – combined transverse tension and in-plane shear

Mode B – combined moderate transverse compression and in-plane shear

Mode C – combined high transverse compression and in-plane shear

These separate phenomena result since (A) transverse tension increases susceptibility to fracture in shear, (B) transverse compression reduces the same and (C) high levels of transverse compression give rise to transverse matrix failure, and this is also affected by the in-plane shear stress.

The authors also specified a method of gradual stiffness reduction as crack propagation was deemed to begin and continue. The failure envelope for a unidirectional glass/epoxy lamina predicted using this theory is shown in Figure 2.5. It can be seen that, as expected, IFF mode A was dominant for transverse tensile stresses, and that IFF mode C dominated transverse compressive behaviour. Fibre failure caused cut-offs to be imposed for high axial loads.

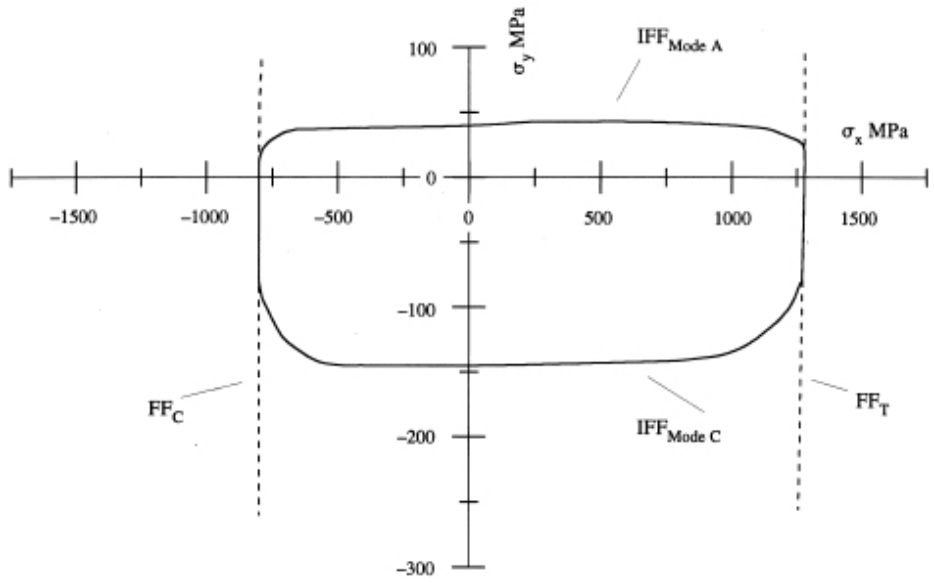

Figure 2.5 Predicted failure envelope for a glass/epoxy unidirectional lamina (V_f = 60%) using the Puck fracture criterion. After Puck and Schürmann [47].

Maximum strain criterion

Since strain can be related to energy stored in a material, and since consideration of strain may avoid the need to consider non-linear material behaviour, the maximum strain criterion was suggested by Pettit and Waddoups [48]. It is analogous to the maximum stress criterion, but formulated in terms of strains. This criterion was

adopted by Bogetti et al [49] in the WWFE, who also incorporated a simple damage model to reduce the stiffnesses of plies within a laminate which were deemed to have exceeded their failure strain.

In order that it was considered in the WWFE (since Bogetti et al [49] were late entrants to the exercise) Hart-Smith [50] produced predictions from both the maximum strain theory and a truncated version of the same, in which the tension-compression quadrants of the σ_1-σ_2 failure envelope were cut off to consider fibre failure in shear, producing failure envelopes reminiscent of the Tresca isotropic criterion. A failure envelope produced using this approach for a unidirectional glass/epoxy lamina is shown in Figure 2.6. It should be noted that since the criterion is formulated in terms of strain, plotting the failure envelope on stress axes gives rise to sloped sides due to the Poisson's ratio of the lamina. This can also be observed in Figure 2.6. In the WWFE, this criterion was referred to as Hart-Smith (2), and this convention will be used during further discussions later in this thesis.

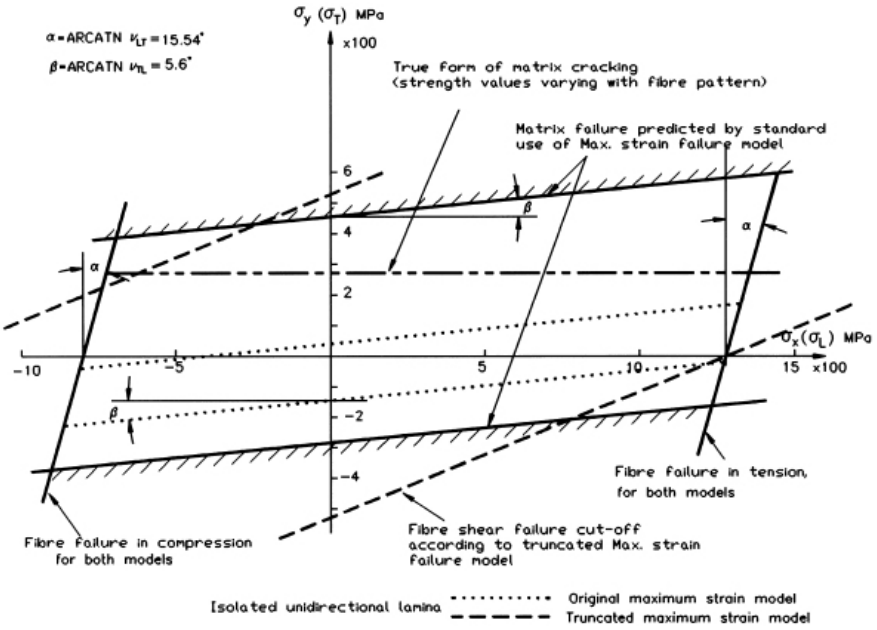

Figure 2.6 Predicted failure envelope for a glass/epoxy unidirectional lamina ($V_f = 60\%$) using the maximum strain theory, with truncations indicated under combined tension-compression loads to consider shear failure. After Hart-Smith [50].

Generalised maximum shear stress criterion

Highlighting the heterogeneous nature of composites, i.e. that they are composed of two different materials, Hart-Smith [51] proposed the use of a method to evaluate the

strains in the fibre and matrix phases of a composite lamina and use these to determine the maximum shear stresses in the phases, superimposing the fibre and matrix envelopes to predict that for the lamina. Hart-Smith's prediction of the failure envelope for a glass/epoxy unidirectional lamina is presented in Figure 2.7. Inspection of this envelope reveals that there are two envelopes for transverse failure, one permitting significantly higher transverse stresses (σ_y) than the other. Hart-Smith states that the in-situ strength of a lamina within a laminate is much higher than that of the same lamina in isolation; hence the lower bounds of this prediction are for the single unidirectional lamina. No reference to other work supporting this statement was made in his paper. The position where the fibre shear failure prediction (the sloping line in the tension/compression quadrant) intercepts the axis of transverse compressive stress was calculated assuming that no matrix failure occurs in order to set the slope of the line. This criterion will subsequently be referred to as Hart-Smith (1) in accordance with the conventions of the WWFE.

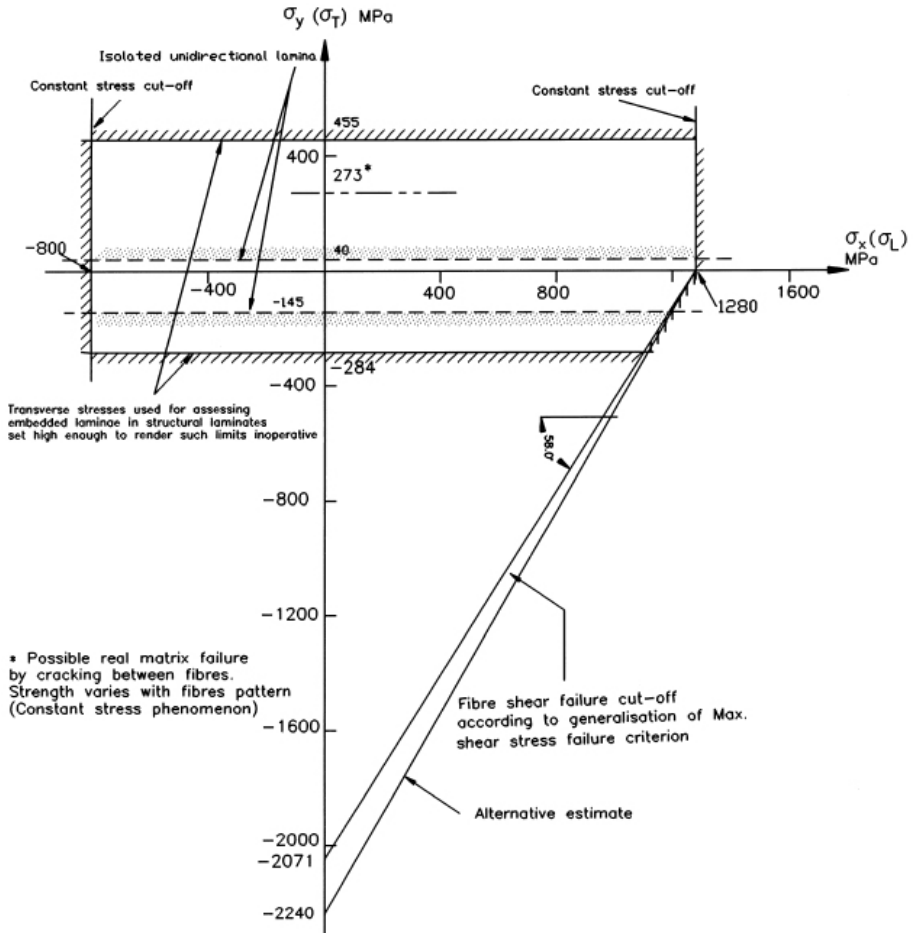

Figure 2.7 Predicted failure envelope for a glass/epoxy unidirectional lamina ($V_f = 60\%$) using the maximum shear stress failure theory. After Hart-Smith [51].

The 'ten-percent rule'

In the second part of the WWFE, Hart-Smith [52] also published results predicted using a technique developed prior to the widespread availability of electronic calculating devices, known as the 'ten-percent rule'. Based almost entirely on 'rules of thumb', the only material data required for input to the model are axial Young's modulus, E_1, and axial strengths in tension and compression, σ_{1ut} and σ_{1uc}. Other properties are inferred from these according to the expressions in Equation 2.14. Hart-Smith also proposes that Poisson's ratio, ν_{12}, of the lamina can be assumed to take the value 0.3 if experimental measurement to the contrary has not been made. The predicted failure envelope for the unidirectional glass/epoxy lamina is shown in Figure 2.8. Note that the author conceded that the lamina transverse strengths would not necessarily match experimental measurements due to their estimation by this theory. For further discussion, this theory will be referred to as Hart-Smith (3).

$$
\begin{aligned}
&\text{The transverse modulus of the lamina, } E_2 = \frac{E_1}{10} \\
&\text{The modulus of a } \pm 45^\circ \text{ angle-ply laminate, } E_{\pm 45^\circ} = E_2 \\
&\text{The transverse lamina strengths, } \sigma_{2ut} = \sigma_{2uc} = \frac{\sigma_{1u}}{10} \\
&\text{The strength of a } \pm 45^\circ \text{ angle-ply laminate, } \sigma_{\pm 45^\circ ut} = \sigma_{\pm 45^\circ uc} = \frac{\sigma_{1u}}{10} \\
&\text{The shear modulus, } G_{12} = G_{0/90} = \frac{E_{\pm 45^\circ}}{2\left(1+\nu_{\pm 45^\circ}\right)} \approx \frac{E_1}{36} = 0.0278\, E_1 \\
&\text{The shear strength of a unidirectional lamina, } \sigma_{12u} = \frac{\sigma_{\pm 45^\circ u}}{2} = 0.05\, \sigma_{1u}
\end{aligned}
\qquad (2.14)
$$

where σ_{1u} is the higher of σ_{1ut} and σ_{1uc}.

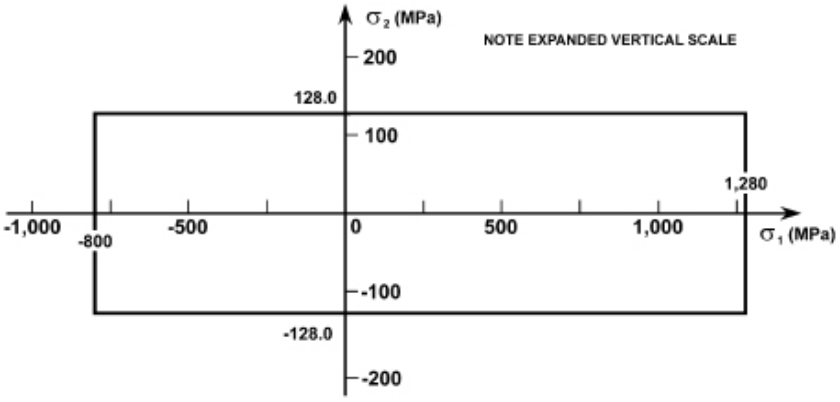

Figure 2.8 Predicted failure envelope for a glass/epoxy unidirectional lamina (V_f = 60%) using the 'ten percent rule'. After Hart-Smith [52].

Rotem criterion

Following his earlier work in collaboration with Hashin [53], Rotem [54] made predictions for the WWFE using separate criteria for the failure of fibres and matrix. Fibre (axial) failure is predicted using the expression in Equation 2.15 (maximum stress criterion), while matrix failure is predicted using the function of all stress terms pertinent to the matrix given in Equation 2.16. The predicted failure envelope of a unidirectional glass/epoxy lamina is shown in Figure 2.9.

$$-\sigma_{1uc} \geq \sigma_1 \geq \sigma_{1ut} \tag{2.15}$$

where σ_1 is the axial stress in the lamina, and σ_{1ut} and σ_{1uc} are tensile and compressive strengths, respectively

$$\left(\frac{E_m(\varepsilon_1)\varepsilon_1}{\pm\sigma_{um}}\right)^2+\left(\frac{\sigma_2}{\pm\sigma_{2ut,c}}\right)^2+\left(\frac{\tau_{12}}{\tau_{12u}}\right)^2 \tag{2.16}$$

where E_m is the Young's modulus of the matrix and σ_{um} is the matrix failure stress.

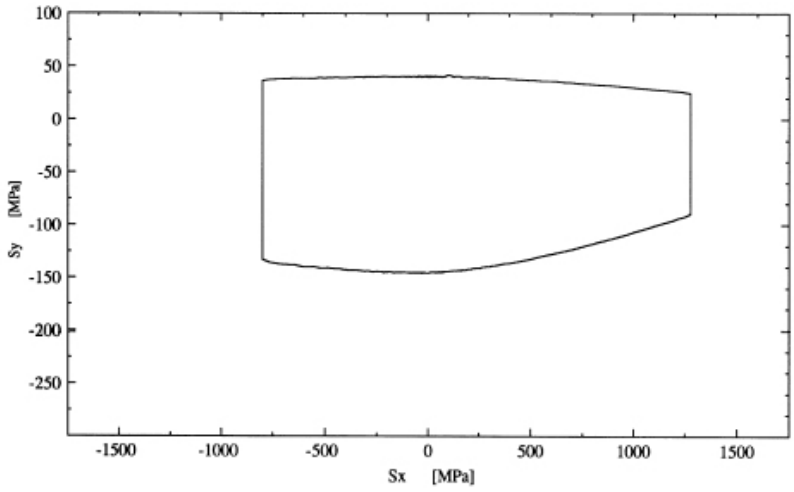

Figure 2.9 Predicted failure envelope for a glass/epoxy unidirectional lamina (V_f = 60%) using the Rotem criterion. After Rotem [54].

It should be noted that Sun & Tao [55] also used Rotem's criterion, although they omitted the first term in Equation 2.16. This had the effect of giving the failure envelope of unidirectional material the classic rectangular shape on the σ_1-σ_2 plane. An alternative method for post-initial failure behaviour was implemented by the authors.

Strain Invariant Failure Theory (SIFT)

Although not part of the WWFE, Hart-Smith has proposed a further failure theory in terms of strain invariants [56]. Known as the strain invariant failure theory (SIFT), this criterion evaluated failure in the fibres and matrix separately, by evaluating certain strain invariants in each phase using micromechanical FE analysis. Although this was based on sound engineering theory, and appears to be very promising, the implementation is still in development.

2.3.3 Interactive failure theories

Tsai-Hill criterion

Tsai [57] applied the yield criterion developed for homogeneous orthotropic plastic materials by Hill [58] to the failure of polymer composites. The resulting 'Tsai-Hill criterion' assesses failure according to the quadratic expression in Equation 2.17

$$\left(\frac{{\sigma_1}^2}{{\sigma_{1u}}^2} - \frac{\sigma_1 \sigma_2}{{\sigma_{1u}}^2} + \frac{{\sigma_2}^2}{{\sigma_{2u}}^2} + \frac{{\tau_{12}}^2}{{\tau_{12u}}^2} \right) = 1 \qquad (2.17)$$

Differences between tensile and compressive failure behaviour are not considered; the same is true of the active failure mechanism. It is possible, however, to estimate the failure mechanism by evaluating the terms in Equation 2.17 individually to assess their contribution to the total.

Tsai-Wu criterion

Later, Tsai and Wu [59] developed a quadratic failure criterion from that proposed by Gol'denblat and Kopnov [60]. This theory is based on experimental observation and curve fitting, and is not founded on the exposition of individual failure mechanisms. In plane stress, failure is evaluated using Equation 2.18:

$$F_1\sigma_1 + F_2\sigma_2 + F_{11}\sigma_1^{\,2} + F_{22}\sigma_2^{\,2} + F_{66}\tau_{12}^{\,2} + 2F_{12}\sigma_1\sigma_2 = 1$$

where: $F_1 = \frac{1}{\sigma_{1ut}} + \frac{1}{\sigma_{1uc}}$; $F_2 = \frac{1}{\sigma_{2ut}} + \frac{1}{\sigma_{2uc}}$;

$$F_{11} = -\frac{1}{\sigma_{1ut}\sigma_{1uc}}; F_{22} = -\frac{1}{\sigma_{2ut}\sigma_{2uc}}; \; F_{66} = \frac{1}{\tau_{12}^{\,2}} \qquad (2.18)$$

$$F_{12} = \frac{1}{2\sigma_{biax}^2}\left[1 - \left(\frac{1}{\sigma_{1ut}} + \frac{1}{\sigma_{1uc}} + \frac{1}{\sigma_{2ut}} + \frac{1}{\sigma_{2uc}}\right)\sigma_{biax} + \left(\frac{1}{\sigma_{1ut}\sigma_{1uc}} + \frac{1}{\sigma_{2ut}\sigma_{2uc}}\right)\sigma_{biax}^2\right]$$

The parameter F_{12} in Equation 2.18 is required to ensure mathematical continuity of the failure envelope through the full range of stress ratios, and controls the shape, orientation and position of the elliptical failure envelope. If test data are available, σ_{biax} represents the failure stress under simultaneous equal loads in the 1 and 2 directions. The F_{12} term may be simplified using an empirical relationship suggested by Tsai and Hahn [61] stating that :

$$F_{12} = f^*\sqrt{F_{11}F_{22}} \quad \text{where } -1 \le f^* \le 1 \quad \text{(Tsai \& Hahn suggest } f^* = -½) \qquad (2.19)$$

Liu and Tsai [62] used this theory as the basis for their predictions in the WWFE. Taking the parameter f* = -½, initial failure was predicted by this criterion whereupon a stiffness degradation scheme was applied to determine post-failure behaviour. The failure envelope of a unidirectional glass/epoxy lamina predicted by Liu and Tsai is shown in Figure 2.10.

It should be noted that there has been a great deal of inferred criticism of this criterion in the literature. Since it essentially fits a quadratic ellipsoid to the uniaxial strengths, Hart-Smith [63] observed that, were the Tsai-Wu criterion used in blind faith, then a stronger submarine hull (subject to biaxial compression) could be designed by using a composite with a lower transverse tensile strength. While this is an extreme example, it is one of the most vaunted weaknesses of the method, and gives an indication of the care required when using this theory.

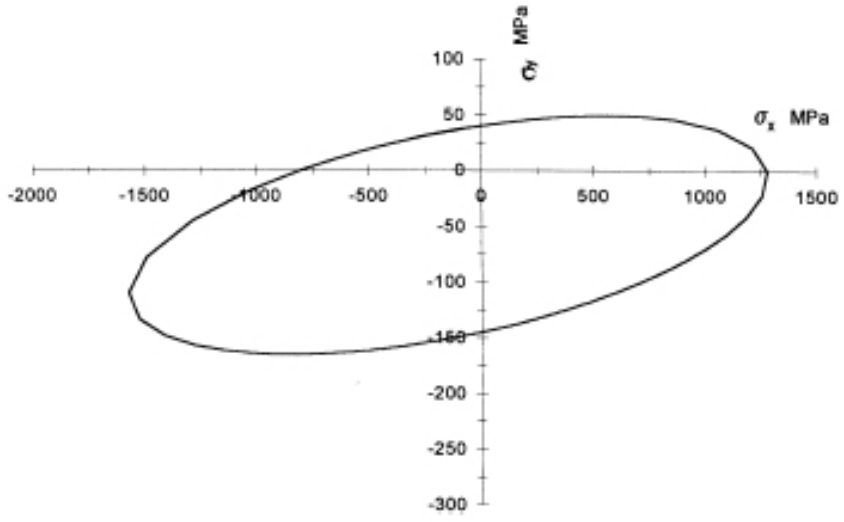

Figure 2.10 Predicted failure envelope for a glass/epoxy unidirectional lamina ($V_f = 60\%$) using the Tsai-Wu criterion. After Liu and Tsai [62].

Wolfe criterion

Wolfe and Butalia [64] gave predictions using a combined stress and strain state criterion based on strain-energy. Their criterion took the form expressed in Equation 2.20.

$$\left(\frac{\int_{\varepsilon_1}^{\varepsilon_1} \sigma_1 \mathrm{d}\varepsilon_1}{\int_{\varepsilon_1}^{\varepsilon_1^u} \sigma_1 \mathrm{d}\varepsilon_1} \right)^{m_1} + \left(\frac{\int_{\varepsilon_2}^{\varepsilon_2} \sigma_2 \mathrm{d}\varepsilon_2}{\int_{\varepsilon_2}^{\varepsilon_2^u} \sigma_2 \mathrm{d}\varepsilon_2} \right)^{m_2} + \left(\frac{\int_{\varepsilon_6}^{\varepsilon_6} \sigma_6 \mathrm{d}\varepsilon_6}{\int_{\varepsilon_6}^{\varepsilon_6^u} \sigma_6 \mathrm{d}\varepsilon_6} \right)^{m_6} = 1 \qquad (2.20)$$

where m_1, m_2 and m_6 are empirical constants determined from biaxial test data in the range $1 \leq m_i \leq 2$, which define the shape of the failure envelope. For the 'blind' predictions presented, the authors used $m_1 = m_2 = m_6 = 1$.

The failure envelope determined using this method for a unidirectional glass-epoxy lamina is shown in Figure 2.11. Although there is no direct comment in the paper on the discontinuities observed on the axial loading axes, the authors state that point B, which falls at approximately half of the measured lamina strength used as input data to the model, suggests a low compressive strength due to the tensile strain induced by Poisson's effect. They suggested that improved predictions would be made if Poisson's ratio were available as a function of the strain.

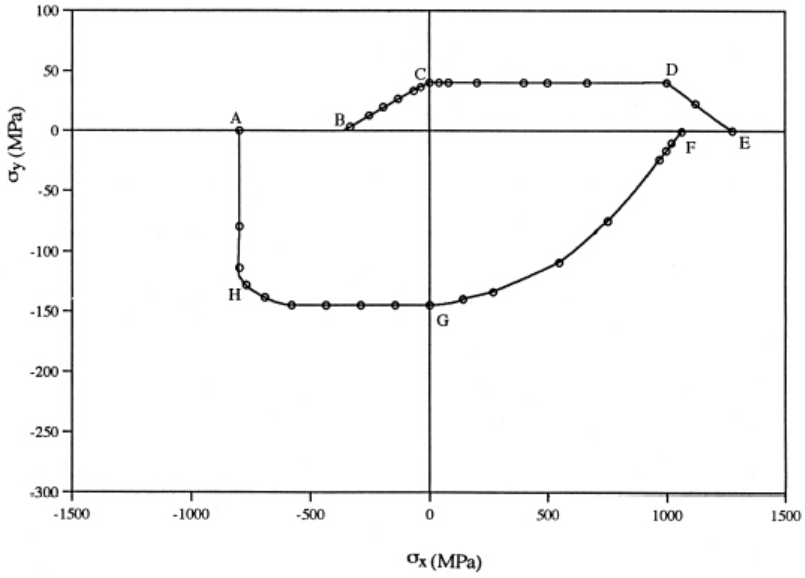

Figure 2.11 Predicted failure envelope for a glass/epoxy unidirectional lamina ($V_f = 60\%$) using a strain energy based criterion. After Wolfe & Butalia [64].

Cuntze criterion

Cuntze and Freund [65] identified distinct fracture mechanisms, rather like those defined by Puck [47], and determined suitable stress invariants to evaluate the failure modes, superimposing the resulting envelopes. However, they also added a 'rounding-off exponent' used to smooth out sharp corners in the failure envelope in what they termed the 'mixed failure domain' at the boundaries between failure modes. For the unidirectional glass/epoxy lamina, the failure envelope predicted using this approach is shown in Figure 2.12.

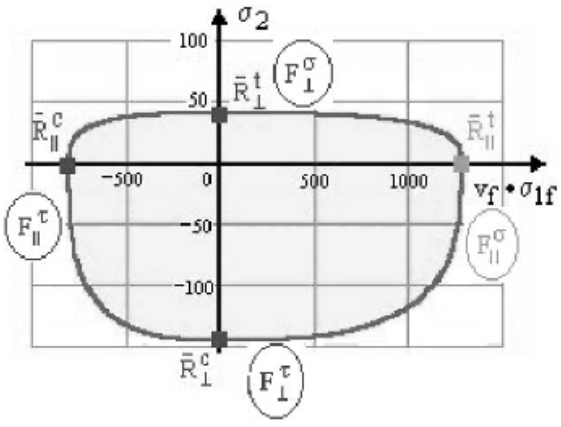

Figure 2.12 Predicted failure envelope for a glass/epoxy unidirectional lamina ($V_f = 60\%$) using a Cuntze's failure theory. After Cuntze & Freund [64].

Gotsis and Chamis criterion

While Gotsis et al [66] used the maximum stress criterion for their predictions of failure for some of the cases in the WWFE using their in-house FE code, CODSTRAN, they also superimposed a maximum distortional energy criterion of the form shown in Equation 2.21.

$$F = 1 - \left[\left(\frac{\sigma_{1t}}{\sigma_{1ut}} \right)^2 + \left(\frac{\sigma_{2c}}{\sigma_{2uc}} \right)^2 - K_{12} \left(\frac{\sigma_{1t}}{\sigma_{1ut}} \right) \left(\frac{\sigma_{2c}}{\sigma_{2uc}} \right) + \left(\frac{\tau_{12}}{\tau_{12u}} \right)^2 \right]$$
$$K_{12} = \frac{(1 + 4\nu_{12} - \nu_{13})E_2 + (1 - \nu_{23})E_1}{[E_1 E_2 (2 + \nu_{12} + \nu_{13})(2 + \nu_{21} + \nu_{23})]^{1/2}} \qquad (2.21)$$

where σ and τ are normal and shear stresses; σ_u and τ_u are the corresponding strengths; subscripts t and c indicate tension and compression respectively.

For the single lamina, the authors used another in-house code, ICAN, based on micromechanics; this code was also used to calculate ply strengths for use with the criterion implemented in their CODSTRAN package, described above. The failure envelope predicted for a unidirectional glass/epoxy lamina is shown in Figure 2.13

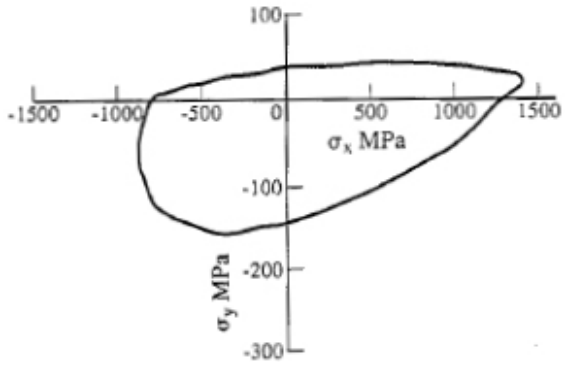

Figure 2.13 Predicted failure envelope for a glass/epoxy unidirectional lamina (V_f = 60%) using micromechanical methods. After Gotsis et al [66].

2.3.4 Summary

The desire to use independent failure theories is easily understood: failure is assumed to occur according to a specific criterion, assumed to be appropriate to the stress state

in the lamina. The active failure mechanism is predicted, and hence reasons for discrepancies may be investigated in an informed fashion. Many authors are immediately critical of interactive failure theories due to their lack of a physical basis. While this is true, the advantages to the designer of a neat, closed form expression to evaluate failure are also clear.

Also worthy of note is that a number of failure criteria are incorporated into finite element packages, such that the user can obtain failure predictions without the use of supplementary software. It should be noted that the Abaqus package [67] has implementations of the Tsai-Hill, Tsai-Wu, maximum stress and maximum strain criteria, although other criteria may be calculated using a user-written subroutine.

Predicted failure envelopes for a unidirectional glass/epoxy lamina are shown with experimental data in Figure 2.14, giving an indication of the differences between some of the theories. Although the findings of the WWFE are too extensive to list, the summary of overall performance of the failure criteria, benchmarked against all of the test cases and requirements, are reproduced in Appendix B of this thesis. However, this is no substitute for reading the conclusions of Hinton et al [68,69], which is a recommended exercise. Recommendations for the design community were also made [4]. It should be noted that Zinoviev's implementation of the maximum stress criterion ranked highly, being particularly good at predicting initial failure, and that the Tsai-Wu criterion, despite the aforementioned reservations, also performed well (although experimental data in states of biaxial compression was limited, leaving the performance of all theories under question in this quadrant). It was stated [68], however, that 'a designer wishing to estimate the stress levels at which initial failure might occur in a multi-directional laminate can only hope to get within ±50% at best, based on current theories'.

While the WWFE is the single most comprehensive study of the predictive capabilities of a number of theories, a number of reviews of the leading failure criteria have also been published (e.g. [70-72]), which are more descriptive in nature and offer criticism at a more fundamental level.

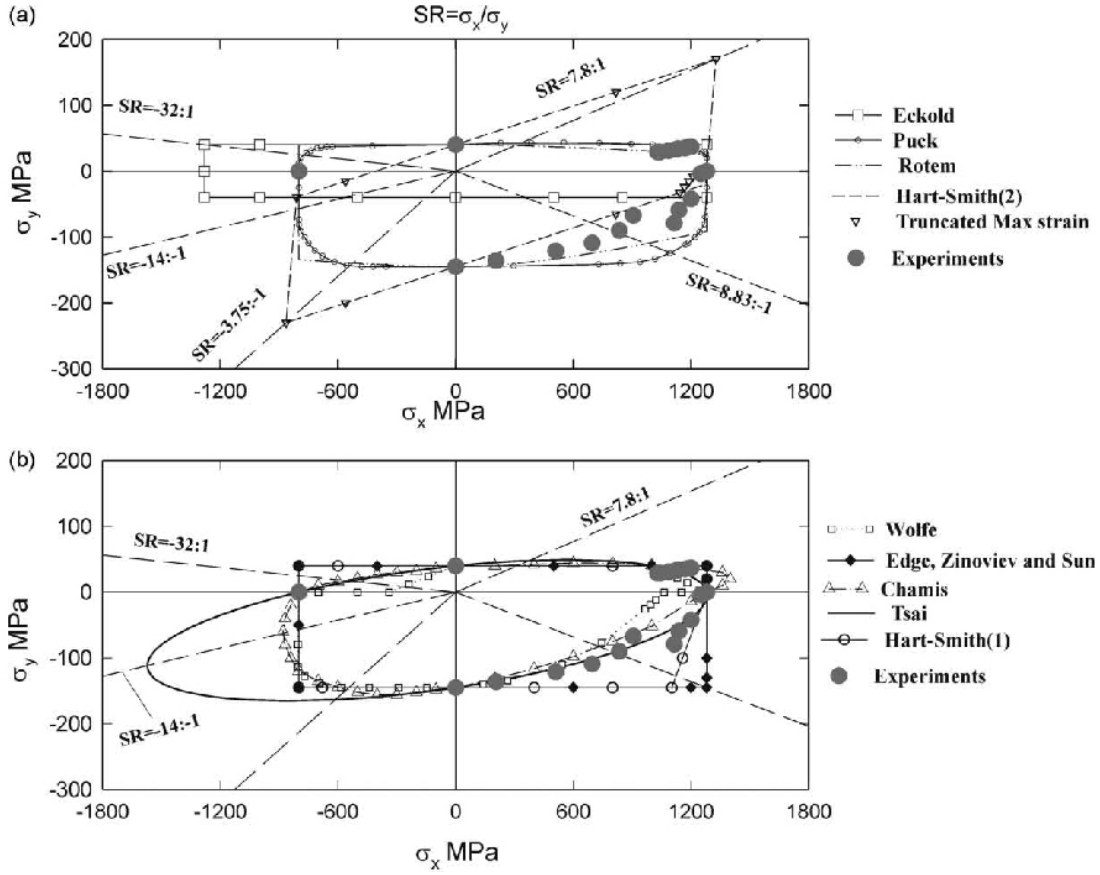

Figure 2.14 Predicted biaxial failure envelopes for a unidirectional glass/epoxy lamina (V_f = 60%), plotted with experimental measurements. Reproduced from [68].

2.4 Models for textile composite laminates

As discussed in Chapter 1, structural composite components are usually manufactured from either multiple layers of unidirectional reinforcement or multidirectional textile reinforcements. While the models described in Sections 2.2 and 2.3 are relevant to composites reinforced with unidirectional fibres, to determine the behaviour of real components some treatment is required to evaluate the behaviour of a laminate produced using multidirectional reinforcements. For non-crimp fabric (NCF) reinforced laminates, where the fibres are present in discrete layers, traditional approaches for laminated unidirectional composites may be used to offer a close approximation to the true material architecture, although for woven fabrics more complex models are required. This section presents published methods for prediction of mechanical properties of textile reinforced composites.

2.4.1 Lamination models

The methods discussed in Section 2.2 can provide a set of stiffness and strength values in the principal directions for transversely orthotropic materials, such as unidirectional fibre reinforced composites. For laminated composites, i.e. those comprised of a number of layers of reinforcement at different orientations, methods must be used to account for the presence of fibres in many orientations within the laminate. Krenchel [73] suggested the use of an efficiency factor to modify the rule of mixtures to account for fibre orientation within a laminate. The modified rule of mixtures is described by Equations 2.22 and 2.23.

$$E_x = \eta E_f V_f + E_m (1 - V_f) \tag{2.22}$$

where E_x is the Young's modulus of the laminate in the x direction, η is the reinforcement efficiency factor, defined in Equation 2.23, E_f and E_m are the Young's moduli of the fibre and matrix respectively, and V_f is the fibre volume fraction.

$$\eta = \sum a_n Cos^4 \theta_n \tag{2.23}$$

where a_n is the proportion of fibres orientated at angle θ_n to the reference (x) direction.

This efficiency factor quantifies the effect that fibres running parallel with the direction of an applied load carry more of that load than those which are not parallel. It has been noted to show good agreement with experimental results for both angle-ply laminates [74,75] and for quasi-isotropic reinforcements (such as continuous filament random mat) [73]. This theory neglects the stiffening effect of transverse fibres due to contraction caused by Poisson's effects, however, as can be seen by inspection of Equation 2.23 (since $\eta = 0$ when all $\theta_n = 90°$). This effect becomes more significant as the angle between the fibres and the load increases, and agreement with experimental data presented by Smith [75] seems to be less satisfactory for angle-ply laminates with $\theta > 50°$. This theory is intended for balanced symmetric laminates and hence neglects any effects caused by tension-shear coupling. There is no associated method for determining local stresses or failure behaviour.

A more rigorous analysis is provided by the well know classical laminate theory. This is well described by a number of authors (e.g. [35,40,61]) and its application within this work is described fully in Chapter 5. This theory uses stress (tensor) transformations and assumes perfect bonding between layers of orthotropic material. It also assumes that plane sections normal to the laminate midplane remain plane, normal and undeformed, i.e. that $\varepsilon_3 = \gamma_{23} = \gamma_{31} = 0$ (this is known as the Kirchhoff hypothesis). A full set of in-plane elastic constants for a laminate can be identified using this method; stresses can also be determined, and hence failure behaviour with the application of an appropriate failure criterion. Since the layers are assumed to be homogeneous, no consideration can be given to reinforcement architecture using this theory alone, although in-plane fibre orientations are considered. It should be noted, however, that experimental studies (e.g. [76]) have shown little difference between composites manufactured from laminated unidirectional material and those produced using stitched NCF reinforcements, suggesting that this theory is suitable for direct application to NCF reinforced laminates, provided that interlaminar displacement is not significant, i.e. that delamination does not occur.

Finite elements may also be used to predict laminate behaviour. A brief description of the finite element method is provided in Section 2.4.4. The Abaqus finite element (FE) code [67] provides thin, thick and general-purpose (suitable for thick or thin problems) plane stress shell elements which may be defined using a number of layers, each with its own material properties and, optionally, material orientation. The thin shell elements require that plane sections remain plane, and also that sections normal to the shell remain normal (Kirchhoff-Love assumptions). This reduces the accuracy of calculations in bending when transverse shear is a significant mode of deformation. This is illustrated in Figure 2.15. To account for this, thick shell solutions allow for transverse shear deformation, but still require that plane sections remain plane (Reissner-Mindlin assumptions). To give full consideration to transverse shear deformation, layered 3D solid elements must be used. When defining material orientations for shell elements, the Abaqus input processor projects the specified orientations into the element plane if necessary (and reports a message to this effect to the data file); this is not performed for solid elements, and hence great care must be taken to define the material orientations correctly for solid

elements. An example of this is shown in Figure 2.16. For a detailed explanation of the behaviour of orthotropic finite elements, the reader is referred to [77].

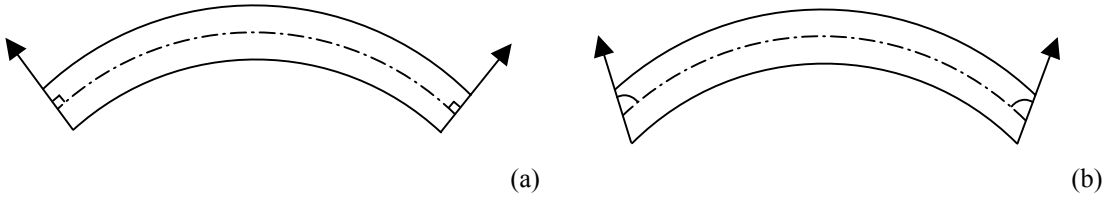

(a) (b)

Figure 2.15 (a) Pure bending and (b) bending incorporating transverse shear

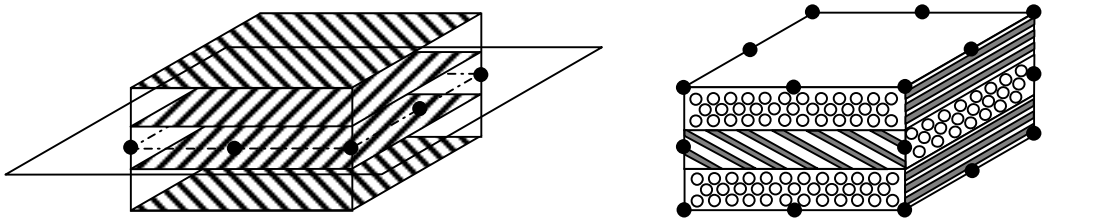

(a) (b)

Figure 2.16 (a) Layered shell element using eight nodes, showing the element reference surface, onto which material orientations are projected and (b) a 20-noded layered solid brick element with orientation mis-specified for the middle layer such that fibres do not lie in the lamina plane

2.4.2 Geometric description of textile composites

As previously mentioned, while lamination models such as those described in Section 2.4.1 may be applied to laminated unidirectional materials, and to non-crimp fabric (NCF) reinforced laminates where discrete layers of unidirectional tows are stitched together to produce a multidirectional reinforcement, their use for textile composites with complex architectures (e.g. woven fabrics) is more limited. Various methods to predict the mechanical properties of woven fabrics have been published, falling into two main categories: analytical models and numerical models. Both of these methods require a mathematical description of the fabric architecture in order to be able to assess its effect on mechanical properties.

The earliest formalisation of woven textile architecture was devised by Pierce [78], who assumed that tows were circular in cross section. Geometric descriptions which are more suitable for woven technical textiles have been developed by others,

notably Lomov et al [79,80], McBride and Chen [81], Hofstee et al [82,83] and Robitaille et al [84,85]. These models differ from many others found in the literature due to their ability to model textiles which have undergone shear deformation during forming. Limitations of the models include requirement of experimentally-determined yarn mechanical data (Lomov), restriction to a single weave style (McBride, Hofstee) and consideration of only the tows, making them unsuitable for three-dimensional analysis of composites produced using liquid moulding techniques since the surrounding resin is not considered (McBride, Hofstee). The code developed by Robitaille and his co-workers is designed to be general in nature such that it is not restricted, for example, to common weave styles or limited assumptions of tow geometry. It also has the ability to describe non-crimp fabrics [86].

Most of the reported mechanical modelling techniques discussed in the following sections also featured a geometric description of the weave structure, ranging from very simple (e.g. Turner [87]) to very general (e.g. Glaessgen et al [88]). Another notable approach was that of Searles et al [89], who fitted polynomial functions to tow cross sections and undulating paths observed in micrographs of eight-harness satin weave composites. Although a good representation of the architecture of a manufactured composite may be produced, the drawback of this approach is that it does not permit analysis of materials for which cross section micrographs are not available, i.e. it is not fully predictive.

2.4.3 Analytical models for textile composites

Various analytical models exist to describe the mechanical behaviour of textile composites. Some of the earliest work in the field was developed by Ishikawa and Chou [90], who used laminate theory to determine mechanical behaviour of composites with woven reinforcements. Ignoring the continuity and undulation of the fibres, simplified ‘mosaic’ models were generated such as those illustrated in Figure 2.17. Upper and lower bounds for stiffness in the tow direction were calculated by assuming constant strain (isostrain) or constant stress (isostress) in the model, respectively.

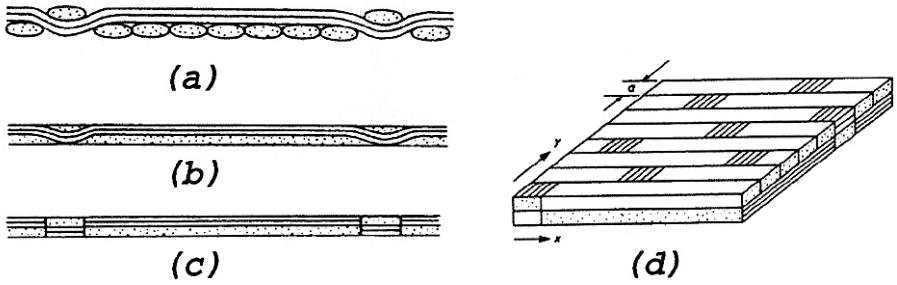

Figure 2.17 Lamination-based model for composite with 8 harness satin weave reinforcement, after Ishikawa and Chou [90]. (a) textile geometry (b) crossing tows assumed to be homogenised (c) stepped simplification of undulating tow (d) approximation to the composite structure.

Addressing the fibre undulation and continuity, Ishikawa and Chou [91] also developed the 'fibre crimp' model, in which the length of one tow in the fabric repeating unit was divided into small sections (dx in Figure 2.18). The geometry of the undulating section of the fabric was defined using a sinusoidal expression, and a straight section of an appropriate length for the weave style was incorporated. Each section along the length of the tow was analysed using laminate theory, and the average compliance was determined assuming constant stress in the x direction. This model only considered loading in the x direction, but did consider general weave patterns. The authors noted that for a single layer of textile, coupling between extension and bending was present since it was not symmetric about the midplane. Lower bounds for stiffness were determined when bending was permitted (i.e. resultant moment was zero), while upper bounds were obtained when curvature was constrained to be zero (producing a resultant bending moment). This was in agreement with the conclusions of Whitcomb et al [92], who later conducted numerical studies of these effects using finite element analysis. In the case of a multilayered laminate, the upper bound approximation is more appropriate, and is exactly true for perfectly symmetric laminates.

Extending their crimp model further, Ishikawa and Chou developed the bridging model [91], which was specifically for composites with satin weave reinforcement. This model recognised that the undulating region of satin woven reinforcement was surrounded by material without undulation, and hence that this small (undulating) region carried a lower load than the surrounding regions due to its lower stiffness. The geometric building blocks, shown in Figure 2.19, were all 0°/90° cross-ply laminates, except for region III, in which the undulating tow was modelled using the

crimp model. Assuming that a load was applied as denoted by N in Figure 2.19, stiffnesses of regions II, III and IV were averaged using an isostrain assumption (since they were in parallel), then the compliances of regions I, (II-II-IV) and V were averaged assuming constant stress (since they were in series), to determine the behaviour of the whole repeating unit.

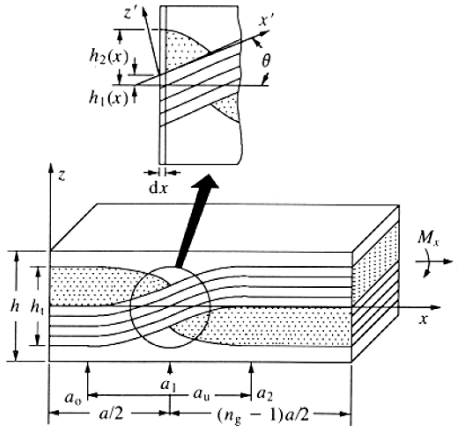

Figure 2.18 Fibre crimp model for woven composite, after Ishikawa and Chou [91].

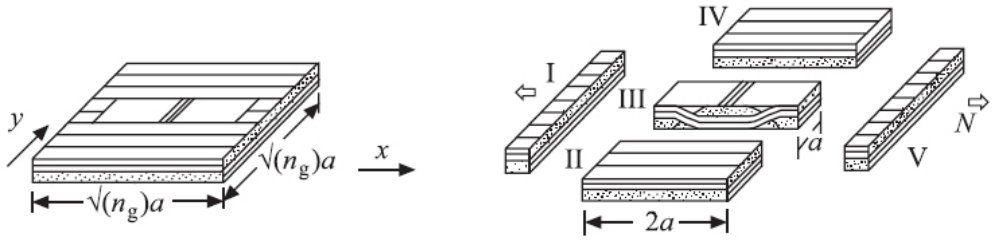

Figure 2.19 Building blocks of the bridging model for satin weave composite, after Ishikawa and Chou [91].

Ishikawa and Chou later compared their models with experimental data for plain weave and 8 harness satin weave composites tested parallel to the warp fibre direction [93] and found that, for the cases examined, the bridging model gave an excellent prediction for stiffness of the satin weave, and that the results for plain weave composites (manufactured with 1, 4, 8 and 20 layers of reinforcement) all fell between the upper and lower bounds from the crimp model, although there was a large difference between the bounds for the crimp model, making the predictions less specific.

The same authors also employed the maximum strain failure criterion to determine a point of initial failure in woven composites [91]. They compared results obtained

with the 'knee point' found in experimental testing for a very limited number of cases, but found agreement to be good.

A very simple geometry was used for analysis of woven reinforced composites by Dimitrienko [94] and by Turner [87]. In their analyses, woven reinforced composites were represented as two layers of tows (lamination model), each layer having homogenised properties considering the effect of the (sinusoidal) waviness in the tow direction. This geometry is illustrated schematically in Figure 2.20. Similar techniques were used to determine elastic behaviour of the wavy lamina, both authors using integration in the tow direction to determine effective properties. Although a more rigorous treatment was given to the homogenisation by Dimitrienko, the implementation was significantly more complicated than that of Turner since non-linear matrix behaviour and through-thickness stresses were considered by the former. Turner [87] stated that the effective Young's modulus in the tow direction could be determined using the simple one-dimensional integration in Equation 2.24, evaluating the transformed compliance matrix (which was defined as a function of the out-of-plane angle) at each point along the tow path. Validation was performed both for woven fabrics (with out-of-plane waviness), and for custom-made materials with high levels of in-plane waviness, and reasonable agreement with experimental measurements was observed. It should be noted that the support provided by the interlacing tows was ignored in these models.

$$\frac{1}{E_{x'}} = \frac{1}{\lambda}\int_0^{\lambda} \bar{S}_{11} - \frac{\bar{S}_{16}^{\,2}}{\bar{S}_{66}}\, dx' \tag{2.24}$$

where x' is the tow direction parallel to the lamina midplane, $E_{x'}$ is the Young's modulus in the x' direction, λ is the wavelength of the sinusoidal tow, and $\bar{S}_{ij}$ are terms in the transformed compliance matrix for the off-axis angle at the appropriate position along the x' axis.

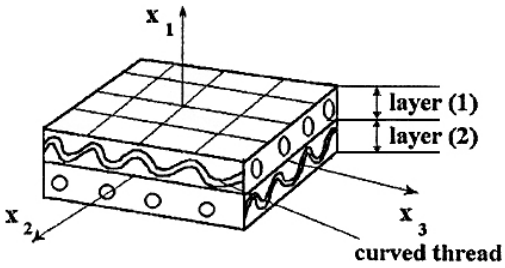

Figure 2.20 Simplified 'wavy laminae' approximation for woven fabric behaviour, after Dimitrienko [94].

Naik and Shembekar [95] developed a model for plain weave composites, extending the existing one-dimensional models of Ishikawa and Chou into two dimensions. Their model allowed different levels of waviness in warp and weft tows, but required that the tow mechanical properties were the same, i.e. manufactured weaves where high tension in the warp tows gives them lower waviness than the weft tows could be modelled, although those with dissimilar materials in the warp and weft tows could not. The tow paths were assumed to follow piecewise curves constructed from straight lines and sinusoids, according to various geometric parameters which were required as input to the model, in a manner similar to that required by Ishikawa and Chou. One-dimensional discretisation was performed in the loading direction according to the 'crimp model' [91] for a number of discrete sections transverse to the loading direction, such that discretisation was performed in two dimensions. Two methods to assemble the resulting discrete sections were proposed: in the series-parallel (SP) model, an isostress assumption was used to assemble the small pieces into sections along the loading direction, and an isostrain assumption was used to assemble these sections across the loading direction; in the parallel-series (PS) model, the small pieces across the loading direction were first assembled using an isostrain assumption then the resulting sections were assembled along the loading direction using an isostress assumption. The geometry used is illustrated in Figure 2.21(a), while the discretisation and assembly for the cell under a load in the x direction using the SP model are considered in Figure 2.21(b) and (c). Using these methods, in-plane elastic constants (Young's and shear moduli and Poisson's ratio) could be determined.

In the same paper [95], Naik and Shembekar compared results of both SP and PS models with experimental data for carbon/epoxy and glass/epoxy plain woven

composites. Three different weave geometries were examined for the glass reinforcement (although experimental results were only presented for two of these). They observed that the models were sensitive to the 'openness' of the weave structure, i.e. the presence of gaps between tows. The SP and PS models gave similar results to one another for the glass/epoxy system, but differed by around 30% for the carbon/epoxy system due to the anisotropic nature of the fibres. They noted that the best all-round agreement between measurement and predictions of Young's modulus in the tow directions was observed for the PS model. These models were limited to loads applied in the tow directions; in a later paper [96], the same authors examined the effects of off-axis loading, but this analysis was limited to the use of stress transformation theory using the on-axis properties, and did not give any new consideration to geometric phenomena. The models by these authors do not consider fabrics with non-orthogonal reinforcements, e.g. braided reinforcements or woven fabrics which have been deformed in shear during forming.

Ganesh and Naik [97] used the method of cells and the Tsai-Wu failure criterion with Naik and Shembekar's earlier models to predict failure in plain weave composites under in-plane shear loads. Damage accumulation was also considered by removing the shear stiffness of subcells where failure was determined to have occurred. Comparisons with experimental data were limited to glass-epoxy systems, but predictions of initial failure were within around 10% of the measured values. More recently, researchers at the same institution [98] investigated the on-axis compressive behaviour of plain weave composites, using analytical techniques for curved beams on an elastic foundation. Load sharing between different subelements of the divided repeating unit was considered, as was the effect of reducing the stiffness of failed subelements by 80%. Failure was determined in this case using the maximum stress criterion. In experimental measurements used to validate their predictions, non-linear behaviour was observed at low strains (ε_c<0.2%) which was not predicted by the model. Predicted compressive stress-strain behaviour exhibited shapes similar to experimental curves, but both stiffness and strength were underestimated.

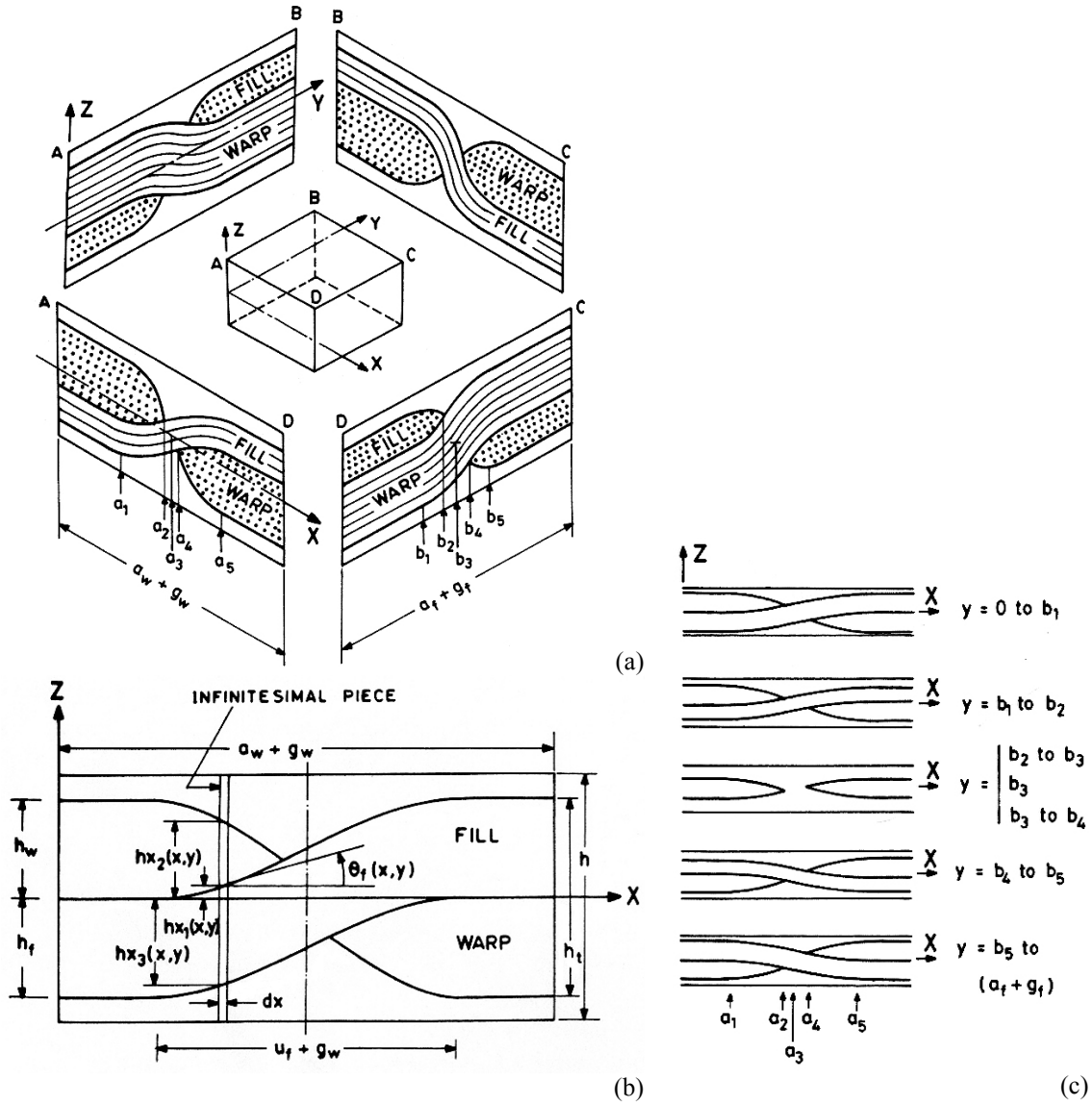

Figure 2.21 The geometric description and discretisation technique used by Naik and Shembekar [95]: (a) the points of subdivision along x and y axes, (b) discretisation along a section in the x direction, (c) sections in the x-z plane at different positions along the y axis.

After proposing a geometric scheme for woven fabrics [99], Vandeurzen et al [100] proceeded to use a discretisation procedure with micromechanics in order to determine homogenised stiffness parameters. They compared their results with both finite element models of the same geometry and experimental data, finding good agreement with FE results and reasonable agreement with experiment. In a later paper, the same authors [101] use a similar homogenisation procedure (bottom-up, i.e. from fibres/matrix up to unit cell level) to determine equivalent elastic behaviour, followed by a reverse process (top-down, from assumed stress on the unit cell down to stresses in fibres/matrix) in order to find the local stresses within the unit cell.

This technique was used subsequently [102] to predict the onset of failure using a modified Tsai-Hill failure criterion, and the effect of damage using a stiffness reduction method for failed microcells. Predicted stress-strain curves appeared to agree closely with experimental measurements on a glass basket weave/epoxy composite in the tow direction, and reasonably for the same material in the bias direction. After a parametric analysis, the authors concluded that the method was sensitive to fabric geometry, and that parameters such as inter-tow gap played a significant role in the predicted behaviour of single-layered fabric structures.

As mentioned in Section 2.4.2, Hofstee et al [82] devised a geometric description for plain weave reinforcements which had undergone in-plane shear deformation during forming. The proposed geometry was relatively simple, based on arcs joined with straight lines, and was able to address (geometrically) the effects of fibre straightening or crimping under tension or compression respectively. Experimental measurements of fabric architecture on a plain weave carbon fibre reinforced thermoplastic were observed to fall within bounds of the geometry predicted using assumptions of maximum stretching or maximum crimp. Hofstee and van Keulen used this geometric formalism in conjunction with a kinematic draping simulation in order to determine the deformed fabric architecture of a draped component to determine local stiffnesses in sheared regions [103]. Closed form analytical expressions were developed such that stiffness was determined for each tow using both isostress and isostrain homogenisation assumptions similar to those used in one-dimensional models discussed previously. However it should be noted that a single tow was considered, and, like the predictions of Dimitrienko [94] and Turner [87], the support afforded by the presence of a crossing tow above or beneath the undulation was neglected. Representative layers for the tows and surrounding matrix were determined, having the properties obtained according to the homogenisation techniques (or those of pure resin where appropriate), and being assigned the principal in-plane tow directions according to the forming-induced shear deformation. Thickness of the layers was calculated such that the appropriate volumes of each tow and the resin were represented. Subsequent analysis of the sheared pseudo-laminate was performed using classical laminate theory. Predicted stiffness envelopes for the sheared materials were presented, indicating the predicted Young's modulus as a function of the angle at which the load is applied. These are

reproduced in Figure 2.22. It should be noted that results obtained using the zero crimp assumption (denoted $E^{\Omega=0}$) are almost the same as those which would be obtained using simple laminate theory giving no account to fibre architecture, with the exception that the fibres are not uniformly distributed (i.e. pure matrix regions exist). Predictions assuming isostrain (E^{ε}) gave Young's moduli almost as high as for zero crimp, while the isostress assumption (E^{σ}) showed significant reductions for the same property. The same authors compared predictions with measurements, both in the tow and bias directions, from specimens with shear deformation present [104]. The predictions offered approximate agreement with experimental measurements, but the differences between the results using different assumptions were small compared with the discrepancies between prediction and experiment. They also observed that the experimentally determined ultimate tensile strength in the tow direction was not significantly or systematically affected by the presence of shear deformation [105].

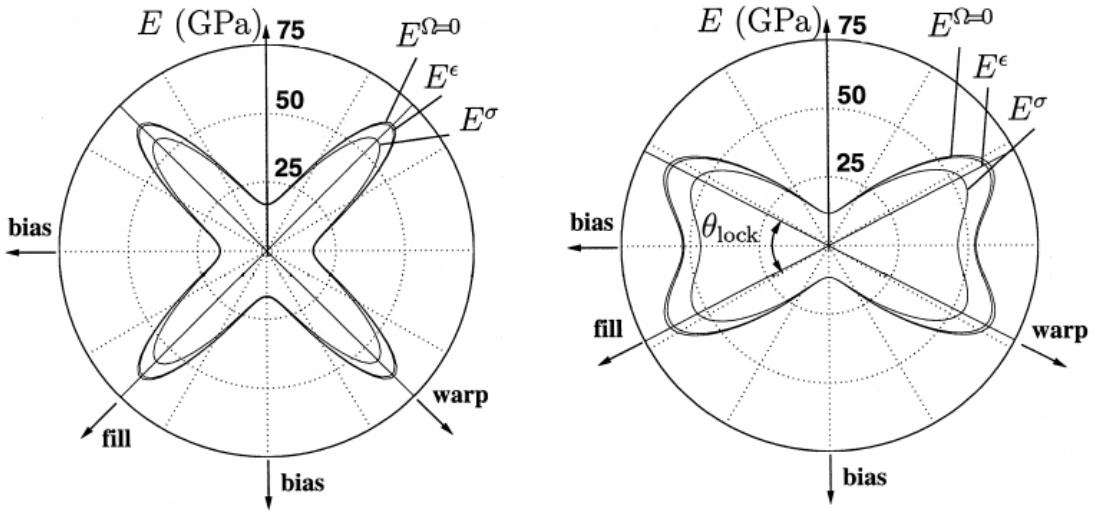

Figure 2.22 Polar plots of stiffness according to the angle of applied loading calculated by Hofstee [103]: (a) an unsheared (±45°) laminate and (b) the same material having been subjected to 35° in-plane shear deformation (i.e. ±27.5°). E^{ε} was calculated assuming constant strain, E^{σ} assuming constant stress, and $E^{\Omega=0}$ was predicted assuming maximum straightening (zero crimp).

While many other authors (e.g. Huang & Ramakrishna [106], Bigaud & Hamelin [107], Tan et al [108], Jiang et al [109]) have produced micromechanics based schemes for homogenisation of woven unit cells, the underlying assumptions of most of such models have been described above. For a broader examination of the background to the published work discussed in this section, the reader is referred to

[110]. In summary, the principal concept of analytical models is to make assumptions regarding the stress or strain field, and use these to develop homogenised elastic properties for the repeating unit cell of the composite. Some of the implementations discussed also describe methods to determine local stresses in the cell under an assumed displacement or loading condition, enabling failure behaviour to be determined. In all cases, a geometric description of the fabric is required; most authors determined their own formalism for fabric structure, although some models could be adapted for other configurations with relative ease. Hofstee was the only author to address sheared fabrics explicitly, although the micromechanics approach of Vandeurzen is understood to be applicable to such materials, according to comments made elsewhere by the same research group [111]. Possibly the limiting factor, other than accuracy of geometric description, in the use of analytical models is the necessity of using an assumed stress or strain field in order to determine behaviour. This requirement is removed by the use of the finite element method, as discussed in the following section, although other problems result. The principal advantage of analytical models is the rapid solution time. For example, results from the simpler models can be calculated almost instantly using a personal computer, while those from the model requiring the most calculations (Vandeurzen [101], 2x2 twill weave) were calculated in three minutes using a Unix workstation in 1998. Using modern computing equipment even these results would be obtained quickly enough to be used for design analysis.

2.4.4 Numerical models for textile composites

As stated in the previous section, the use of analytical models requires assumptions to be made regarding the stress or strain fields in the composite; this is not the case when numerical models, such as those using the finite element (FE) method, are used. In the finite element method, discrete blocks, known as elements, have individual stiffness matrices determined from the elastic properties of the material and the formulation of the element. These elements are defined by their corners, known as nodes, at which they join to other elements. The set of elements representing the structure are assembled together in a mesh, boundary conditions are applied to constrain the model and forces or displacements are applied as appropriate. An FE software package is used to solve equations of equilibrium for

each element in the whole model simultaneously, on the basis that resultant forces must be zero at the nodes. This enables the response of a complete, discretised, structure to be analysed as a function of externally applied loads or displacements. An explanation of finite element formulation is beyond the scope of this thesis, but it is well documented elsewhere, e.g. in [112].

Many authors have used the finite element method to determine the mechanical behaviour of representative unit cells of textile composites. Provided that a geometric description of the material is available, a mesh can be generated containing elements describing the tow and resin regions. If the appropriate mechanical properties are assigned to each element, and material orientation is specified for the orthotropic elements making up the tow, then behaviour of the unit cell can be determined, which is assumed to be representative of the material.

Some of the earliest examples of application of the finite element method to mechanical evaluation of textile composite behaviour were conducted by Woo and Whitcomb, first in two dimensions [113] and subsequently extended to three dimensions [114]. They used macroelements (Figure 2.23a), which were subdivided into smaller domains to calculate the stiffness matrix; a mesh of several macroelements was used to represent the whole structure and nodal displacements were calculated. The nodal displacements were subsequently used as the boundary conditions for a refined submodel of the unit cell constructed from conventional finite elements (Figure 2.23b), used to determine the local stress/strain behaviour. Although savings in computational effort were significant, discrepancies at the boundaries of the global/local domain were observed, requiring further investigation.

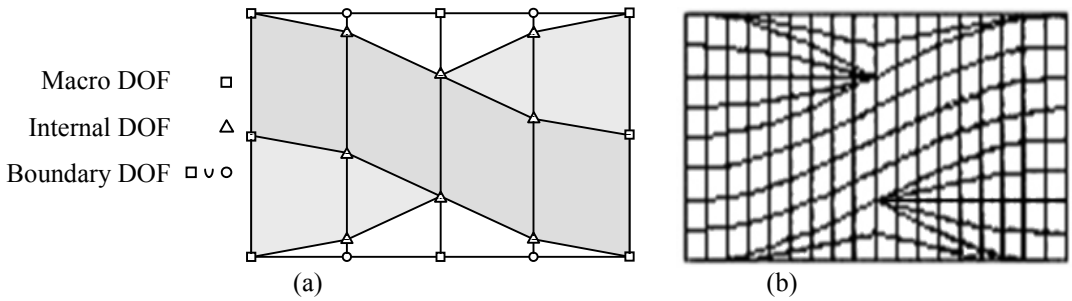

Figure 2.23 A typical submesh for (a) a macroelement, comprised of one undulating axial tow and two half cross sections of transverse tows, and showing internal and global degrees of freedom and (b) conducting a local (refined) analysis with conventional finite elements. After Woo and Whitcomb [113].

Using conventional finite elements and assuming a sinusoidal tow path, Chapman and Whitcomb [115] studied the stress distributions within the unit cells of plain weave composites. In the interests of computational efficiency, they exploited the symmetry of the plain weave unit cell, analysing a $^1/_{32}$ section of the geometry under the appropriate periodic boundary conditions. A rigorous convergence study was conducted to determine the number of elements necessary to obtain accurate results, using two different methods of specifying the material orientation within the tow. In the first method, a single orientation was specified for each element within the tow and used for calculation; in the second method, an interpolation scheme was used between adjacent tow elements to determine orientation at each calculation (integration) point. For the 20-noded isoparametric brick elements which they used, there were 27 integration points, hence each element contained 27 material orientations. Convergence of force/displacement behaviour was observed using just 32 elements with multiple orientation, but required 192 elements with single orientation. It is interesting to note that they did not observe complete convergence of stress results even with 400 elements with multiple orientations. Some of the meshes used for this convergence study are shown in Figure 2.24. The authors used their analysis technique to determine equivalent elastic properties for the cells, examining the effect of changing waviness. They observed that the most significant effects of waviness were on Poisson's ratio, ν_{xy}, which increased from 0.018 to 0.151, and on Young's modulus, E_x, which fell from 68 GPa to 26 GPa as the waviness ratio (defined as cell thickness divided by sinusoid wavelength) increased from $^1/_{20}$ to $^1/_3$. Although failure indices were calculated using a modified Tsai-Hill criterion, predictions of failure stress were not presented explicitly.

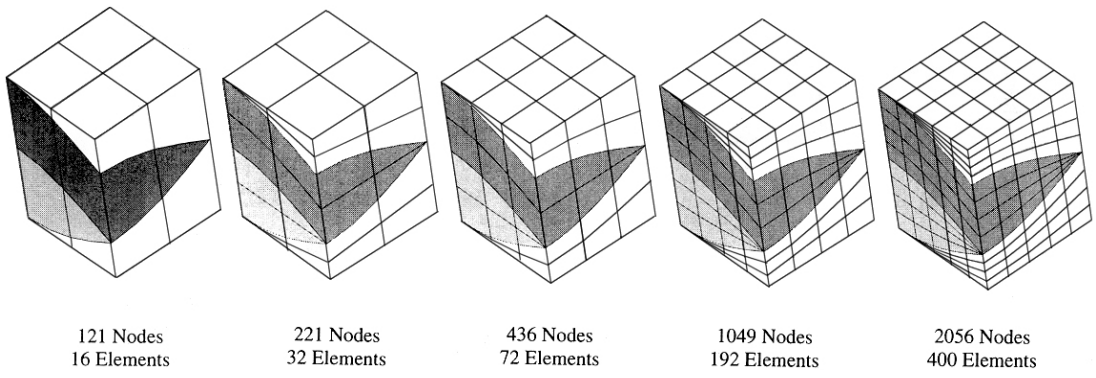

Figure 2.24 Finite element meshes used for a convergence study for a $^1/_{32}$ of a plain weave composite unit cell. After Chapman and Whitcomb [115].

A number of research groups have used conventional 3D finite element analysis to examine elastic and failure behaviour of repeating unit cells. Glaessgen et al [88] described a method to implement the unit cell FE technique using the I-DEAS geometric/FE modelling software to build solid meshes. They presented a model for a plain weave composite, but the method was general to woven textile forms. Results were limited to this single illustrative example, and comparisons with other models or experimental data were not made.

Parametric studies using FE analysis were conducted using the Abaqus FE package by Feng et al [116]. They found that increasing the waviness ratio (defined as the tow height divided by the length of the undulating tow region) from zero (no crimp) to 0.3 could reduce failure strength in the tow direction by 50%, and concluded that this result indicated that tow waviness should be carefully controlled in the manufacturing process. The same authors also examined the effect of the presence of a small gap between the yarns, concluding that this had little significance.

Tan et al [108] found good agreement between experimentally determined elastic constants and those found using FE analysis for a carbon/epoxy plain weave composite. Only one unit cell geometry was analysed using finite elements, and FE analysis was not used to determine failure behaviour.

The work of Carvelli and Poggi [117,118] differed from that discussed so far within this section, since measured or assumed values for the mechanical properties of the tow were not used. They employed a two-scale homogenisation procedure, where 3D FE analysis was conducted at the fibre/matrix scale to determine homogenised properties of the tow for subsequent analysis of a woven fabric unit cell. A simple damage model was incorporated by reducing stiffness terms for elements which exceeded their failure stress. Limited validation studies were presented but the predicted stress-strain curve presented in [118] seemed only to agree with experimental data in the elastic region, while predicted stress-strain behaviour presented in [117] showed very limited agreement with experiment. A single geometry was analysed, and no comment was made regarding geometric model generation.

Similar homogenisation studies have been undertaken by other authors, e.g. D'Amato [119], Rupnowski and Kumosa [120] and Ivanov et al [121]. The latter is noteworthy since the unit cell of a plain weave composite having been subjected to shear deformation during forming was analysed. One of the difficulties which the authors reported was the generation of meshes with matched opposite faces for the application of periodic boundary conditions. This appeared to impede the meshing process and restrict the level of mesh refinement which was readily available. The outer edges of the mesh which they used are shown in Figure 2.25.

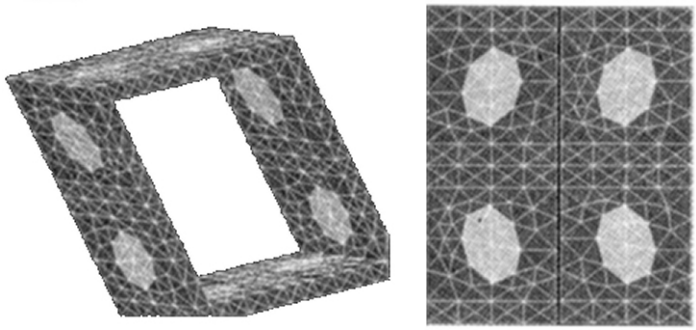

Figure 2.25 The outer boundaries of a 3D finite element mesh of a sheared plain weave composite unit cell with matching opposite faces for the application of symmetric boundary conditions. After Ivanov et al [121].

One of the overriding themes in the work to date on 3D FE analysis of repeating unit cells is that accurate mesh generation (i.e. providing a good geometric description of the structure with sufficient elements to obtain good accuracy) coupled with the need to keep the mathematical problem size within the limits of practical computation is one of the limiting problems in the field. The use of the adaptive meshing technique, where elements containing high gradients of solution variables (i.e. stress and strain) are subdivided until the behaviour is captured with sufficient accuracy, may offer a means to overcome such problems, and has become more common in commercial FE packages in recent years. Alternative methods are also being developed, such as the 'voxel' method suggested by Kim and Swan [122]. This technique, borrowed from the field of image processing (the name meaning a 3D pixel), offers an automated method to produce locally-refined meshes which describe complex 3D geometries accurately. It is essentially designed to refine hexahedral elements around a tow/matrix interface by subdivision such that, as the number of elements tends to infinity, the tow volume fraction (i.e. the volume of tow in the element divided by the volume of matrix in the same) tends to discrete values of 0 and 1. In practice,

some criterion is specified to limit the number refinement levels and, in one variation of the technique, to limit the number of refinement 'generations' between adjacent elements. An example of voxel refinement is shown in cross section in Figure 2.26.

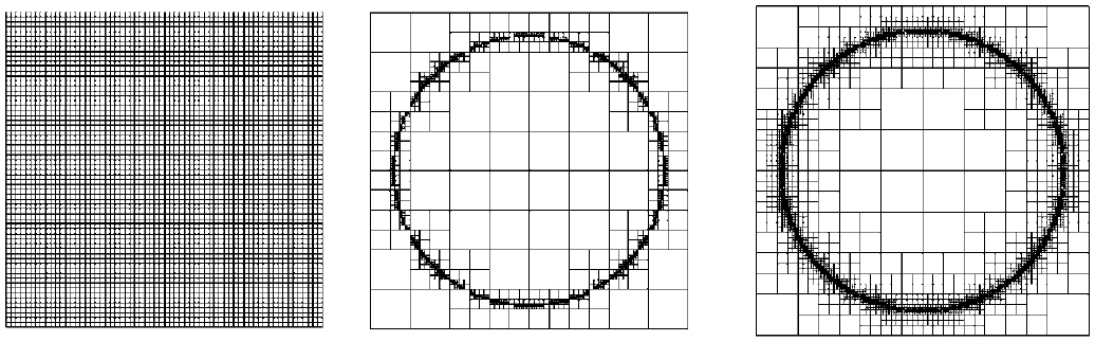

(a) (b) (c)

Figure 2.26 Voxel mesh refinement (a) uniform refinement, (b) selective refinement (refinement to improve definition of edge) and (c) constrained selective refinement (refinement to improve definition of edge but allow only one refinement 'generation' between adjacent elements). After Kim and Swan [122].

Since new nodes are formed on existing element boundaries, the use of kinematic constraints is required to maintain continuity of the displacement field. An example of this is shown in Figure 2.27. The authors do not discuss the effect of this phenomenon on stress/strain results, although they do suggest the use of the voxel technique for geometric refinement in conjunction with the adaptive meshing technique for refinement for the purpose of solution convergence.

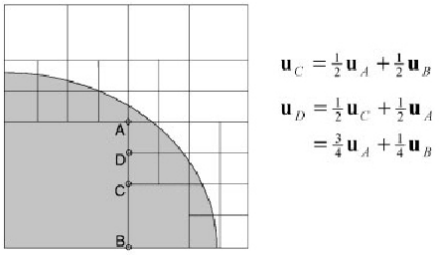

(a) (b)

Figure 2.27 Schematic showing the need for nodal enslavement to enforce displacement continuity in selectively refined voxel or pixel meshes: (a) hierarchical mesh with enslaved nodes; and (b) dependencies among master and slave nodes (where **u** is a displacement vector). After Kim and Swan [122].

Using the Pro/Engineer commercial 3D computer aided design (CAD) package to construct geometric models of unit cells, Hu et al [123,124] addressed some of the issues associated with meshing the complex volumes in a unit cell by using p-type high order finite elements within the structural analysis module of the same software

(Pro/Mechanica). Using this formulation, meshes which would normally be considered of 'poor quality' (i.e. coarse meshes of elements with high aspect ratios) can be expected to give good results due to the use of a high order polynomial interpolation function to calculate solution variables. A typical mesh for a plain weave composite is shown in Figure 2.28. Analysis results were published purely for illustration of the capabilities of the technique, and no parametric investigation or comparison with other models or experiment was undertaken.

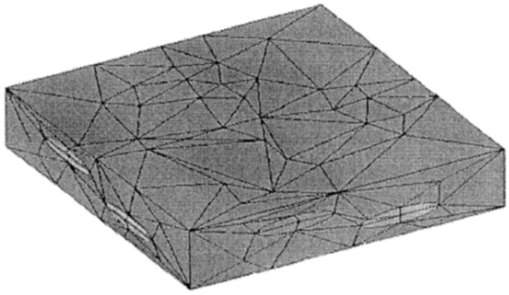

Figure 2.28 A unit cell mesh of a plain weave composite for use with p-type finite elements. After Hu et al [123].

The use of meshes where the tow/matrix interface is joined using junction elements instead of the traditional requirement of mesh continuity (where nodes are shared between elements either side of the interface to form a continuum) was suggested by Durville [125]. The approach was applied to bundles of aramid fibres reinforcing a rubber matrix, but results were not validated. No comment was made on the effect of this method on results of stress and strain calculations.

The problem of generation of complex meshes was circumvented by the method proposed by Cox et al [126,127]. This method, known as the binary model, used 1D line elements to represent the tow axial stiffness, fixed within 3D elements using multi-point constraints. The 3D elements represented what the authors termed the 'effective medium', providing the matrix-dominated mechanical properties (transverse stiffness, Poisson's ratio etc.). The line elements were used to form a piecewise linear approximation to the curved tow paths. Although this method could produce results of elastic behaviour with relatively little computational effort, prediction of failure behaviour remains unproven. However, more recently Yang and Cox [128] presented a strain averaging technique for use with the binary model, which appeared to offer reasonable agreement with full-field strain measurements

taken from a 3D woven C/SiC composite under tension in the weft direction. They suggested that this method would provide a route for strength prediction, although predictions of strength were not made. A typical mesh used for this technique is shown in Figure 2.29.

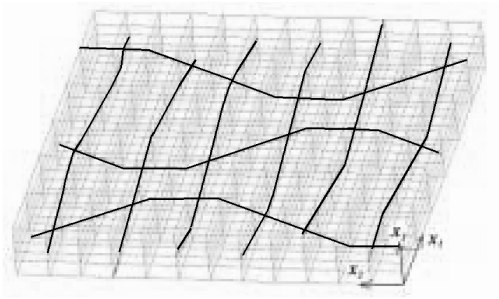

Figure 2.29 A unit cell mesh of a woven composite using the binary model. After Cox et al [128].

Mesh generation can also be simplified by examining behaviour of a single cross section through the composite thickness. This technique has been used recently by Le Page et al [129], who used generalised plane strain elements, which are defined in two dimensions and formulated such that strain in the third dimension is constant (but not necessarily zero) for the whole model. As stated by the authors, this may be a simplification of the true strain field in a woven composite, but the technique offers easy mesh generation and fast solution times. It was used in this case to evaluate effects of laminate stacking geometry and hence will be discussed in Section 2.4.5. A typical mesh for use with this technique is illustrated in Figure 2.30.

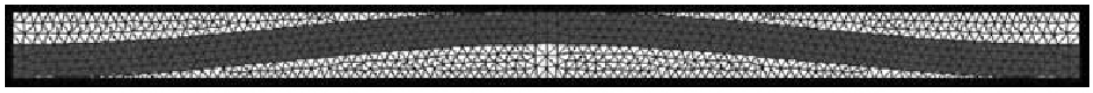

Figure 2.30 A mesh of a section through a woven composite for use with generalised plane strain finite elements. Dark regions represent longitudinal tows; lighter regions represent transverse tows. After Le Page et al [129].

2.4.5 Models for stacked textile composite laminates

Although many methods have been discussed in the preceding sections for the analysis of single layers of textile composites, it is important to consider the behaviour of a layer within a multilayered structure, as encountered in real components. The effects associated with this include the manufacture of symmetric laminates, i.e. those which are symmetric about the midplane, and the constraint

imposed when the upper and lower surfaces of a material layer within the laminate are not free to deform due to the presence of other material layers above and below. In this section published studies of these effects are reviewed.

Ishikawa and Chou [91] noted that under an applied in-plane load, a single layer of woven fabric reinforced composite would exhibit local curvatures due to its non-symmetric nature. In their modelling, they proposed two limiting assumptions to determine the material behaviour. The initial assumption was that the resultant bending moment must be zero, i.e. that bending was permitted; the alternative was to prevent bending by constraining curvature to be zero at all points in the laminate. The former gave lower bounds for stiffness prediction, while the latter gave upper bounds. A significant difference between these bounds was observed and, when making comparisons with experimental data [93], the authors found that test results in the tow directions of plain weave composites manufactured with a single layer of reinforcement ($E \approx 48$ GPa) fell slightly closer to the lower bound than to the upper, while those with 8 or 20 layers of reinforcement ($E \approx 60$ GPa) fell closer to the upper bound. The authors suggested that this was due to the constraint imposed on curvature by the presence of extra layers.

This was in agreement with the conclusions of Whitcomb et al [92], who later conducted numerical studies of these effects using finite element analysis. In the case of a multilayered laminate, the upper bound approximation is more appropriate, and is exactly true for perfectly symmetric laminates. They found that stiffness increased with the number of layers analysed, and that when 8 or more layers were considered, the results tended to the upper bound approximation obtained by the application of periodic boundary conditions (suitable for an infinite number of layers).

Feng et al [116] used FE analysis of the unit cell to evaluate the effect of boundary conditions applied to a single layer of plain weave composites on their failure behaviour. Their approach was used to determine the effects of constraint at the surfaces to enforce geometric compatibility, and shift between layers was not considered. They concluded that, although stress in the tows was almost unchanged, the principal stress in pure resin regions near the surfaces of a single layer increased

by around 30% when no constraint was applied, compared with the value obtained when displacement at the surfaces in the through-thickness direction was constrained to be zero (i.e. plane strain conditions). Much smaller differences in stress were observed in the tow regions.

Shembekar and Naik [130] extended their studies of woven fabric behaviour to examine the effects of applying in-plane phase shifts to the laminae when building a laminate, such that the tow centrelines in adjacent layers moved out of phase with one another. Some of the configurations analysed are illustrated in Figure 2.31. They observed almost no difference between results of their models (both parallel-series and series-parallel approaches) for the different configurations analysed, except in one case, where a small change in the Poisson's ratio was observed. They also noted in another paper [131] that in the presence of shift between layers, the in-plane elastic constants converged to a constant value when eight or more layers were considered. This can be understood intuitively since as more layers are added with in-plane shifts the degree of asymmetry about the midplane reduces.

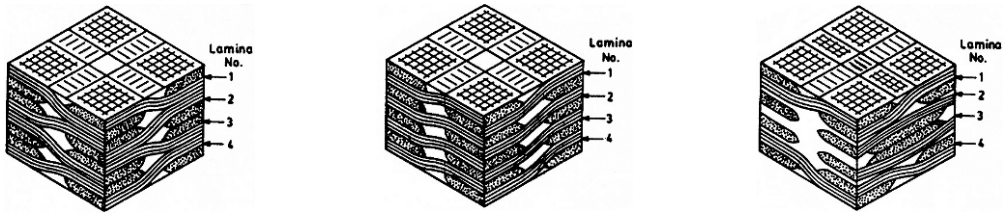

Figure 2.31 Plain weave composite unit cells exhibiting different shifts between the layers. After Shembekar and Naik [130].

Numerical studies of this phenomenon were conducted by Kurashiki et al [132], who evaluated stress-strain response considering damage development using finite element analysis for plain weave composites with and without phase shifts between the layers. They concluded that the onset of damage occurred earlier in laminates with zero phase shift due to the local bending stresses which were present, but that the change in Young's modulus due to shift was small. This and the findings of Shembekar and Naik [130] were in contrast to those of Woo and Whitcomb [133], who reported an increase in Young's modulus from 23 GPa to 29 GPa as the phase shift between two layers increased from zero to $\lambda/2$ (where λ is the wavelength of the

sinusoidal tow path) according to results from their finite element model (using macroelements).

Using generalised plane strain finite element analysis of cross sections of woven composites, Le Page et al [129] also investigated the effects of phase shifts between layers. They too found that the difference between Young's moduli of symmetric and anti-symmetric two-layered woven laminates was only around 4%, although they observed more significant differences in the energy release rate due to cracking, which was the focus of the work.

In summary, although stacked laminates may exhibit different mechanical behaviour from that of a single layer of woven fabric composite due to the change in asymmetry about the laminate midplane and the resultant constraints on local curvature, the differences in elastic behaviour are generally expected to be small. Similarly, studies where the effect of incorporating in-plane phase shifts between adjacent layers, such that the tow paths are not in phase, have shown little effect on elastic behaviour. Larger differences in damage and failure behaviours may be expected, particularly in matrix cracking, although the presence of in-plane phase shifts between layers in multilayered laminates appears to become less significant as the number of layers increases.

2.5 Manufacturing process simulation

When considering the structural behaviour of textile composite components it is necessary to consider the reinforcement orientation. While it may be reasonable to assume that fibres remain orthogonal in components which are nearly flat, for those parts which have been manufactured by forming the reinforcement into a doubly-curved three-dimensional shape it is important to know the orientations of the fibres in the manufactured configuration. Various studies of reinforcement deformation during forming have been undertaken, and published work in the field is discussed in this section.

Studies of the forming behaviour of dry textile reinforcements (draping) have been undertaken by a number of authors. Most common is the 'pin-jointed net' or 'fisherman's net' approach, in which fibres are considered to be straight (between joints) and inextensible, and crossover points between tows are assumed to act as pinned joints, permitting 'trellis-like' shear but not permitting fibre slip. Fabric deformation modes are shown in Figure 2.32. Such algorithms have been applied to composites forming since the 1980s, when Robertson et al [134] determined the position of tow crossovers by calculating the intersection of the arcs which describe the possible endpoints of the tows on the surface to be covered. This is illustrated schematically in Figure 2.33.

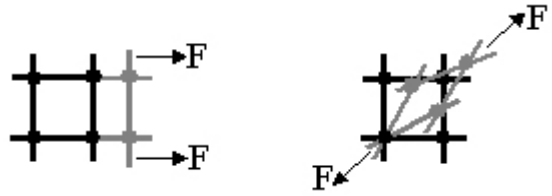

Figure 2.32 Significant modes of fabric deformation during forming. (a) Fibre slip; (b) Shear deformation (trellis-like shear). Reproduced from [19]

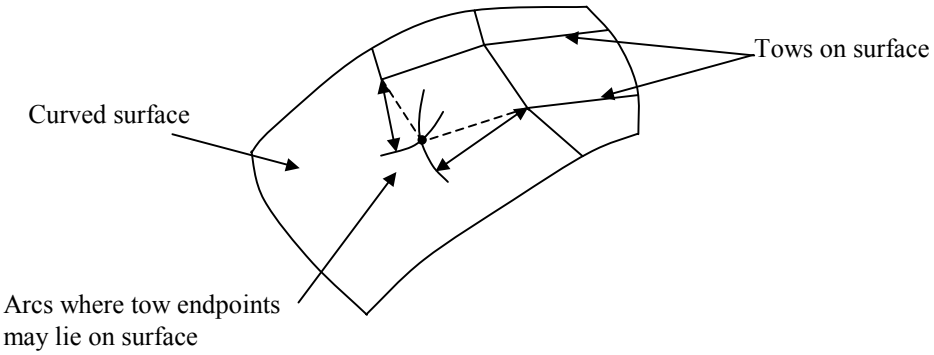

Figure 2.33 Determination of tow positions on a curved surface using a pin-jointed net algorithm.

This type of forming simulation has been developed by a number of authors, and is implemented in various commercial composite design packages, including FiberSIM (produced by Vistagy) and Laminate Modeller (produced by MSC software). The assumption that in-plane shear is the only significant mode of deformation was validated for three non-crimp fabric reinforcements by Long [135], who found that fibre slip was less than 10% in the tests which he conducted. He did note, however, that this assumption may not be valid if the biaxial forces applied to the material

during forming are not of approximately equal magnitude. Pin-jointed net forming simulations are purely geometric, and rely on the definition of initial fibre paths to define the rest of the geometry. As such, they are not suitable for reinforcements which exhibit a preferential shearing direction, i.e. which have a higher shear compliance in one direction than the other (often the case for non-crimp fabrics). This issue was addressed by Souter [19], who measured the shear compliance of reinforcements in both directions, and incorporated this data into a pin-jointed net simulation with an energy minimisation algorithm. Predictions of non-crimp fabric deformation made using this approach were found to be in good agreement with experimental measurements.

Finite element simulations were also used by a number of authors (e.g. Boisse [136]) to predict the forming behaviour of reinforcements due to the flexibility and generality of the method. The main drawbacks of this approach are the computational cost, since simulations typically take hours compared with seconds for kinematic solutions, and the degree of materials characterisation required. Potluri [137] addressed the latter issue, proposing robotic test methods for fabric behaviour in order to improve repeatability and confidence in the results; this does not, however, remove the need to have fabric and equipment available for testing. Finite element simulations are also in common use to simulate the forming of reinforcements in a viscous matrix, i.e. prepregs or thermoplastic composites [138-140]. For further investigation of the field of composites forming, a comprehensive review has been published by Lim and Ramakrishna [141].

2.6 Structural analysis of component-scale geometry

Although much work has been published on reinforcement forming, and on the mechanical properties of textile composites, relatively little consideration has been given to the impact of the former on the latter. Rudd et al [142] manufactured a composite wheel hub from non-crimp fabric (NCF) reinforcement using resin transfer moulding. They observed that, under a diametric pinch loading, elastic response of the component changed at different positions around the geometry, concluding that this could be attributed to the effects of fibre reorientation and local

increases in fibre volume fraction due to shearing of the reinforcement. Smith et al [143] later manufactured and tested flat specimens from both woven and NCF reinforcement which had been subjected to uniform in-plane shear deformation, and concluded that classical laminate theory could be used to give a reasonable estimate of elastic behaviour for such materials if they were assumed to consist of two layers of unidirectional materials, having the same principal orientations as the fibres in the sheared reinforcements. No simulation of component behaviour was presented.

Analysis of a protective toe cap manufactured from thermoformed satin weave glass-fibre/thermoplastic polyurethane material was presented by Kuhn et al [144]. The authors stated that fibre orientation and local thickness data were exported from a forming simulation (PAMStamp) into a structural analysis package (Ansys). No description of the material models used was provided, and the results presented focussed on the design optimisation of the component lay-up. No validation with experimental data was presented.

Studies of filament wound structures were conducted by Jones [145], who developed a link to export fibre orientation data from a process simulation such that it could be used in subsequent FE analysis of the structure using layered shell elements. While suitable for the application, the implementation was intended only for the filament winding process, and considered only elastic behaviour. More recent studies of long-term mechanical behaviour of components manufactured using the same process were conducted by Richard and Perreux [146], who concluded that an accurate knowledge of the winding angle was the single most important factor when conducting structural analysis.

Using his geometric draping software [147] to provide information on fibre orientation and deformation, Bergsma [148] suggested the use of Naik's model [95] to obtain effective elastic properties for layers of material used to represent sheared woven fabrics. He also stated that this method could be used in conjunction with an FE package for component analysis. No validation with experimental measurements of coupons or components was performed, and failure behaviour was not considered.

More recently, studies have been undertaken on the mechanical performance of components at the University of Leuven by van den Broucke et al [111]. Using a kinematic draping algorithm, fibre orientations were predicted for three component geometries (a large and a small hemisphere and a motorcycle mudguard). Calculations of local stiffnesses were performed using the TexComp micromechanics-based model [100,79], accounting for fibre reorientation and the resulting change in fibre volume fraction. These stiffnesses were subsequently used to define the properties of shell elements in the commercially available SysPly FE package, which was used to predict the elastic response of the components. Although good agreement with experimental load-displacement curves was observed for the small hemispherical geometry, stiffness of the mudguard and the large hemisphere were underestimated by around 25%. Similarly, locally measured and predicted strains were compared at different positions on the components; reasonable agreement was observed for the hemispherical geometries but significant differences (predicted ~0.25% vs. measured ~0.05%) were found for the mudguard. In some cases, classical laminate theory predictions for element stiffnesses accounting for fibre reorientation gave improved agreement compared with the TexComp model. Distortions due to resin shrinkage were not considered in the analyses, which may offer a possible explanation for the observation of good agreement only in axisymmetric components. (Lamers [149] showed that process-induced distortions in non-axisymmetric components were significantly larger than those in a hemisphere.) Component failure was not considered in van den Broucke's study.

In addition to the studies discussed above, a number of commercial analysis codes are available to predict the structural performance of composite components. Many general-purpose FE codes have the ability to model layered shell structures, but it is necessary to prepare the appropriate data to determine mechanical properties and orientations for each element. A package such as FiberSIM (produced by Vistagy) can be used to export ply orientation data for use with general-purpose FE packages, but this does not incorporate material models, instead relying on user input for mechanical properties of the plies. Other packages for analysis of composite structures, namely SysPly (ESI group), ESAComp (produced by Componeering Inc. in conjunction with the European Space Agency), Lusas Composite (Finite Element Analysis Ltd.) and Composite Star (MATERIAL) are aimed at analysis of laminates

made from unidirectional plies, and do not incorporate models for draping or for mechanical properties of bi-directional reinforcements. In the 2003 release of their Laminate Modeller package, MSC software incorporated the ability to model changing properties as a function of the shear deformation in the reinforcement, but their implementation required the user to enter mechanical data into a look-up table for discrete ranges of shear angle; no predictive capability was incorporated.

2.7 Conclusions

Published work in the field of composite mechanical properties prediction has been reviewed. The unidirectional reinforced composite has been identified as the basic building block for composite properties. Various micromechanical methods to determine the elastic behaviour of unidirectional composites have been discussed, in addition to those for failure under a uniaxial load. The field of failure under complex biaxial loads has been noted as an area of significant ongoing research and some of the most prominent theories have been discussed. Conclusions arising from the world-wide failure exercise (WWFE) have been summarised.

Published methods to determine the mechanical behaviour of both laminates comprising layers of unidirectional material and woven fabric laminates have been discussed in some detail. It has been noted that most models for woven fabric behaviour are not directly applicable to fabrics which have undergone shear deformation during the manufacturing process. It was also observed that most woven fabric models are limited to a single weave style (e.g. plain weave), or to the assumption that tow undulations follow a sinusoidal path. Analytical models for woven fabric behaviour have been observed to depend upon assumptions of constant stress or strain over certain regions of the unit cell; this can be overcome with the use of numerical (finite element) models at the expense of computational time and increased complexity in model generation.

Although the mechanisms of forming itself are not of direct concern for the purposes of the work in this thesis, some means is required to characterise the fibre orientations after forming reliably and quickly for input into mechanical models.

Various techniques are available, falling into two basic categories: kinematic models and finite element simulations. Published studies in this field have been reviewed briefly.

It has been noted that various published studies exist concerning the effects of reinforcement deformation on composite mechanical properties, but that none of the published studies has presented an integrated approach to analysis of composite components up to the point of failure with validation from experimental measurements. A number of commercial packages for analysis of composite components have also been reviewed, but these are either intended for components manufactured from layers of unidirectional reinforcement, or lack material models to describe changes in local material properties due to forming where bi-directional reinforcements are considered.

This review highlights the need for a purely predictive modelling approach by which component behaviour may be understood from a knowledge of the mechanical properties of the fibre and matrix materials, and the architecture of the reinforcement textile. Potential ways to achieve this are suggested in Chapter 5 of this thesis, where comparisons with experimental measurements presented in Chapter 4 are made for the purpose of validation. The materials and the manufacturing techniques used for the experimental studies presented are described in Chapter 3

3 EXPERIMENTAL TECHNIQUES

3.1 Introduction

Experimental work has been undertaken to develop an understanding of the role of reinforcement deformation on the mechanical behaviour of the resultant composite. This chapter describes the techniques employed to produce laminates with a uniform level of in-plane shear in the fabric reinforcement, in order to verify quantitatively and in isolation the effect on stiffness and strength of this mode of deformation. Unidirectional laminates were also manufactured at a range of fibre volume fractions in order to provide material comparable with the multidirectional laminates suitable for determination of the lamina properties, to enable validation of micromechanics models. The procedures carried out to manufacture a three-dimensional component, used to determine the effects of reinforcement draping on mechanical performance at the part level, and also to validate predictions from the models presented later in this thesis, are also described. Mechanical test methods and characterisation techniques used to measure such effects are also presented, in addition to a description of the equipment and materials used throughout the experimental programme.

3.2 Materials used

3.2.1 Reinforcement materials

Throughout this work, E-glass fibre reinforcement materials have been used to produce specimens and components. The reinforcements used are summarised below, and photographs of the reinforcements are shown in Figure 3.2. Geometric parameters associated with the textile reinforcements are reported in Table 3.1, while the properties of E-glass fibres are detailed in Table 3.2.

Saint-Gobain BTI EBX hd 936: A ±45° tricot-stitched non-crimp fabric manufactured from 600 tex glass fibre tows, having a superficial density of 936 gm^{-2}.

Formax FGE-106: A ±45° tricot-stitched non-crimp fabric manufactured from 600 tex glass fibre tows, having a superficial density of 936 gm^{-2}. This reinforcement

was very similar to EBX hd 936, although the stitching geometry was slightly different; details can be found in Table 3.1.

Formax UD-468: A custom-manufactured stitched unidirectional material manufactured in the same manner as FGE-106 but having only one set of tows, hence forming a unidirectional +45° tricot-stitched reinforcement. The nominal superficial density of this material was approximately 468 gm^{-2}, although this was very sensitive to deformation during handling.

Saint-Gobain Vetrotex RT600: A plain weave textile reinforcement made from 1200 tex glass fibre tows, having a superficial density of 600 gm^{-2}.

Saint-Gobain Vetrotex Unifilo U101-220: Continuous filament random mat manufactured from 25 tex strands laid in swirls, held together using approximately 4.5% powdered thermoplastic polyester binder. The nominal superficial density of this reinforcement is 220 gm^{-2}, although the random nature of the structure is such that local variations are present.

Table 3.1 Approximate measured geometric parameters of textile reinforcements used.

Parameter	EBX hd 936	FGE-106	UD-468	RT600
Tow linear density, ρ_t (tex)	600	600	600	1200
Tow width, w_t (mm)	1.5	1.5	1.5	3.0
Tow height, h_t (mm)	0.5	0.5	0.5	0.25
Tow spacing (pitch), s_t (mm)	1.5	1.5	1.5	4.0
Stitch length, l_s (mm)[a]	2.0	2.5	2.5	-
Stitch spacing (pitch), s_s (mm)[a]	4.2	4.2	4.2	-

[a] Parameters defined in Figure 3.1

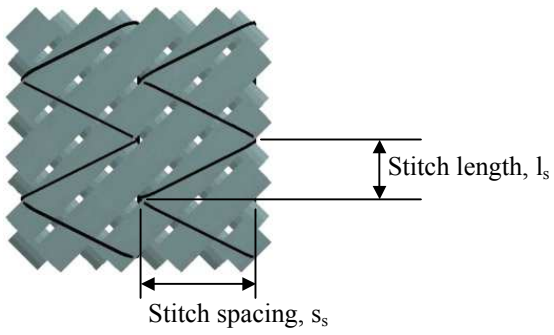

Figure 3.1 Definition of geometric parameters of the stitching in non-crimp fabrics.

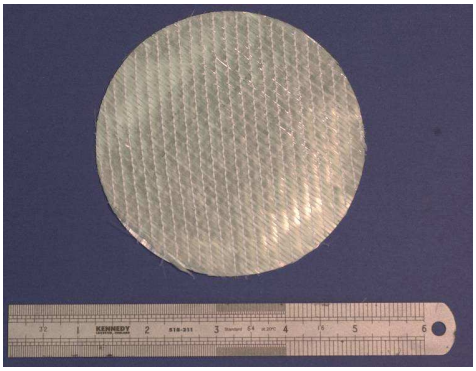

(a) EBX hd 936 (front)

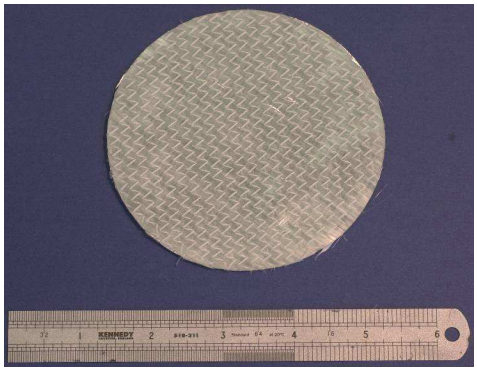

(b) EBX hd 936 (back)

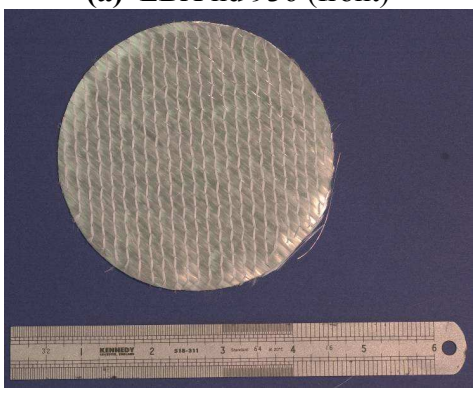

(c) FGE-106 (front)

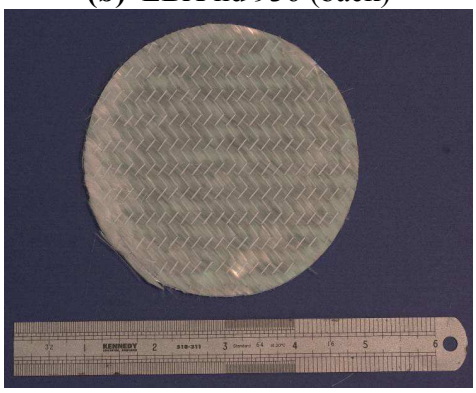

(d) FGE-106 (back)

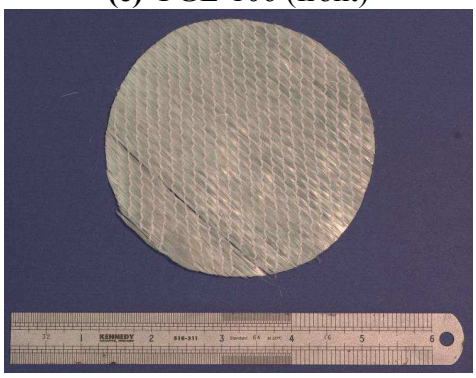

(e) UD-468 (front)

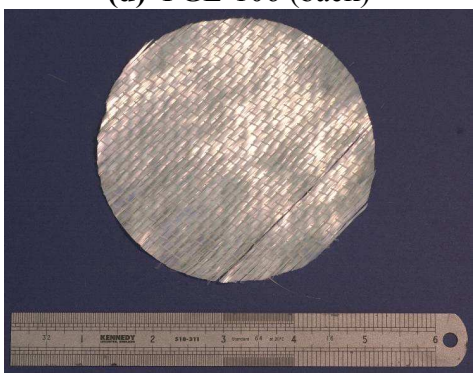

(f) UD-468 (back)

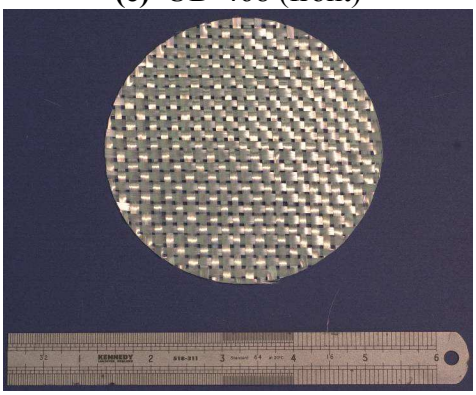

(g) RT600

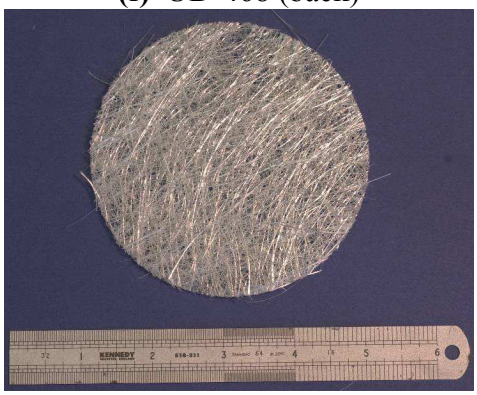

(h) Unifilo U101-220

Figure 3.2 Photographs of all reinforcements used in the course of this thesis

3.2.2 Thermosetting resins

Two unsaturated polyester thermosetting resins have been used throughout this work. Polyester resins were used due to their low cost, frequent application in industry (particularly automotive) and relative ease of processing (i.e. no heating of the resin was required to assist flow or to initiate the curing reaction). Reichhold Norpol 440-M750 resin is a pre-accelerated system, while Reichhold Norpol 420-100 was accelerated using Akzo-Nobel NL49P 1% cobalt accelerator. In each case the curing process was initiated using Butanox M50 catalyst. Norpol 440-M750 resin was used for initial experimental work, although the 420-100 system was found to have improved processing characteristics and was used for later work. The mechanical and physical properties of these resins, as provided by the manufacturer, are presented in Table 3.2.

Table 3.2 Mechanical and physical properties of resins used (manufacturer's data in fully cured state) and of E-glass fibre (after [150])

Parameter	440-M750	420-100	E-glass
Young's modulus, E (GPa)	4.6	3.7	73
Ultimate tensile strength, σ_u (MPa)	50	70	2000
Poisson's ratio, ν	0.25	0.26	0.22
Density, ρ (kg m^{-3})	1100	1100	2620

3.2.3 Ancillary materials

DSM Neoxil 940: This powdered thermoplastic polyester binder was applied by hand to improve the handling characteristics of preforms manufactured from sheared fabric reinforcement.

Chemlease PMR-90: This mould release agent, containing trimethylbenzene, was applied with a cloth to the tool faces for all mouldings produced to facilitate removal of the cured part from the aluminium mould.

Reichhold Norpol 320-3200: This thermosetting polyester resin was used to mount specimens of material to facilitate polishing and subsequent optical microscopy. Approximately 0.5% NL49P cobalt accelerator and 1.5% M50 catalyst were used to initiate the curing process. When cured this resin is transparent.

3.3 Manufacturing techniques

This section describes the manufacturing techniques used to produce specimens and components for mechanical testing. For the parts presented in this thesis, resin transfer moulding (RTM) has been used exclusively. In this process, liquid resin is mixed with a catalyst to initiate cross-linking, and is immediately injected into a closed mould under pressure before the reaction is complete, and hence while the resin is still liquid. Solidification occurs inside the mould which, in the case of the polyester resins used in this thesis, minimises toxic styrene emissions.

3.3.1 Introduction of in-plane shear deformation into textile reinforcements

To investigate the effect of in-plane shear deformation in the reinforcement on the mechanical properties of the resultant composite, a number of plaques were manufactured from textile reinforcements which had been subjected to uniform shear deformation. Angle-ply laminates were produced at a range of ply angles. Ply angle is defined in Figure 3.3, and is related to the angle through which the reinforcement is sheared according to Equation 3.1.

$$\phi = \pm \frac{90° - \theta}{2} \tag{3.1}$$

where ϕ is the ply angle and θ is the angle through which the reinforcement is sheared (the shear angle).

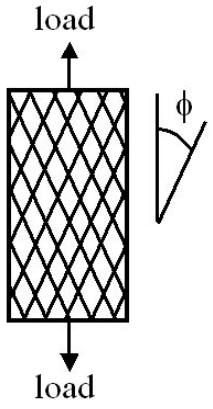

Figure 3.3 Specification of ply angle, ϕ, for laminate specimens

Reinforcement material was cut to an appropriate size from the roll. It was then placed into a hinged rig (1200 x 900 mm) such that the fibre tows were aligned with the sides of the rig, as shown in Figure 3.4. The fabric was clamped between the steel frame and a stiff clamping bar with a rubber strip which helped to grip the fabric along its whole length. This operation was carried out with the rig in its rectangular starting position. The fabric needed to be aligned accurately to avoid wrinkling when shearing took place. A force was subsequently applied to the moving bar such that the fabric was subjected to simple shear deformation.

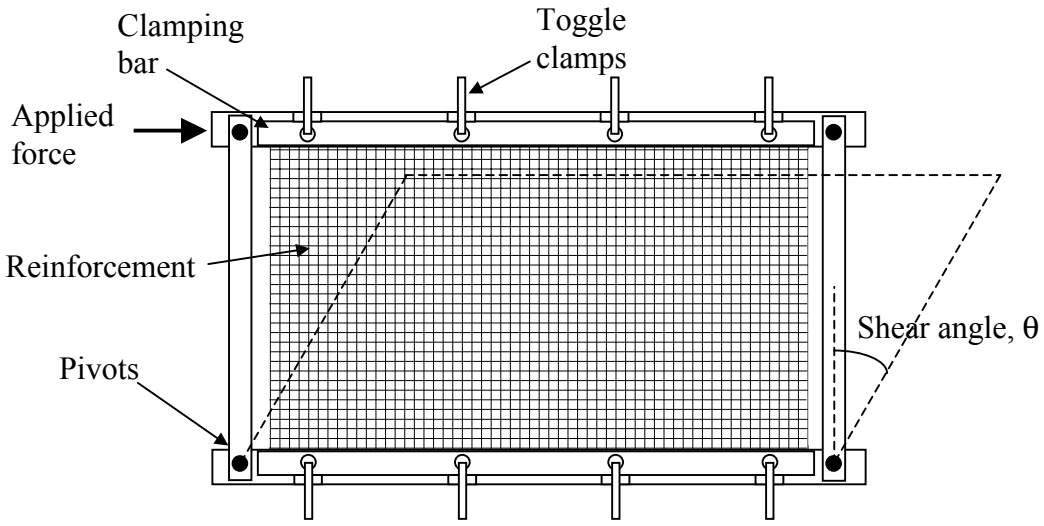

Figure 3.4 Parallelogram rig used to induce simple shear in fabric reinforcement

Before removing the clamping force, the fabric was stapled to a wooden frame beneath it to ensure that the deformation remained unchanged after removal from the shearing rig. The excess fabric was cut from the frame, and 1±0.25 g of Neoxil powdered thermoplastic binder was sprinkled onto the fabric's upper surface and spread out by hand. As subsequent layers were sheared to produce a preform for moulding, these were stapled over the top such that at the end of the process the wooden frame had the required number of fabric layers stapled to it, all sheared by the same amount and laying in the same orientation with the bias direction parallel to the long side of the frame, as shown in Figure 3.5. This assembly was then placed between MDF boards in a heated hydraulic press. The press was maintained at 70°C and a compaction load of 15 tonnes was applied for 20 minutes. After this time, the reinforcement was left between the boards but removed from the press and allowed to cool naturally, causing the binder to stiffen. Once cooled, the binder provided

enough stiffness to enable the preform (300 x 460 mm) to be cut away from the centre of the frame using a sharp knife while still retaining its shape.

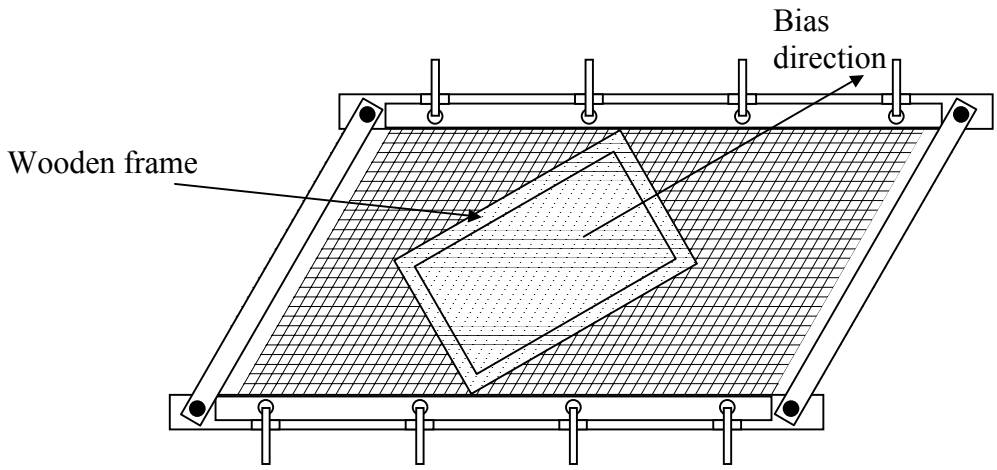

Figure 3.5 Fixing the sheared fabric to a wooden frame at the appropriate orientation

This preform was subsequently used to mould a flat plaque by RTM; this process is described in the following section.

3.3.2 Resin transfer moulding of flat plaques

Flat plaques were manufactured from unidirectional reinforcement (Formax UD-468) and from two textile reinforcements (Formax FGE-106, Vetrotex RT600), the textile reinforcements having been subjected to in-plane shear deformation as described in the preceding section. For this moulding process a two part aluminium mould tool was used containing a cavity of 3.8 mm thickness, which could be increased through the use of shims. The mould was sealed with a 4 mm o-ring and closed using a hydraulic press. Injection was accomplished using a central injection port, with the resin under a positive pressure of approximately 3 bar, in addition to the application of a vacuum at the mould vents, located at either end of the mould, to improve moulding quality. Reichhold Norpol 420-100 polyester resin was used, in conjunction with Butanox M50 catalyst and Akzo Nobel NL49P accelerator (0.75% each by mass). Resin typically reached the outlet vents after approximately two minutes, whereupon the vacuum was removed. Injection continued under positive pressure until no bubbles were observed in the output stream, typically after a further five minutes. At this point the vents were sealed; the inlet was also sealed shortly

afterwards such that the system was pressurised during the cure cycle. Plaques were allowed to cure in the mould overnight at room temperature, and subsequently were post-cured, according to the resin manufacturer's instructions, in a fan-assisted oven at 80°C (2 hours heating from ambient temperature to target temperature, 2 hours at target temperature and 2 hours cooling).

In order to isolate the effects of fibre orientation on mechanical properties, it was decided to manufacture all laminates at approximately the same fibre volume fraction, necessitating different mould thicknesses since reinforcement superficial density increases due to shear deformation. Since in RTM the mould cavity has a fixed height, shims were used to modify the mould height to satisfy constant fibre volume fraction according to the relationship in Equation 3.2. In practice, shim thicknesses were chosen to coincide with Standard Wire Gauge (SWG) dimensions, and appropriate shear angles were derived such that aluminium sheet could be obtained and used to make the shims. Table 3.3 shows the shim thicknesses used for the shear angles employed in this thesis. The target fibre volume fraction for angle-ply laminates was that obtained using four layers of FGE-106 reinforcement with no shear deformation and no shims, i.e. approximately 38%.

$$h = \frac{nS_0}{\rho_{glass} V_f \cos\theta} \tag{3.2}$$

where h is the mould cavity height, n is the number of reinforcement layers in the laminate, S_0 is the reinforcement superficial density (mass per unit area), ρ_{glass} is the bulk density of glass, V_f is the target fibre volume fraction and θ is the reinforcement shear angle.

Table 3.3 Shim thicknesses used to produce mouldings at constant fibre volume fraction (unshimmed mould cavity height was 3.8mm)

Shear angle, θ (°)	Ply angle, ϕ (°)	Shim thickness (mm)
0	45	0
10	40 & 50	0
30	30 & 60	0.60
36	27 & 63	0.91
40	25 & 65	1.22

3.3.3 Resin transfer moulding of a jet engine nose cone

In order to validate models presented in this thesis it was necessary to manufacture and test a component which would demonstrate the effect on mechanical properties of forming textile reinforcement to a three dimensional geometry. A jet engine nose cone geometry was chosen for this purpose since RTM tooling was available and because its axisymmetric shape enabled comparison between tests at different positions around the component. A schematic diagram of the tooling is shown in Figure 3.6. The diameter at the base of the cone was approximately 200 mm, while the component height was approximately 230 mm.

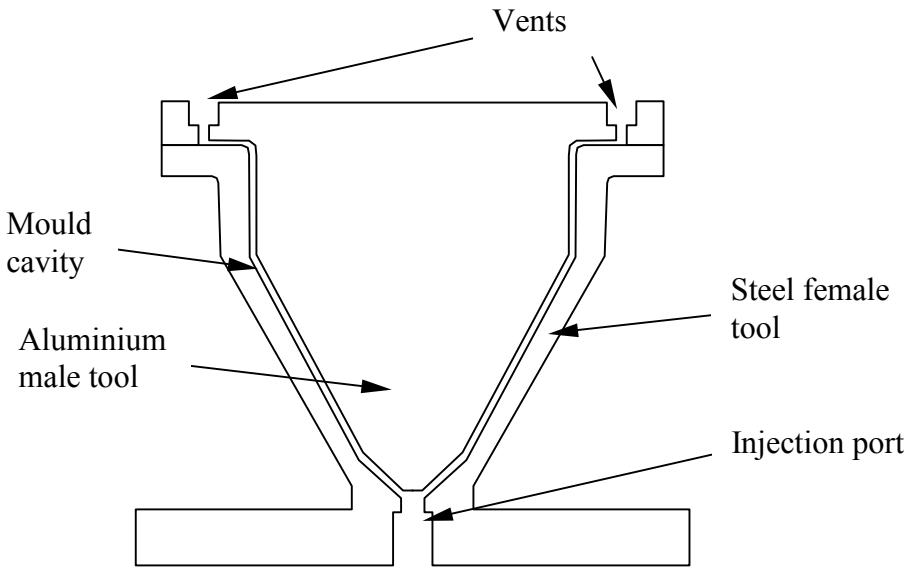

Figure 3.6 Schematic diagram of the RTM tooling used to produce the nose cone component

The reinforcement fabric used to manufacture this component was EBX hd 936, which was formed to shape over the male tool by hand such that no wrinkles were observed. Three layers of this fabric were used; these were interleaved with pairs of layers of Unifilo U101-220 according to the lay-up shown in Figure 3.7. The Unifilo was added to reduce the large change in fibre volume fraction observed between regions of high and low reinforcement deformation around the geometry, which caused problems in filling the mould due to the effect on permeability. The layers of Unifilo were tailored to fit the geometry without being subjected to any in-plane deformation. The approximate deformation pattern of the textile reinforcement can

be seen in Figure 3.8, which shows a computer-simulated plan view of the formed reinforcement, with gridlines parallel to the fibre directions. Dark lines indicate low shear (i.e. fibres nearly orthogonal) while light grey is indicative of high levels of in-plane shear deformation. The computer simulation tool used to produce this image is discussed in Chapter 5.

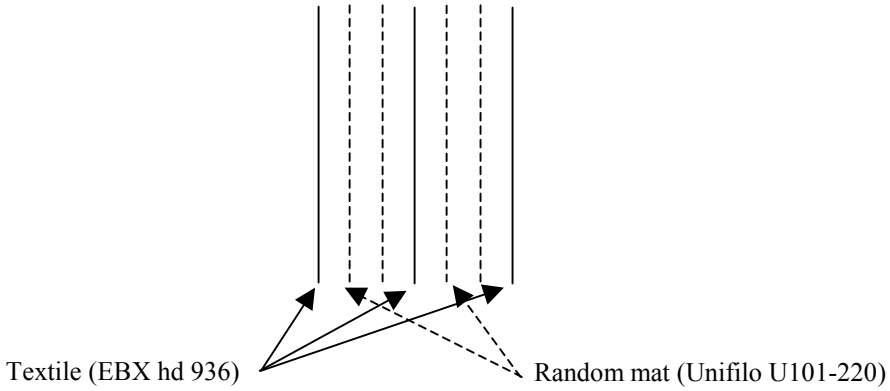

Figure 3.7 Schematic diagram of the reinforcement lay-up used to produce the nose cone component

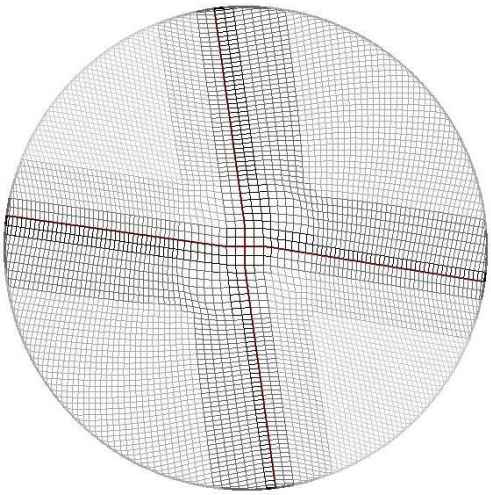

Figure 3.8 Draped reinforcement pattern of EBX hd 936 non crimp fabric formed to the shape of a jet engine nose cone predicted using the energy minimisation based Drape Model. Dark lines indicate areas where little shear deformation has been induced (i.e. fibres nearly orthogonal) while light lines indicate areas of high shear. Note that the deformation is not quarter-symmetric due to the shear asymmetry exhibited by the reinforcement.

The mould was sealed using an o-ring and evacuated from two vents connected inside the tool with a gallery around the base of the cone. Norpol 440-M750 resin was mixed with 1% Butanox M50 catalyst and injected through the central injection port at the tip of the cone under a positive pressure of 3 bar. Once resin began to appear at the outlet vents, the vacuum was removed and flow was allowed to continue for several minutes to ensure complete filling of the part. The vents were

subsequently closed and the inlet pressure was increased to 6 bar before closing the inlet such that the mould contents remained under pressure during the cure cycle. Curing took place at room temperature overnight, and the part was subsequently de-moulded and post-cured in a fan-assisted oven at 80°C (2 hours heating from ambient temperature to target temperature, 2 hours at target temperature and 2 hours cooling). Due to difficulties in forming the reinforcement and filling the mould, the flange at the base of the cone did not contain a consistent volume of reinforcement. In order to facilitate interpretation of test data, the bottom 50mm of the part was removed using a diamond cutting wheel.

3.4 Mechanical testing

This section describes the mechanical test methods used to determine elastic and failure behaviour, both for standard test coupons and three-dimensional components. All mechanical testing was performed using an Instron 1195 universal testing machine, having an electro-mechanical action and dedicated PC-based data logging facilities to record data from both the 50 kN tension/compression load cell and an extensometer continuously throughout the duration of each test. Where strain gauges have been used, data from these were recorded continuously throughout the test duration using an Instrunet 100 PC-based data logging system.

3.4.1 Tensile testing

Tensile testing was performed according to the guidelines set out in ASTM D3039-95. Specimen dimensions used were in accordance with this test method, and are shown in Table 3.4. For testing of angle-ply laminates, specimens were cut such that the bias direction of the reinforcement lay in the machine direction. Since failure was consistently observed to occur away from the grips, tabs were not used.

Table 3.4 Specimen dimensions used for tensile test coupons.

Specimen type	Width (mm)	Length (mm)
Angle-ply (bias)	25	250
Unidirectional (on-axis)	15	250
Unidirectional (transverse)	25	175

Tests were performed using a constant cross-head speed of 2 mm/min. A clip-on extensometer, having a gauge length of 50 mm, was attached to each specimen to measure extension in the direction of loading, while a foil strain gauge, having a gauge length of 10 mm, was bonded to the specimen surface to measure the strain in the transverse direction. Readings from these devices and the load cell were taken and recorded at approximately 2 Hz. Four repeat specimens were tested in most cases; exceptions will be noted where results are presented. Since the materials tested exhibited small failure strains, engineering strains were used; strain in the loading direction was calculated according to Equation 3.3.

$$\varepsilon_x = \frac{\delta l_x}{l_x} \tag{3.3}$$

where l_x is the gauge length (also in the loading direction) and δl_x is the change in the gauge length, or the extension.

Similarly, engineering (nominal) stress in the loading direction was calculated using Equation 3.4, assuming that cross-sectional area remained constant.

$$\sigma_x = \frac{F_x}{A} \tag{3.4}$$

where F_x is the applied load and A is the initial cross-sectional area of the specimen, the product of its width and thickness which were measured using digital vernier callipers.

Young's modulus of specimens was determined from the gradient of the stress-strain curve in the range $0 < \varepsilon_x < 0.2\%$, where stress-strain behaviour was always approximately linear. Poisson's ratio was calculated using Equation 3.5, using data from within the same strain range as that used to calculate Young's modulus.

$$\nu_{12} = \frac{|\varepsilon_2|}{|\varepsilon_1|} \tag{3.5}$$

Different techniques were used to obtain failure stress according to the type of specimen being tested. The procedure used in each case will be described where results are presented.

3.4.2 In-plane shear testing

The measurement of in-plane shear properties of aligned fibre composites is an area of considerable debate, and a significant amount of work has been published in the scientific literature on the matter. Although the v-notched beam, or Iosipescu, method (standard test method ASTM D5379-93) is widely used, concerns have been raised about the potential for stress concentrations induced by the notches and for parasitic transverse compressive stresses due to the boundary conditions. A popular alternative to the Iosipescu test is the 10° off-axis tensile test, proposed by Chamis and Sinclair [151], in which a unidirectional composite specimen is prepared with the fibres at an angle of 10° to the loading axis.

One of the most frequently reported problems with the 10° off-axis test is that, due to the non-symmetric nature of the specimen, application of a tensile load introduces in-plane bending deformation in the specimen, as shown in Figure 3.9. To overcome this problem, some researchers have suggested the use of grips which are free to rotate [152,153], while others have suggested the use of specimens fitted with specially designed tabs to allow homogeneous deformation throughout the specimen gauge length [154-157]. Notably, Sun and Chung [155] observed that the component of displacement in the loading direction, u, for an off-axis tensile specimen could be maintained uniformly on a straight line, defined as a function of the transformed compliance matrix as indicated in Equation 3.6.

$$u = \left(\overline{S}_{11}x + \overline{S}_{16}y\right)\sigma \tag{3.6}$$

where $\overline{S}_{11}$ and $\overline{S}_{16}$ are terms in the transformed compliance matrix for the material under investigation at the appropriate off-axis angle, x and y are geometric coordinates and σ is the applied stress.

By inspection of Equation 3.6, they stated that the angle, ϕ, between the line of isodisplacement and the loading (x) direction could be calculated according to Equation 3.7.

$$\cot\phi = -\frac{\overline{S}_{16}}{\overline{S}_{11}} \tag{3.7}$$

They suggested that the use of bonded rigid end tabs, cut such that the tab edge was at an angle ϕ to the loading direction, would remove the bending moment imposed by normal grips. In order to verify this, the authors performed both finite element analysis and experimental verification with a number of strain gauges, showing that the strain field was very close to uniform when oblique tabs were used, in contrast to the inhomogeneous strain field observed with rectangular tabs. They did note, however, that contraction due to Poisson's ratio would be prevented close to the tab. Also, the oblique angle for the tab is dependent on the material properties of the specimen.

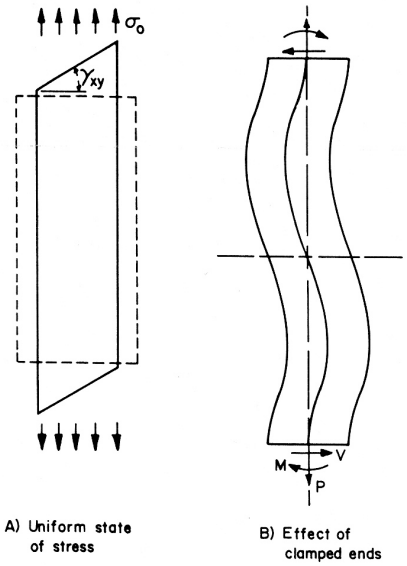

Figure 3.9 The influence of end constraints in the off-axis tensile test, after Pagano and Halpin [158].

Commenting on this method, Pierron and Vautrin [156] found that the use of ±45° composite tabs in place of aluminium gave improved experimental results due to the reduced resistance to Poisson's contraction, although they noted from finite element analysis that small transverse tensile stresses were present, which would be likely to cause reported strengths to be lower than the true shear strength. They suggested that

the Iosipescu test offered an improved opportunity to obtain a state of pure shear [159].

Since disparity was observed in the literature on this matter, both Iosipescu and 10° off-axis tests were carried out in the present work for evaluation of the test methods in the context of the materials under investigation. Rectangular off-axis tensile specimens (25 x 250 mm) were cut from unidirectional plaques, made with UD-468 reinforcement using the method in Section 3.3.2, with the fibres running at 10° to the length of the specimen. Using the micromechanics models described in Chapter 2 (rule of mixtures and Halpin-Tsai equations) in conjunction with Equation 3.7, the oblique angle for the tabs was found to be approximately 45°. Tabs were cut from ±45° glass/polyester laminate, following the suggestions of Pierron and Vautrin [156]. A stacked three strain gauge rosette (0°/45°/90°, gauge length 3mm) was used to record the strain in the centre of the specimen, strains being transformed using the relationship stated by Chamis and Sinclair (Equation 12 in [151]). No extensometer was used. The remainder of the procedure used was the same as that for on-axis tensile testing, described in Section 3.4.1. Three repeat specimens were tested, and the results were compared with those obtained by Iosipescu testing of specimens from the same plaque. The Iosipescu test method is described in detail in the following paragraphs. Results for shear strength and modulus from the two methods were observed to be within 15% of one another, with Iosipescu strengths being higher than those from the off-axis test, suggesting that either test would be suitable for determination of the in-plane shear properties. The Iosipescu test was selected for the remaining studies for a number of reasons:

- The time required for specimen preparation was smaller than for off-axis specimens, since tabs were not used.
- Since the specimens were smaller, more could be obtained from each plaque.
- The off-axis testing required a three strain gauge rosette, costing approximately double the amount of the two gauge rosettes required for Iosipescu testing.

The procedure used for in-plane shear testing of unidirectional laminates by the v-notched beam, or Iosipescu, method was in accordance with ASTM D5379-93. Rectangular specimens were cut from manufactured plaques such that the fibres ran parallel to the long side of the specimens, then notches were machined using an

appropriate milling cutter such that they were symmetric about the axis of the specimen. A 90° two gauge rosette foil type strain gauge (gauge length 2 mm) was adhesively bonded to the surface of the specimen in the centre. A schematic diagram of the specimen is shown in Figure 3.10.

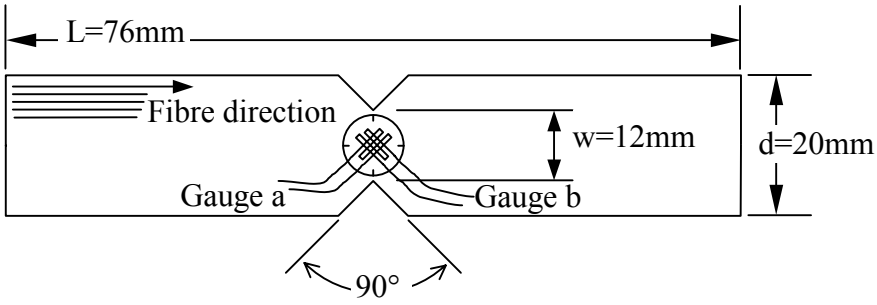

Figure 3.10 Schematic diagram of an Iosipescu (v-notched beam) in-plane shear test specimen fitted with 90° strain gauge rosette

The specimen was constrained on one side of the notch and a vertical load was applied on the other side using a fixture which did not permit rotation of the specimen, in order to obtain a state of pure shear in the centre of the specimen. The fixture is illustrated in Figure 3.11. Loading was applied using the Instron testing machine with a constant cross-head speed of 2 mm/min. Strain and load data were recorded at a rate of approximately 2 Hz. Four repeat specimens were tested in each case. Engineering shear strain in the specimen was calculated using Equation 3.8, according to the standard test method.

$$\gamma_{12} = \left|\varepsilon_{\text{gauge a}}\right| + \left|\varepsilon_{\text{gauge b}}\right| \tag{3.8}$$

where $\varepsilon_{\text{gauge a}}$ and $\varepsilon_{\text{gauge b}}$ are the strains recorded from gauges a and b respectively.

Shear stress in the specimen was calculated using Equation 3.9.

$$\tau_{12} = \frac{F}{wh} \tag{3.9}$$

where F is the applied load, w is the width across the notch root and h is the specimen thickness; w and h were measured using digital vernier callipers.

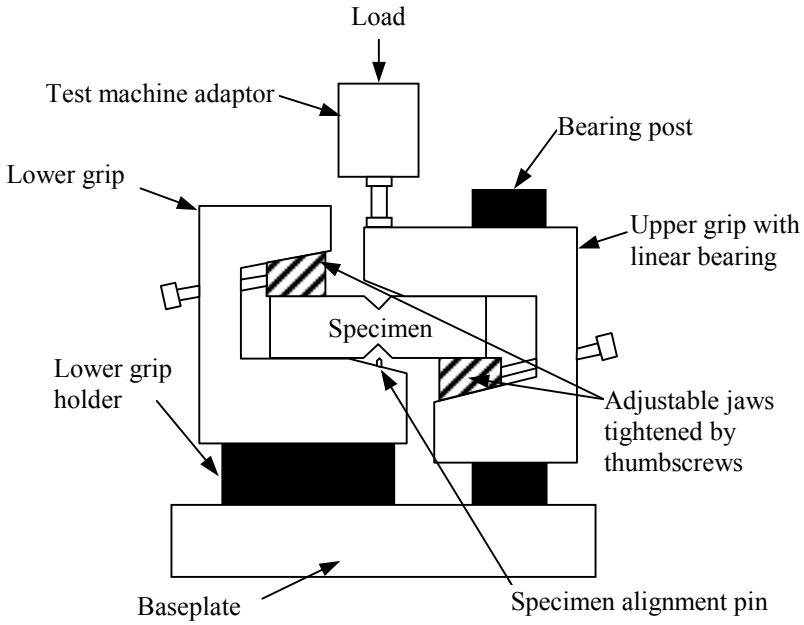

Figure 3.11 Schematic diagram of the Iosipescu (v-notched beam) in-plane shear test fixture (after ASTM D5379)

Ultimate shear strength, τ_{12u}, was calculated by substituting the maximum applied load into Equation 3.9. In all cases presented in this thesis, specimens were observed to fail in a way considered acceptable according the test standard (i.e. failure occurred within the area between the notches and not at the point of application of the load). A typical specimen having failed is shown in Figure 3.12.

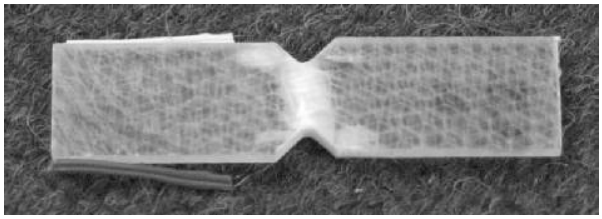

Figure 3.12 Typical failure within the gauge area observed in unidirectional glass reinforced polyester Iosipescu test specimens

Shear modulus was calculated by obtaining the gradient of an appropriate linear portion of the shear stress-shear strain curve, typically in the range $0<\gamma_{12}<0.01$. A typical shear stress-shear strain curve for unidirectional glass reinforced polyester is shown in Figure 3.13.

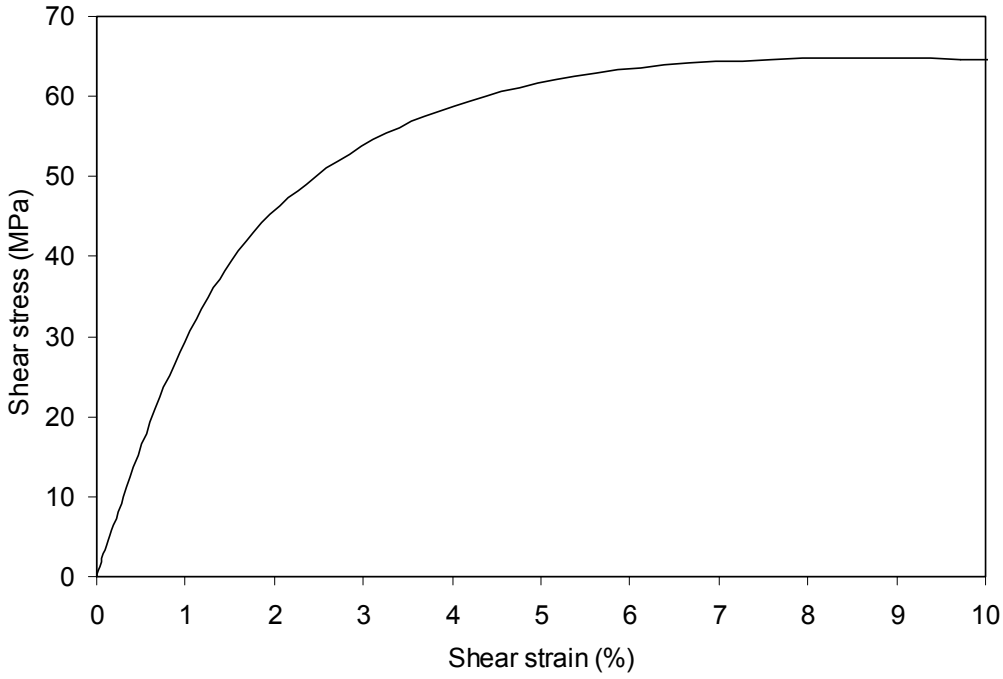

Figure 3.13 Typical shear stress-shear strain curve for unidirectional glass reinforced polyester laminates obtained using the Iosipescu test method.

3.4.3 Mechanical testing of a jet engine nose cone

The component described in Section 3.3.3 was tested under a pinching load across the diameter of the base. This load was applied using custom made curved jaws, having the same curvature as that of the part (radius = 100 mm) and being 60 mm wide, which were fixed into the Instron testing machine. A photograph of the apparatus is shown in Figure 3.14.

Figure 3.14 Jet engine nose cone mechanical test apparatus.

A displacement of 1 mm was applied using a crosshead speed of 1 mm/min. Load and displacement data were recorded at a rate of approximately 1 Hz. After the

prescribed displacement was reached, the loading was removed and the component was rotated through 30° about its axis. This procedure was performed six times in order to evaluate the effect of draping the reinforcement fabric on the mechanical properties of the component, after which it was repeated using 2 mm, 3 mm and 4 mm displacement levels in turn. A schematic of the testing apparatus showing the axes of loading with respect to the draped fabric reinforcement pattern is shown in Figure 3.15.

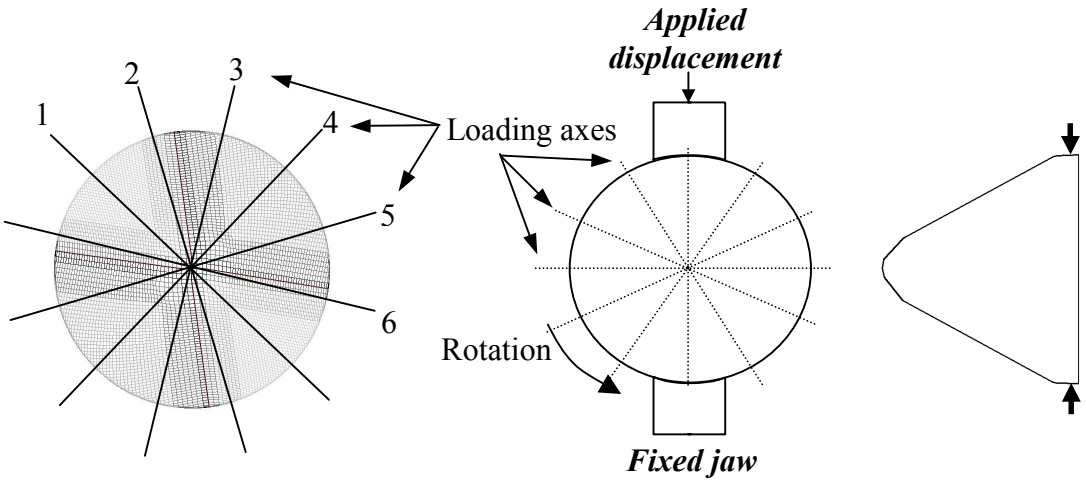

Figure 3.15 Schematic of jet engine nose cone mechanical test apparatus with respect to the draped reinforcement pattern. The centre of sheared region (direction 1) defines the 0° orientation.

Results of all mechanical testing performed are presented in Chapter 4.

3.5 Characterisation techniques

This section describes the techniques used to characterise the composite laminates which were produced. Characterisation was required to determine or verify parameters which were predicted from a knowledge of the constituent materials.

3.5.1 Determination of fibre volume fraction by ignition loss

Although it is possible to estimate the fibre volume fraction (V_f) of a laminate from the mass of the reinforcement preform and the volume of the moulding, to obtain a more accurate measurement the ignition loss, or burn off, technique was used.

Testing by this method was performed according to ASTM D2584-94. Specimens were cut from different areas of each plaque to be analysed in order to obtain an indication of local variations in V_f in addition to an average value representative of the whole plaque. Specimen dimensions were approximately 25 x 25 mm. Between three and five specimens were tested from each plaque.

A crucible was weighed using digital electronic scales, then weighed again after having a specimen placed in it. The crucible was placed inside a Carbolite AAF1100 electric muffle furnace equipped with extraction and an afterburner (shown in Figure 3.16), and maintained at a temperature of approximately 550°C for 45 minutes. After this time all carbonaceous residue was observed to have been removed, leaving only glass reinforcement. The crucible was removed and allowed to cool before the mass was measured for a third time. Fibre volume fraction of each specimen was calculated from the mass fraction and the appropriate phase densities using Equation 3.10.

$$V_f = \frac{m_3 - m_1}{(m_3 - m_1) + \left(\frac{\rho_f \left((m_2 - m_1) - (m_3 - m_1) \right)}{\rho_m} \right)} \tag{3.10}$$

where m_1 is the mass of the crucible, m_2 is the mass of the crucible with the specimen, m_3 is the mass of the crucible with the specimen residue after resin removal in the furnace, ρ_f is the density of glass fibre and ρ_m is the density of the matrix resin.

Figure 3.16 Carbolite AAF1100 electric muffle furnace used for fibre volume fraction measurement by ignition loss

No consideration was given to the presence of voids in the material (void content). The void level was thought to be low due to the use of a vacuum during moulding; this view was reinforced by the highly transparent nature of the moulded laminates, although no void content measurement was performed.

3.5.2 Optical microscopy

In order to examine the internal structure of the materials studied, optical microscopy was performed. Specimens with a length of 20-30 mm and a width of approximately 20 mm were cut from the laminates to be examined. These were placed into plastic pots with detachable bases of 40 mm diameter, stood on edge and held in place with a small amount of epoxy based adhesive. Catalyst and accelerator were mixed with Norpol 320-3200 casting resin and this was poured into the pots and allowed to cure at room temperature overnight such that the specimen was encased in solid resin.

After removing the cured specimens from the mounting pots, the specimens were cut to a thickness of approximately 14 mm. Initially, the two faces of the specimens were ground using coarse abrasive paper to obtain parallel faces. The grinding operation was carried out on Struers DAP-7 machine equipped with an automatic holder (Struers Pedemin-S), using 240 rpm motor speed. The cast samples were

ground using waterproof abrasive papers and washed. To obtain a good polished surface, at least four abrasive papers (e.g., 240, 600, 1200 and 4000 grit) with increasing grit number were used for not less than five minutes each. After polishing using grinding paper the specimens were polished with 1 μm alumina paste consisting of 20% by volume of powder and the balance of water on a flocked wheel.

Specimens were examined under a Zeiss Axiolab optical microscope fitted with a CCD camera connected to a PC for image acquisition. A typical image is shown in Figure 3.17. Where absolute dimensions were required, a graticule was used for calibration.

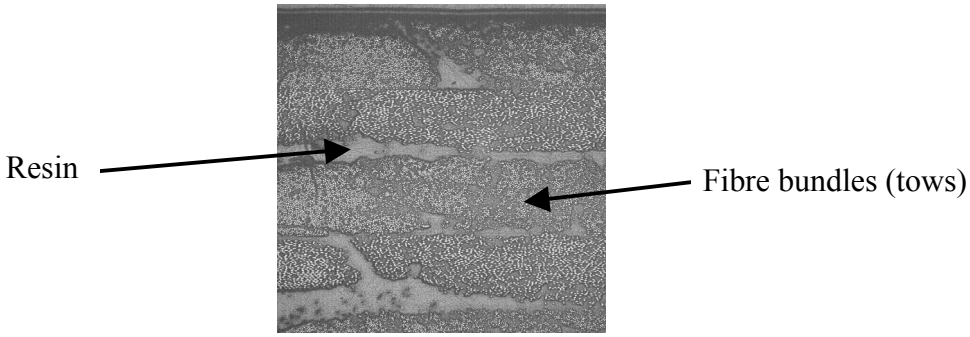

Figure 3.17 Typical optical micrograph obtained at low magnification (50x).

3.6 Conclusions

The procedures used for resin transfer moulding have been described in detail in this chapter; the mechanical test methods adopted for the specimens produced were also described, and justified where appropriate. At every stage great care has been taken to ensure accuracy and consistency throughout the work, such that results which are presented in Chapter 4 are thought to be comparable. For example, the unidirectional laminates manufactured to verify the lamina mechanical properties were manufactured using similar materials and processing parameters as those used to manufacture fabric reinforced angle-ply laminates. As a result, it was possible to have high confidence in the lamina properties required when predictions of the mechanical behaviour of the angle-ply laminates were made in Chapter 5.

4 EXPERIMENTAL TESTING AND RESULTS

4.1 Introduction

As discussed in Chapter 3, experimental testing was performed in order to determine the effects of certain parameters such as fibre volume fraction and reinforcement deformation on stiffness and strength, principally to validate the models described in Chapter 5. While the materials and techniques used are described in detail in Chapter 3, in this chapter results of mechanical testing are presented alongside a discussion of the treatments required to facilitate sensible interpretation of the data. Summary data are presented in this chapter, while detailed results are tabulated in Appendix C.

Unidirectional laminates, manufactured at three fibre volume fractions, were tested to failure in the axial and transverse directions and in in-plane shear, such that the elastic constants and principal strengths were determined. Flat plaques were manufactured from both woven fabric and NCF reinforcement which had been subject to a range of levels of shear deformation in order to isolate the effects on mechanical behaviour, since this is the principal mechanism for reinforcement deformation during component manufacture. These laminates were tested to failure in the bias direction and the behaviour was observed to change according to the ply angle. Typical stress-strain curves are presented and a method to determine the initial failure where non-linear behaviour was observed is described. A component containing significant levels of shear deformation in the reinforcement due to the draping process was also produced and tested, showing that the behaviour was dependent on these effects.

4.2 Unidirectional laminates

4.2.1 Introduction

Flat plaques, with dimensions 300 mm x 460 mm and a thickness of 3.8 mm, were manufactured by the resin transfer moulding (RTM) process, using Formax UD-468 unidirectional reinforcement material (Figure 3.2(e) and (f)) and Reichhold Norpol 420-100 unsaturated polyester resin. The reinforcement was orientated such that the

fibres ran parallel to the long side of the aluminium mould, with all layers being at the same orientation. Plaques were made with different numbers of layers of reinforcement in order to obtain different fibre volume fraction levels. In total, four plaques were manufactured using this reinforcement. The first was used exclusively for evaluation of shear test methods, discussed in Section 3.4.2. The other three plaques were designated according to Table 4.1, which also shows the number of layers of reinforcement used, the fibre volume fraction calculated using Equation 3.2, and that measured using the ignition loss technique described in Section 3.5.1.

Table 4.1 Designation and fibre volume fraction of unidirectional plaques

Plaque designation	No. reinforcement layers	Nominal (calculated) V_f (%)	Measured V_f (ignition loss, %)
UD2	7	32.9	34.1
UD3	8	37.6	39.6
UD4	9	42.3	42.2

4.2.2 On-axis tensile testing

Mechanical test specimens were cut from each plaque, having dimensions of 15 mm x 250 mm in accordance with ASTM D3039-95. Tensile testing was performed on these specimens using the procedure described in Section 3.4.1, where mechanical property calculation methods are also described. A typical stress-strain curve is shown in Figure 4.1. Linear stress-strain behaviour until the point of sudden failure was observed in all cases. Failure was noted to occur in a violent manner, involving fibre breakage and the presence of longitudinal cracks.

Figure 4.2 shows a summary of the Young's moduli obtained from on-axis tensile testing of the unidirectional plaques. Modulus is observed to increase with increasing fibre volume fraction, as expected from classical micromechanics models, although a significant spread in the values obtained can be noted. For example, values of E_1 for specimens prepared from the UD4 plaque ranged from approximately 30 GPa to 40 GPa, this spread being around 29% of the average value.

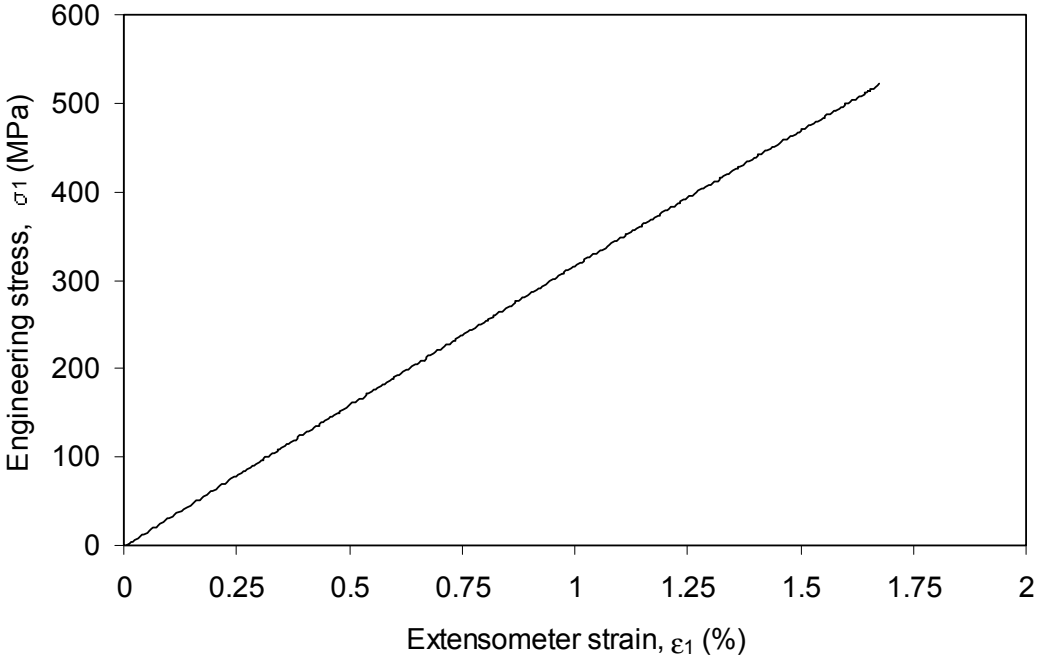

Figure 4.1 Typical stress-strain curve obtained from on-axis tensile test of unidirectional material. This curve was obtained from a specimen cut from the UD2 plaque, which exhibited a modulus of 32.9 GPa and a failure stress of 521 MPa. The linear form is typical of tests on this type of material.

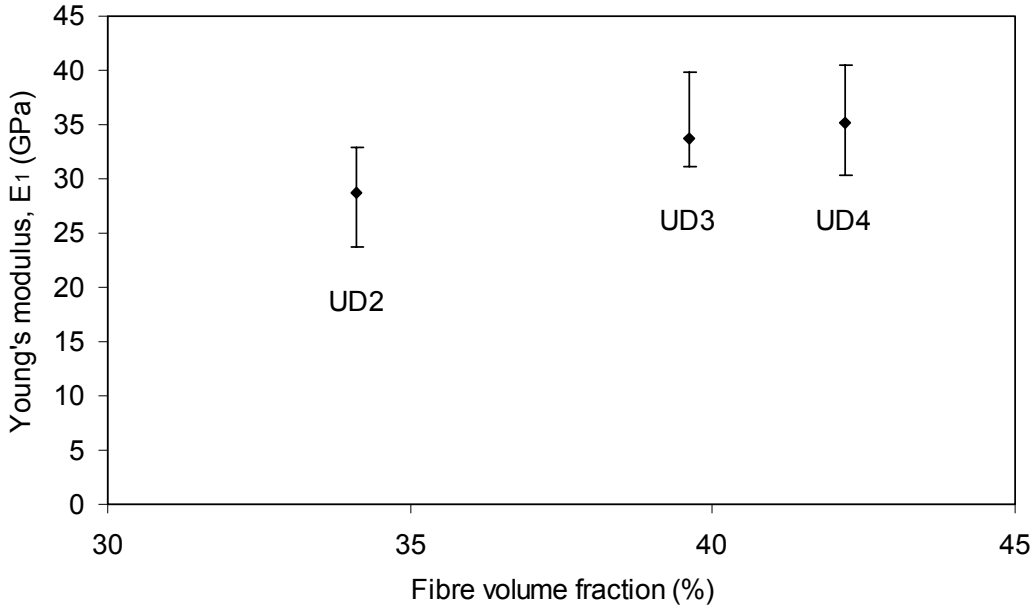

Figure 4.2 Longitudinal Young's modulus obtained from mechanical testing of unidirectional plaques UD2 (5 repeat specimens), UD3 (5 repeats) and UD4 (4 repeats). Error bars indicate maximum and minimum values obtained.

Poisson's ratio values, calculated using Equation 3.5, are presented in Figure 4.3. There is no obvious trend relating the Poisson's ratio to the measured fibre volume fraction. Since the Poisson's ratios of the fibre and matrix phases, given in Table 3.2, are similar it can be expected that changing V_f would have only a small effect on

the value for the laminates. The difference between maximum and minimum values obtained from repeat specimens (indicated by the error bars) is between 0.04 or 14% of the average value (UD4) and 0.07 or 22% of the average (UD2).

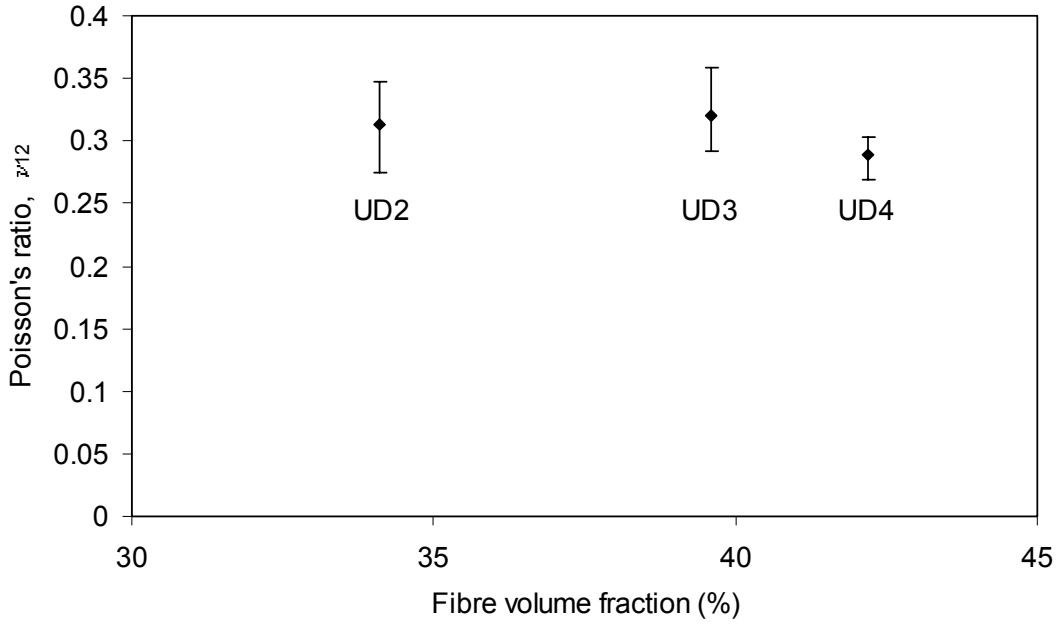

Figure 4.3 Poisson's ratio values obtained from mechanical testing of unidirectional plaques UD2, UD3 and UD4. Error bars indicate maximum and minimum values obtained.

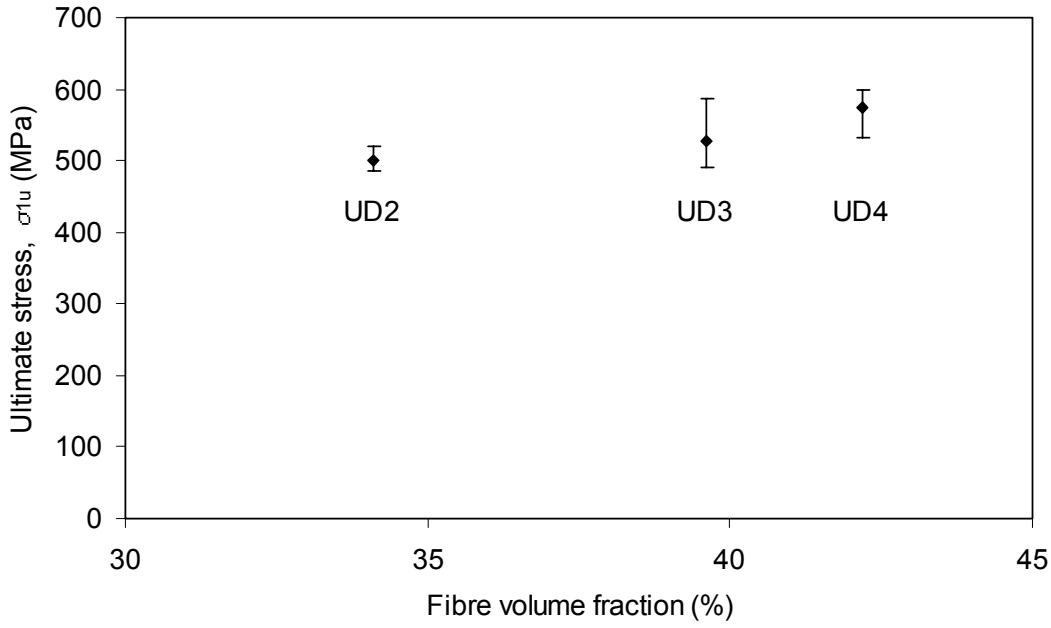

Figure 4.4 Ultimate stress values obtained from mechanical testing of unidirectional plaques UD2, UD3 and UD4. Error bars indicate maximum and minimum values obtained.

Failure stresses observed during testing are summarised in Figure 4.4. Average values can be seen to increase with fibre volume fraction, which was expected since

the fibres are much stronger than the matrix, and the scatter is significantly smaller than that observed in the elastic properties obtained from the same tests.

4.2.3 Transverse tensile testing

Specimens used for transverse tensile testing were 25 mm x 175 mm, in accordance with ASTM D3039-95. Tensile testing was performed on these specimens using the procedure described in Section 3.4.1. A typical stress-strain curve is shown in Figure 4.5. Linear stress-strain behaviour until the point of sudden failure was observed in all cases. Failure was almost instantaneous, although not violent, consisting of a single crack running across the width of the specimen.

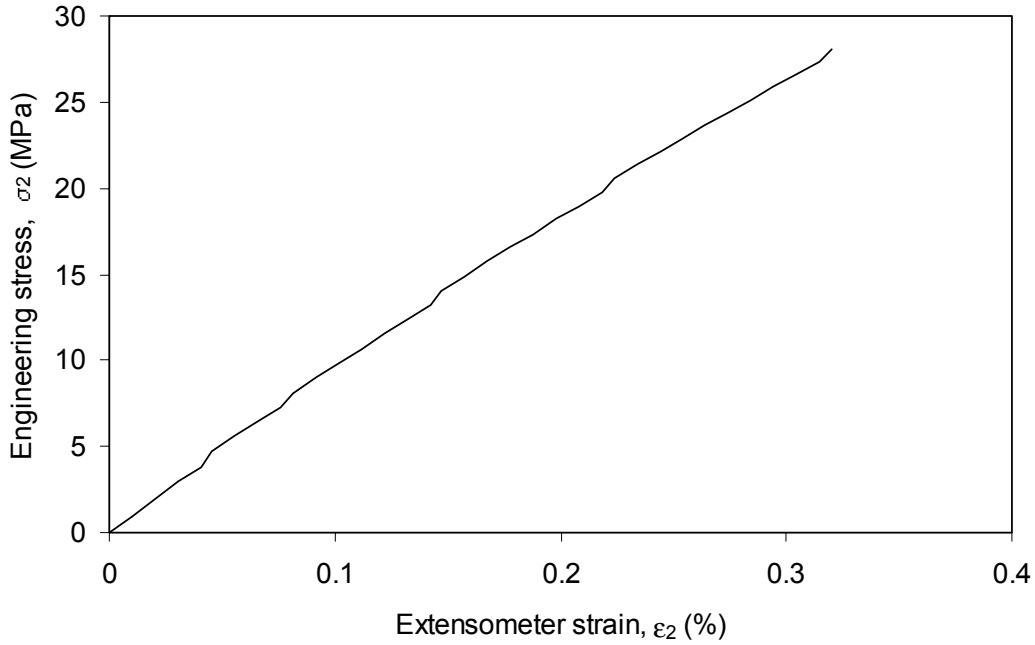

Figure 4.5 Typical stress-strain curve obtained from transverse tensile test of unidirectional material. This curve was obtained from a specimen cut from the UD2 plaque, which exhibited a modulus of 9.8 GPa and a failure stress of 28.1 MPa. All of the tests followed this pattern of linear behaviour. The apparent wavy nature of the plot is related to the resolution and frequency of the data acquisition system and is not thought to represent non-linear material behaviour.

The Young's modulus values obtained from these tests are summarised in Figure 4.6. It can be seen from the data presented that E_2 increased with increasing fibre volume fraction; this trend is also predicted by micromechanics models for E_2. A small spread in the results was observed, with the greatest difference between maximum

and minimum values for a single set of specimens being approximately 900 MPa, or 10% of the average (UD2).

Transverse strengths obtained from the same tests are summarised in Figure 4.7. The spread in the results is greater than that observed for E_2, the largest being 7 MPa, or 20% of the average, between maximum and minimum values (UD4). It can be seen that σ_{2u} also increased with fibre volume fraction, contrary to the predictions of micromechanics models, which suggest that the introduction of transverse fibres reduces the load bearing capacity of the matrix.

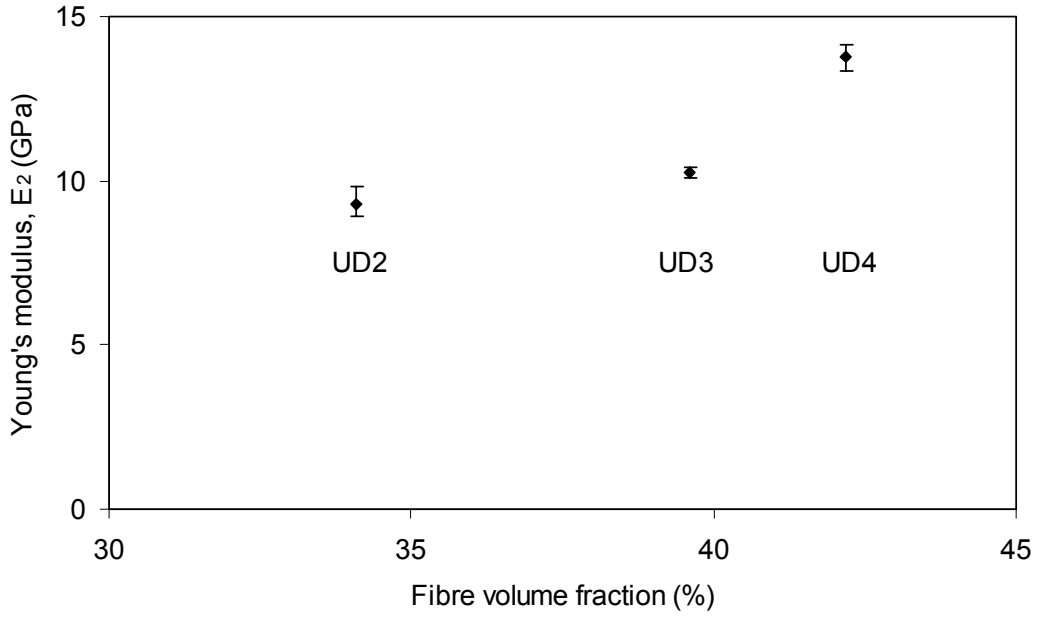

Figure 4.6 Transverse Young's modulus obtained from mechanical testing of unidirectional plaques UD2, UD3 and UD4. Four repeat specimens were tested in each case; error bars indicate maximum and minimum values obtained.

4.2.4 In-plane shear testing

As discussed in Section 3.4.2, the Iosipescu, or v-notched beam, test was selected to determine mechanical properties under an in-plane shear loading. Specimens were prepared with the reinforcement fibres running along their length. A 90° strain gauge rosette was bonded to the specimen between the notches in order to measure the shear strain. A typical shear stress-shear strain curve is shown in Figure 4.8. Curves from all specimens took approximately the same shape, exhibiting nearly

linear behaviour until around 1.75% shear strain, with the curve being nearly flat by around 5% shear strain.

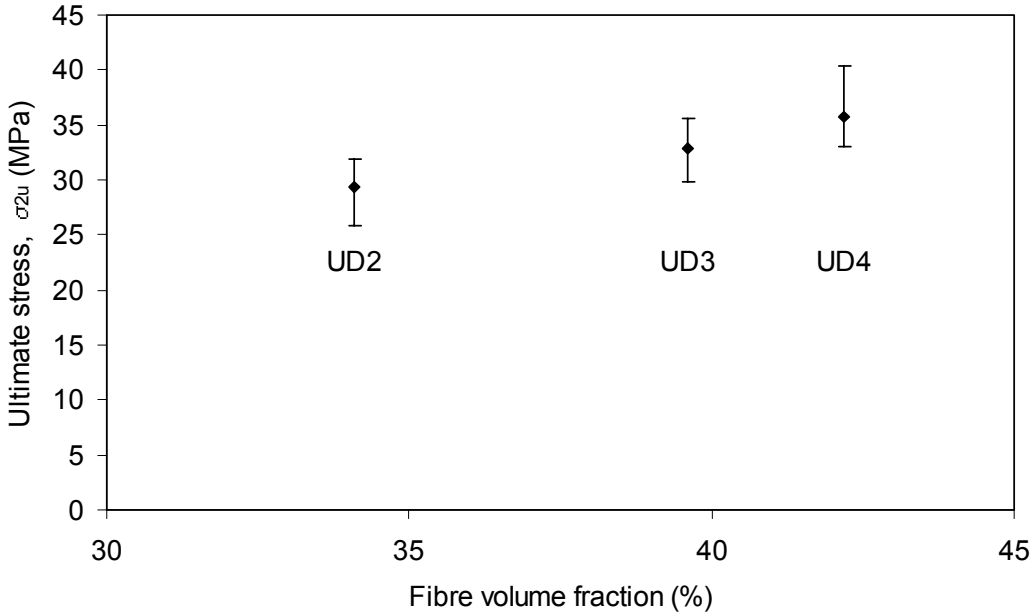

Figure 4.7 Ultimate transverse stress values obtained from mechanical testing of unidirectional plaques UD2, UD3 and UD4. Four repeat specimens were tested in each case; error bars indicate maximum and minimum values obtained.

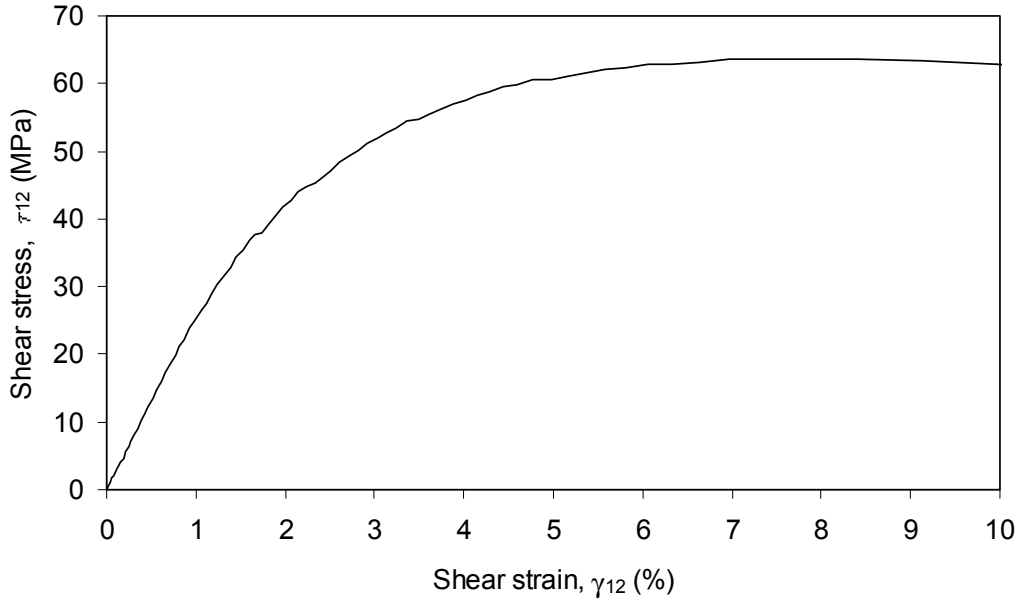

Figure 4.8 Typical shear stress-shear strain curve obtained from Iosipescu shear test on unidirectional material. This is a typical curve, which was obtained from a specimen cut from the UD2 plaque, which exhibited a shear modulus of 2.5 GPa and an ultimate shear stress of 63.6 MPa.

The shear modulus was determined from the gradient of the curve in the region $0 < \gamma_{12} < 1\%$, where linear behaviour was observed in all cases. The shear moduli

obtained from the specimens tested are summarised in Figure 4.9. Although the shear modulus appeared to increase with increasing fibre volume fraction, the spread in the experimental data was quite large, as high as 700 MPa or 28% of the average value (UD2), so this may not be a valid conclusion from the data available, although this is trend predicted by the Halpin-Tsai equations.

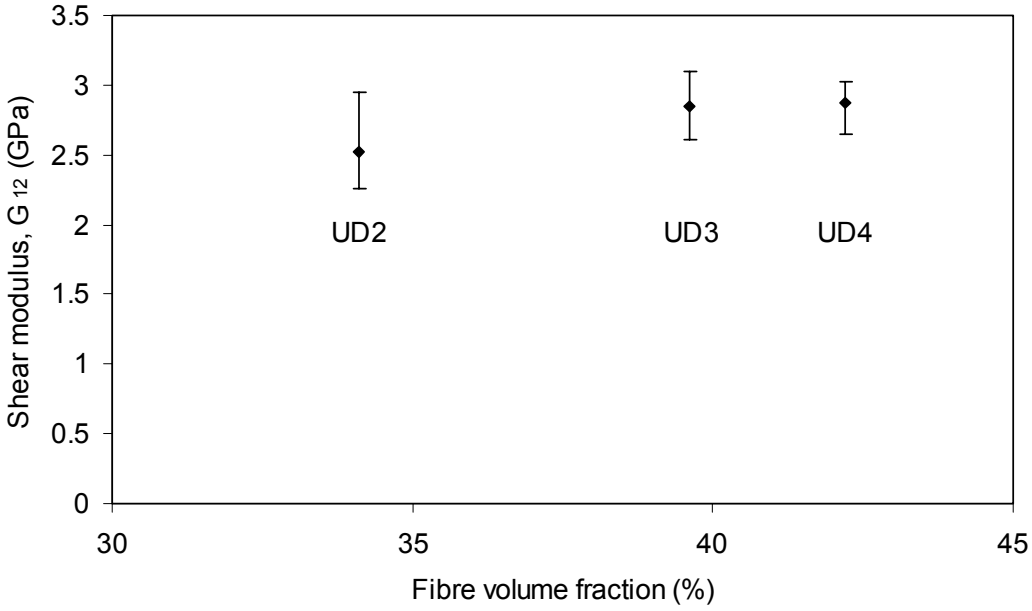

Figure 4.9 Summary data of shear moduli obtained from Iosipescu shear test on unidirectional material. Four repeat specimens were tested in each case; error bars indicate maximum and minimum values obtained.

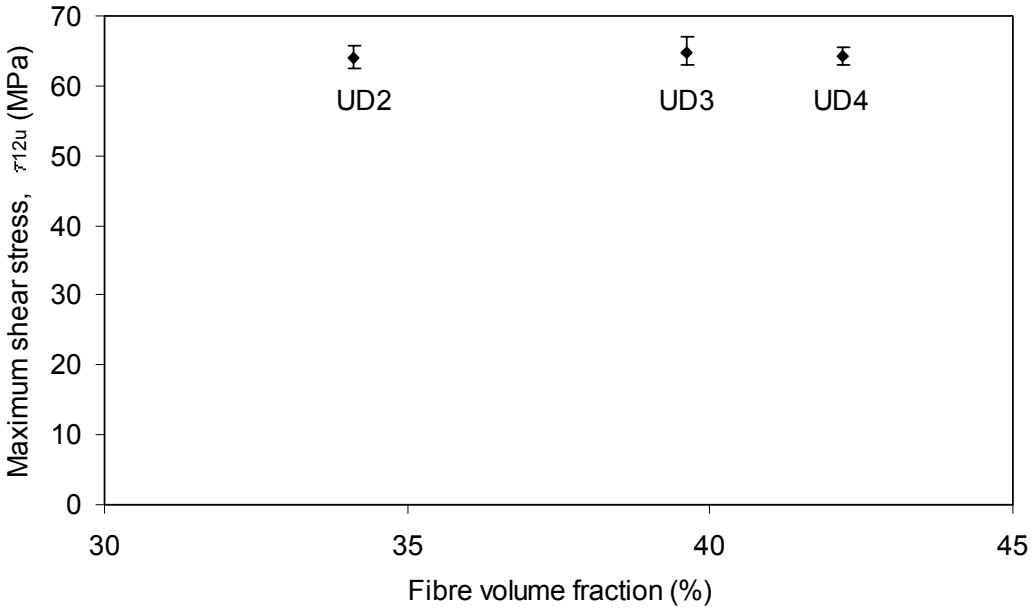

Figure 4.10 Maximum shear stress data obtained from Iosipescu shear test on unidirectional material. Four repeat specimens were tested in each case; error bars indicate maximum and minimum values obtained.

Measured values of ultimate shear stress were very consistent, exhibiting a maximum spread of 3.9 MPa, or 6% of the average value. Average values at each fibre volume fraction were within 0.7 MPa of one another, i.e. no significant change in ultimate shear stress was observed within the range of fibre volume fractions tested. Values are summarised in Figure 4.10.

4.3 Angle-ply laminates

4.3.1 Introduction

In order to determine the effects of fibre reorientation during forming on textile composite mechanical behaviour, reinforcement was subjected to in-plane shear deformation and used to manufacture flat plaques. Plaques were manufactured from Formax FGE-106 biaxial warp-knitted textile reinforcement material (Figure 3.2(c) and (d)) and Vetrotex RT600 plain weave reinforcement (Figure 3.2(g)) with Reichhold Norpol 420-100 unsaturated polyester resin, using the RTM process. The reinforcement was deformed before moulding using the technique described in Section 3.3.1. All layers of reinforcement in a single moulding were at the same orientation and were subjected to the same amount of in-plane shear, such that angle-ply laminates were produced having equal amounts of fibre at angles $+\phi$ and $-\phi$ to the bias (neutral) direction, which was parallel with the side of the rectangular mould. Plaques were made with four layers (FGE-106) or seven layers (RT600) of reinforcement, and shims were incorporated between the mould faces to modify the plaque thickness in order to maintain constant fibre volume fraction levels at all ply angles. This is required to counteract the effect described by Equation 3.2. Six plaques were manufactured from FGE-106 reinforcement, and five from RT600 reinforcement. By preparing tensile specimens cut both parallel and perpendicular to the long side of the mould, specimens at eleven ply angles were produced from FGE-106 and at nine ply angles from RT600. Plaque designations and specimen ply angles are summarised in Table 4.2 together with fibre volume fraction data, measured using the ignition loss technique. Although the intention was to produce laminates at the same fibre volume fraction, it can be seen from the data in Table 4.2 that some deviation from the nominal value of 37.6% was observed, possibly due to variations in the reinforcement. This has not been considered in subsequent

modelling of angle-ply laminates presented, but may have a small effect on the results for the laminates affected.

Table 4.2 Designation and fibre volume fraction of angle-ply laminates

Plaque designation	Reinforcement material	Reinforcement shear deformation induced, θ	Ply angle, ϕ	Measured V_f (ignition loss, %)
FGE-25	FGE-106	40°	25° & 65°	36.4
FGE-27	FGE-106	36°	27° & 63°	42.0
FGE-30	FGE-106	30°	30° & 60°	36.8
FGE-35	FGE-106	20°	35° & 55°	40.9
FGE-40	FGE-106	10°	40° & 50°	36.5
FGE-45	FGE-106	0°	45°	36.3
RT-25	RT600	40°	25° & 65°	37.4
RT-27	RT600	36°	27° & 63°	37.2
RT-30	RT600	30°	30° & 60°	42.8
RT-40	RT600	10°	40° & 50°	39.1
RT-45	RT600	0°	45°	37.2

4.3.2 Tensile testing

Tensile testing was performed as described in Section 3.4.1. Recorded stress-strain data were similar for plaques manufactured from the two reinforcement fabrics, but changed shape according to the ply angle of the specimen. The stress-strain curves could be categorised into four likely shapes, each indicated in Figure 4.11. Typical shapes are given designations in Table 4.3, while Table 4.4 shows which specimens fell into each category.

Table 4.3 Designation and description of typical stress-strain curve types shown in Figure 4.11.

Designation	Ply angle, ϕ, indicated in Figure 4.11	Description
a	±27°	Having small curvature until sudden failure at high stress
b	±40°	Almost no linearity; one long curve
c	±45°	Similar to type b, but exhibiting a distinctive 'knee' indicative of gradual failure whereupon the load was still supported at high extensions (typically 8-15% strain)
d	±63°	Linear or nearly linear until sudden failure at low stress

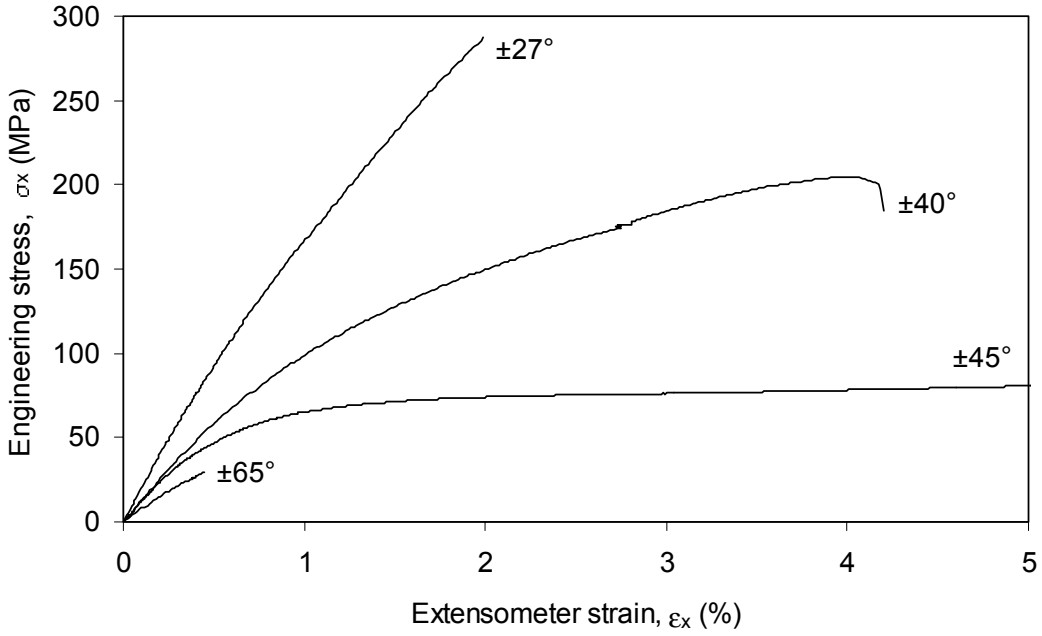

Figure 4.11 Typical stress-strain curves obtained from bias tensile test on angle-ply laminates. These curves are typical of laminates manufactured from both reinforcements, and show the significant differences in behaviour observed with changing ply angle.

Although non-linearity was observed in much of the stress-strain behaviour recorded, curvature of the initial portion of the stress-strain plot, i.e. $0<\varepsilon_x<0.2\%$, was small in all cases; hence Young's modulus in the direction of loading (bias direction), E_x, was calculated by taking the gradient of the stress-strain curve in this range, which was considered to be representative for all of the cases investigated. Results obtained are summarised in Figure 4.12. It can be seen that E_x decreased significantly with increasing ply angle in the range $25°<\phi<45°$, whereupon it remained approximately constant for $45°<\phi<65°$. Specimens manufactured from woven reinforcement generally exhibited higher Young's moduli than corresponding NCF reinforced specimens, although the models discussed in Section 2.4.3 would predict the opposite to be the case due to the crimped nature of the woven reinforcement. Similarly, the result that E_x appeared to be lower for $\phi=25°$ than for $\phi=27°$ was not expected. This suggests either that inaccuracies in the manufacturing process may have caused the fibres to be orientated away from their nominal positions, or that another factor, such as a change in textile geometry after forming, was introduced which is not considered by a traditional laminate analysis. Values obtained exhibited a relatively small spread, up to a maximum of 21% of the average value (approx. 1850MPa) for the FGE-106 ±40° samples.

Table 4.4 Categorisation of stress-strain behaviour of angle-ply laminates.

Plaque designation[a]	Ply angle, ϕ	Stress-strain behaviour type[b]
FGE-25	25°	a
FGE-27	27°	a
FGE-30	30°	a
FGE-35	35°	b
FGE-40	40°	b
FGE-45	45°	c
FGE-40	50°	c/d
FGE-35	55°	d
FGE-30	60°	d
FGE-27	63°	d
FGE-25	65°	d
RT-25	25°	a
RT-27	27°	a
RT-30	30°	a
RT-40	40°	b
RT-45	45°	c
RT-40	50°	c
RT-30	60°	d
RT-27	63°	d
RT-25	65°	d

[a] From Table 4.2
[b] From Table 4.3

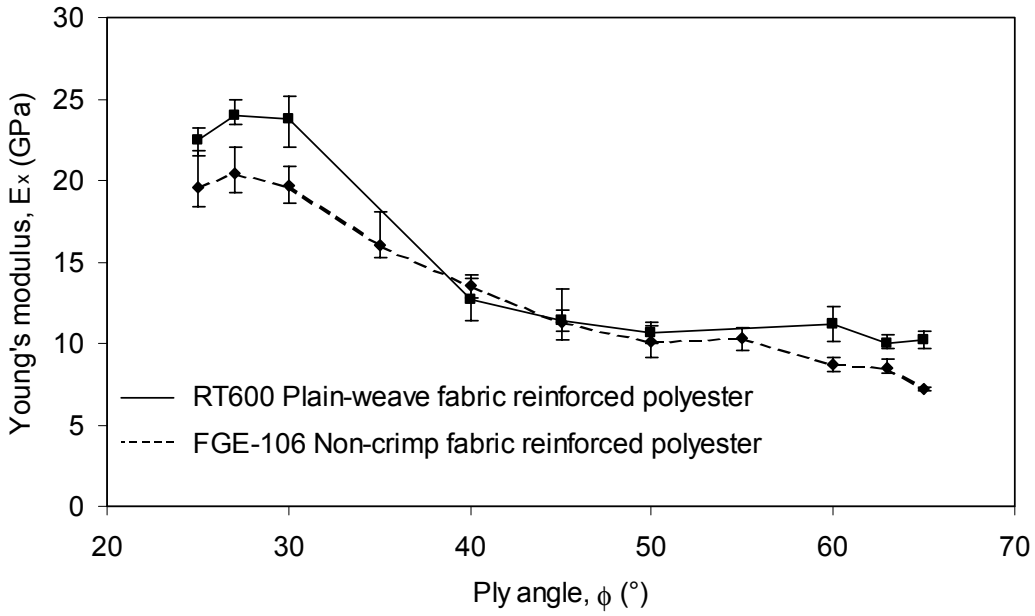

Figure 4.12 Summary data of Young's moduli, E_x, obtained from tensile testing of angle-ply laminates manufactured from both non-crimp and woven fabric reinforcements. Error bars indicate maximum and minimum individual values obtained from four repeat specimens for each value (except ±45°, 8 specimens, and RT600 ±25°, 7 specimens).

Since transverse strain gauges were mounted on the specimens, it was possible to calculate the Poisson's ratio, ν_{xy}, using Equation 3.5. Results of this calculation are given in Figure 4.13. The spread in Poisson's ratio values is very large in some cases: up to 60% of the average value (FGE-106 ±35°), although it is more typically 20%-30% of the average. Nonetheless, a distinct trend in values of ν_{xy} can be observed, with values dropping consistently with increasing ply angle in the range $40° < \phi < 65°$; an increase in values of ν_{xy} with increasing ply angle is apparent in the range $25° < \phi < 40°$, although this portion of the data exhibits greater variation so this may not be a true effect.

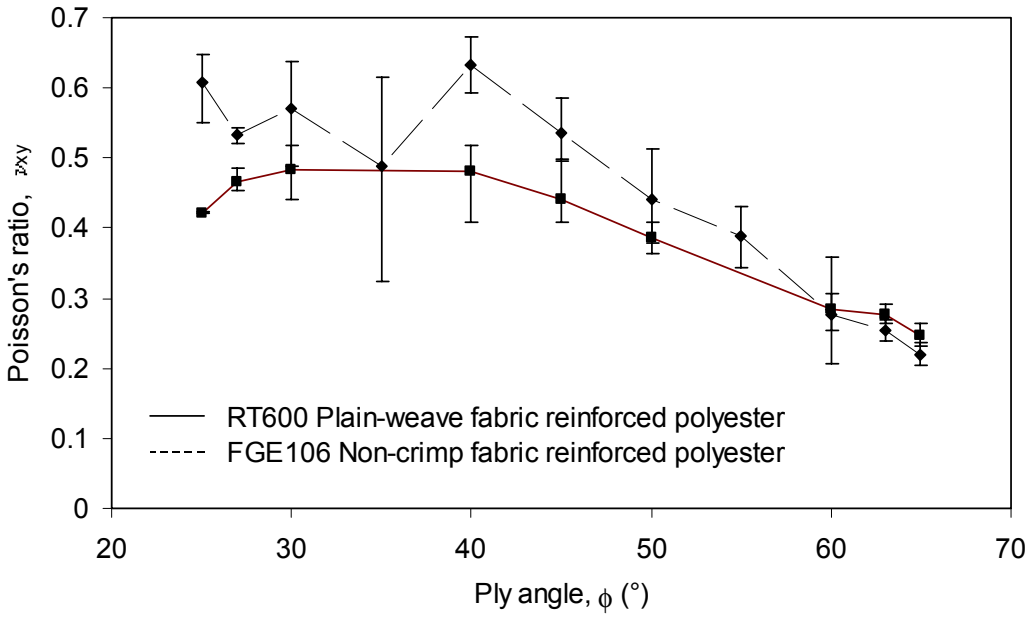

Figure 4.13 Summary data of Poisson's ratio, ν_{xy}, obtained from tensile testing of angle-ply laminates manufactured from both non-crimp and woven fabric reinforcements. Error bars indicate maximum and minimum individual values obtained from four repeat specimens for each value (except ±45°, 8 specimens, FGE-106 ±40°, 3 specimens, RT600 ±25°, 2 specimens, and RT600 ±65°, 3 specimens).

The maximum stress supported by each specimen is summarised in Figure 4.14. While this is a useful indication of the failure stress for specimens exhibiting near-linear stress-strain behaviour such as that denoted type d (Table 4.3), its value for specimens with type a, b or c behaviour is limited, since visible cracking had occurred at stresses below the maximum, after which an engineering component would be taken out of service. Since all specimens were tested to ultimate displacement, attempts to characterise the failure mode by examination of the failed specimens did not yield any significant findings, suggesting that examination of the

recorded stress-strain behaviour was more useful. It can be observed from Figure 4.15 that the ultimate stress occurred at high strains for ply angles in the range $40°<\phi<50°$, which is indicative of the stress-strain behaviour denoted by type c in Figure 4.11, where the stress continued to rise after an obvious onset of failure. It was noted during testing that a large amount of matrix cracking developed throughout these specimens before final failure to support a load occurred. As a result of this phenomenon, the 0.2% proof stress technique has been used to determine a consistent maximum design stress, at which initial failure is deemed to have occurred. This treatment was originally devised for metals where no clear yield point could be determined, and remains a value frequently quoted in materials databases. The use of this technique is recommended in ASTM D3518-94, which outlines procedures for evaluation of shear behaviour using ±45° bias tensile testing. Although the test described therein is not identical to the work presented in this section (since the ASTM standard only refers to ±45° laminates and shear stresses and strains, while this work refers to general angle-ply laminates and direct engineering quantities), the nature of the stress-strain behaviour is similar. Figure 4.16 shows a typical application of this technique to a ±45° laminate tested within this study, which serves to recommend its use in such cases since the 0.2% proof stress falls immediately before the 'knee' in the stress-strain curve. The proof stress is obtained by finding the intersection of a straight line, having a gradient=E_x and intersecting the x axis at ε=0.2%, with the stress-strain curve. The coordinates of this point indicate the 0.2% proof stress and the corresponding strain. This method has been implemented numerically using the raw experimental data within a spreadsheet. Where the offset line did not have an intersection with the stress-strain curve, the maximum stress value was used.

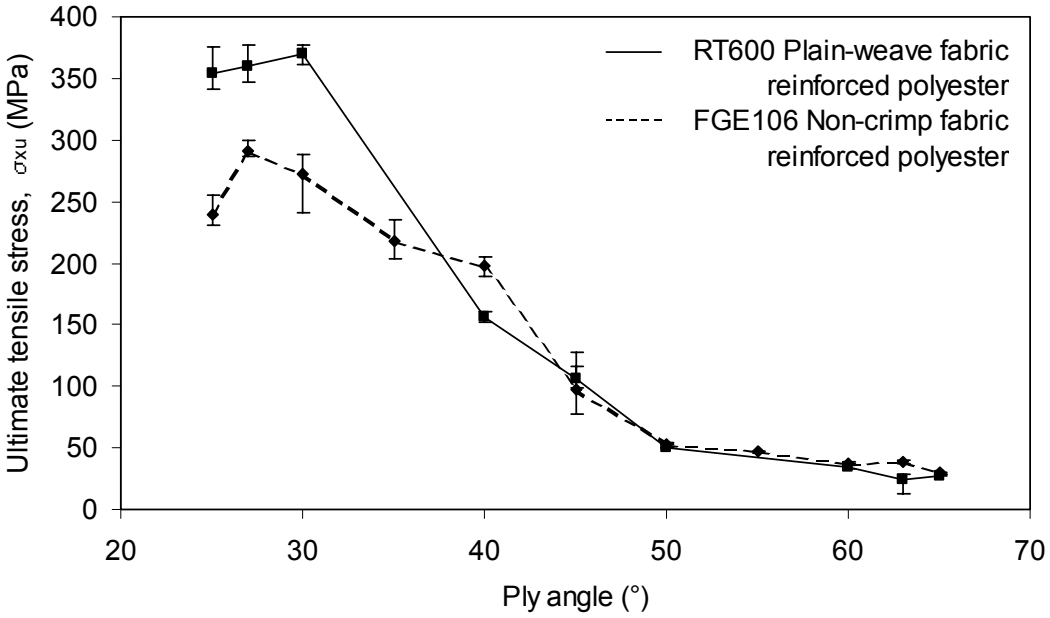

Figure 4.14 Summary data of ultimate tensile stress, σ_{xu}, obtained from tensile testing of angle-ply laminates manufactured from both non-crimp and woven fabric reinforcements. Error bars indicate maximum and minimum individual values obtained from four repeat specimens for each value (except ±45°, 8 specimens, and RT600 ±25°, 7 specimens).

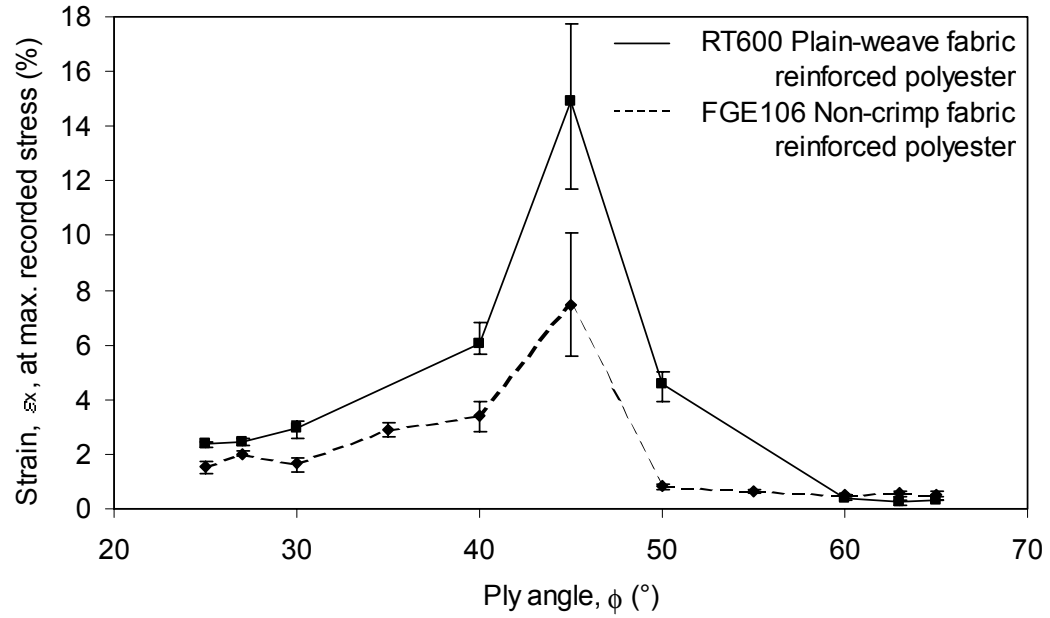

Figure 4.15 Summary data of recorded extensometer strain, ε_x, at the maximum stress level observed during tensile testing of angle-ply laminates manufactured from both non-crimp and woven fabric reinforcements. Error bars indicate maximum and minimum individual values obtained from four repeat specimens for each value (except ±45°, 8 specimens, and RT600 ±25°, 7 specimens).

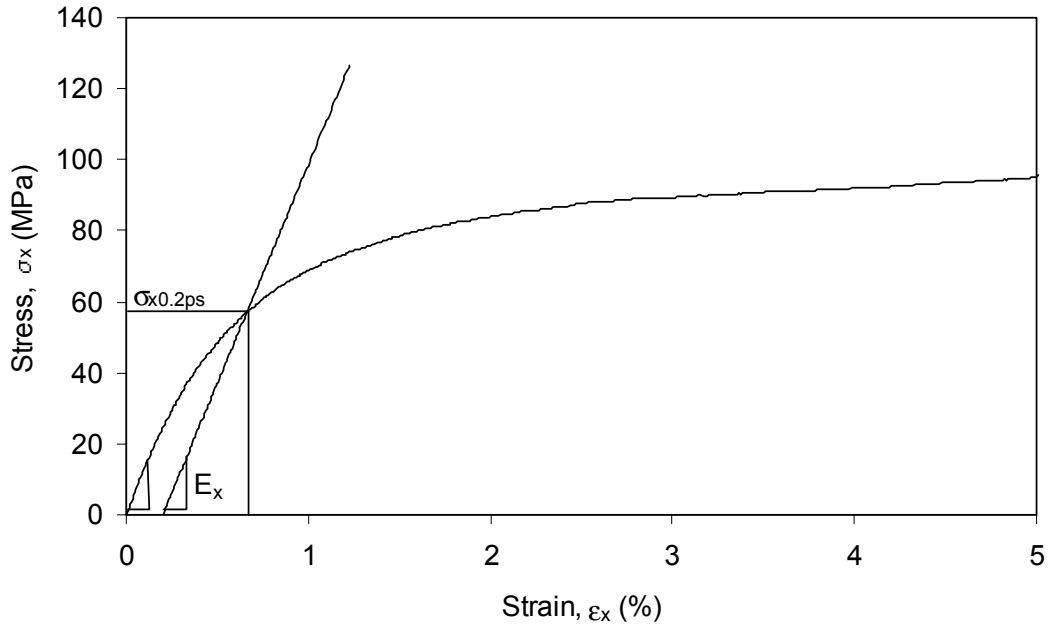

Figure 4.16 Stress-strain behaviour of RT600 ±45° specimen showing the intersection of the 0.2% strain offset line used to determine the 0.2% proof stress (Figure 4.17), and the corresponding strain (Figure 4.18).

As expected from the nature of the method, the 0.2% proof stress is significantly lower than the ultimate tensile stress for specimens where $\phi<50°$. These specimens all exhibited non-linear stress-strain behaviour. Conversely, for $\phi\geq50°$, the 0.2% proof stress is very similar to the ultimate tensile stress, due to the linear stress-strain behaviour coupled with sudden failure. Proof stress data are compared with UTS data in Figure 4.17. It should also be noted that, in general, the spread of proof stress data is slightly smaller than that observed in UTS values. It is evident from the difference between the UTS values for woven and NCF laminates that the woven materials were able to support a greater load; however, the 0.2% proof stress values for the two materials are very similar. As for Young's modulus, the models described in Section 2.4.3 predict that woven fabric reinforced materials have a lower initial failure stress than NCF laminates. This suggests that, although the onset of failure may not depend significantly on the architecture of the reinforcement, the post-failure behaviour of the plain weave reinforced laminates was substantially better than that of those reinforced with NCF, perhaps due to the resistance to delamination caused by the interwoven nature of the tows. This idea is corroborated by the recorded strains at the 0.2% proof stress and UTS, which are reported in Figure 4.18, since the woven fabric reinforced laminates reached higher strains (at UTS) than the NCF laminates. It is evident that the proof stress technique reports

lower strains to failure than the maximum stress approach for specimens where $\phi<50°$. More significantly, the large peak in the range $40°\leq\phi\leq50°$ is removed using this method, giving a more physically realistic strain to failure.

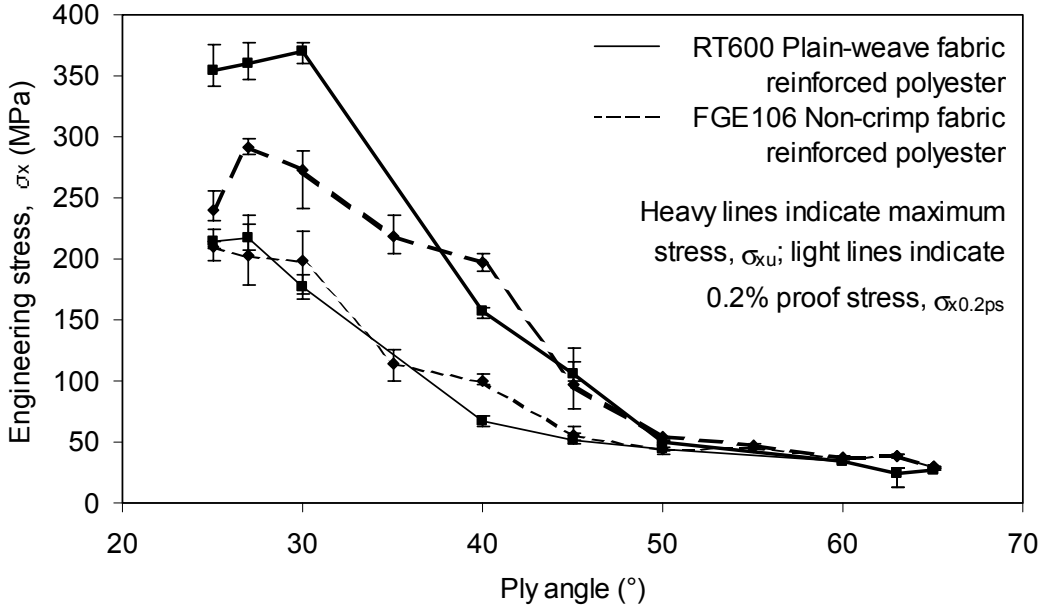

Figure 4.17 Summary data of the stress level at the onset of failure, $\sigma_{x0.2ps}$, determined using the 0.2% proof stress technique on stress-strain curves obtained from tensile testing of angle-ply laminates manufactured from both non-crimp and woven fabric reinforcements, and compared with the maximum observed stress. Error bars indicate maximum and minimum individual values obtained from four repeat specimens for each value (except ±45°, 8 specimens, and RT600 ±25°, 7 specimens).

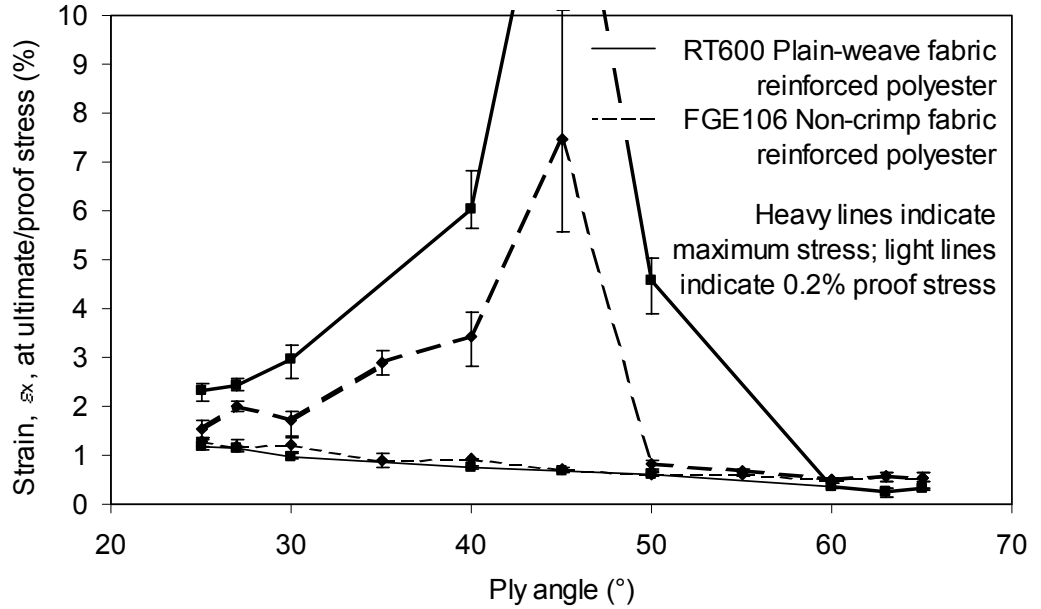

Figure 4.18 Summary data of recorded extensometer strain, ε_x, at the onset of failure (determined using the 0.2% proof stress) compared with that at the maximum observed stress during tensile testing of angle-ply laminates manufactured from both non-crimp and woven fabric reinforcements. Error bars indicate maximum and minimum individual values obtained from four repeat specimens for each value (except ±45°, 8 specimens, and RT600 ±25°, 7 specimens).

4.4 Jet engine nose cone

4.4.1 Introduction

In order to examine the effect of reinforcement deformation during forming on the mechanical behaviour of a three-dimensional component, a jet engine nose cone tool was used to manufacture cones from EBX hd 936 non-crimp fabric and U101-220 continuous filament random mat reinforcements, with Norpol 440M-750 polyester resin using the RTM process. All layers of textile reinforcement were formed over the male tool by hand, without darting, and placed at the same orientation. The manufacturing process is described in detail in Section 3.3.3.

4.4.2 Testing under a diametric pinching load

The component was tested under a diametric pinching load, applied using custom-made curved jaws mounted in a universal testing machine. Tests were performed to a small displacement (initially 1 mm) before removing the load and rotating the component through 30° about its symmetry axis. Once six tests had been performed, the component was returned to its initial position and the procedure was repeated to a higher displacement. This was repeated in 1 mm increments up to 4 mm displacement. The testing procedure is detailed in Section 3.4.3.

It can be seen from Figure 4.19 that the force required to produce a given displacement reduced for each set of tests. This suggests that some form of damage occurred within the material during testing, causing its stiffness to reduce. There were no significant features in the force-displacement curves which indicated any specific occurrence of failure or damage. Because of this, results presented in Figure 4.20, which show the force required to produce a 1 mm displacement, were all taken from the first series of tests in order to minimise the potential impact of these effects on the results.

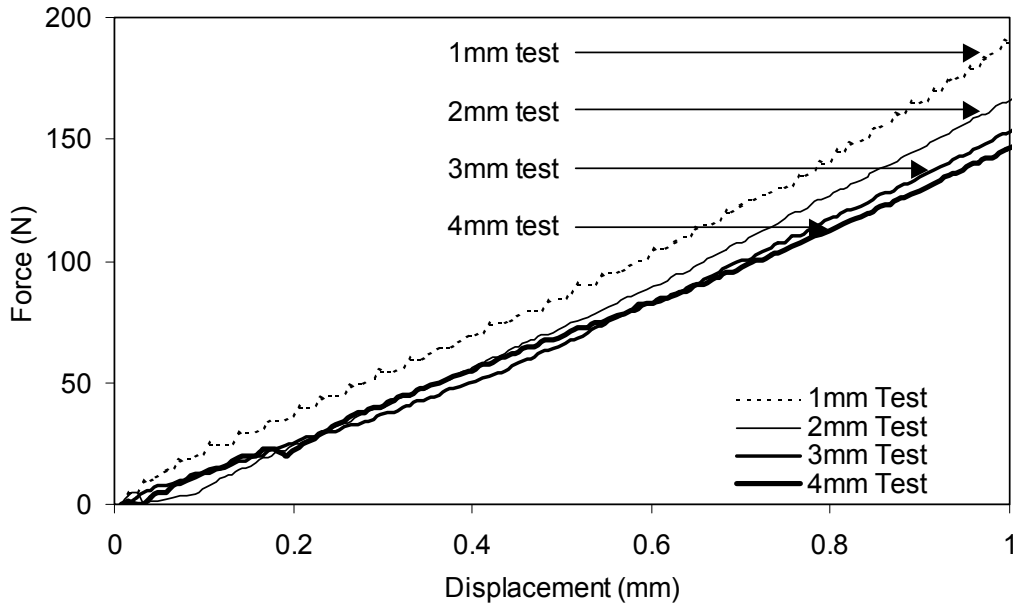

Figure 4.19 Force-displacement behaviour of the jet engine nose cone at the same orientation, but in a series of tests which were undertaken to different ultimate displacements. This shows that some form of damage caused the component to become more compliant in later tests.

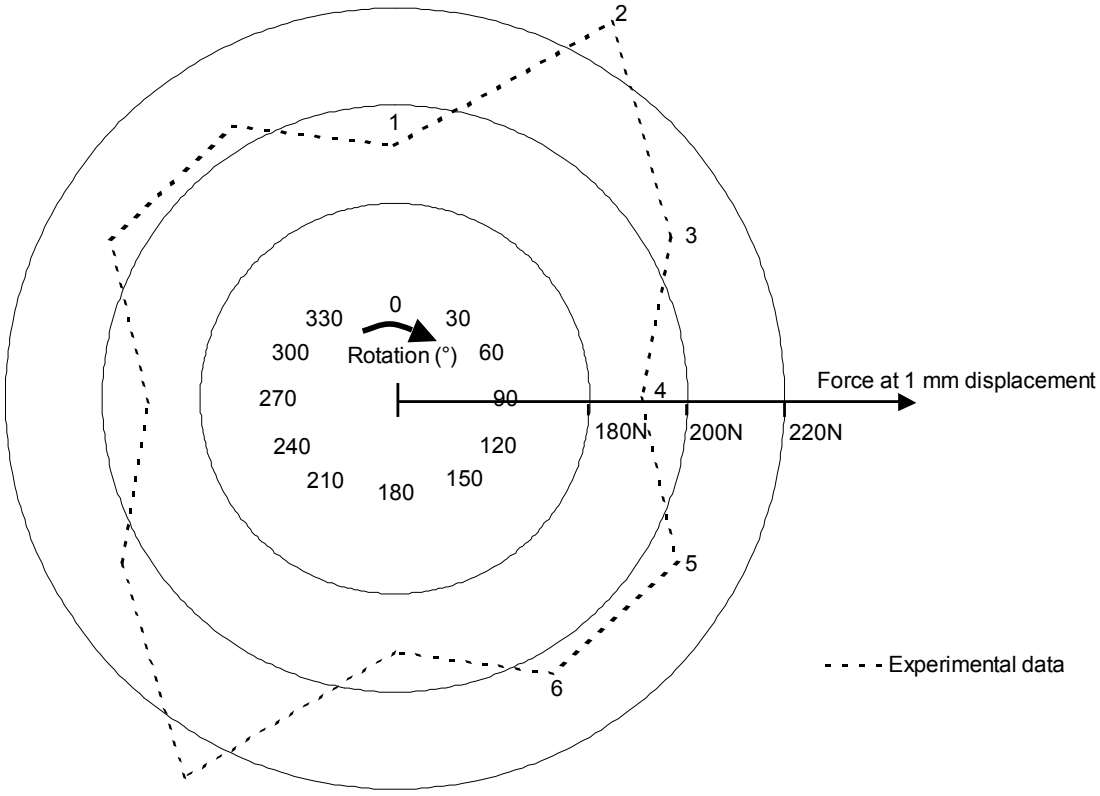

Figure 4.20 Force required to produce 1 mm displacement across the diameter of the jet engine nose cone at different points around the geometry, which shows the non-uniformity of the mechanical response of the component. Note that the scale does not begin at zero in the centre. Data labels indicate orientation number, defined in Figure 3.15.

The results presented in Figure 4.20 show that there was a significant difference in the elastic response of the nose cone as the pinching load was applied at different points around its circumference. Full data are tabulated in Appendix C. During the first set of tests (to 1 mm displacement), the maximum force required to produce 1mm displacement was 229 N, while the minimum was 191 N, indicating a change in stiffness across the component diameter of approximately 20%. Although this represents a significant change in behaviour, this non-uniformity is not usually considered in structural analysis of composite components, and the need to incorporate information about the reinforcement orientation and deformation into analysis procedures is highlighted by these results. Furthermore, the effect can be shown to be related to the reinforcement structure since the pattern remained the same in subsequent tests conducted to higher displacements, although the accumulation of damage caused the absolute values to be lower. The force required to produce 1mm displacement in each set of tests is reported in Figure 4.21.

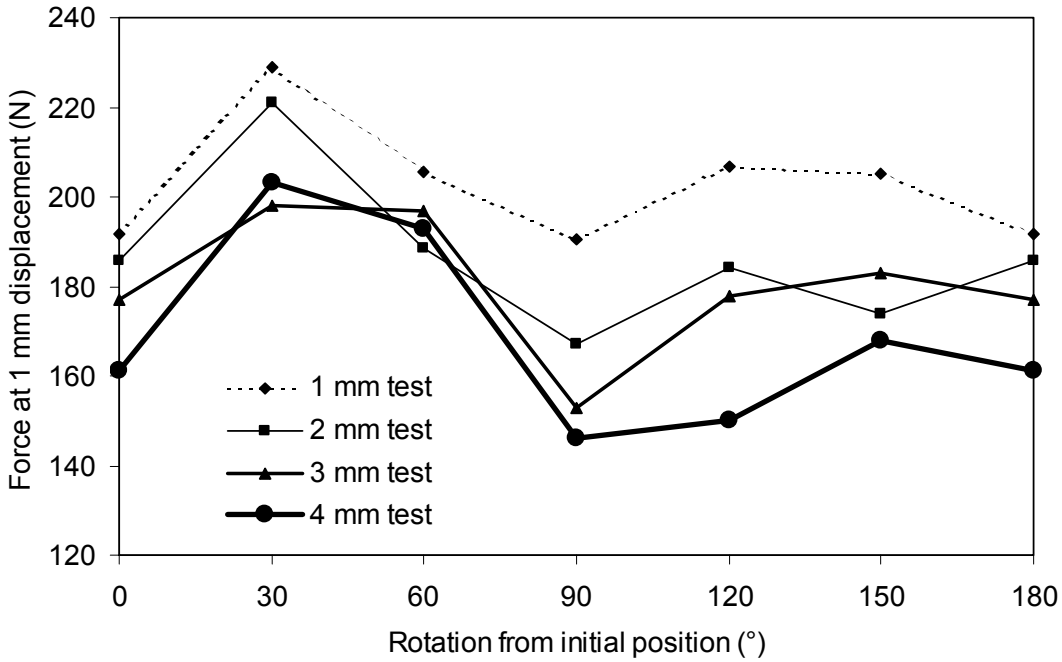

Figure 4.21 Force required to produce 1 mm displacement across the diameter of the jet engine nose cone at different points around the geometry in a series of tests which were undertaken to different ultimate displacements. This shows that some form of damage caused the component to become more compliant in later tests, but also that the trend in the component response remained the same.

4.5 Conclusions

Results of mechanical testing undertaken during the course of this work are presented. Unidirectional laminates were tested, showing the effect of fibre volume fraction on several properties: E_1, E_2, G_{12}, ν_{12}, σ_{1u}, σ_{2u} and τ_{12u}. In the range of fibre volume fractions tested ($34\%<V_f<42\%$) most properties (E_1, E_2, G_{12}, σ_{1u}, and σ_{2u}) were seen to increase with increasing V_f, as expected in most cases, although Poisson's ratio, ν_{12}, and shear strength, τ_{12u}, appeared to remain approximately constant. Tensile testing was also performed on angle-ply laminates manufactured from both non-crimp and woven fabric reinforcements. Tests were performed in the bias direction, providing values for E_x, ν_{xy}, σ_{xu} and ε_{xu} as a function of the off-axis angle (ply angle), ϕ. Non-linear behaviour was observed in some specimens, making the determination of the onset of failure difficult and making the value of σ_{xu} unsuitable for design calculations. In these cases, the 0.2% offset proof stress was calculated in order to approximate the stress and strain at initial failure, $\sigma_{x0.2ps}$ and $\varepsilon_{x0.2ps}$, respectively. These data are also presented. Proof stresses for laminates where $\phi\leq45°$ were lower than the reported UTS values, although the trends remained the same. In general, both E_x and $\sigma_{x0.2ps}$ decreased as ϕ increased; Poisson's ratio, ν_{xy}, appeared to have a maximum value when $\phi=40°$, and decreased as ply angle deviated from this. The strain at UTS exhibited a large peak for specimens where $40°\leq\phi\leq50°$ due to their continued ability to support a load after significant inelastic deformation. This feature was not present in $\varepsilon_{0.2ps}$ data. This is of particular relevance to the design community for applications such as pipes and pressure vessels, where it is essential that component integrity is maintained after initial failure so that catastrophic failure does not occur (this is known as the leak-before-break condition). The 0.2% proof stress has been shown to give more suitable strength data for design calculations where the onset of failure must be prevented.

A conical component was manufactured from textile reinforcement and tested under a diametric pinch loading at different positions around its circumference. Results of these tests are presented and show a significant non-uniformity in the elastic response of the component which is thought to be caused by the deformation and re-orientation of the reinforcement during forming.

Models to describe the mechanical behaviour of such composites are presented in Chapter 2, and details of their application to the problems considered in this chapter are discussed in Chapter 5. Unidirectional materials are discussed first, and the appropriate stages involved in calculating response of three-dimensional components manufactured from textile reinforced composites are described subsequently.

5 MODELLING STRATEGIES FOR TEXTILE COMPOSITE MECHANICAL BEHAVIOUR

5.1 Introduction

In this chapter a description is given of the methods used to apply some of the models introduced in Chapter 2 to the experimental situations described in Chapter 4 in order to predict the elastic and failure behaviour of composite components, and to develop or extend these models where necessary. Starting with the building block of unidirectional composite, material models are described and evaluated with consideration of the experimental data presented in Chapter 4. The application of classical laminate theory (CLT) to angle-ply laminates is described and, through the use of a failure criterion, predictions of both stiffness and strength of angle-ply laminates are presented using this theory. Once again, results are compared with experimental observations. Comparisons are also made with predictions made with layered shell finite elements. A simple model for woven fabric laminates is implemented and extended to consider failure behaviour, and the potential effects of tow waviness on composite stiffness and strength are discussed. Finally, a computer based kinematic draping simulation is used to determine fibre orientations to enable implementation of the models described for application to real composite components, considering the effects of reinforcement deformation on fibre orientation and volume fraction, using finite element analysis. In order to make predictions of the behaviour of the jet engine nose cone described in Section 4.4.2, a simple compaction model is also implemented to account for the change in relative layer thicknesses of CFRM and NCF reinforcements. The models described are implemented into the draping software, providing an integrated method for the production of finite element analysis input files for predictive modelling of component mechanical behaviour.

The methods used in the implementation of the models are presented in addition to the underlying assumptions. Results predicted by the models are compared with those obtained by experimental measurement at each stage and possible reasons for discrepancies are discussed.

5.2 Micromechanics prediction of UD composite mechanical properties

As discussed in Chapter 2, if textile reinforced composites are to be represented as layers, or laminae, of orthotropic unidirectional material, then the first steps involved in the modelling process involve the calculation of the mechanical properties of the unidirectional materials. This has been undertaken using micromechanics models. It should be noted that, as a result of material symmetry, $E_2 = E_3$, $G_{12} = G_{13}$, $\sigma_{2u} = \sigma_{3u}$ and $\tau_{12u} = \tau_{13u}$. Calculated properties were based on Norpol 420-100 resin, except where stated otherwise. Material properties used for the constituent phases are given in Table 3.2.

5.2.1 Elastic behaviour

The rule of mixtures (Equations 2.1 and 2.2) was used to calculate the longitudinal Young's modulus, E_1, and the Poisson's ratio, ν_{12}, of the lamina. Linear relationships between these properties and fibre volume fraction were predicted, evident from the form of the equations. Predictions are compared with experimental data in Figure 5.1 (E_1) and Figure 5.2 (ν_{12}). It was assumed that $\nu_{12} = \nu_{13} = \nu_{23}$. Young's modulus values obtained using this method show excellent agreement with experimental data, falling within the bounds of the error bars in all cases. Predictions of Poisson's ratio are somewhat lower than experimental values. Typical published values of ν_m for thermosetting polyester resins are in the region of 0.35, whereas the value provided by the resin manufacturer was 0.26. Using the former value would have provided an excellent fit with experimental data, but this cannot be justified without further experimental characterisation of the pure resin.

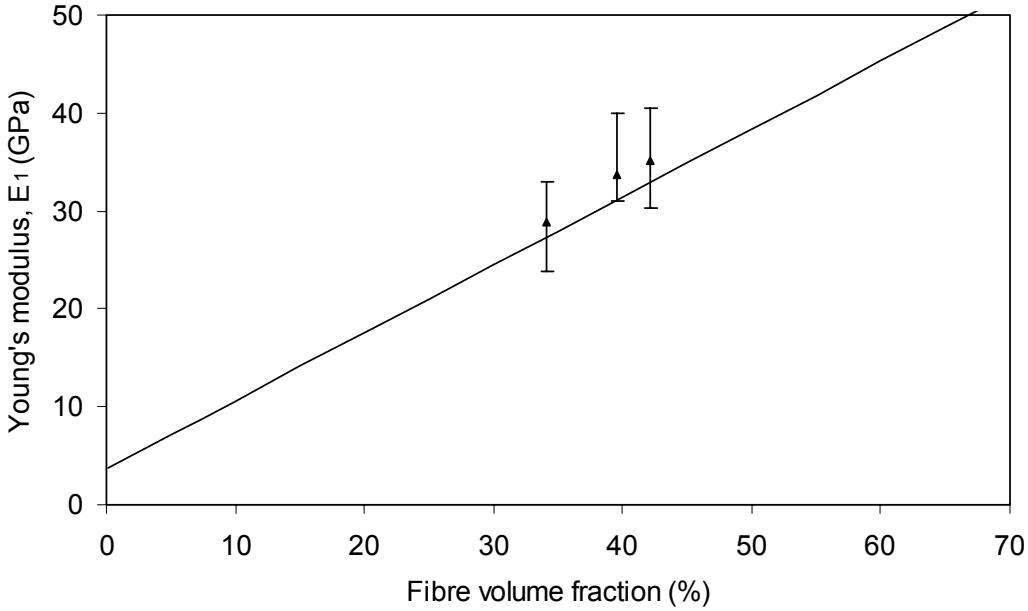

Figure 5.1 Prediction of Young's modulus, E_1, made using the rule of mixtures (solid line) plotted with experimental data (points). Error bars show maximum and minimum values obtained during experimental testing.

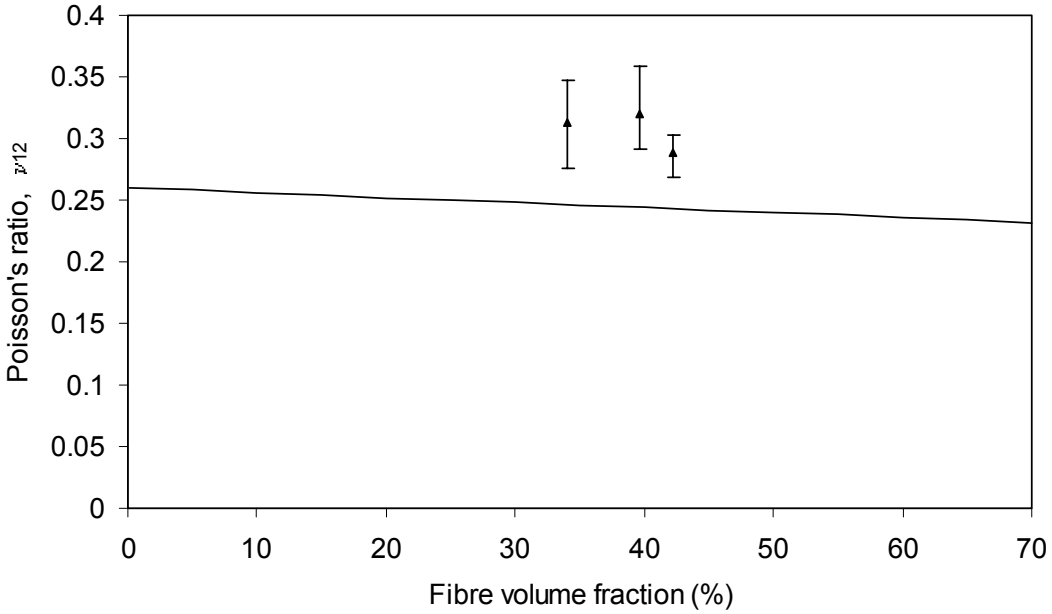

Figure 5.2 Prediction of Poisson's ratio, ν_{12}, made using the rule of mixtures (solid line) plotted with experimental data (points). Error bars show maximum and minimum values obtained during experimental testing.

To predict the Young's modulus of unidirectional composites in the transverse direction, E_2, and the in-plane shear modulus, G_{12}, the Halpin-Tsai relationship (Equations 2.4 and 2.5) was used. The parameter, ξ, was assumed to have a value of 2 when calculating E_2, and a value of 1 when calculating G_{12}, as suggested by Daniel

and Ishai [29]. Shear moduli of the isotropic constituent phases were calculated using the well known relationship in Equation 5.1.

$$G_{12} = \frac{E}{2(1+\nu_{12})} \tag{5.1}$$

Predictions from these equations did not exhibit linear relationships with V_f, as observed in Figure 5.3 (E_2) and Figure 5.4 (G_{12}), where they are compared with experimental data. Calculated values of E_2 exhibited reasonable agreement with experiment, falling around 10% lower than the average experimental values at the first two points, but 27% below the average experimental value for $V_f = 42.2\%$. Although a better fit could have been obtained by using a higher value of ξ, the intended goal of a purely predictive modelling route, using published approximations where necessary, discouraged the use of a posteriori empirical constants. For G_{12}, good agreement between predictions and experiment was observed, with predicted values falling within the bounds of the error bars for some of the experimental measurements.

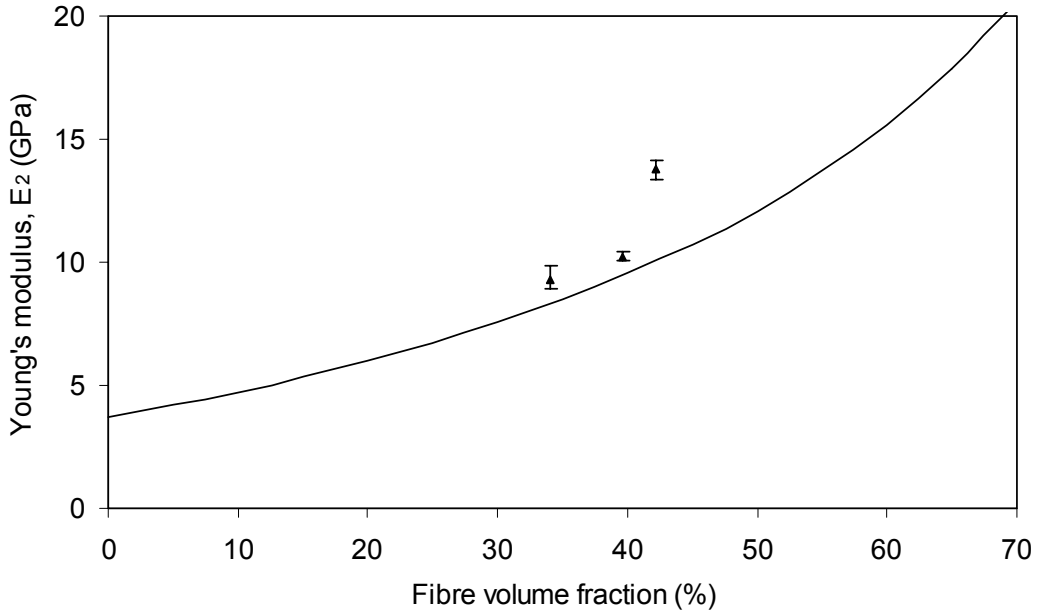

Figure 5.3 Prediction of transverse Young's modulus, E_2, made using the Halpin-Tsai equations (solid line) plotted with experimental data (points). Error bars show maximum and minimum values obtained during experimental testing.

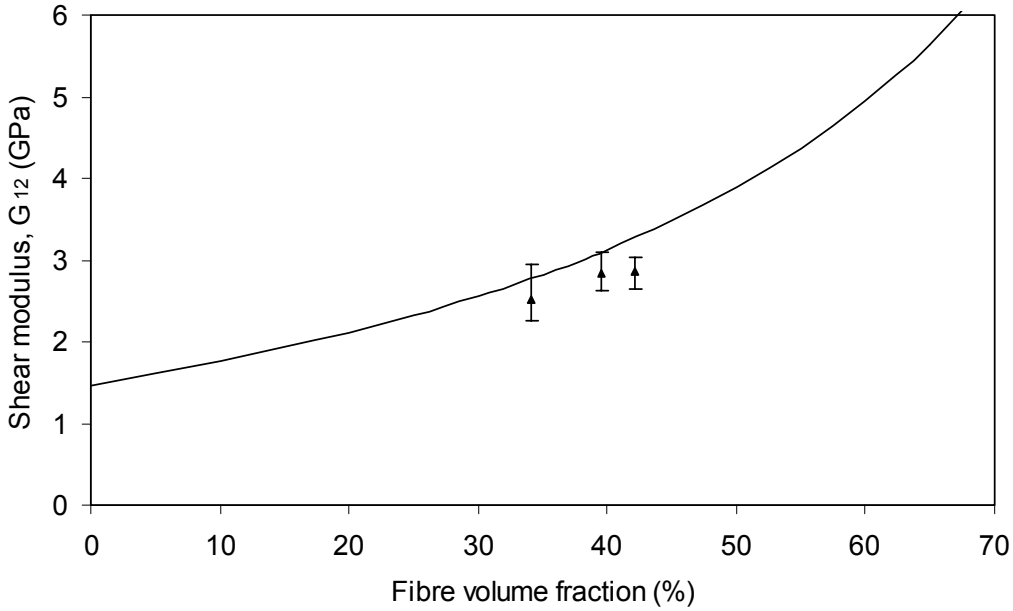

Figure 5.4 Predictions of in-plane shear modulus, G_{12}, made using the Halpin-Tsai equations (solid line) plotted with experimental data (points). Error bars show maximum and minimum values obtained during experimental testing.

5.2.2 Strength of the lamina

As discussed in Section 2.2.3, the strength of a lamina in the direction of the reinforcement fibres, σ_{1u}, was assumed to be proportional to the fibre volume fraction, according to Equation 2.6, since $\sigma_{fu} >> \sigma_{mu}$. The resulting prediction of σ_{1u} with respect to V_f is presented in Figure 5.5 with comparable experimental data. It is evident that experimental values were significantly lower than predictions, the difference being 26%-30%. A close fit would have been obtained if it was assumed that σ_{fu} = 1400 MPa, but there was no precedent for this assumption, and the range of fibre volume fractions in the experimental data was too small to justify fitting the curve in such a manner. More fundamental reasons for avoiding empirical fitting were discussed in Section 5.2.1. Various physical phenomena were neglected in the models used for lamina strength, including the effects of resin shrinkage after curing, the presence of voids and the effects of the stitching on the distribution of fibres, which was assumed to be regular. Though these parameters may be expected to affect the transverse strength, their effect on axial strength was not expected to be significant. However, fibre misalignment would be expected to affect axial strength values significantly, with small deviations from the loading direction giving rise to large changes in strength. This may occur globally, if specimens are cut slightly off-

axis, or locally due to in-plane fibre waviness. Although this was not measured in the experimental specimens, it is anticipated that this would be the most likely cause for the discrepancies observed, assuming that the failure stress of the fibres was close to the published value used (in Table 3.2).

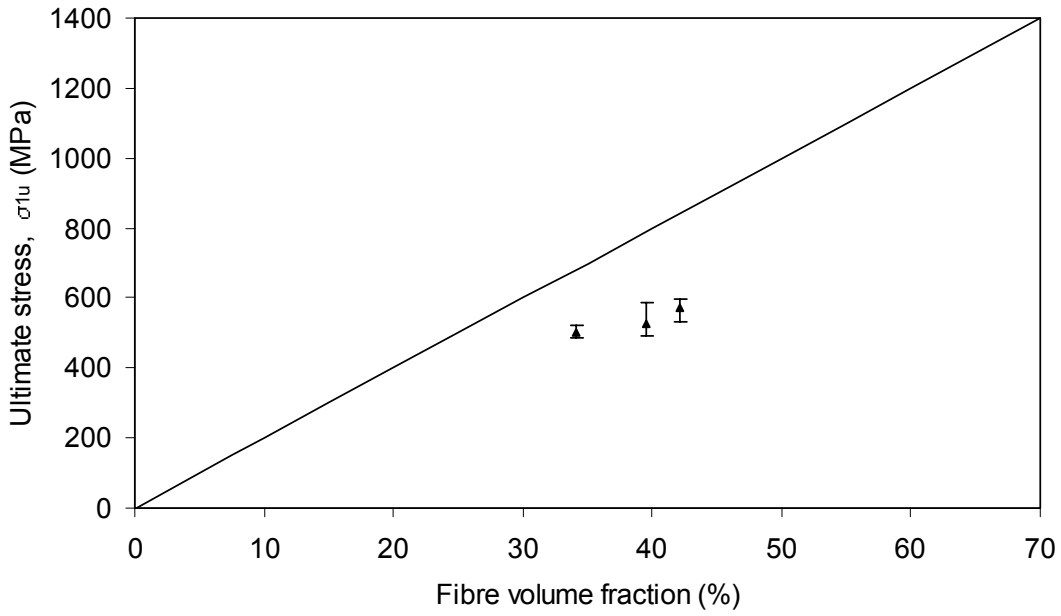

Figure 5.5 Predictions of on-axis strength, σ_{1u}, made using Equation 2.6 (solid line) plotted with experimental data (points). Error bars show maximum and minimum values obtained during experimental testing.

Prediction of failure under transverse loading was undertaken using a modification to the model proposed by Kies [36], discussed in Section 2.2.3. Simplifying the random packing arrangement of fibres found in real composites, Kies assumed that the fibres were distributed in a square-packed array within the composite to develop the relationship between global and local maximum strains within the material, described by Equation 5.2.

$$k_{\varepsilon 2} = \frac{\varepsilon_{\max}}{\varepsilon_2} = \frac{1}{\frac{2r_f}{s_f}\left[\frac{E_m}{E_f} - 1\right] + 1} \tag{5.2}$$

where $k_{\varepsilon 2}$ is the strain concentration factor relating the average transverse strain, ε_2 to the peak local strain, ε_{max}; r_f is the fibre diameter and s_f is the fibre spacing, or pitch.

If the fibre diameter is known, then the relationship between fibre spacing and volume fraction can be expressed by Equation 5.3. Fibre diameter was assumed to be 15.8 μm.

$$s_f = 2r_f + \frac{\sqrt{\pi r_f^2} - 2r_f\sqrt{V_f}}{\sqrt{V_f}} \tag{5.3}$$

The stress concentration factor, $k_{\sigma 2}$, relates global and local stresses according to Equation 5.4.

$$k_{\sigma 2} = \frac{\sigma_{\max}}{\sigma_2} \tag{5.4}$$

Since the factor is used to determine maximum stress occurring in the matrix region, Equation 5.4 can be written:

$$k_{\sigma 2} = \frac{E_m \varepsilon_{\max}}{E_2 \varepsilon_2} \tag{5.5}$$

where E_2 is the transverse Young's modulus of the composite

Incorporating the relationship in Equation 5.2 yields:

$$k_{\sigma 2} = \left(\frac{E_m}{E_2}\right) k_{\varepsilon 2} = \frac{E_m}{E_2\left(\frac{2r_f}{s_f}\left[\frac{E_m}{E_f} - 1\right] + 1\right)} \tag{5.6}$$

Hence, the failure stress of the composite can be found using Equation 5.7:

$$\sigma_{2u} = \frac{\sigma_{mu}}{k_{\sigma 2}} = \sigma_{mu}\left(\frac{E_2}{E_m}\right)\left(\frac{2r_f}{s_f}\left[\frac{E_m}{E_f} - 1\right] + 1\right) \tag{5.7}$$

This neglects the effect of any residual stresses in the resin, so may be expected to overestimate the transverse tensile strength. Where residual stresses are known, however, they may be incorporated into the expression as in Equation 5.8.

$$\sigma_{2u} = \left(\sigma_{mu} - \sigma_{rm}\right)\left(\frac{E_2}{E_m}\right)\left(\frac{2r_f}{s_f}\left[\frac{E_m}{E_f} - 1\right] + 1\right) \tag{5.8}$$

where σ_{rm} is the residual stress in the matrix.

The effect of fibre volume fraction on transverse strength according to Equation 5.7 is shown in Figure 5.6. Experimentally determined values for transverse strength were 30%-45% lower than predicted values using the approach described. This may indicate that the problem is dominated not by resin failure, but by crack initiation at the fibre/matrix interface. Another factor contributing to the discrepancy may be that the lamina is composed of bundles of fibres in which the local fibre volume fraction is greater than the average volume fraction of the composite, whereas the micromechanics approaches all assume that fibres are evenly distributed. It may be perceived that the controlling factor in this case would be the maximum local volume fraction within the specimen being tested. This is investigated in more detail in Chapter 6, where the potential effects of reinforcement architecture on transverse behaviour are evaluated using finite element analysis. Perhaps more significantly, residual stresses due to resin shrinkage have been assumed to be negligible. Since unsaturated polyester resins usually experience significant shrinkage due to the curing process (typically 5-7%), this assumption may be the primary cause of the difference between experiment and predictions, and remains an area for further investigation. Similarly, void contents of the samples were not measured, although laminates were highly transparent which suggested that void content was low. The effects of voids on the mechanical behaviour were neglected, which also presents an opportunity for further study.

The same model is used to predict transverse shear strength, τ_{23u}, according to Equation 5.9, which is analogous to Equation 5.7.

$$\tau_{23u} = \frac{\tau_{mu}}{k_{\tau 23}} = \tau_{mu}\left(\frac{G_{23}}{G_m}\right)\left(\frac{2r_f}{s_f}\left[\frac{G_m}{G_f}-1\right]+1\right) \tag{5.9}$$

where $k_{\tau 23}$ is the shear stress concentration factor.

Following a number of authors (e.g. [160-162]), the Tresca isotropic yield criterion was used to determine the matrix shear strength, τ_{mu}, according to Equation 5.10.

$$\tau_{mu} = \sigma_{mt}\left(\frac{\sigma_{mc}}{\sigma_{mt} + \sigma_{mc}}\right) \tag{5.10}$$

where τ_{mu} is the matrix shear strength, σ_{mt} is the matrix tensile strength and σ_{mc} is the matrix compressive strength.

Due to the brittle nature of the polyester resin used, the matrix strength in compression was assumed to be twice the tensile strength, based on approximations made from published experimental data [e.g. 39,150,163]. When $\sigma_{mc} = 2\sigma_{mt}$ the expression for shear strength reduces to Equation 5.11.

$$\tau_{mu} = \frac{2}{3}\sigma_{mt} \tag{5.11}$$

Predicted values of transverse shear strength are presented in Figure 5.7. Since no experimental characterisation of transverse shear response was performed, no validation of this model has been made, although it should be noted that this strength value was only used in the studies of unit cells presented in Chapter 6, and that transverse shear stresses did not approach the predicted strengths.

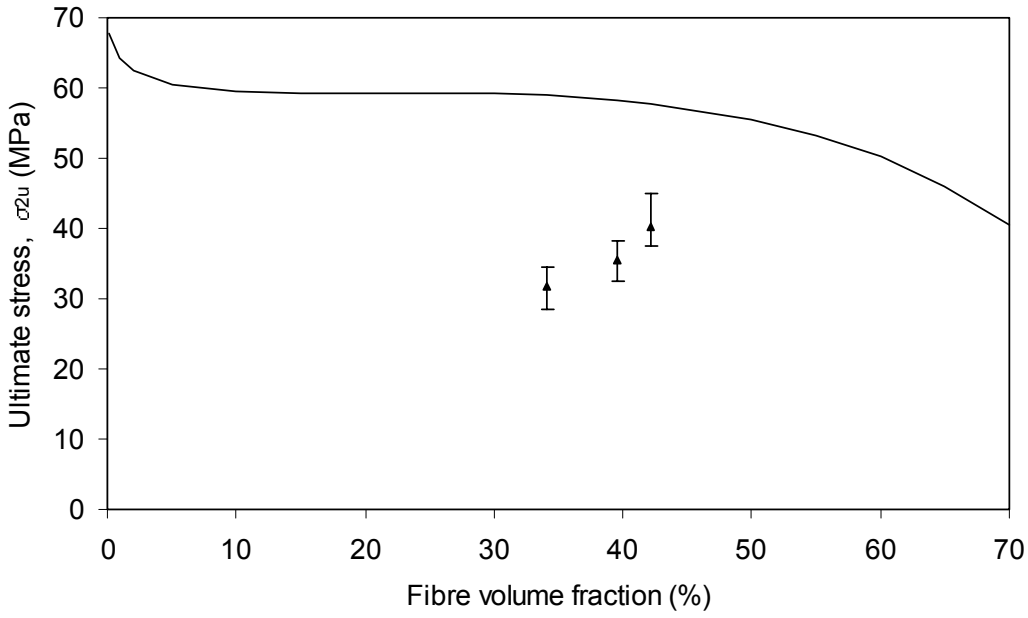

Figure 5.6 Predictions of transverse strength, σ_{2u}, made using the strain concentration model proposed by Kies [36], (solid line) plotted with experimental data (points). Error bars show maximum and minimum values obtained during experimental testing.

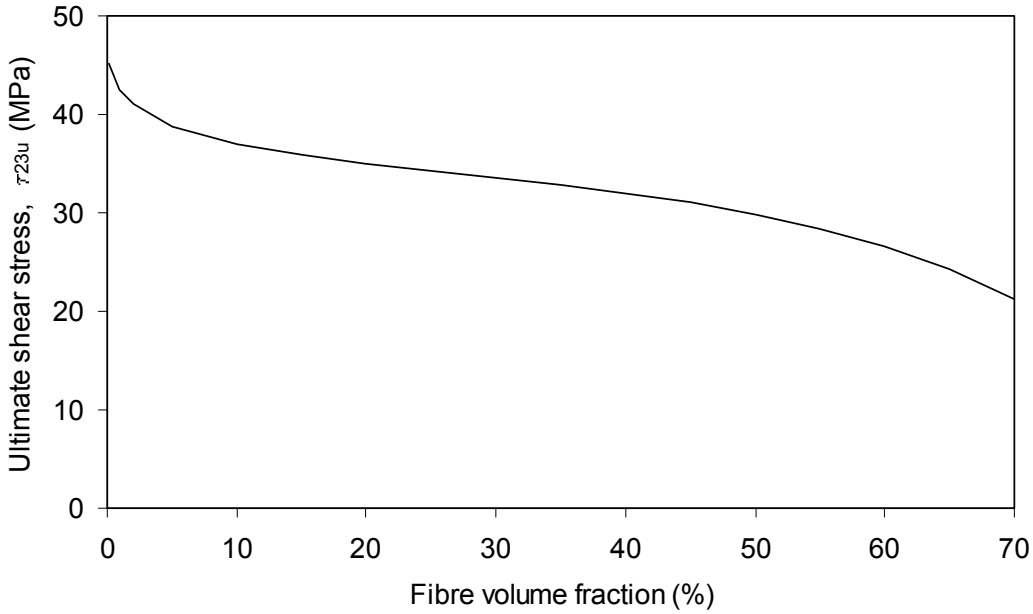

Figure 5.7 Predictions of transverse shear strength, τ_{23u}, made using the strain concentration model proposed by Kies [36]. No comparable experimental measurements were made.

Although Kies states in his report that it is also applicable for τ_{12u}, experimental data published as part of the World Wide Failure Exercise (WWFE) showed that values of τ_{12u} of the UD laminae tested were higher than those of the base resins [39], contradicting predictions from this model. In the absence of a reliable micromechanics model for the in-plane shear strength, and noting the small deviation observed in the experimental data within the range of fibre volume fractions characterised in Section 4.2.4, it was assumed that τ_{12u} held a constant value. Notwithstanding reservations expressed previously about the use of experimental data for predictive modelling, the average of the reported experimental values was used, i.e. $\tau_{12u} = 64.4$ MPa. This value is greater than the shear strength obtained for pure resin using Equation 5.11, notionally agreeing with published data [39].

5.3 Application of classical laminate theory for non-crimp fabric laminates

Classical laminate theory (CLT) has been implemented to facilitate predictions of mechanical behaviour of the angle-ply laminates tested. Using this theory elastic behaviour of multidirectional reinforced laminates can be predicted; stresses in the fibre directions of each layer can also be determined, enabling the incorporation of a failure criterion.

Since the non-crimp fabrics used in the experimental study are manufactured by stitching together discrete layers of unidirectional tows, it has been assumed that these layers behave as unidirectional laminae in the laminate. Hence for a laminate made from four layers of bi-directional fabric, eight laminae are present. For a thin lamina with orthotropic symmetry in a plane stress state, i.e. $\sigma_3 = \tau_{23} = \tau_{31} = 0$, Equation 5.12 describes the elastic behaviour in terms of the lamina compliance matrix, [S].

$$\begin{bmatrix} \varepsilon_1 \\ \varepsilon_2 \\ \gamma_{12} \end{bmatrix} = \begin{bmatrix} S_{11} & S_{12} & 0 \\ S_{12} & S_{22} & 0 \\ 0 & 0 & S_{66} \end{bmatrix} \begin{bmatrix} \sigma_1 \\ \sigma_2 \\ \tau_{12} \end{bmatrix} \tag{5.12}$$

where

$$S_{11} = \frac{1}{E_1} \qquad S_{12} = -\frac{\nu_{12}}{E_1}$$

$$S_{22} = \frac{1}{E_2} \qquad S_{66} = \frac{1}{G_{12}}$$

Elastic properties of the unidirectional laminae were found using the micromechanics models described Section 5.2, incorporating the input data for the constituent phases given in Table 3.2. Properties were calculated for Norpol 420-100 resin containing 38% E-glass fibres by volume, in order to give predictions which were comparable to results of experimental testing. Properties calculated for the lamina are presented in Table 5.1.

Table 5.1 Mechanical properties for the unidirectional laminae employed for calculations using classical laminate theory.

Parameter	Value
Fibre volume fraction, V_f (%)	37.6
Young's modulus, E_1 (GPa)	29.8
Young's modulus, E_2 (GPa)	9.02
Poisson's ratio, ν_{12}	0.245
In-plane shear modulus, G_{12} (GPa)	2.99
Ultimate tensile strength, σ_{1u} (MPa)	752
Ultimate tensile strength, σ_{2u} (MPa)	58.5
Ultimate shear strength, τ_{12u} (MPa)	64.4

In order to determine the elastic response of the lamina to an in-plane load applied in an arbitrary direction, x, a transformation must be applied using an appropriate transformation matrix, [T], defined in Equation 5.13

$$[T]=\begin{bmatrix} c^2 & s^2 & 2cs \\ s^2 & c^2 & -2cs \\ -cs & cs & c^2-s^2 \end{bmatrix} \tag{5.13}$$

where c = cos ϕ and s = sin ϕ if ϕ is the angle between the fibre (1) direction and the reference or loading (x) direction.

This matrix was used to transform the stress components according to Equation 5.14, to determine stresses in the fibre directions from those in the loading direction.

$$\begin{bmatrix} \sigma_1 \\ \sigma_2 \\ \tau_{12} \end{bmatrix} = [T] \begin{bmatrix} \sigma_x \\ \sigma_y \\ \tau_{xy} \end{bmatrix} \tag{5.14}$$

Similarly, the modified transformation matrix, [T'], defined in Equation 5.15, was employed to transform the engineering strains from the loading axis system to the lamina axis system as in Equation 5.16.

$$[T']=\begin{bmatrix} c^2 & s^2 & cs \\ s^2 & c^2 & -cs \\ -2cs & 2cs & c^2-s^2 \end{bmatrix} \tag{5.15}$$

$$\begin{bmatrix} \varepsilon_1 \\ \varepsilon_2 \\ \gamma_{12} \end{bmatrix} = [T'] \begin{bmatrix} \varepsilon_x \\ \varepsilon_y \\ \gamma_{xy} \end{bmatrix} \tag{5.16}$$

To express the elastic behaviour of a lamina fully in terms of the stresses and strains in the loading direction, Equations 5.12-5.16 were combined, multiplying the matrices to form the transformed compliance matrix, $[\bar{S}]$, as indicated in Equation 5.17.

$$\begin{bmatrix} \varepsilon_x \\ \varepsilon_y \\ \gamma_{xy} \end{bmatrix} = [T']^{-1}[S][T] \begin{bmatrix} \sigma_x \\ \sigma_y \\ \tau_{xy} \end{bmatrix} = [\bar{S}] \begin{bmatrix} \sigma_x \\ \sigma_y \\ \tau_{xy} \end{bmatrix} \tag{5.17}$$

The lamina stiffness matrix, [C], is the inverse of the compliance matrix, [S], i.e. $[C] = [S]^{-1}$ and $[\bar{C}] = [\bar{S}]^{-1}$. This relationship was required when calculating the behaviour of a laminate, since this was performed by the summation of the stiffness matrices of the constituent laminae with respect to their thicknesses according to Equation 5.18. This expression yields the stiffness matrix for the laminate, $[\bar{C}_l]$, and depends on the assumption that plane sections normal to the laminate midplane remain normal and plane (i.e. the Kirchhoff constraint); hence for in-plane loads, the strain field is the same in all laminae and the laminae are perfectly bonded.

$$\bar{C}_{l(ij)} = \frac{\sum_{k=1}^{2n} (\bar{C}_{k(ij)} h_k)}{\sum_{k=1}^{2n} h_k} \tag{5.18}$$

where $\bar{C}_{l(ij)}$ are the components of the transformed laminate stiffness matrix (which has dimensions i x j), $\bar{C}_{k(ij)}$ are the components of the transformed stiffness matrix of the k^{th} lamina, h_k is the thickness of the k^{th} lamina and 2n is the number of laminae, assuming that the laminate comprises n layers of bi-directional reinforcement fabric.

Once the stiffness matrix for the whole laminate, $[\bar{C}_l]$, was known then elastic behaviour under loading could be described, and the engineering constants for the laminate were obtained by finding the compliance matrix, $[\bar{S}_l]$ (the matrix inverse of $[\bar{C}_l]$) and using the relationships defined in Equation 5.12.

This method was applied to determine the engineering constants of balanced, symmetric angle-ply (±ϕ) laminates, such as those manufactured from NCF reinforcement, and results are compared with those determined experimentally. Calculations were performed within a spreadsheet. Predictions of Young's modulus in the bias direction, E_x, are presented in Figure 5.8 with experimental measurements of the same property. Across the range of volume fractions studied, the modulus was seen to fall sharply from approximately 22 GPa for $\phi = 20°$ to 10 GPa for $\phi = 45°$, before levelling off in the range $45° \leq \phi \leq 70°$. Close agreement was observed, with some experimental data falling on either side of the predicted curve. The majority of experimental points were above the curve, with the largest difference being approximately 21% (±55°).

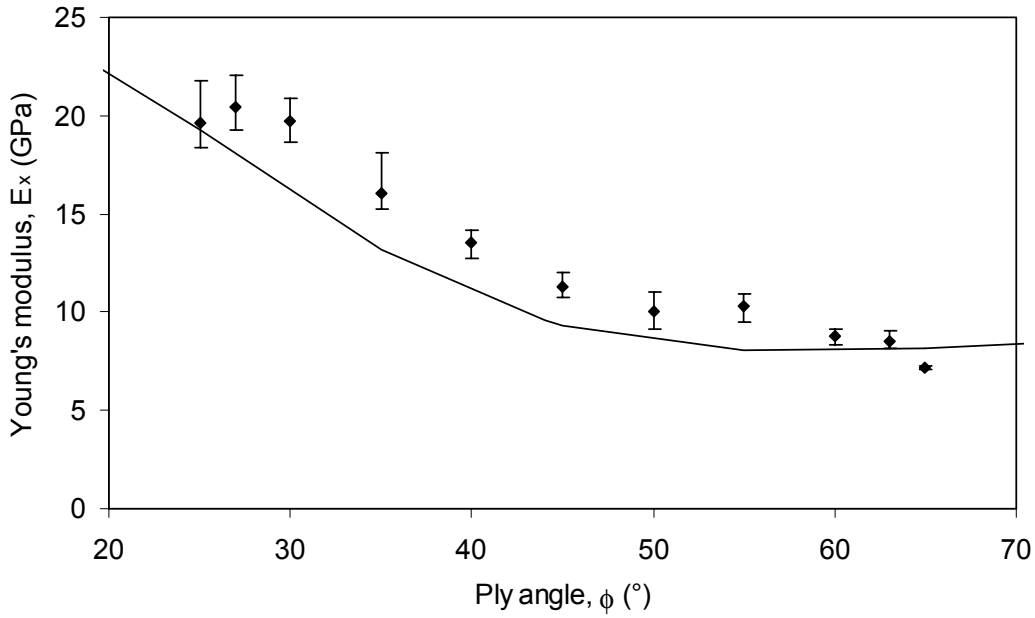

Figure 5.8 Predictions of Young's modulus in the bias direction of an angle-ply laminate, E_x, (solid line) compared with results of experimental testing of NCF reinforced laminates (points). Error bars indicate maximum and minimum values obtained in experimental tests.

Predictions of Poisson's ratio, ν_{xy}, extracted from the laminate compliance matrix, are presented in Figure 5.9. It can be observed that a maximum value was exhibited at $\phi = 35°$, where $\nu_{xy} = 0.65$, with values reducing as the ply angle deviates from this in either direction. When $\phi = 70°$, the predicted value of ν_{xy} had fallen to 0.19. The predicted values showed excellent agreement with the experimental data, the only significant discrepancy occurring for $\phi = 35°$, where a large spread in experimental measurements was present but all of the points fell below the predicted value. In all

other cases the difference between the predicted and average experimental values was less than 10%, with the predicted curve passing between the experimental error bars in most cases.

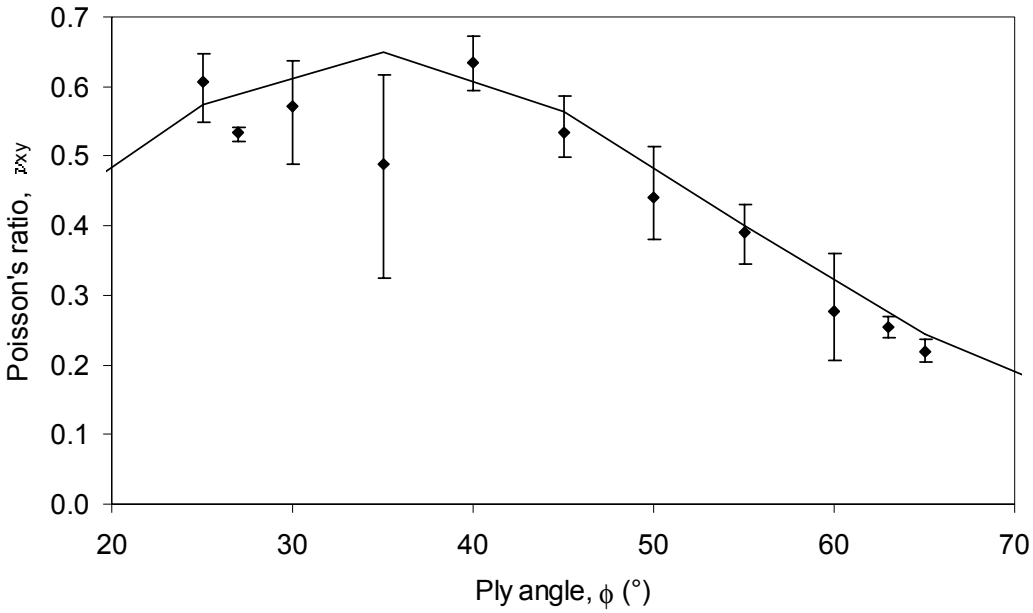

Figure 5.9 Predictions of Poisson's ratio of an angle-ply laminate, ν_{xy}, (solid line) compared with results of experimental testing of NCF reinforced laminates (points). Error bars indicate maximum and minimum values obtained in experimental tests.

In-plane shear modulus, G_{xy}, was also predicted, and this data is presented in Figure 5.10. Maximum shear modulus was predicted when $\phi = 45°$, when $G_{xy} = 8.5$ GPa. The shear modulus reduced as the ply angle moved away from this value, the curve being symmetric about $\phi = 45°$. When $\phi = 20°$ or 70°, $G_{xy} = 5.2$ GPa. No experimental determination of shear properties was performed on angle-ply laminates, so it was not possible to make such a comparison, but the symmetric nature of the curve would be expected intuitively since a ±30° laminate is simply a ±60° laminate rotated through 90°, and the sign of the shear stress does not affect the behaviour.

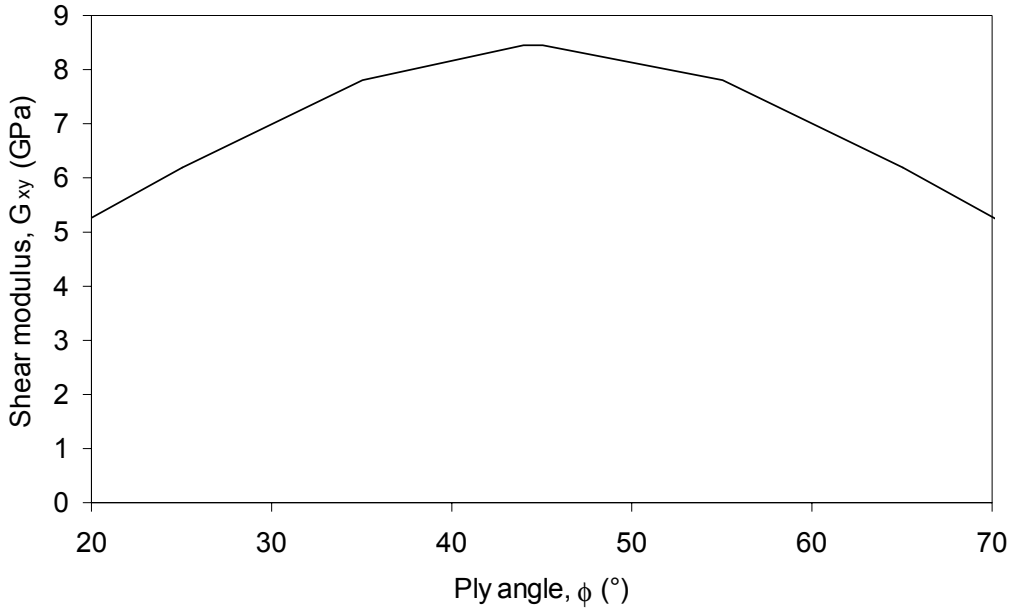

Figure 5.10 Predictions of shear modulus of an angle-ply laminate, G_{xy}, obtained using classical laminate theory. No comparable experimental data were produced.

5.4 Implementation of failure criteria using CLT

Classical laminate theory has been shown to give good agreement with experimental measurements of the elastic constants for angle-ply laminates under plane stress conditions. Since this theory relates the strain and stress fields in the laminate, it can also be used to determine their failure behaviour. In order to do so, the stresses in the principal material directions of each of the laminae must be determined.

Since it is assumed that the strain field is uniform in all layers, the strain in the lamina coordinate system for the k^{th} ply with its fibre (1) direction at an angle ϕ from the reference (x) direction can be found using Equation 5.19.

$$\begin{bmatrix} \varepsilon_{1k} \\ \varepsilon_{2k} \\ \gamma_{12k} \end{bmatrix} = [T']_{\phi} \begin{bmatrix} \varepsilon_{x} \\ \varepsilon_{y} \\ \gamma_{xy} \end{bmatrix} \tag{5.19}$$

where $[T']_{\phi}$ is the strain transformation matrix for an angle, ϕ, defined in Equation 5.15.

This result would enable the use of a strain based failure criterion, such as the maximum strain criterion, but to enable the use of a stress based criterion the stresses in the ply must be found from the strains using the stiffness matrix for that ply as in Equation 5.20.

$$\begin{bmatrix} \sigma_{1k} \\ \sigma_{2k} \\ \tau_{12k} \end{bmatrix} = [C]_k \begin{bmatrix} \varepsilon_{1k} \\ \varepsilon_{2k} \\ \gamma_{12k} \end{bmatrix} \tag{5.20}$$

where [C] is the stiffness matrix in the lamina coordinate system, and all terms pertain to the k^{th} lamina.

Once the stress state resulting from an assumed applied strain is known, any of the stress based failure criteria may be applied. A flowchart showing the basic steps of such an analysis is shown in Figure 5.11. Using an iterative approach, it is possible to increase the applied stress until the highest value of failure index computed for any lamina reaches unity, indicating that this ply has failed. By defining a stress ratio, s.r., between applied longitudinal and transverse stresses such that σ_y = s.r. x σ_x, it is also possible to determine the onset of failure under biaxial loading.

This calculation procedure was followed in order to predict the failure stresses of angle-ply laminates, such as those which were manufactured from NCF reinforcement, in order to enable comparisons with experimental data to be made. Three failure criteria were compared: maximum stress (Equation 2.13), Tsai-Hill (Equation 2.17) and Tsai-Wu (Equation 2.18). Since the Tsai-Wu criterion requires compressive strength values, it was assumed that transverse strength in compression, σ_{2uc}, was three times that in tension, σ_{2ut}, and that σ_{1uc} = 0.6 x σ_{1ut}. Both of these approximations were inferred from published data for unidirectional glass/epoxy [29,39,61], and their applicability to glass/polyester systems was assumed. These parameters were used only for generation of a quadratic ellipsoid and they have relatively little effect on the tension-tension quadrant; this was considered acceptable for the cases presented since predictions under compressive loading were not made. It was assumed that the interaction parameter, f^* = -0.5, as suggested by Liu and Tsai [62]. Results from these criteria are presented with experimental data (both UTS and $\sigma_{0.2ps}$) for comparison in Figure 5.12. Results from all criteria were similar, although

the peak at $\phi = 51°$ was a distinctive feature of the maximum stress criterion. As mentioned previously, and unlike the other failure criteria, the maximum stress criterion indicated the dominant failure mechanism, and the switch from shear to transverse failure was coincident with the aforementioned peak. This appeared to occur at too high a ply angle compared with the position of the drop in failure stress observed in experimental data. The mode of failure in experimental tests was not obvious from visual examination of the specimens after testing, particularly since tests were conducted beyond the point of initial failure, whereupon a significant amount of delamination occurred within the region of failure. All criteria overestimated ultimate strengths at large ply angles, due to overestimation of transverse strength by the micromechanics model described in Section 5.2.2. Predictions overestimated initial failure (proof stress) at all ply angles. The Tsai-Wu criterion appeared to give the best fit to the experimental UTS data, although for initial failure the Tsai-Hill criterion seemed to give better agreement with the trend of the proof stress measurements.

Replacing the lamina failure stresses, σ_{1u} and σ_{2u}, with average experimental values from tests on unidirectional composites yielded significantly improved predictions from the same laminate theory approach, suggesting that the method was suitable given appropriate lamina data. These results are presented in Figure 5.13. In this case, the transition from shear to transverse failure mode predicted by the maximum stress criterion fell at $\phi = 45°$, which appeared to show reasonable agreement with the experimental data. All three criteria gave similar results for ply angles in the range $50° \leq \phi \leq 70°$, and the two interactive criteria (Tsai-Hill and Tsai-Wu) gave almost identical predictions for $35° \leq \phi \leq 70°$. Overall, the Tsai-Wu criterion appeared to give the best fit to the experimental data for UTS, although the maximum stress criterion also offered reasonable agreement in addition to predicting the failure mode. When compared with proof stress measurements, however, the Tsai-Hill criterion gave significantly better predictions than the others for $\phi < 35°$. Note that, although better agreement with experimental data was observed by using the measured lamina strengths, this was performed to assess the capability of the laminate theory model when used with a failure criterion independently of the

micromechanics models used. Hence the purely predictive nature intended is not present in the results shown in Figure 5.13.

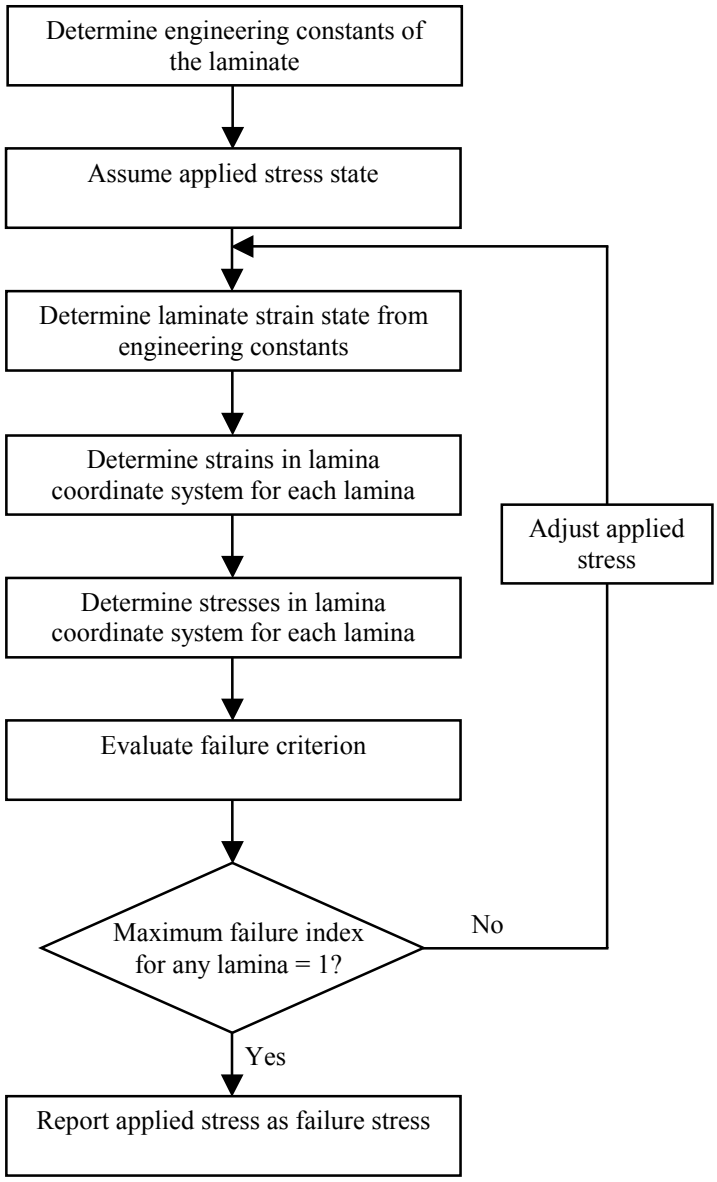

Figure 5.11 Outline flowchart showing steps used to determine initial failure stress of composite laminates using classical laminate theory in conjunction with a stress based failure criterion.

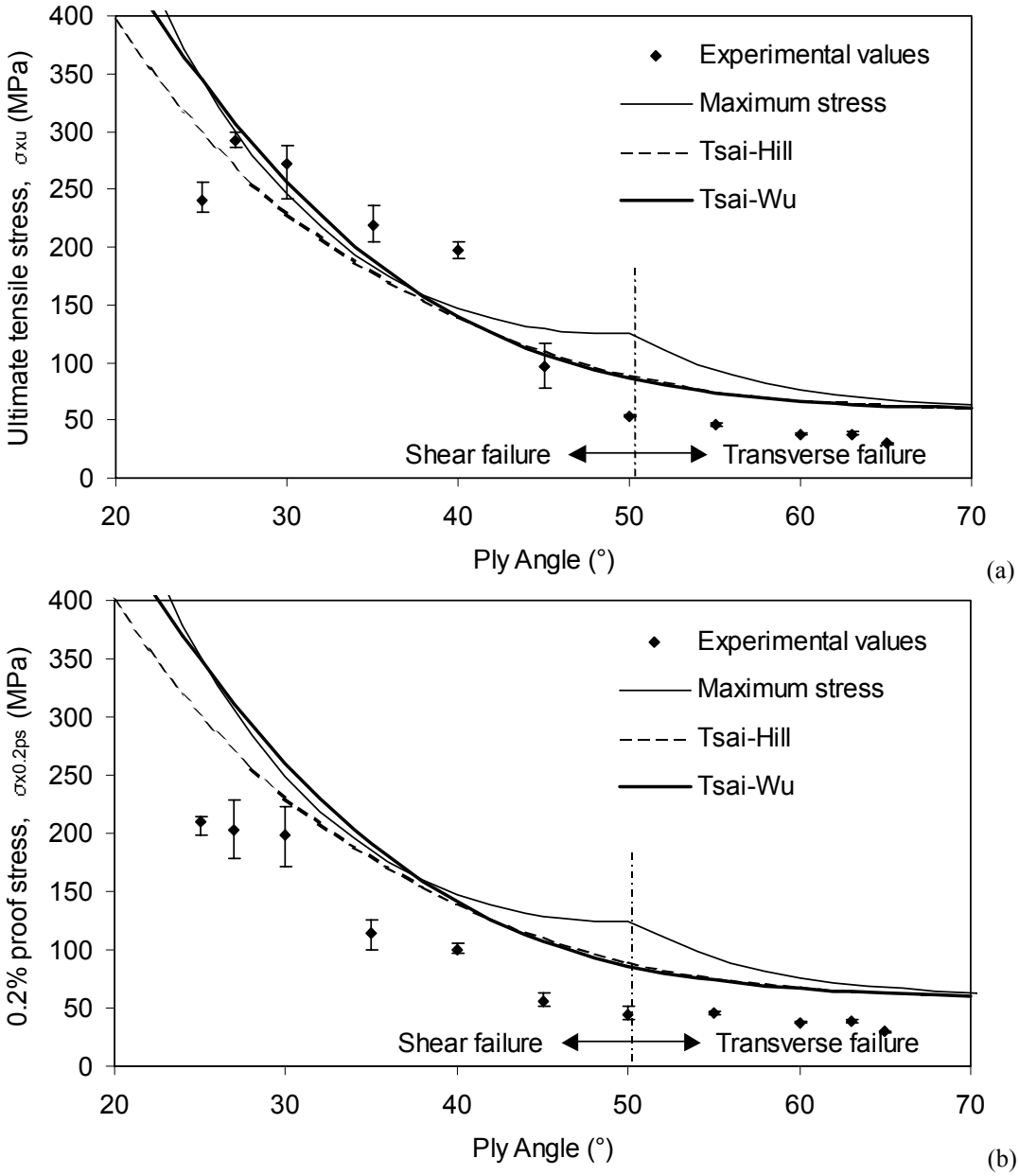

Figure 5.12 Predictions of failure stress of an angle-ply laminate, σ_{xu}, obtained using classical laminate theory with a failure criterion, compared with results of (a) UTS and (b) 0.2% proof stress, obtained by experimental testing of NCF reinforced laminates. Failure mode (shear/transverse) was predicted by maximum stress criterion. Error bars indicate maximum and minimum values obtained in experimental tests.

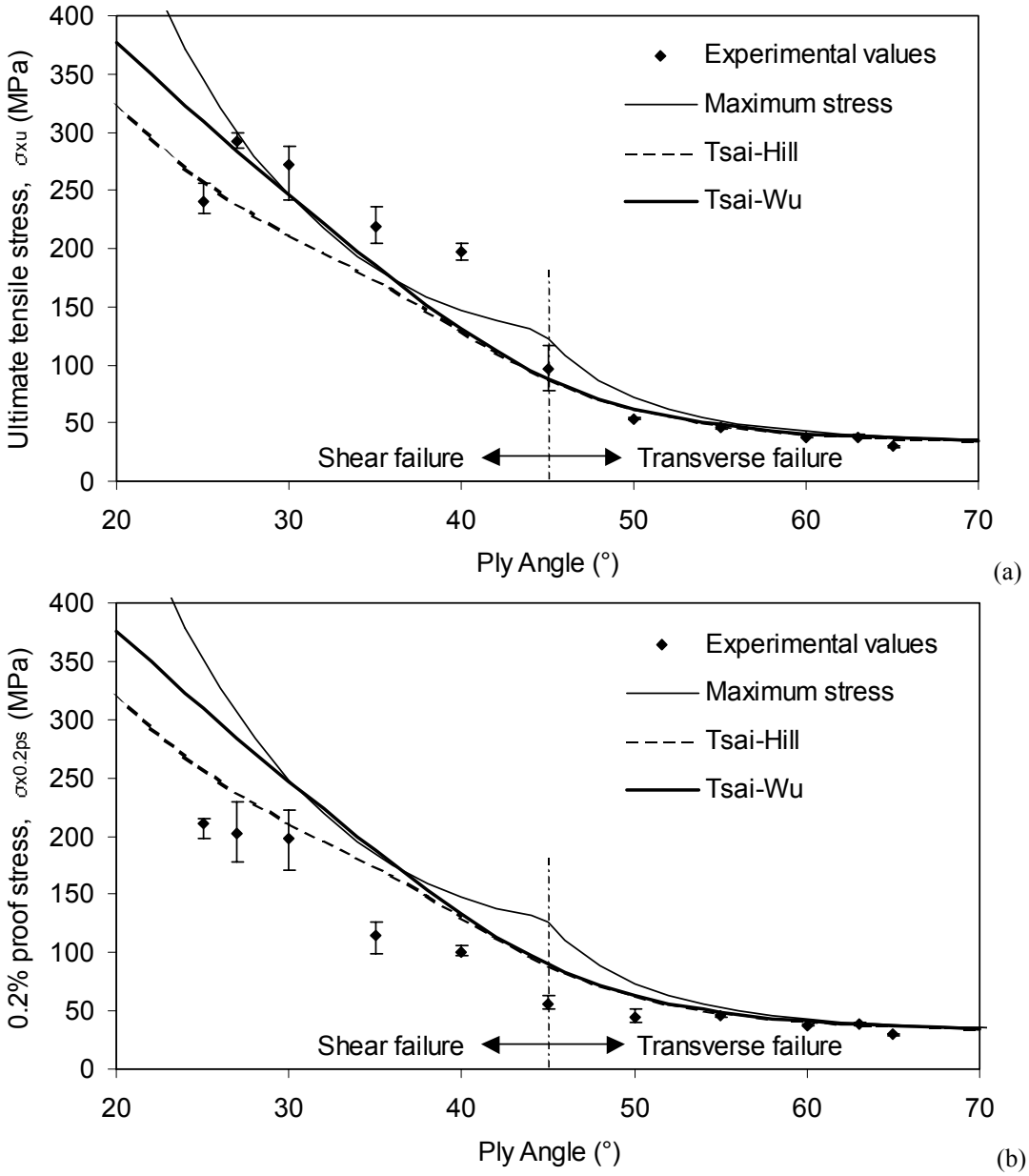

Figure 5.13 Predictions of failure stress of an angle-ply laminate, σ_{xu}, obtained using classical laminate theory with three failure criteria, compared with results of (a) UTS and (b) 0.2% proof stress, obtained by experimental testing of NCF reinforced laminates. Lamina failure stresses used for predictions were average experimental values. Failure mode (shear/transverse) was predicted by maximum stress criterion. Error bars indicate maximum and minimum values obtained in experimental tests.

Failure envelopes predicting failure behaviour of angle-ply laminates under a combination of axial and transverse stresses were also produced using the same technique, reverting to predicted values for lamina strengths; these are presented for ±25° and ±45° laminates in Figure 5.14. Predictions were only made for the tension-tension quadrant since detailed consideration was not given to lamina failure behaviour in compression. As stated previously, assumptions were made to provide

compressive lamina failure stresses required for the Tsai-Wu criterion. In general, the Tsai-Hill criterion gave the most conservative predictions, falling inside the failure envelopes predicted by the other criteria except for a small region close to the axes (i.e. nearly uniaxial load) for the ±45° laminate. The envelopes predicted by the maximum stress criterion comprised linear sections, each corresponding to a particular mode of failure. It can be seen from the results presented that high failure stresses were predicted at the points of transition between different failure modes. This is due to the nature of the criterion, i.e. that the lamina is expected to support 99% of its ultimate transverse load simultaneously with 99% of its ultimate shear load without failure being initiated. Predicted failure stresses from the Tsai-Wu criterion were higher than those from the maximum stress criterion around the 'nose' of the failure envelope, but were lower in the regions where the maximum stress criterion was previously noted to give particularly high predictions. Due to their nature, no indication of the active failure mechanism was given by either of the interactive criteria.

In the absence of biaxial test data, comparisons with experimental results could not be made, but it should be noted that this procedure could be implemented for general laminates, and that any failure criterion could be used. The failure criteria employed for the predictions in this thesis were used for comparative purposes, and the choice of angle-ply laminates was made to complement the experimental work performed.

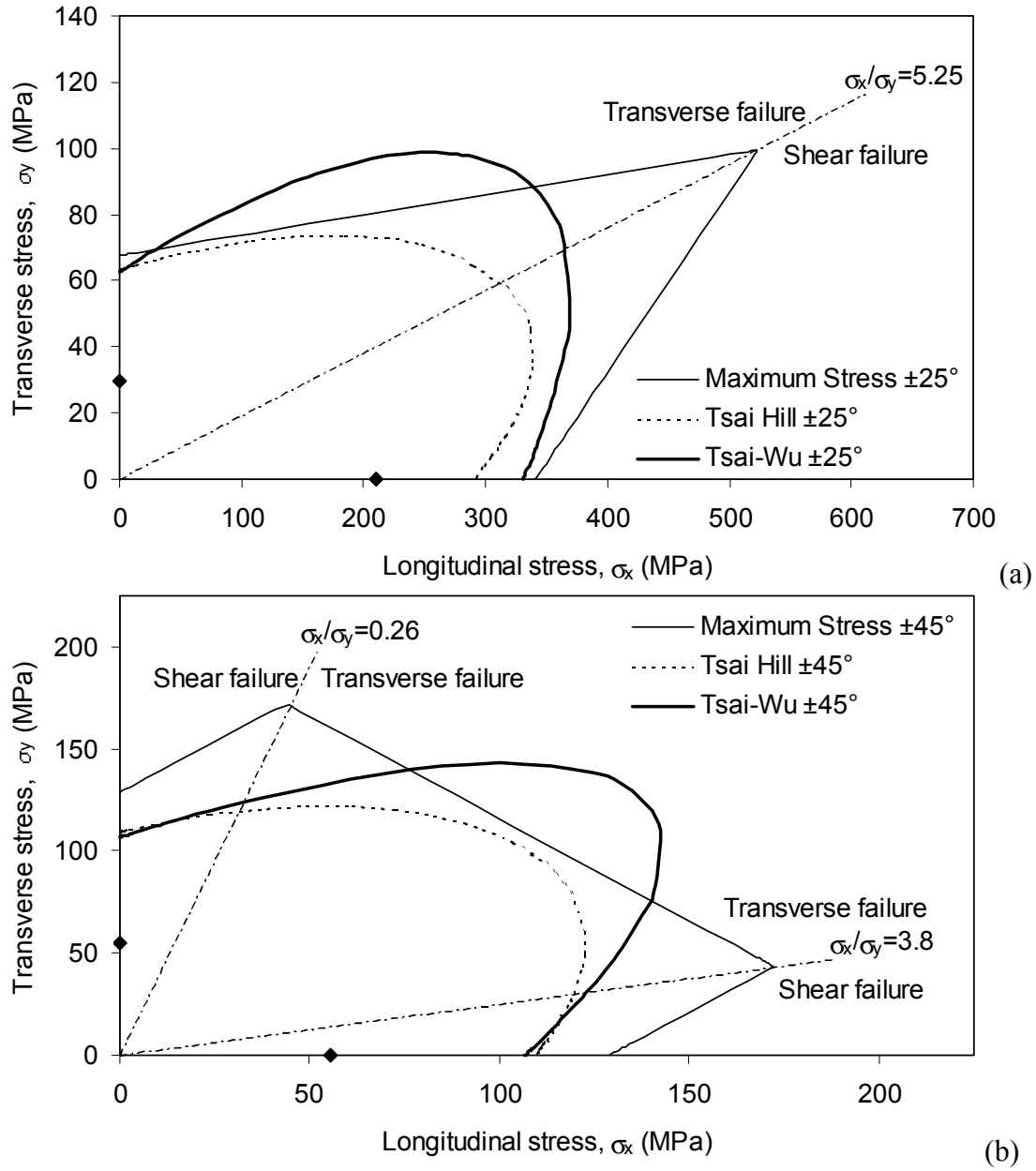

Figure 5.14 Predicted failure envelopes of (a) a ±25° and (b) a ±45° angle-ply laminate under biaxial loading conditions obtained using classical laminate theory with three failure criteria. Lamina failure stresses used are in Table 5.1. Failure mode (shear/transverse) was predicted by maximum stress criterion. Measured values of 0.2% proof stress under uniaxial loads are indicated by points on the axes.

5.5 Laminate behaviour using layered shell finite elements

While classical laminate theory (CLT) has been used to give a useful insight into the behaviour of textile reinforced composites, and to predict the behaviour of such materials when manufactured in a flat configuration, if the behaviour of formed three-dimensional components is to be predicted an alternative approach must be

employed. The finite element (FE) method was used, where layered shell elements were assumed to represent textile reinforced composites in the same way as CLT, i.e. one layer of fabric reinforcement was represented by two unidirectional layers in a shell. The use of FE permits structural analysis of complex geometries. For the work presented in this thesis, the Abaqus implicit FE code [67] was used exclusively. All of the analyses conducted used linear elastic material behaviour, and the assumption was made that deformations were small. As discussed in Section 2.4, plane stress conditions (i.e. $\sigma_3 = 0$) were assumed in the formulation of the layered shell elements used. The elements used were quadratic triangular thin shell elements (Abaqus element designation STRI65), having six nodes and five degrees of freedom per node. Thin shell solutions enforce the Kirchhoff constraint, i.e. that $\varepsilon_3 = \gamma_{23} = \gamma_{31} = 0$ (normal sections remain normal to the element reference surface), while thick shell solutions permit transverse shear deformation (normal plane sections remain plane but not necessarily normal). Since no triangular thick shell elements with quadratic interpolation were available in the Abaqus software, the suitability of thin shell elements for analyses presented in this chapter was verified by comparing results from linear thin shells (STRI3) and general purpose shells (S3); general purpose shell elements converge to the thin shell solution as the thickness reduces. Results from the general purpose and exclusive thin shell elements were compared and found to be identical for the analyses presented in this chapter, indicating that thin shell approximations were valid for these models. Since greater accuracy is afforded by the use of six noded (quadratic interpolation) elements, these were selected for analysis of a shaped component.

5.5.1 Implementation procedure

To model a structure using layered shell elements requires a considerable amount of user input. A discretised mesh consisting of nodes and elements is used to define the geometry, while mechanical properties must be assigned to each element. For orthotropic materials, orientations must be specified for each layer. In the case of draped components, it may be necessary to define unique mechanical properties and orientations for every element, although for regular structures such as flat plates, these may be defined once and applied to groups of elements. The exact syntax used is described in detail in Appendix D.

The data described above must be assembled to form a complete input file, which is used by the FE package. The code solves the governing equations and calculates displacements, forces, stresses and strains, writing the results to an output file. Failure behaviour for the laminates may also be calculated internally within Abaqus, which evaluates a failure index (effectively the ratio of the stress to the failure stress) at each material calculation point. The maximum stress, Tsai-Hill and Tsai-Wu criteria are all available for orthotropic plane stress elements, and results are written to the output file on request, provided that the `*FAIL STRESS` option has been used. Other failure criteria may be encoded using a user subroutine similar to that described in Section 6.3. This output file may be read and interpreted directly, or by using a post-processing package such as Abaqus Viewer. Both techniques were used in the determination of results presented in this thesis.

5.5.2 Results

Angle-ply laminates were modelled using layered shell elements in the manner described in Section 5.5.1. The tensile tests undertaken experimentally were modelled using idealised boundary conditions, indicated in Figure 5.15. The angle-ply laminate behaviour was determined using Equations 5.21-5.23

$$\varepsilon_x = \frac{\delta l}{l} \tag{5.21}$$

where l is the length of the specimen and δl is the prescribed displacement

$$\sigma_x = \frac{\sum RF_x}{wh} \tag{5.22}$$

where w is the width and h is the thickness of the specimen and ΣRF_x is the total reaction force at the displaced edge

$$E_x = \frac{\sigma_x}{\varepsilon_x} \tag{5.23}$$

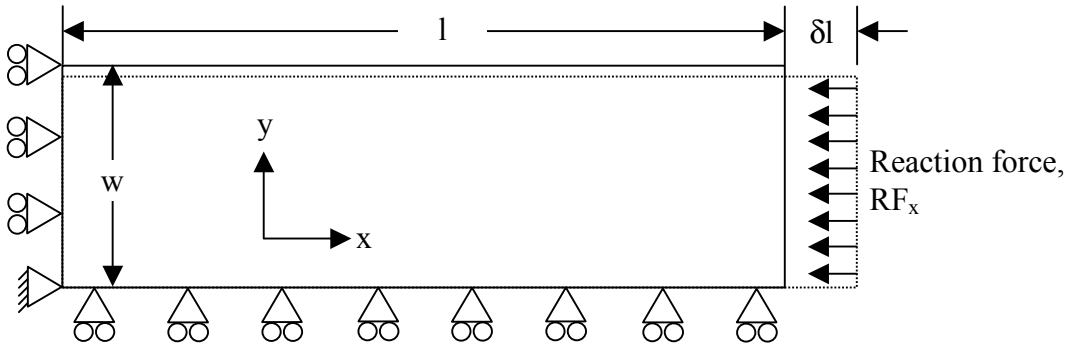

Figure 5.15 Schematic illustration of the model used for simulation of tensile testing with Abaqus. A displacement boundary condition was applied at the right hand side; displaced shape is indicated by a dashed line.

The boundary conditions used produced constant strain and stress fields, i.e. strain and stress were constant at every point in the specimen. Failure index was calculated by the Abaqus code at each calculation point, which gave a constant value due to the nature of the stress field. Since the analysis was linear, failure stress was determined using Equation 5.24.

$$\sigma_{xu} = \frac{\sigma_x}{FI_{\max}} \tag{5.24}$$

where FI_{max} is the maximum calculated failure index.

Results obtained for Young's modulus, E_x, and failure stress, σ_{xu}, using this technique agreed exactly with those presented in Sections 5.3 and 5.4, obtained using CLT. This provided high confidence in the results of both methods; consequently this FE based method was adopted for analysis of three-dimensional structures, as described in Section 5.7.

5.6 Models for behaviour of woven fabric laminates

Although the techniques described in Sections 5.3-5.5 were shown to be applicable to non-crimp fabric reinforced composite laminates, analysis of composites reinforced with woven fabric required some consideration of the fibre waviness introduced by the weaving process, i.e. that the fibres were no longer parallel to the lamina plane along their whole length. A discussion of some of the analytical models available in

the literature to calculate the effects of fibre waviness on laminate mechanical properties is presented in Section 2.4.3. A published method [87] is presented in this section which used stress transformations to determine the effective modulus of composites reinforced with plain woven fabric, by assuming that the composite could be represented as two discrete layers of wavy tows; this model was extended to predict failure stress. Properties for the constituent wavy laminae were then used with CLT, applied in the same way as for NCF reinforcements in Sections 5.3 and 5.4, to determine laminate behaviour.

5.6.1 Assumptions and implementation

While the tows comprising a woven fabric are straight when viewed from above, in section they undulate around the tows with which they are interwoven. This out-of-plane waviness can be observed in Figure 5.16. For the purposes of this section only, it is assumed that the tow under investigation runs in the x' direction of the laminate.

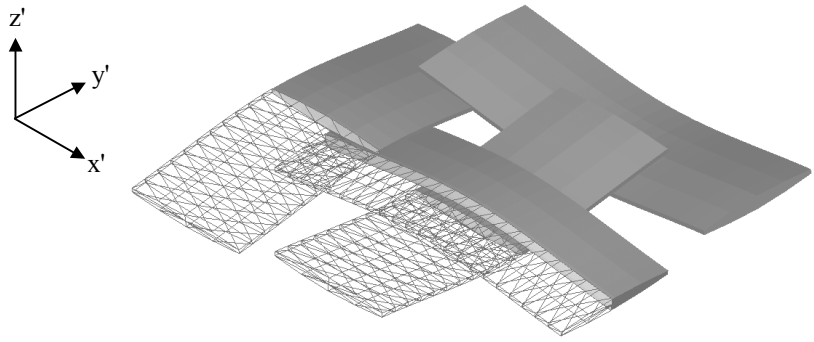

Figure 5.16 Schematic of plain-weave fabric showing out-of-plane tow waviness

If the path which the tow follows is known, then an expression can be derived for the angle between the local fibre direction and the plane of the laminate, α. Figure 5.17 illustrates this idea for a sinusoidal tow path.

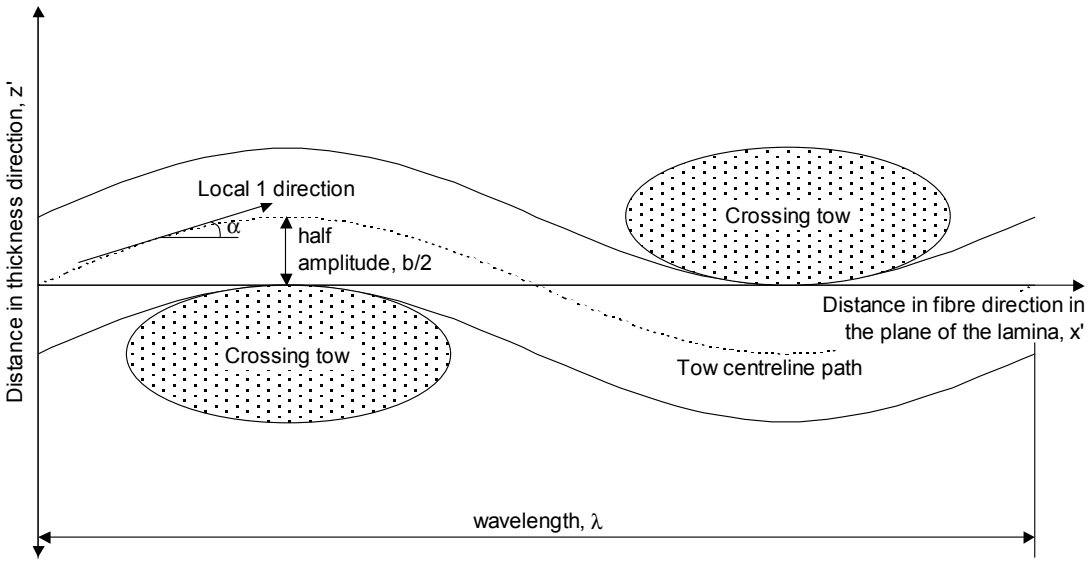

Figure 5.17 Specification of terms defining the angle between the fibre and the laminate plane for reinforcements with out-of-plane fibre waviness (sinusoidal tow path shown)

The theory used to transform stress and strain fields in orthotropic materials is presented in Section 5.3. The result of a series of transformations is the off-axis compliance matrix, $[\bar{S}]$, which relates stress and strain in the tow direction in the plane of the lamina (x') according to Equation 5.25.

$$\begin{bmatrix} \varepsilon_{x'} \\ \varepsilon_{z'} \\ \gamma_{x'z'}=0 \end{bmatrix} = \begin{bmatrix} \bar{S}_{11} & \bar{S}_{13} & \bar{S}_{16} \\ \bar{S}_{13} & \bar{S}_{33} & \bar{S}_{36} \\ \bar{S}_{16} & \bar{S}_{36} & \bar{S}_{66} \end{bmatrix} \begin{bmatrix} \sigma_{x'} \\ \sigma_{z'}=0 \\ \tau_{x'z'} \end{bmatrix} \tag{5.25}$$

where it can be shown that:

$$\bar{S}_{11} = S_{11}\cos^4\alpha + S_{33}\sin^4\alpha + (2S_{13} + S_{66})\sin^2\alpha\cos^2\alpha$$

$$\bar{S}_{13} = S_{13}(\cos^4\alpha + \sin^4\alpha) + (S_{11} + S_{33} - S_{66})\sin^2\alpha\cos^2\alpha$$

$$\bar{S}_{16} = (2S_{11} - 2S_{13} - S_{66})\sin\alpha\cos^3\alpha - (2S_{33} - 2S_{13} - S_{66})\sin^3\alpha\cos\alpha$$

$$\bar{S}_{33} = S_{11}\sin^4\alpha + S_{33}\cos^4\alpha + (2S_{13} + S_{66})\sin^2\alpha\cos^2\alpha$$

$$\bar{S}_{36} = (2S_{11} - 2S_{13} - S_{66})\sin^3\alpha\cos\alpha - (2S_{33} - 2S_{13} - S_{66})\sin\alpha\cos^3\alpha$$

$$\bar{S}_{66} = 2(2S_{11} + 2S_{33} - 4S_{13} - S_{66})\sin^2\alpha\cos^2\alpha + S_{66}(\sin^4\alpha + \cos^4\alpha)$$

where α is the out of plane angle, and where

$$S_{11} = \frac{1}{E_1}\ ,\ S_{33} = \frac{1}{E_3}\ ,\ S_{13} = -\frac{\nu_{13}}{E_1}\ ,\ S_{66} = \frac{1}{G_{13}}$$

This expression assumes plane stress in the x'-z' plane, i.e. $\sigma_{y'} = \tau_{x'y'} = 0$. Since in any woven fabric, there are many adjacent tows 'stacked' in the y' direction, such that where α is positive for one tow, there will be another for which α is negative and has approximately the same magnitude; hence, the 'laminate' in the x'-z' plane was assumed to be balanced, such that under a uniaxial load in the x' direction, the shear strain, $\gamma_{x'z'} = 0$. In his model, Turner [87] assumed that $\sigma_{z'} = 0$ since there was no applied stress in this direction.

Equation 5.25 reduces to the expressions in Equation 5.26:

$$\begin{aligned} \varepsilon_{x'} &= \overline{S}_{11}\sigma_{x'} + \overline{S}_{16}\tau_{x'z'} \quad \text{(a)} \\ \varepsilon_{z'} &= \overline{S}_{13}\sigma_{x'} + \overline{S}_{36}\tau_{x'z'} \quad \text{(b)} \\ \gamma_{x'z'} &= \overline{S}_{16}\sigma_{x'} + \overline{S}_{66}\tau_{x'z'} = 0 \quad \text{(c)} \end{aligned} \tag{5.26}$$

Rearranging (c) to find $\tau_{x'z'}$ and substituting into (a) yields Equation 5.27

$$\varepsilon_{x'} = \left(\overline{S}_{11} - \frac{\overline{S}_{16}^{\,2}}{\overline{S}_{66}} \right) \sigma_{x'} \tag{5.27}$$

This relationship enables the local composite modulus to be determined according to Equation 5.28

$$\frac{1}{E_{x'}} = \overline{S}_{11} - \frac{\overline{S}_{16}^{\,2}}{\overline{S}_{66}} \tag{5.28}$$

Equation 5.28 yields a value for modulus for a single out-of-plane angle. To obtain the effective modulus of the material, this must be integrated along a full wavelength of the tow with respect to distance in the principal direction, x', as described in Equation 5.29.

$$\frac{1}{E_{x'}} = \frac{1}{\lambda} \int_0^{\lambda} \overline{S}_{11} - \frac{\overline{S}_{16}^{\,2}}{\overline{S}_{66}} \, dx' \tag{5.29}$$

Since compliance terms are averaged, Equation 5.29 assumes constant stress in each interval. For the constant strain assumption, stiffnesses must be averaged, according to Equation 5.30.

$$E_{x'} = \frac{1}{\lambda} \int_0^{\lambda} \left(\overline{S}_{11} - \frac{\overline{S}_{16}^{\,2}}{\overline{S}_{66}} \right)^{-1} dx' \tag{5.30}$$

These expressions were evaluated using a numerical integration scheme (trapezium rule with 200 intervals) within a spreadsheet.

Since the out-of-plane angle between the fibre and the lamina plane was known for each interval used to calculate the integral in Equation 5.29, it was possible to transform the stresses in the lamina x' direction into the principal local directions of the tow. By using an isostrain assumption (i.e. assuming that strain was constant in the lamina x' direction), a strain level, $\varepsilon_{x'u}$, was determined at which the maximum stress failure criterion (Equation 2.13) was first satisfied for a single out-of-plane angle and hence the axial failure stress, $\sigma_{x'u}$, was calculated using Equation 5.31.

$$\sigma_{x'u} = \varepsilon_{x'u} E_{x'} \tag{5.31}$$

An isostress assumption was also made to determine failure stress. In this case, a constant value of stress in the x' direction was assumed, which was transformed into the material directions for each out-of-plane angle. The maximum stress failure criterion was evaluated to determine the axial failure stress, $\sigma_{x'u}$.

The modulus, $E_{x'}$, and strength, $\sigma_{x'u}$, values obtained for a single wavy lamina were used as input parameters for the classical laminate theory (CLT) model described in Sections 5.3 and 5.4 to find the elastic response and failure behaviour of angle-ply laminates. To summarise, the steps used to calculate woven laminate mechanical properties are illustrated in Figure 5.18.

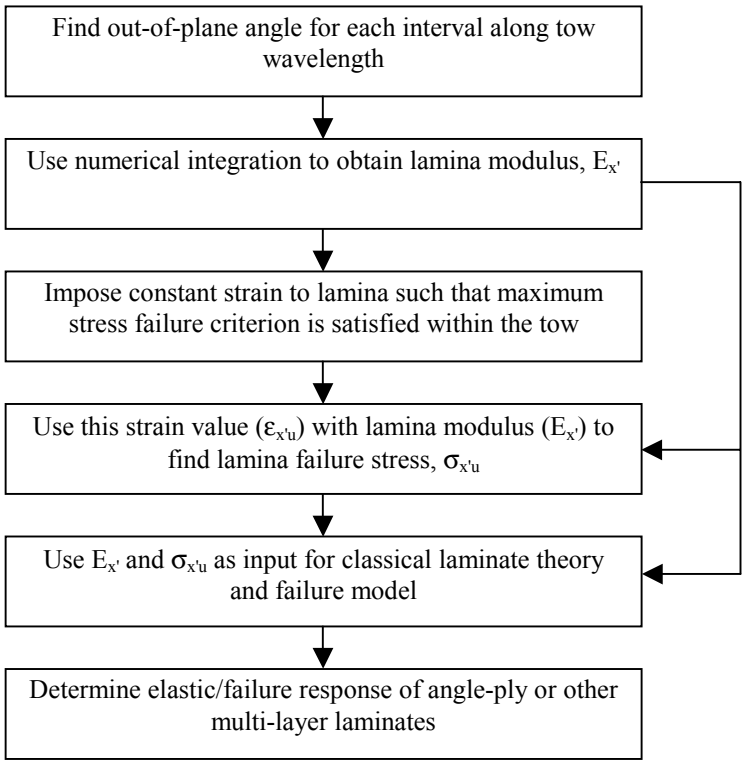

Figure 5.18 Outline summary of steps used to calculate mechanical properties of woven fabric composite laminates

5.6.2 Results

Using the assumption that the tows followed a sinusoidal path, values of Young's modulus, $E_{x'}$, and failure stress, $\sigma_{x'u}$, of the effective lamina were calculated for different levels of fibre waviness, expressed as the ratio between the amplitude and wavelength of the tow centreline path, b/λ. Material property data for the constituent phases used to calculate these values are provided in Table 3.2, while the resulting properties of unidirectional composite, obtained using micromechanics, are shown in Table 5.1. The relationship between Young's modulus and waviness is shown in Figure 5.19, while that between failure stress and waviness is shown in Figure 5.20. The waviness of RT600 plain weave reinforcement is indicated on each of these figures. The waviness of most common reinforcement fabrics is likely to fall somewhere in the range $0<b/\lambda<0.05$, the higher values pertaining to tightly woven plain weave fabrics; values greater than this may be seen in reinforcements such as thick 3D woven fabrics. The results showed that in the range mentioned, Young's modulus, $E_{x'}$, fell by approximately 30%, while failure stress, $\sigma_{x'u}$, fell by approximately 65%. Failure stress was particularly sensitive to waviness in the range

$0.0125<b/\lambda<0.04$. It should be noted that the RT600 plain weave reinforcement used in experimental testing exhibited a waviness of $b/\lambda=0.03125$, which fell within this region of high sensitivity.

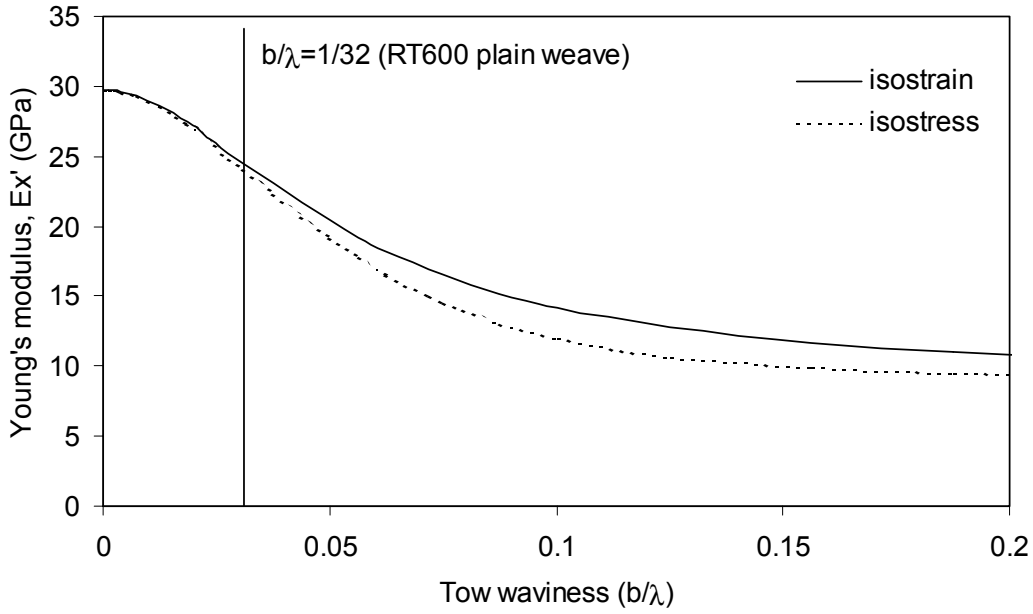

Figure 5.19 Young's modulus, $E_{x'}$, of a lamina having fibres parallel to the direction of loading with out-of-plane sinusoidal waviness, plotted as a function of the ratio of amplitude of the sinusoid to its wavelength.

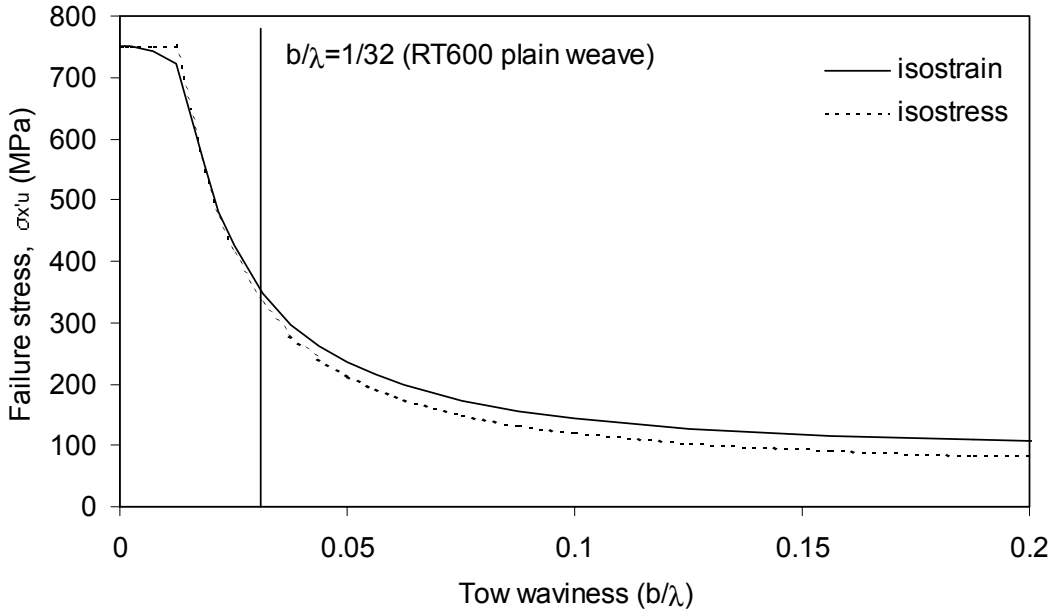

Figure 5.20 Failure stress, $\sigma_{x'u}$, determined using the maximum stress criterion, of a lamina having fibres parallel to the direction of loading with out-of-plane sinusoidal waviness, plotted as a function of the ratio of amplitude of the sinusoid to its wavelength.

It can be seen from Figure 5.19 that for the plain-weave fabric indicated, the predicted modulus, $E_{x'}$, was reduced by approximately 19% (isostress) or 18% (isostrain) compared with that of the unidirectional composite. Figure 5.20 shows that the predicted failure stress, $\sigma_{x'u}$, for the same material reduced by approximately 56% (isostress) or 54% (isostrain). Results of these calculations are provided in Table 5.2. It should be noted that the model assumed that waviness remained constant at all shear angles. In practice, the waviness of the tows in a woven fabric is likely to increase with increasing shear angle, but this effect was not accounted for by the predictions presented. Using the techniques implemented, it would be possible to change the tow path as a function of the shear angle in order to evaluate this effect if an expression for the tow path was assumed.

Table 5.2 Calculated on-axis mechanical properties for a unidirectional lamina having the same tow waviness as RT600 plain weave reinforcement.

Parameter	Value
Tow waviness, b/λ	1/32
Young's modulus, $E_{x'}$ (GPa) (isostress)	24.05
Young's modulus, $E_{x'}$ (GPa) (isostrain)	24.49
Ultimate tensile strength, $\sigma_{x'u}$ (MPa) (isostress)	332.2
Ultimate tensile strength, $\sigma_{x'u}$ (MPa) (isostrain)	347.5

In order to evaluate the effect of waviness on the properties of angle-ply laminates such as those tested experimentally, the values of Young's modulus, $E_{x'}$, and failure stress, $\sigma_{x'u}$, given in Table 5.2 were used in the CLT model. Figure 5.21 shows how the introduction of revised on-axis modulus affected the elastic behaviour of angle-ply laminates; similarly, the effects of revised on-axis modulus and strength on bias tensile strength of angle-ply laminates are presented in Figure 5.22. In each of these figures, results of the models incorporating waviness are compared with predictions for non-crimp fabric reinforcement at the same fibre volume fraction, in addition to results of experimental data for woven reinforcements. It can be seen from the results presented, and from inspection of the equations, that this model predicts lower moduli and failure stresses for the woven material than those predicted for a non-crimp fabric. Comparison of the values of on-axis stiffness and strength in Table 5.2 with those calculated for a unidirectional lamina in Table 5.1 (which were used for NCF materials and as input for the woven fabric model) shows the significance of tow waviness, particularly on strength, as predicted by this model. However,

experimental results showed that laminates manufactured from woven reinforcement exhibited higher stiffness and strength than those manufactured from NCF reinforcement in most cases, although the differences observed between reinforcement types were relatively small.

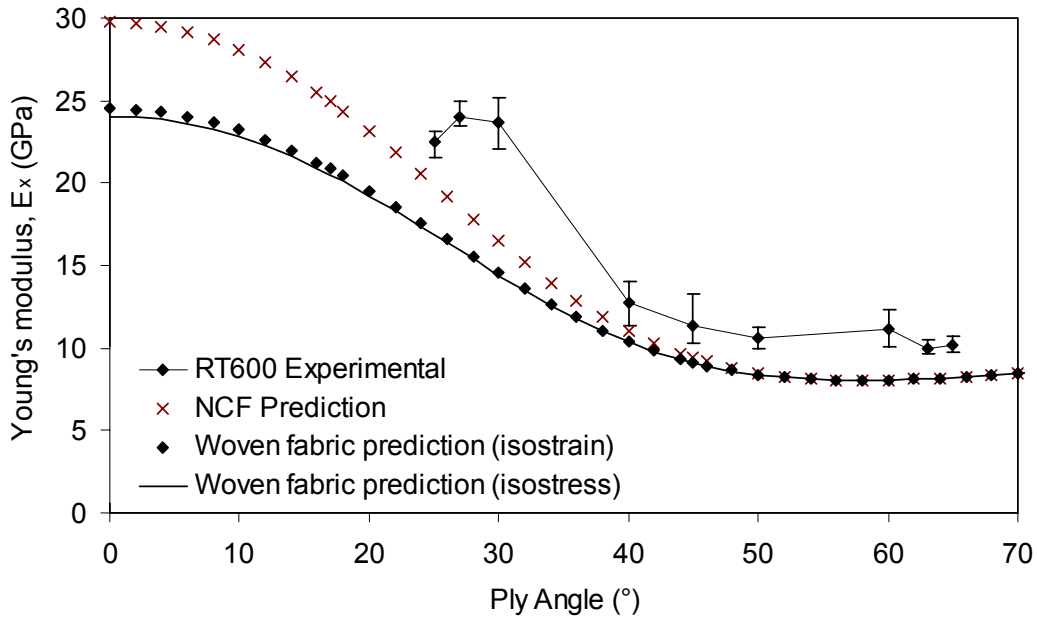

Figure 5.21 Predicted Young's modulus vs. ply angle for angle ply laminates made from woven & non-crimp reinforced composites compared with values obtained by experimental testing.

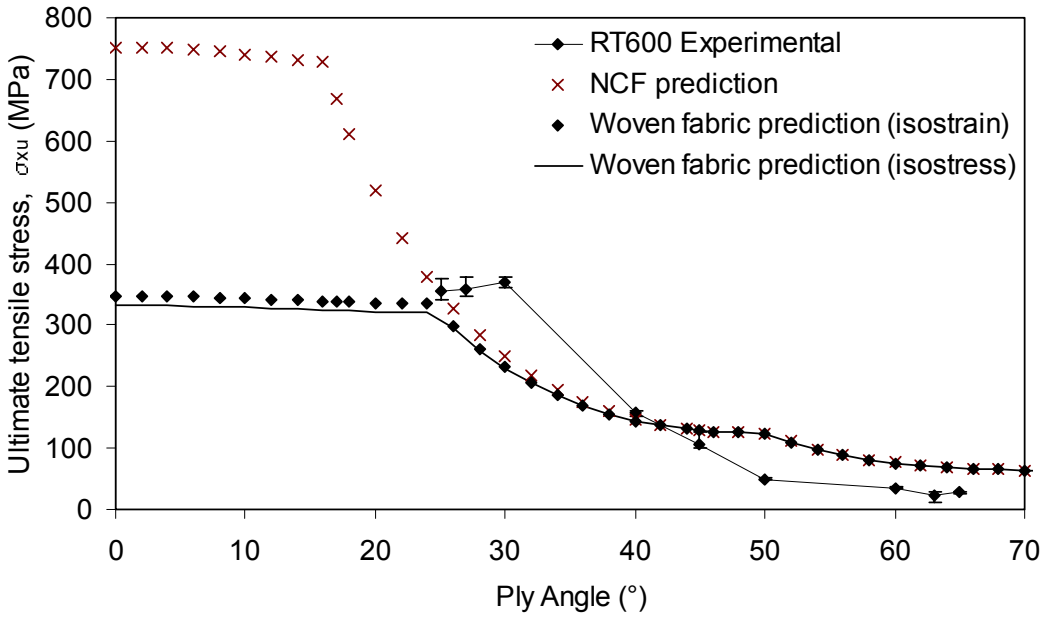

Figure 5.22 Predicted failure stress (maximum stress criterion) vs. ply angle for angle ply laminates made from woven & non-crimp reinforced composites compared with values obtained by experimental testing.

It should be noted that within the range of ply angles studied experimentally the incorporation of tow waviness had very little effect on predicted failure stress of angle-ply laminates; shear and transverse behaviour of the lamina were more significant than on-axis behaviour for $20°<\phi<70°$. This may suggest that the differences between reinforcement types observed in experimental measurements were caused by other features of laminate not considered here. For example, Piggott [13] and Ganesh [97] suggested that the in-plane shear strength may be expected to increase due to tow waviness due to the interruption of planes of pure resin, but this is not calculated by the present model. Similarly, the effect of reinforcement deformation on waviness was not known, but the waviness may be expected to have increased as the fabric was sheared.

More complex models for woven materials such as those published by Hofstee [103] and Naik [95] predict a set of in-plane elastic constants for a given fabric architecture, but are somewhat restricted in the geometries which can be analysed. Although inherently more limited in the output data which may be obtained, the method presented here has the ability to describe easily tows following any repeating path. Although a sine wave tow path was assumed for the results presented here, a continuous function for α is not required, i.e. piecewise curves, or even lines from experimental measurements, may be used to describe the tow path, providing a high level of generality. Analytical models require certain assumptions to be made, most frequently those of plane stress conditions, and most notably that either stress or strain in the x' direction is constant. While these assumptions enable easy solution techniques to be used, the true states of stress and strain in a woven fabric reinforced laminate will be non-uniform. To capture this behaviour accurately, more complex numerical techniques must be used, such as finite element (FE) analysis of the repeating unit cell. Although a more detailed discussion of this method is presented in Section 6.7, it should be noted at this stage that the technique is significantly more time consuming, requires much greater computational effort, and requires a three-dimensional model of the unit cell. In spite of these limitations, unit cell FE may provide a route to determining the effects of any aspect of reinforcement architecture on both elastic and strength behaviour, particularly as affordable computing power increases and the development of textile geometric modelling continues.

5.7 Post-forming structural analysis of textile composite components

Having identified a number of techniques which may be used for predicting the mechanical properties of textile reinforced composites in different situations, it became necessary to link these models together in such a way that they may be used to analyse the structural behaviour of manufactured components. To illustrate how this procedure may be applied in a practical context, the jet engine nose cone component has been modelled in order to simulate the tests undertaken such that the results of FE analysis may be compared with those determined experimentally, presented in Section 4.4.2.

5.7.1 Predicting the fibre pattern of the formed reinforcement

As discussed in Chapter 2, when a textile reinforcement consisting of orthogonal fibres is formed into a three-dimensional shape, in-plane shear deformation occurs such that the fibres cease to be orthogonal. While various methods exist to predict this behaviour, the approach adopted for the work in this thesis is essentially a geometric solution coupled with a shear strain energy minimisation algorithm. This algorithm uses an experimentally-determined shear stress-shear strain curve to provide the characteristics of the reinforcement, and builds a pin-jointed net working outwards from a user-selected starting point, minimising the additional shear strain energy for each step. This enables the behaviour of reinforcements which do not deform in a symmetric manner to be simulated; the architecture of the warp-knitted non crimp fabrics used for the experimental work in this thesis is such that less effort is required to induce shear in one direction (positive shear) than in the other (negative shear). This is due to the fact that negative shear places the stitching in tension, while positive shear compresses the stitch. A more detailed discussion of these issues, together with a comprehensive description of the method of drape prediction, can be found elsewhere [19]. The algorithm was implemented previously within a computer application written in the C programming language, and the source code was available for extension/modification by the present author. This application is referred to as DrapeIt. The same application has also been used to determine local reinforcement properties for flow simulation [135].

The use of such a model for predicting textile reorientation during forming provided data for fibre orientations and shear angle around the geometry of the component being analysed. Since DrapeIt required the geometric description of the component to be provided in the form of nodes and elements, it was convenient to use the finite element mesh which was to be used for structural analysis at a later stage. The tip of the cone was used as the starting point for the draping simulation, just as this was the starting point for forming the reinforcement under experimental conditions. Shear stress-shear strain data for EBX hd 936 reinforcement had been measured previously, and this was used to describe the forming behaviour of the material. The forming analysis was performed and the draped reinforcement pattern is shown in Figure 3.8. This result showed good agreement with the reinforcement deformation observed experimentally using grid strain analysis, published elsewhere [164].

5.7.2 Specification of lamina material properties and orientations

The reinforcement deformation pattern was defined computationally as a number of nodes interconnected by lines indicating the fibre orientation. When determining the properties defined in Section 5.5.1 which were required to conduct an FE shell analysis, the initial problem was to generate data for every finite element, rather than only for those in which a node of the draped mesh was located. This was accomplished using a simple interpolation algorithm, which determined the average of the orientation vectors for each of the two fibre orientations from the surrounding elements. Once both fibre orientations were known for each element, these were transformed such that they lay in the element plane using the following procedure:

- The vectors of two of the element sides were calculated, *S12* and *S13*.
- The element normal, *T3*, was calculated using the vectorial product (cross product) of *S12* and *S13*.
- The vectorial product of the element normal and the material orientation was calculated to yield a vector, *T2*, which was mutually perpendicular to both of these; hence, *T2* was in the plane of the element.
- The vectorial product of *T2* and the element normal was calculated, giving a vector, *T1*, which was parallel to the orientation vector and in the plane of the element. This vector was used to specify the material orientation.

- The above procedure was carried out for both of the fibre directions for each element.

This procedure was necessary since fibre orientation vectors were calculated using the positions of two nodes of the draped mesh, which were frequently not located in the same geometric element; hence, if the elements containing the draped nodes were not coplanar, the direction vector was not in an element plane. Subsequently the included angle, 2ϕ, between the two fibre directions was determined using the scalar product (dot product) of the orientation vectors. Since the angle through which the reinforcement had been sheared was expressed according to Equation 5.32, this permitted calculation of the fibre volume fraction according to Equation 5.33, values for the required parameters being entered by the user. It was assumed that each reinforcement layer occupied the same thickness within the mould cavity.

$$\theta = 90° - 2\phi \tag{5.32}$$

where θ is the angle through which the reinforcement is sheared (the shear angle) and ϕ is the ply angle.

$$V_f = \frac{nS_0}{\rho_{glass} h \cos\theta} \tag{5.33}$$

where h is the mould cavity height, n is the number of reinforcement layers in the laminate, S_0 is the reinforcement superficial density (mass per unit area), ρ_{glass} is the bulk density of glass, V_f is the fibre volume fraction. Values of these parameters are provided in Chapter 3.

Once the fibre volume fraction was known for each element, then the mechanical properties of a constituent unidirectional lamina were calculated, using user defined properties of the constituent phases. For analysis of this component, mechanical properties for Norpol 440-M750 polyester resin and E-glass fibre were used (Table 3.2). The procedure differs from commercially available packages due to the incorporation of these material models to determine local properties automatically from the constituent phase properties and the calculated fibre volume fraction. Each element was assigned its own material property type, which was assumed to be the same for all layers. Although four layers of reinforcement textile were defined as

eight laminae (i.e. eight layers in the shell element), only two fibre orientations were required per element since all reinforcement layers were assumed to have the same orientation and deformation. Since these two orientations had already been calculated for each element, it was possible to write an input file for the Abaqus FE code containing nodes, elements, material properties (one per element), orientations (two per element) and shell section definitions (one per element). Boundary conditions were added manually to complete the information required to perform the structural analysis.

5.7.3 Modelling the compaction behaviour of components containing dissimilar reinforcements

As discussed in Chapter 3 of this thesis, when manufacturing the nose cone component, it became necessary to interleave layers of continuous filament random mat (CFRM) reinforcement with the non crimp fabric due to problems with the manufacturing process. The manufactured component had a lay-up of three layers of EBX hd 936 textile reinforcement, interleaved with two pairs of layers of U101-220 CFRM, as illustrated in Figure 3.7. To incorporate this in a structural model of the part required a knowledge of the thicknesses and fibre volume fractions of each of the reinforcement layers, necessitating an understanding of the compaction behaviour of the reinforcements. Compaction modelling of multiple reinforcement types is beyond the scope of integrated composites structural design packages which are presently available.

Relative layer thicknesses were modelled by Robitaille and Gauvin [165] using an empirical compaction model relating fibre volume fraction to compaction pressure using the relationship in Equation 5.34.

$$V_f = AP^B \tag{5.34}$$

A and B are empirically determined constants for each reinforcement material. Robitaille and Gauvin found values for A and B for EBX hd 936 textile reinforcement and a CFRM reinforcement (Vetrotex Unifilo U101-450, 450 gm^{-2}). Since U101-220 was used in the nose cone solely in pairs of layers, and since Equation 5.34 is

independent of the number of layers provided that nesting is not significant, it was assumed that compaction data for a single layer of U101-450 would be representative of the CFRM in each case. Values for A and B used in this thesis are given in Table 5.3. The constants for the textile reinforcement may change with shear angle, although analytical models reported in the literature [166,167] indicate that compaction pressure is a function of fibre volume fraction only. While most of these models are not applicable to heterogeneous fibre distributions, the fabric in question can be considered as a homogeneous distribution since the tows are not crimped, and adjacent tow edges are in contact even before shearing begins. The relationship in Equation 5.34 can be used in predicting layer thicknesses since the compaction pressure applied to each layer in a multi-layer preform must be equal. The total preform thickness, H, is the sum of the thicknesses of each layer, as in Equation 5.35.

$$H = \sum_{i=1}^{n} h_i \tag{5.35}$$

The thickness of the i^{th} textile layer, h_i, can be calculated using the relationship in Equation 5.36.

$$h_i = \frac{S_0}{\rho_{glass} V_f \cos\theta} \tag{5.36}$$

where S_0 is the superficial density of the reinforcement in the unsheared condition and θ is the shear angle. Note that the same expression is used to find the thickness of the CFRM layers, but the cos θ term is omitted since this reinforcement is not subject to any in-plane deformation in this case.

In the RTM process, the total preform thickness, H, is determined by the thickness of the mould cavity; hence a compaction pressure can be found which satisfies Equation 5.35, determining the thickness and fibre volume fraction of each layer of reinforcement. Solving this equation at a range of shear angles enables a relationship to be plotted between the relative layer thicknesses and the shear angle. Figure 5.23 shows this relationship for the reinforcement configuration used in the nose cone component.

Table 5.3 Reinforcement compaction constants

Material	Superficial Density, S_0 (gm^{-2})	Architecture	A (10^{-2})	B (10^{-2})
EBX hd 936	936	warp-knitted ±45°	12.6	13.1
U101-220	220	CFRM		
U101-450	450	CFRM	1.89	23.3

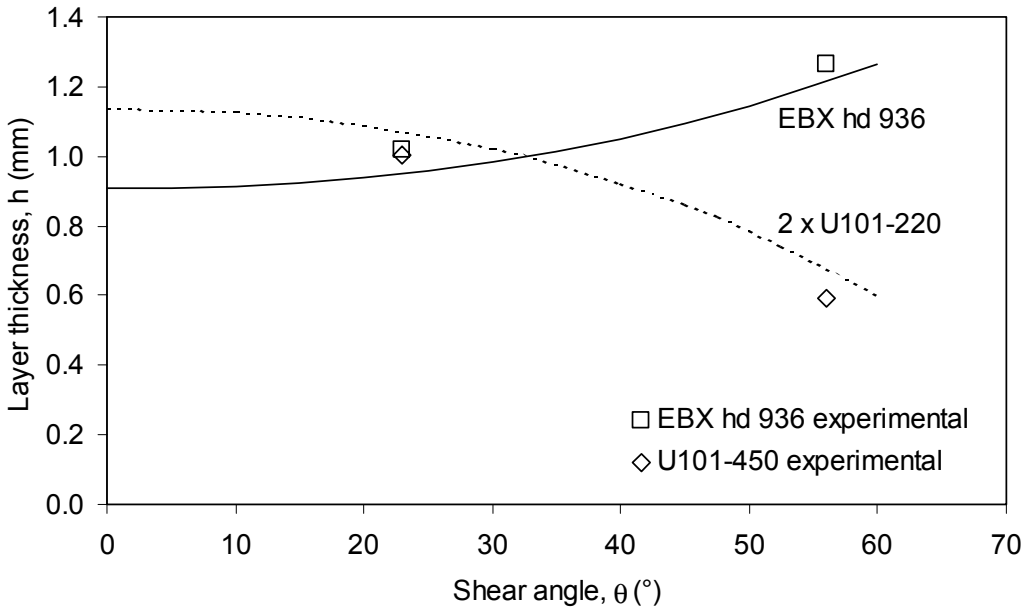

Figure 5.23 The predicted relationship between relative layer thicknesses of EBX hd 936 and U101 reinforcements and shear angle of EBX hd 936, assuming uniform compaction pressure and fixed mould cavity thickness, compared with experimental data measured from sections shown in Figure 5.24 and Figure 5.25.

In order to obtain an indication of the validity of these predictions, sections were cut from the manufactured component and optical microscopy was performed. Figure 5.24 shows a cross section where the textile reinforcement was sheared through approximately 23°, while the textile reinforcement in the section shown in Figure 5.25 was sheared through approximately 56°. Agreement between the predictions of the compaction model in Figure 5.23 and the measured thicknesses was observed to be reasonable for the two cases examined. It should be noted that the reinforcement in Figure 5.25 has wrinkled during the preforming process; this effect can not be predicted by the modelling approaches presented. According to the models used for tow waviness described in Section 5.6, the effect of local wrinkling on component behaviour may be significant. Another effect of the wrinkling observed in Figure 5.25 was that the central layer of reinforcement was offset from the laminate midplane, potentially affecting the properties in bending. Savci et al [168] observed local weaknesses where wrinkling occurred in a weft knit reinforced component

produced by RTM. They found that this was due to the presence of a high void concentration around such irregularities due to local changes in permeability. No such void concentrations could be observed from the micrograph shown in Figure 5.25, but the possibility of this phenomenon exists and the presence of voids was not accounted for by the modelling approach presented.

This simple compaction model was incorporated into DrapeIt such that the actual component was represented more accurately, and its effect on the elastic behaviour of the nose cone, determined by FE analysis, can be seen in Figure 5.27. Elastic properties of the CFRM layers were calculated using the modified rule of mixtures (Equations 2.22 and 2.23).

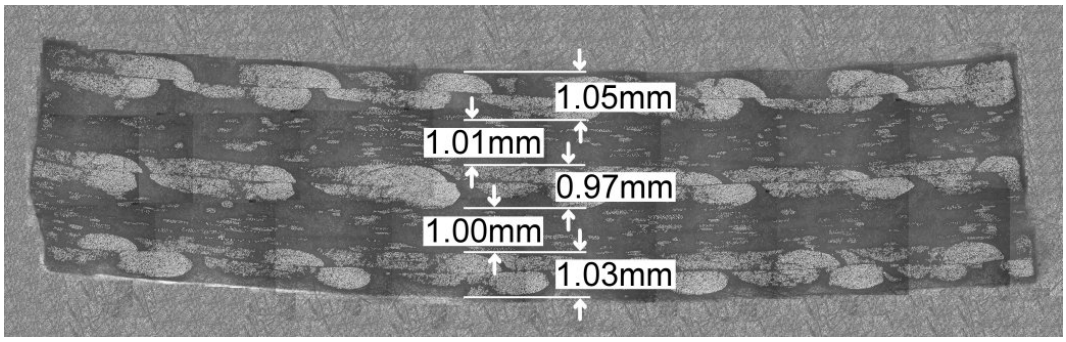

Figure 5.24 Optical micrograph of section taken through multi-layered laminate, the textile having been sheared through approximately 23°. Lay-up stacking sequence is presented in Figure 3.7.

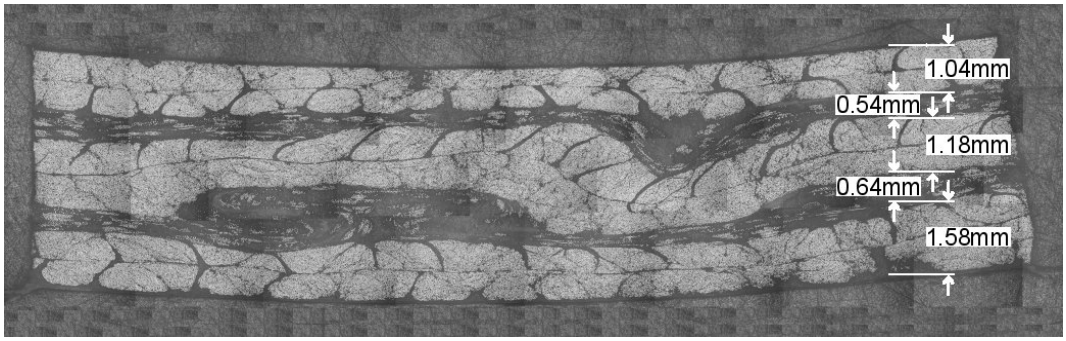

Figure 5.25 Optical micrograph of section taken through multi-layered laminate, the textile having been sheared through approximately 56°.

5.7.4 Results of structural FE analysis of a jet engine nose cone

Input files for the Abaqus FE package were written using the methods described in Sections 5.7.1-5.7.3 to describe the geometry and distribution of material properties and fibre orientations. Approximately 3,100 six noded triangular layered shell elements were used, following a convergence study comparing results of other

meshes (~2,000, ~2,500 and ~3,700 elements) for a single loadcase. Two separate analyses were conducted: in the first, the effects of the CFRM reinforcement were ignored and the structure was assumed to consist of four layers of EBX hd 936; in the second, a more accurate representation of the reinforcement was provided through the use of the compaction model, accounting for the true lay-up. Boundary conditions were added manually and were designed to give a reasonably accurate representation of the experimental procedure, while avoiding additional complications such as modelling of the test fixtures and the contact conditions between these and the part. As such, nodal displacement boundary conditions were used, placing constraints only at the points where the corners of the machined jaws used for loading in the experimental case came into contact with the part. This assumption was made since these were the only points on the geometry where the experimental displacements were known categorically, and to minimise the possibility of over-constraining the model; the boundary conditions are illustrated schematically in Figure 5.26.

Eight sets of boundary conditions were applied at different rotational positions around the geometry within eight discrete analysis steps. The prescribed displacement was 1 mm in each case. Reaction forces at the nodes where displacement was applied were written to the output file and summed to give the force required to produce 1 mm diametric displacement. These data are presented for both analyses in Figure 5.27, where they are compared with experimental data.

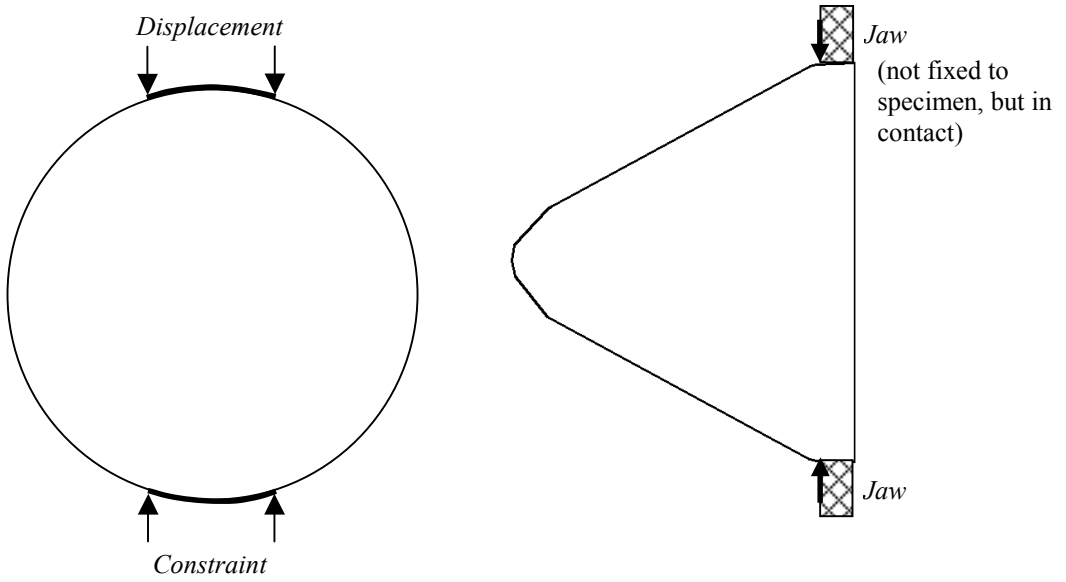

Figure 5.26 Schematic illustration of prescribed-displacement boundary conditions (not to scale)

Excellent agreement between experimental data and predictions from both models was observed, with the exception of the experimental test at position 2, where the response of the component was much stiffer than predicted. Results from the model incorporating CFRM reinforcement and compaction behaviour appeared to agree slightly more closely with those from experimental testing, although the difference between the two models was small. Possible reasons for the differences between experiment and analysis include the fact that the boundary conditions were simplified, assuming point constraints, and that forces were reported at different rotational positions around the geometry (i.e. every 30° for experimental and every 22.5° for FE) such that direct comparisons could only be made at 0° and 90° points. Also, the geometry of the reinforcement was considered to be perfectly identical in every layer, which would not be achievable in the manufactured component due to issues of repeatability when forming reinforcement by hand. However, had a traditional structural analysis been undertaken, where each element was assigned the same 'smeared' properties, no change in force would have been observed as the boundary conditions were moved around the cone. That such an analysis has been performed with so little experimental input, that the procedure is automated, and that such good agreement with validative testing was observed, suggests that this is a powerful technique for analysis of general composite components made with textile reinforcements.

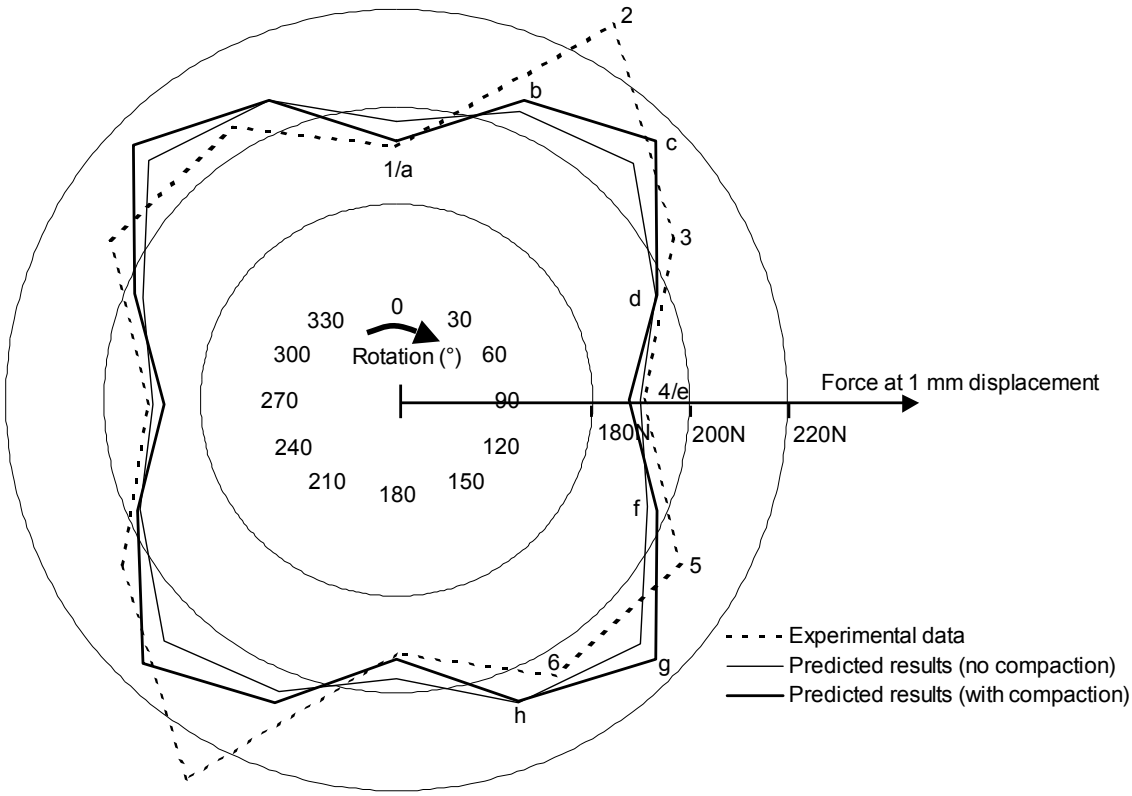

Figure 5.27 Results of component response predicted using layered shell finite element analysis compared with experimental data (dashed line). Analysis results are presented from the model which disregards compaction and the presence of CFRM reinforcement (light line) and from the model which considers the presence of CFRM reinforcement, incorporating a simple model for compaction (heavy line). Experimental data points are labelled 1-6, while those from FE analysis are labelled a-h. Note that the scale does not begin at zero in the centre.

Although a distinct point of failure was not determined when testing the nose cone, predictions of initial failure were obtained from the FE analysis, principally for purposes of illustration. As mentioned in Section 5.5, the maximum stress failure criterion may be evaluated on request by the Abaqus package provided that the `*FAIL STRESS` option was used to define principal failure stresses for each material type, and these results were available for post-processing. Since these orthotropic failure criteria were not applicable to the layers of CFRM reinforcement, failure predictions were made using the analysis in which the reinforcement structure was modelled as four layers of textile reinforcement (i.e. eight laminae).

Figure 5.28 shows contour plots of the failure index, calculated using the maximum stress criterion, for two of the load cases used for the nose cone. The applied pinching displacement of 1 mm was orientated as indicated in Figure 5.28(a) and (c). Values plotted in (b) and (d) were reported in the outer material layer. It can be seen

that the highest values of failure index, i.e. the points closest to failure, occurred at approximately 90° to the direction of application of the applied displacements, where the local change in curvature due to bending was highest due to the geometry of the structure. The maximum failure index values at 1mm displacement were 0.090 and 0.113 for the first and second load cases respectively. Since the analysis was geometrically linear and employed linear elastic material types, it was extrapolated that failure would occur at respective displacement levels of 11.06 mm and 8.87 mm. Assuming linear behaviour, this would correspond to loads of approximately 2.18 kN and 1.81 kN respectively. This indicates a difference in displacement to failure of approximately 20%, with the difference in failure loads being slightly smaller; this is significantly larger than the difference between the reaction forces for the same load cases (which only differed by approximately 3.5%).

It should be noted that although a mesh convergence study was performed for force/displacement results, stress results were not examined in relation to mesh density, and it is possible that inaccuracies in the reported failure behaviour may be present as a result. Since the predictions were not validated with experimental measurements, a time-consuming mesh convergence study for stresses was not perceived to be justifiable. Failure predictions are presented for this component as an indication of the capabilities of the technique, and to highlight the non-intuitive behaviour which may be observed in components manufactured from draped reinforcement. It should also be noted that geometric non-linearity was not accounted for, which may be significant at the high deflections where failure was predicted to occur.

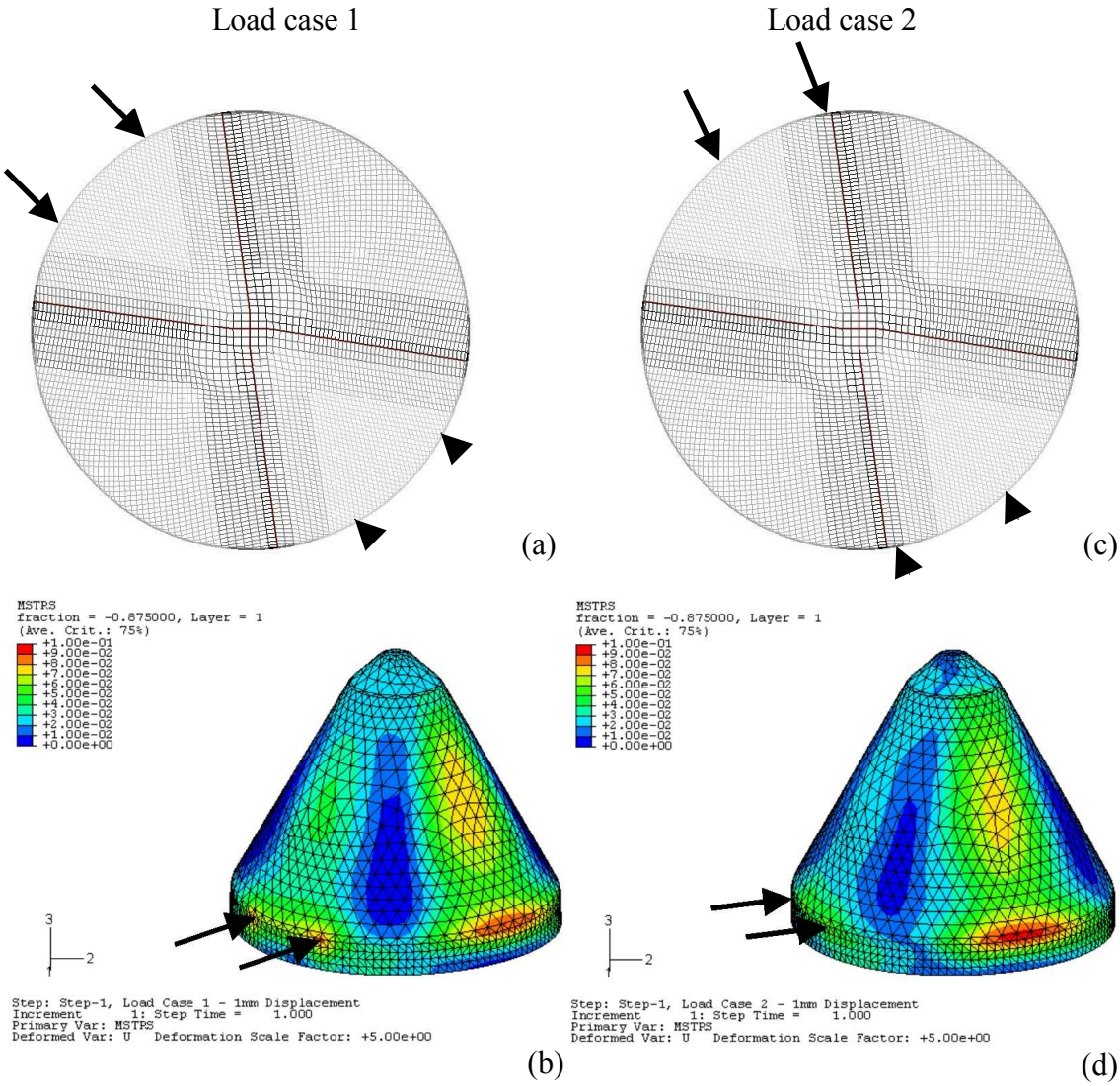

Figure 5.28 (a) and (c) Position of load cases 1and 2 with respect to the draped reinforcement pattern of EBX hd 936 non crimp fabric reinforced nose cone; (b) and (d) contour plots showing the failure index calculated using the maximum stress criterion within the Abaqus FE package. Values on the scale run from 0 (blue) to 0.1 (red).

5.8 Conclusions

A series of models for composite materials has been presented, beginning with micromechanics theories to predict unidirectional composite behaviour at the fibre/matrix level. Subsequently simple ways to consider fabric architecture at the so-called 'meso-scale' were introduced. Finally a method to combine these techniques with finite element analysis to predict the behaviour of a complex structure was presented. Consideration was given to the way in which mechanical properties changed locally as a result of forming, or draping, of the reinforcement, in addition to ensuring that correct fibre orientations were specified for each element in the FE analysis.

At each stage predicted results were compared with results of experimental testing presented in Chapter 4. In general, reasonable agreement was observed for micromechanics predictions, with the exception of transverse strength which was overestimated by the strain concentration model used. No analytical model for in-plane shear strength was presented, instead experimental data were required to be used.

Elastic constants of angle-ply laminates were predicted using classical laminate theory and good agreement with experimental data for NCF reinforced laminates was observed. The same technique was extended to determine lamina stresses in angle-ply laminates, whereupon three failure criteria were used to determine the laminate failure stress. Agreement was reasonable, and was noted to improve when experimentally determined values for lamina strengths were substituted for those predicted with micromechanics.

Although the micromechanics/CLT approach was considered to be suitable for non-crimp fabric reinforced laminates where fibres are straight, those manufactured from woven reinforcements may be expected to behave differently. A simple model to characterise the effects of tow undulation (waviness) was introduced, and was used to make revised predictions of lamina on-axis stiffness. It was also extended to predict on-axis strength. The underlying assumption that each layer of woven fabric could be represented as two discrete layers of wavy tows is certainly a simplification

of the real case, and may not be valid, since the support of the crossing tows is neglected. More significantly, however, since this model only calculated changes in on-axis behaviour, the predicted effect on angle-ply laminates was small. More significance would be observed for other configurations, e.g. 0°/90° cross-ply laminates, but experimental testing of such laminates was not performed. It was noted that analytical models to account for fabric architecture are frequently limited either in the range of textiles which may be described, the range of ancillary geometric parameters (e.g. tow shape) which may be examined, or the ability to predict failure behaviour. In almost all cases, analytical models require an assumption of either constant stress or constant strain in the tow direction, which is not the case in real woven fabric reinforced composites. Some of these issues may be addressed using FE analysis of the repeating unit cell; an introductory study of this method is presented in Chapter 6.

The use of layered shell finite elements was described. Results for in-plane loading of angle-ply laminates were found to be exactly the same as those obtained using CLT, giving confidence in the appropriate application of the techniques. Well-established failure criteria were implemented within the Abaqus FE code, and results from these were also the same as those from the CLT-based model. Other failure criteria may be implemented via a user subroutine, written in Fortran, called by the FE software during analysis. An example of this procedure undertaken for solid elements is given in Section 6.3.

Having established confidence in the finite element method to predict composite properties, a novel and integrated means of predicting the behaviour of composite components was described. Reinforcement draping behaviour was predicted using a computer-based kinematic draping simulation incorporating an energy minimisation algorithm to account for reinforcements exhibiting asymmetric shear behaviour. Information obtained from this simulation was used to record fibre orientations and to calculate fibre volume fraction and mechanical properties for each finite element. A simple model to determine the compaction behaviour of dissimilar reinforcements present within the same component was implemented and integrated into the application, together with the necessary programming steps for automated preparation of finite element analysis input files. A jet engine nose cone component

was analysed using these techniques, and elastic behaviour was seen to change significantly around the geometry due to the nature of the reinforcement architecture. These results were compared with experimental data and very good agreement was observed. Failure analysis of the same component was also performed, which showed that a significant variation in failure behaviour around the geometry was predicted.

Various phenomena which were not considered may offer some explanation for differences between predictions and experiment, including:

- The variation present in fibre orientations in different layers.
- The presence of voids, and the possibility of imperfect fibre/matrix bonding.
- The presence of process-induced residual stresses and distortions.
- Deformation of the reinforcement by mechanisms other than in-plane shear, including fibre slip and wrinkling; the latter was shown to be present.
- The effects of interlaminar shear and delamination.

A more detailed discussion of the areas requiring further study can be found in Section 7.4.

6 FINITE ELEMENT MODELLING OF TEXTILE COMPOSITE UNIT CELLS

6.1 Introduction

In Chapter 5, various differences between predicted and measured mechanical properties were observed. As stated, the predictive models employed rely on various assumptions, e.g. assumptions regarding the stress and strain fields in the material, and that fibres are distributed uniformly rather than grouped in bundles. In order to address some of these issues and, more significantly, to determine their significance, finite element (FE) models of textile composite unit cells may be used to give a more accurate description of the reinforcement architecture, and to remove the necessity to assume constant stress or strain.

In this chapter the work undertaken to investigate the use of finite element (FE) models of textile composite unit cells in order to predict the mechanical behaviour of the bulk material is described. The work presented in this chapter is part of an ongoing collective effort towards fully automated modelling of general textile geometric architectures within the University of Nottingham [169]; many of the underlying geometric algorithms have been described previously [84-85]. A geometric modelling software tool is being developed for use in various aspects of process simulation in addition to mechanical analysis of textile composite structures. One of the fundamental design criteria for this package is the ability to model not only different weave styles, but also to enable modification of each geometric parameter (tow cross-section, tow spacing, crimp etc.) easily within a model of a textile. Statistical variation of fabric architecture may also be incorporated using an appropriate distribution. Models of textiles which have undergone in-plane shear deformation during forming may also be generated. A robust algorithm to generate the complex resin volumes enables geometric modelling of the entire composite unit cell. While geometric modelling of textiles is beyond the scope of this thesis and is not discussed in any detail, the focus of this chapter is on the application of textile modelling to prediction of mechanical properties. As discussed in Chapter 2, using three dimensional FE analysis of composite unit cells (meso-scale) generated with this model would permit prediction of mechanical properties within different areas of draped components made from many different fabrics accounting for their natural

variability. Properties obtained in this manner would subsequently be used as input data for FE analysis at the part level (macro-scale).

Measurements of reinforcement tows within manufactured laminates are presented with methods to characterise the tow shape. A method to evaluate effective modulus and failure stress of a unit cell using the Abaqus implicit FE package with a user defined failure criterion is presented, which is applicable to analyses conducted in two or three dimensions.

Before proceeding with a large number of computationally intensive studies into various textile structures, it is important to have a clear understanding of the individual effects of different material properties and of geometric parameters. Although some researchers (e.g. [90,91,95,100,115]) have examined the effects of the assumed tow path and tow spacing in woven laminates, rigorous studies of the effects of tow cross-sectional geometry have not been reported in the literature. Such work is presented in this chapter using analysis of two-dimensional cross sections through a single tow. Effects of various parameters are evaluated systematically and their sensitivity in analysis of stiffness and failure in transverse tension is reported. Stiffness results from solid models of angle-ply laminates are also presented together with comparable experimental data. Note that in this chapter, the subscripts t and c are used to denote properties pertaining to tows and unit cells respectively, as distinct from their use in the rest of this thesis where they denote tensile and compressive properties.

6.2 Characterisation of tow shapes within textile composites

In order to construct a geometric model of a textile composite unit cell, a knowledge of the cross-sectional shape of the reinforcement tows was required. Optical microscopy was performed on sections of laminates, detailed in Table 4.2, manufactured from FGE-106 non-crimp fabric reinforcement at various shear angles. For analysis of manufactured laminates, sections were cut such that the cutting plane was perpendicular to the fibre direction in one layer of tows in each layer of fabric, as indicated in Figure 6.1. Only the tows perpendicular to the cutting plane were analysed. The specimen preparation and microscopy procedures are outlined in

Section 3.5.2. Images were imported into an image analysis software package, ImageTool (provided free of charge by the University of Texas Health Science Centre in San Antonio), for analysis.

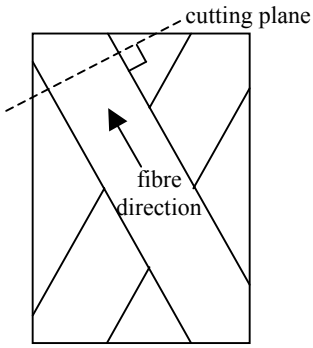

Figure 6.1 Cutting plane used for manufacture of cross-sectional microscopy specimen.

Individual tows were analysed using two measurements. Firstly, a bounding rectangle was drawn around the tow in order to determine the width, w_t, and height, h_t. The tow aspect ratio, a_t, is defined as the ratio of the tow width to the tow height. A freehand shape was subsequently drawn around the edge of the tow, mimicking its shape; the area of this shape was reported by the software, hence the cross-sectional area of the tow, A_t, was known. The shape of the tow was characterised according to the ratio of the cross-sectional area of the tow to the area of the bounding rectangle. This term (r_a) was calculated using Equation 6.1. Figure 6.2 shows the steps involved in measuring a tow in a typical micrograph.

$$r_a = \frac{A_t}{w_t h_t} \tag{6.1}$$

where r_a is the tow area ratio, A_t is the cross-sectional area of the tow, w_t is the tow width and h_t is the tow height.

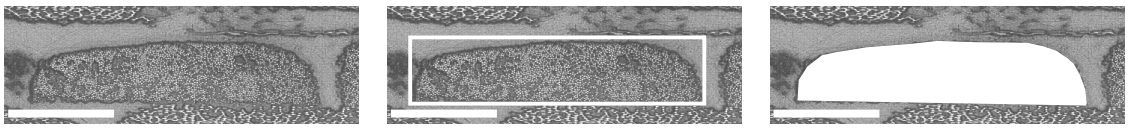

Figure 6.2 Analysing the geometry of a tow cross section. (a) a micrograph of a tow (b) a bounding rectangle used to determine height and width and (c) a freeform shape used to determine area. Scale bar represents 1mm.

Although the tow shown in Figure 6.2 is clearly defined, it can be seen from Figure 6.3 that other laminates presented some challenge in determining the tow boundaries in order to characterise the geometry of the tows. For laminates where tows were not easily distinguishable, fewer measurements are available. Results of measurement of four laminates are presented in Figure 6.4.

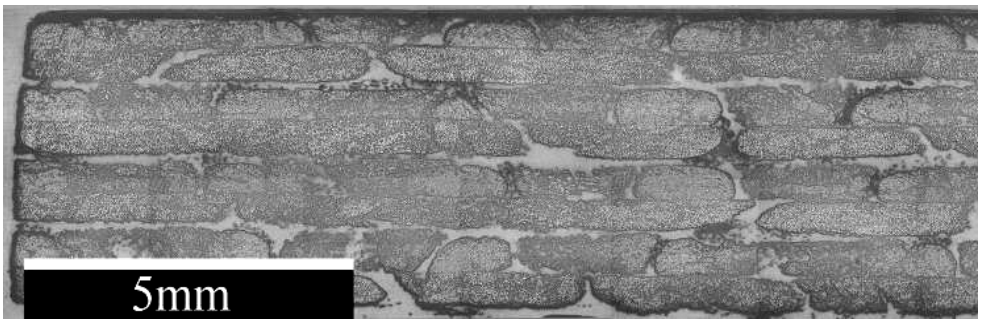

Figure 6.3 Poorly defined tow shapes within a section from a ±27° laminate. Upper tow layers are perpendicular to the section, i.e. the top layer and alternate layers thereafter.

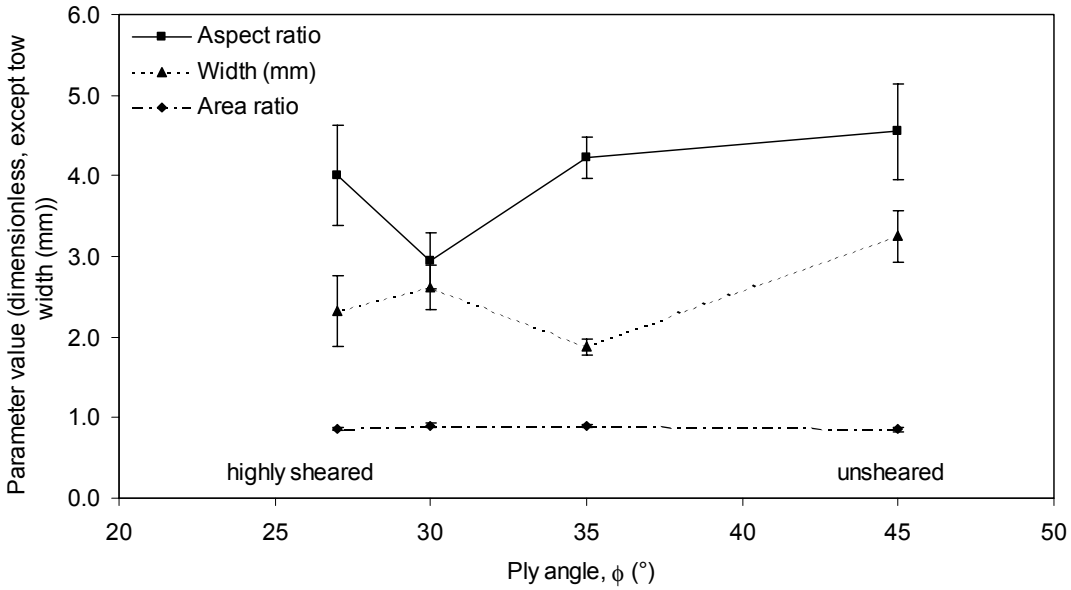

Figure 6.4 Tow geometry data measured by optical microscopy and digital image analysis (averaged values from 15-25 measurements per point). Error bars show 90% confidence interval. Ply angle is defined in Figure 3.3.

The data collected are summarised in Figure 6.4. Three data series are indicated; aspect ratio (width/height) and area ratio (area of tow/area of bounding rectangle) are dimensionless, while tow width is plotted in mm. It can be seen from Figure 6.4 that any change in tow shape caused by shearing of the fabric is too small to be evident within the range of shear angles studied and within the confidence limits of the available data. Standard deviation of measured quantities ranges between

approximately 15-40% for width, 16-32% for aspect ratio and 4-8% for the area ratio, suggesting that mean values obtained are unlikely to be sufficiently significant to observe trends within the scales encountered. Moreover, the large variation in tow geometry suggests that a stochastic approach to simulation, in which geometric parameters are chosen according to a statistical distribution, may be the most appropriate technique in the longer term. For the purposes of an initial study, the findings suggest that constant tow geometry at all shear angles may be assumed, considerably simplifying the work undertaken and reducing the number of variables in a model used to characterise a single material. The overall mean values are given in Table 6.1.

Table 6.1 Mean measured tow geometry parameters from FGE-106 reinforced laminates

Parameter	Value
Tow width (mm)	2.5
Aspect ratio	3.9
Area ratio	0.88

For the purposes of a geometric model, a flexible function was required to describe the tow cross section. Equation 6.2 describes a generalised ellipse:

$$\pm y = \pm\left(\frac{h_t}{2}\right)\left(1-\frac{x^2}{\left(\frac{h_t a_t}{2}\right)^2}\right)^n \tag{6.2}$$

where x and y are geometric coordinates, h_t is the tow height, a_t is the tow aspect ratio and n is the tow shape parameter.

This equation is used to determine the shape of a general ellipse. The tow shape parameter, n, defines the shape of the curve, with n=0.5 producing a natural ellipse and n=0 producing a rectangle. For values in the range 1>n>0.5 a lenticular shape is generated, although for the cases presented in this thesis, values in the range 0.5≥n>0 were used exclusively. Coordinates had to be generated separately for each quadrant; this also permitted the production of non-symmetric shapes. A sample of tow shapes generated using Equation 6.2 is shown in Figure 6.5.

The area of each quadrant of the generalised ellipse was calculated in a spreadsheet using numerical integration techniques (the trapezium rule with approximately 100 intervals). Using an iterative approach, it was also possible to determine the value of n which produced a specified ratio of the tow area to that of its bounding rectangle (r_a).

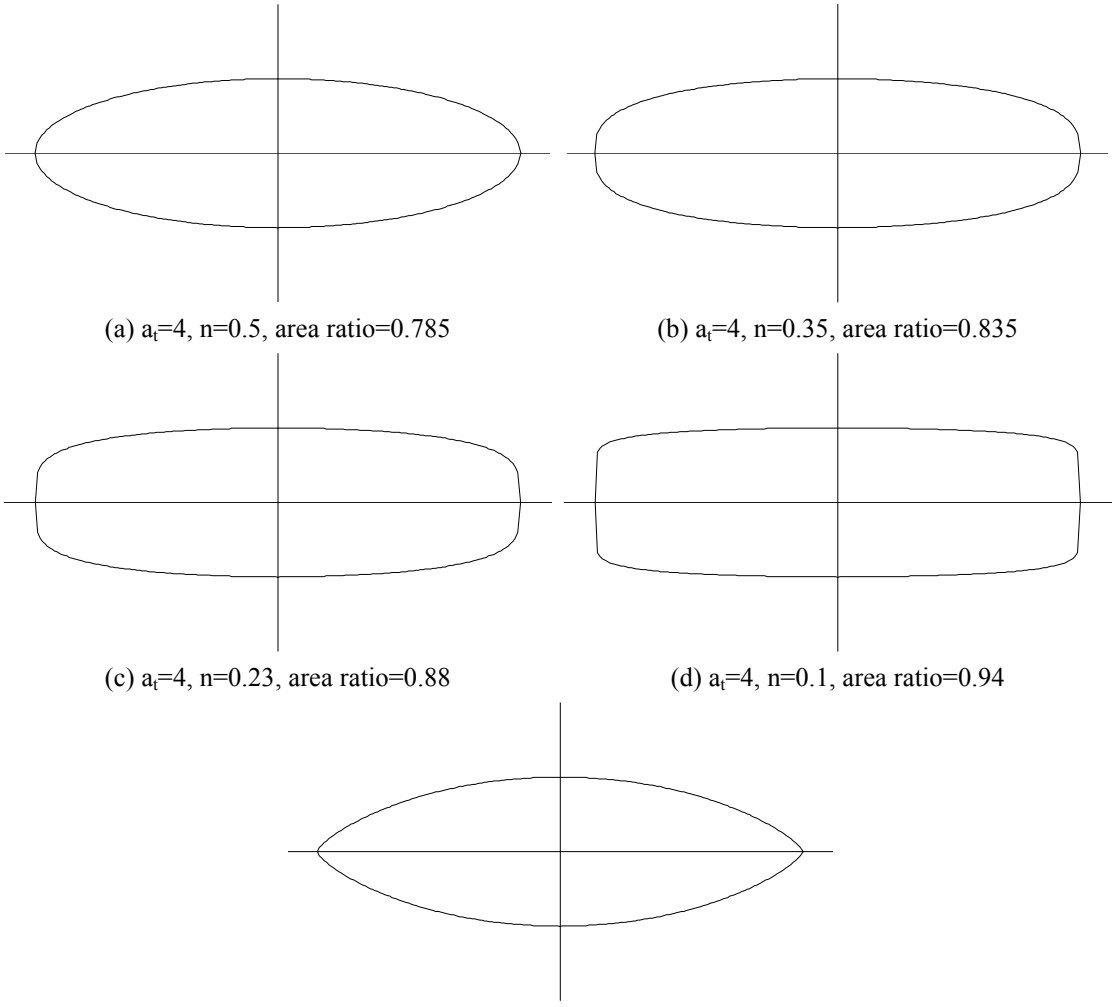

(a) a_t=4, n=0.5, area ratio=0.785

(b) a_t=4, n=0.35, area ratio=0.835

(c) a_t=4, n=0.23, area ratio=0.88

(d) a_t=4, n=0.1, area ratio=0.94

(e) a_t=4, n=0.75, area ratio=0.72

Figure 6.5 Tow shapes produced using Equation 6.2 (a)-(d) show evolution of tow shape with n; (e) shows the lenticular shape produced for 0.5<n<1, which would be applicable to tows in woven or braided reinforcements.

6.3 Finite element modelling of a single tow cross-section

The systematic study presented in this section concentrated on the effect of various parameters on transverse tensile behaviour of composites, i.e. behaviour when load was applied perpendicular to the fibre direction. Models of a single tow cross-section in the 2-3 plane within a rectangular cell were made in two dimensions, and

quadratic triangular generalised plane strain elements were employed within the Abaqus implicit FE code (element designation CPEG6). These elements permitted through-thickness strain, but required this to remain constant for the whole model, i.e. faces remained plane but were able to move in the material 1 direction. Unit thickness was assumed. Displacement was applied to the right hand vertical edge in the 2 direction, while the left hand vertical edge was restrained in the 2 direction. Both vertical edges were free to move in the 3 direction. The lower edge was free to move in the 2 direction and restrained in the 3 direction. The upper edge was free to move in both directions, but forced to remain flat by coupling the displacement degree of freedom in the 3 direction for all nodes on this edge using the *EQUATION option in Abaqus. This was performed to satisfy requirements of geometric compatibility, assuming that the section being analysed was part of a continuum. Although it may be argued that periodic boundary conditions are more appropriate for such models, if a stochastic approach to calculation is used then periodic assumptions are not valid since surrounding cells are not identical. The axis system and boundary conditions are defined in Figure 6.6.

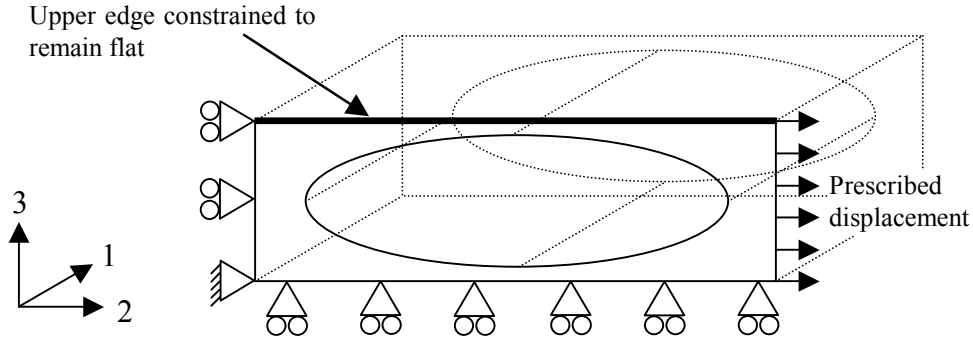

Figure 6.6 Specification of material axes and boundary conditions used for FE modelling

The transverse modulus of the cell, E_{2c}, was calculated by obtaining the applied strain in the cell, ε_{2c}, from the prescribed displacement and cell length according to Equation 6.3, and the resultant stress, σ_{2c}, from the sum of the reaction forces in the 2 direction at the nodes on the edge where displacement was applied and the cross-sectional area in the 1-3 plane, as in Equation 6.4. This enabled direct calculation of the effective modulus of the cell using Equation 6.5.

$$\varepsilon_{2c} = \frac{\delta w_c}{w_c} \tag{6.3}$$

where w_c is the width of the unit cell and δw_c is the prescribed displacement (Figure 6.7)

$$\sigma_{2c} = \frac{\sum RF_2}{h_c} \quad \text{(assuming unit thickness in the 1 direction)} \tag{6.4}$$

where h_c is the height of the unit cell and ΣRF_2 is the total reaction force at the displaced edge (Figure 6.7)

$$E_{2c} = \frac{\sigma_{2c}}{\varepsilon_{2c}} \tag{6.5}$$

Failure stress for the cell was determined using the maximum stress failure criterion within the tow and the von Mises criterion in the resin. As discussed in Chapter 2, the maximum stress criterion states that if any of the principal stresses exceeds the corresponding failure stress in that direction then failure is deemed to occur; for the isotropic resin phase, the von Mises stress invariant was compared with the resin failure stress to determine whether failure occurred. A failure index was calculated at each integration point using a user subroutine within Abaqus according to Equations 6.6 and 6.7.

$$FI_t = \max\left(\left|\frac{\sigma_1}{\sigma_{1ut}}\right|, \left|\frac{\sigma_2}{\sigma_{2ut}}\right|, \left|\frac{\sigma_3}{\sigma_{3ut}}\right|, \left|\frac{\tau_{12}}{\tau_{12ut}}\right|, \left|\frac{\tau_{13}}{\tau_{13ut}}\right|, \left|\frac{\tau_{23}}{\tau_{23ut}}\right|\right) \tag{6.6}$$

$$FI_m = \frac{\sigma_{vonMises}}{\sigma_{um}} \tag{6.7}$$

The user subroutine was a program written in the Fortran language, which was called by the Abaqus package when the analysis was run for each material calculation point in the model. The variables which it calculated were subsequently available for postprocessing. A listing of the code used for this subroutine can be found in Appendix E. Since the analysis was linear, the maximum failure index obtained in the model was proportional to the prescribed displacement and hence to the resultant stress, enabling the initial failure stress to be determined directly.

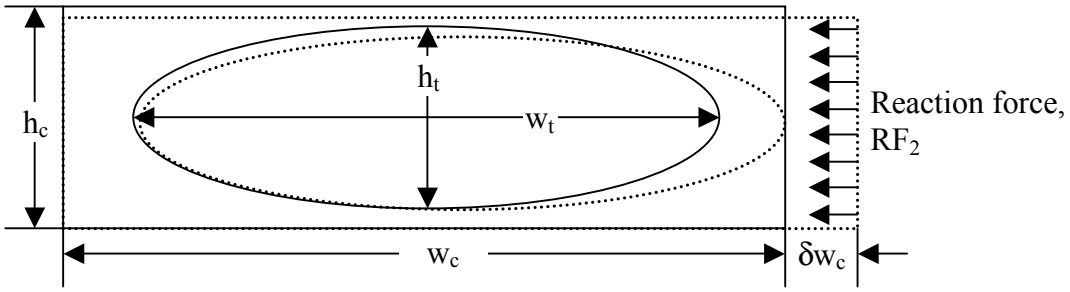

Figure 6.7 Dimensions of the 2D unit cell model, with displaced shape indicated by a dashed line

6.4 Mechanical property calculation for the composite tow

The subject of micromechanics models is discussed in Section 2.2, however it is pertinent to mention briefly the models used for this section of the work here. Micromechanics models were used to determine mechanical behaviour of the unidirectional composite forming the tow. The rule of mixtures (Equation 2.1) was used for Young's modulus in the fibre direction and for Poisson's ratio, while the Halpin-Tsai equations (Equation 2.4) were used to calculate transverse and shear moduli. The ultimate strength in the fibre direction was considered to be fibre dominated according to Equation 2.6. Transverse tensile strength within the tow was predicted using a micromechanics model devised by Kies [36], which evaluated stress concentration induced by the presence of stiff cylindrical fibres within the matrix. Consequently, the transverse failure stress was given by Equations 2.9 and 2.10. A model of the same form, proposed by the same author, was used for shear strength of the unidirectional composite in the 2-3 plane (τ_{23ut}), according to Equations 2.11 and 2.12. In the absence of a simple model for in-plane shear strength, a constant value of $\tau_{12ut} = \tau_{13ut} = 64.4$ MPa was assumed, as discussed in Section 5.2.2. The application of these equations to the materials in question is described in Chapter 2. The properties of the constituent phases were variables under investigation, but were of the same order of magnitude as those of Norpol 420-100 polyester resin and E-glass fibres, which are provided in Table 3.2.

Although σ_{1ut}, τ_{12ut} and τ_{13ut}.are used as input parameters for the failure criterion, it should be noted that, in the analyses presented in this chapter, none of the associated failure mechanisms is active. Similarly the failure indices calculated throughout the

isotropic resin phase are significantly smaller than those for the transverse tension mode within the tow region. In all cases presented in this thesis, failure index for modes other than transverse tension in the tow remains below 0.6 throughout the models when failure initiates within the tow (i.e. maximum failure index reaches unity). Hence the sensitivity of these parameters has not been assessed.

6.5 Planning of analyses

The initial stages of a systematic evaluation of sensitivity of the model to a number of material and geometric parameters have been undertaken. In preparing this evaluation, a number of independent geometric parameters were identified; care was taken to ensure that parameters were completely independent in order that the array of cells generated could be used in future studies employing a statistical 'design of experiments' technique to determine the effects of interaction between parameters. Investigation of the same parameters on resin flow behaviour was also performed [170], and the assistance of Dr. F. Robitaille in the selection of independent variables is gratefully acknowledged. The analyses presented in this thesis were conducted in small groups, modifying individual parameters while maintaining all others at the nominal values. These parameters are listed in Table 6.2. While not all parameters were investigated in the present work, they are all explained for the sake of completeness.

Table 6.2 Independent geometric and material parameters pertaining to analysis of transverse behaviour in unit cells. (See notes below on parameter choices and definitions.)

Designation	Parameter	Proposed values
Geometric parameters:		
A	Tow aspect ratio, a_t	3, 4, 5, 6, 7
B	Upper and lower tow shape parameters, n_{upper} & n_{lower}	0.1, 0.2, 0.3, 0.4, 0.5
C	Cell fibre volume fraction, V_{fc}	(0.7, 0.8, 0.9) x V_{fcmax}
D	Cell aspect ratio, a_c	$(a_{cmin}+a_t)/2$, a_t, $(a_{cmax}+a_t)/2$
E	Horizontal and vertical shift	(0.5, 0.25, 0) x max possible shift
Material parameters:		
F	Number of filaments in the tow	6000, 8000, 10000, 12000, 14000
G	Young's modulus of resin, E_m	3, 3.5, 4, 4.5, 5 GPa
H	Young's modulus of fibre, E_f	60, 65, 70, 75, 80 GPa
I	Poisson's ratio of resin, ν_{12m}	0.22, 0.26, 0.3, 0.34, 0.38
J	Poisson's ratio of fibre, ν_{12f}	0.22, 0.26, 0.3, 0.34, 0.38
K	Ultimate strength of resin, σ_{um}	40, 50, 60, 70, 80 MPa

Notes:

A. Tow aspect ratio values were chosen directly to be within the range measured in laminates in Section 6.2. The area of the tow bounding box (the product of tow width, w_t and tow height, h_t) was kept constant such that w_t and h_t were defined as a function of the aspect ratio, a_t.

B. Separate tow shape parameters could be selected for each quadrant of the generalised ellipse. In all cases presented here, tows exhibited symmetry about their horizontal and vertical axes, i.e. n (Equation 6.2) was constant for all quadrants.

C. Cell fibre volume fraction, V_{fc}, was defined as a multiple of the maximum possible cell fibre volume fraction (i.e. that when $w_c=w_t$ and $h_c=h_t$) and was used to determine the dimensions of the cell relative to those of the tow. The nominal case was used for all analyses presented in this thesis.

D. Cell aspect ratio, a_c, was defined as the quotient of cell width, w_c, and cell height, h_c (related to the tow aspect ratio such that the tow always remained inside the cell without touching the edges). This was expressed as a function of the nominal case ($a_c=a_t$) and the minimum and maximum possible values. Values of a_{cmin} and a_{cmax} were calculated such that $w_c=w_t$ (min) and $h_c=h_t$ (max). For all cases presented in this thesis, the nominal value of a_c was used.

E. Values of horizontal and vertical shift were chosen to move the centre of the tow away from the centre of the cell. These values were defined in terms of the tow and cell dimensions such that the tow remained within the cell at all times. The maximum possible shift was that which caused the tow to touch the edge of the cell. No shift was applied to the cases presented in this thesis.

F. The number of glass fibre filaments was used to define the amount of glass in each tow, and hence in each cell; this was a more fundamental approach than the direct use of V_f since it allowed the fibre volume fraction to change as a function of geometric parameters, just as that of a laminate changes as a function of the mould cavity thickness or the level of compaction. The nominal case contained 10000 fibres of diameter 15.8 μm.

G,H,I,J,K. Values of constituent material properties were chosen to indicate the model sensitivity to these parameters within reasonable limits around the manufacturers' quoted values. Shear moduli for the isotropic constituents were calculated using the relationship defined in Equation 5.1. Values of Poisson's ratio remained constant in the cases presented in this thesis. Note that failure stress of the fibre phase was not listed as a parameter since fibre dominated failure was not an active phenomenon in the transverse analyses presented.

Table 6.3 Parameters used for 2D generalised plane strain FE analyses (parameter under investigation shown in bold for each case). Overall fibre volume fractions in the tow and cell, which vary with some parameters, are also shown for each case.

Case designation	Parameters investigated						Resultant fibre vol. fractions	
	Fibre modulus, E_f (GPa)	Matrix modulus, E_m (GPa)	Matrix failure stress, σ_{um} (MPa)	No. fibres	Tow aspect ratio, a_t	Tow shape parameter, n	Tow, V_{ft} (%)	Cell, V_{fc} (%)
1 (nominal)	70	4	60	10000	5	0.3	46	32
2	**60**	4	60	10000	5	0.3	46	32
3	**65**	4	60	10000	5	0.3	46	32
4	**75**	4	60	10000	5	0.3	46	32
5	**80**	4	60	10000	5	0.3	46	32
6	70	**3**	60	10000	5	0.3	46	32
7	70	**3.5**	60	10000	5	0.3	46	32
8	70	**4.5**	60	10000	5	0.3	46	32
9	70	**5**	60	10000	5	0.3	46	32
10	70	4	**40**	10000	5	0.3	46	32
11	70	4	**50**	10000	5	0.3	46	32
12	70	4	**70**	10000	5	0.3	46	32
13	70	4	**80**	10000	5	0.3	46	32
14	70	4	60	**6000**	5	0.3	28	19
15	70	4	60	**8000**	5	0.3	37	25
16	70	4	60	**12000**	5	0.3	55	38
17	70	4	60	**14000**	5	0.3	64	44
18	70	4	60	10000	**3**	0.3	46	32
19	70	4	60	10000	**4**	0.3	46	32
20	70	4	60	10000	**6**	0.3	46	32
21	70	4	60	10000	**7**	0.3	46	32
22	70	4	60	10000	5	**0.1**	42	32
23	70	4	60	10000	5	**0.2**	44	32
24	70	4	60	10000	5	**0.4**	48	32
25	70	4	60	10000	5	**0.5**	50	32

By modifying the values of these parameters a large array of unit cells representing sections of composite parts can be created. The 25 combinations of parameters selected for this study appear in Table 6.3. The long-term aim of this work is to document the effect on mechanical properties of all parameters used in defining any unit-cell from within a full 3D multi-layer preform, however it is beyond the scope of this thesis to explore this field in great detail; hence a selection of results is presented which gives some insight into the potential effects of certain parameters. Further discussion of the issues surrounding unit cell modelling can be found in Chapter 7.

6.6 Results

Results are presented for transverse modulus, E_{2c}, and failure stress, σ_{2uc}, with respect to the parameters examined within the study. Results presented isolate individual variables as described in Section 6.5. In all of the two-dimensional cases studied, the failure mechanism was transverse tension within the tow region. This was in agreement with the experimental findings for plain-weave textile composites of Pandita et al [171], amongst other authors. A summary of the values calculated for each case is presented in Table 6.4. Figure 6.8(a) shows a typical FE mesh, comprised of 2324 elements and 4817 nodes, while Figure 6.8(b) and (c) show the transverse stress distribution in the nominal case and case 22 respectively. Most analyses within the study presented had a stress distribution similar to that of the nominal case, and failure was predicted to occur near one of the ends of the tow. As the tow shape factor, n, decreased, the stress distribution tended to that seen in Figure 6.8(c), where stress was almost constant through the whole section of the tow, with areas of slightly raised stress at the four apices, where failure was predicted to occur. It should be noted that published experimental findings for 0°/90° laminates (e.g. [171]) often suggest that failure occurs at the centre of the tow; the effect on the stress field caused by the presence of a perpendicular tow has not been evaluated in the present study, and may cause the predicted position of initial failure to change.

Table 6.4 Results obtained using 2D generalised plane strain FE analysis.

Case designation	Active parameter	Cell modulus, E_{2c} (GPa)	Cell failure stress, σ_{2uc} (MPa)	Micromech. modulus, E_{2c} (GPa)[a]	Micromech. failure stress, σ_{2uc} (MPa)[b]
1 (nominal)		8.37	34.11	8.46	50.5
2	E_f = 60 GPa	8.21	33.52	8.29	50.3
3	E_f = 65 GPa	8.29	33.84	8.38	50.4
4	E_f = 75 GPa	8.43	34.39	8.52	50.6
5	E_f = 80 GPa	8.49	34.60	8.58	50.7
6	E_m = 3 GPa	6.47	35.10	6.54	50.9
7	E_m = 3.5 GPa	7.43	34.60	7.51	50.7
8	E_m = 4.5 GPa	9.28	33.65	9.38	50.3
9	E_m = 5 GPa	10.16	33.17	10.27	50.2
10	σ_{um} = 40 MPa	8.37	22.76	8.46	33.7
11	σ_{um} = 50 MPa	8.37	28.45	8.46	42.1
12	σ_{um} = 70 MPa	8.37	39.83	8.46	58.9
13	σ_{um} = 80 MPa	8.37	45.52	8.46	67.3
14	No.fibres = 6000	6.28	39.70	6.30	50.7
15	No.fibres = 8000	7.25	36.99	7.22	50.7
16	No.fibres = 12000	9.66	30.65	9.69	50.0
17	No.fibres = 14000	11.19	26.07	11.12	49.1
18	a_t = 3	8.29	46.03	8.46	50.5
19	a_t = 4	8.35	35.70	8.46	50.5
20	a_t = 6	8.40	35.07	8.46	50.5
21	a_t = 7	8.42	34.94	8.46	50.5
22	n = 0.1	8.33	39.21	8.46	50.5
23	n = 0.2	8.34	38.22	8.46	50.5
24	n = 0.4	8.38	32.14	8.46	50.5
25	n = 0.5	8.90	32.99	8.46	50.5

[a] Predicted Young's modulus of the cell based on overall fibre volume fraction, calculated using Equation 2.4.

[b] Predicted transverse failure stress of the cell based on overall fibre volume fraction, calculated using Equations 2.9 and 2.10.

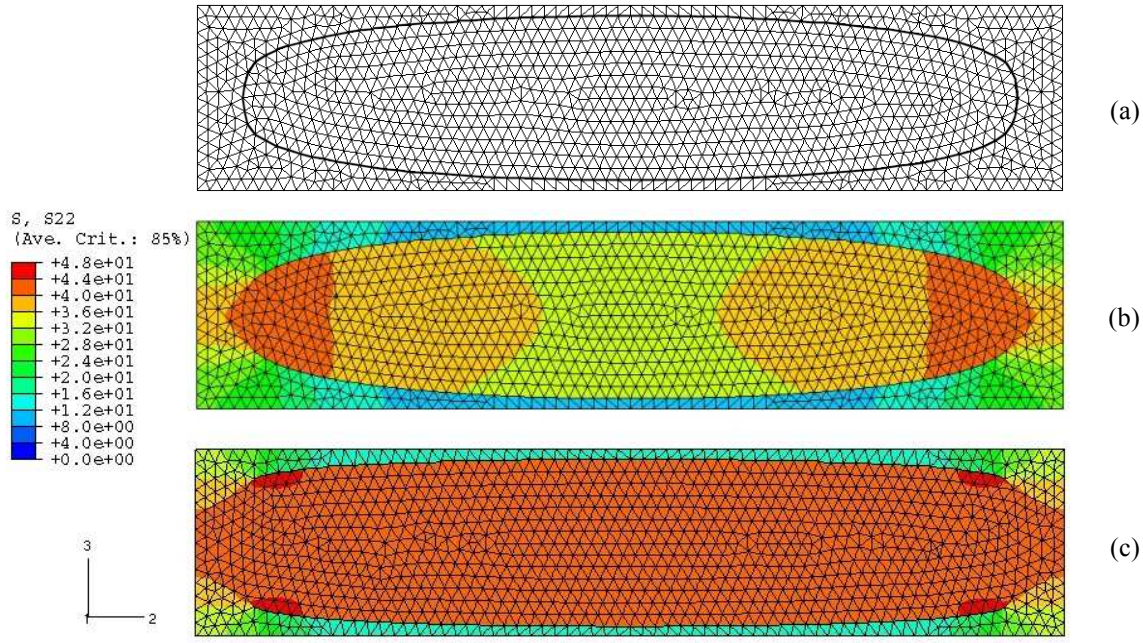

Figure 6.8 (a) Finite element mesh for the nominal case (case 1); Distribution of transverse stress in (b) nominal case and (c) case 22 (tow shape parameter, n=0.1).

Figure 6.9 shows the effect of fibre modulus, E_f, on mechanical behaviour. It is clear that while E_f is well known to have a dominant effect on properties in the fibre direction, it has little significance for the transverse properties.

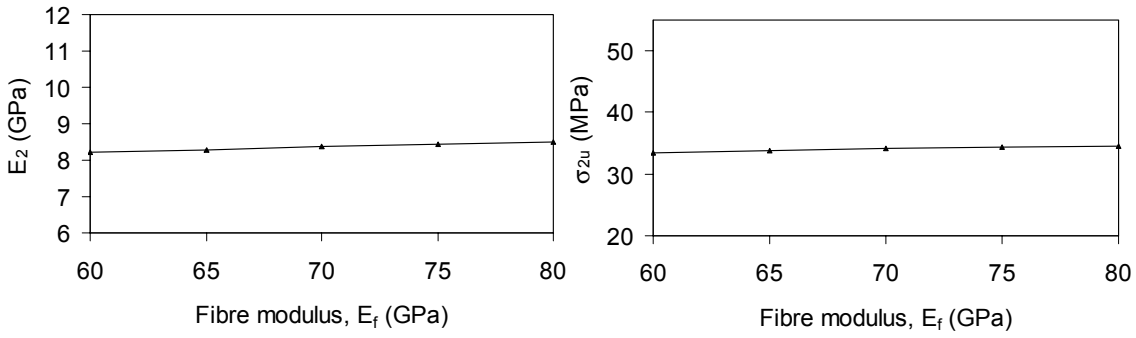

Figure 6.9 Effect of fibre modulus on the elastic and failure behaviour of the unit cell.

Conversely, the Young's modulus of the matrix phase plays a much more significant role in the transverse elastic behaviour of the unit cell, as demonstrated in Figure 6.10. While this may be observed from the Halpin-Tsai equations, the effect on the failure behaviour of the cell is less obvious, and the change predicted using FE analysis was significantly larger than that suggested by micromechanics models alone. This can be seen from the data in Table 6.4.

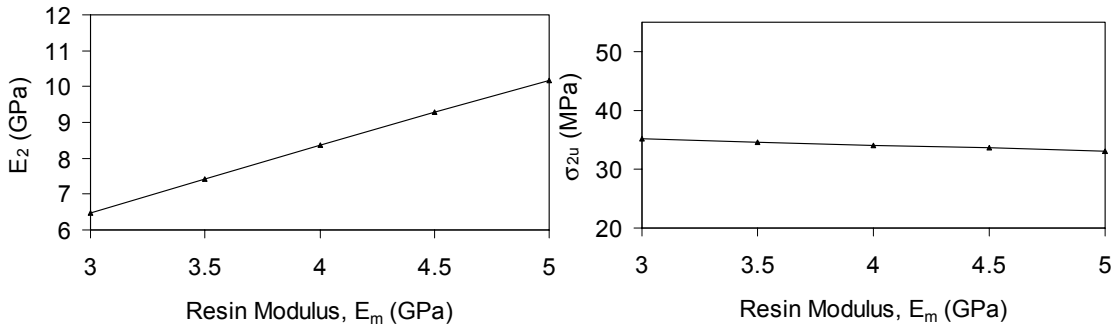

Figure 6.10 Effect of resin modulus on the elastic and failure behaviour of the unit cell.

Although the strength of the matrix phase has no direct influence on the composite elastic behaviour, it is the parameter with the most significant effect on the transverse failure stress; this is clear from Figure 6.11. The relationship between σ_{2uc} and σ_{um} is one of direct proportionality when all other parameters are maintained constant. As long as failure is known to be by transverse tension within the tow, this relationship can be deduced directly from Equation 2.9.

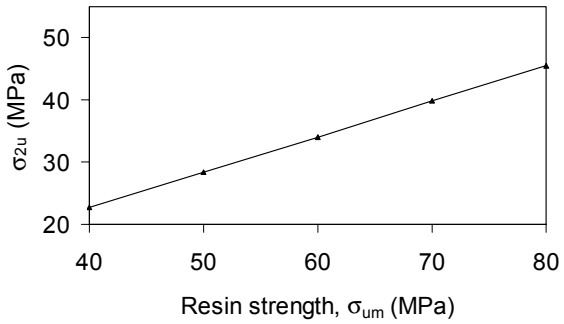

Figure 6.11 Effect of resin strength on the failure behaviour of the unit cell.

As discussed in the planning section, the number of fibres contained within the tow has been used to determine the fibre volume fraction of the tow, V_{ft}, and the cell, V_{fc}. In the cases presented in Figure 6.12, the relationship between the number of fibres and both V_{ft} and V_{fc} is proportional. If modulus is calculated for the whole cell using the Halpin-Tsai equations assuming an even distribution of fibres within the cell having fibre volume fraction, V_{fc}, the results overlay those produced using the FE approach almost exactly in this case. However, if the same assumption is used with the micromechanics model for σ_{2u} (Equations 2.9 and 2.10), the strength is considerably overestimated. The principal cause of this would appear to be that the unit cell models employ a much higher volume fraction within the tow region, which

subsequently fails at lower stresses. In most design analysis environments, however, this issue would almost certainly be overlooked.

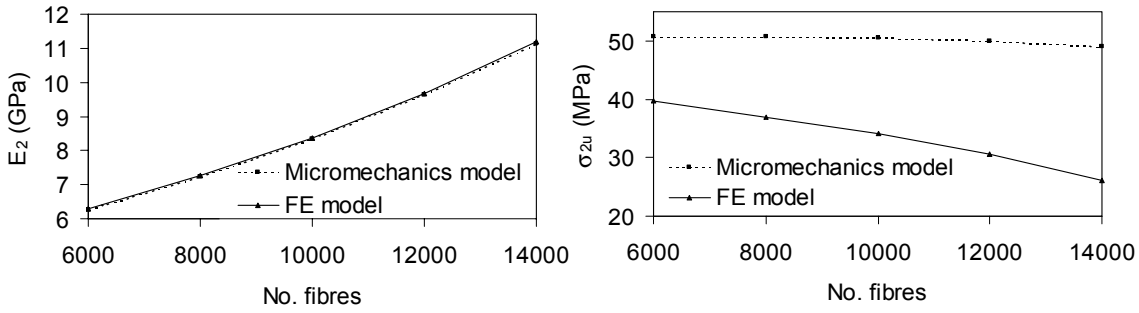

Figure 6.12 Effect of number of fibres on the elastic and failure behaviour of the unit cell. Behaviour observed in the FE model is compared with that determined by assuming a uniform fibre distribution within the unit cell having the same number of fibres using the micromechanics approach in Equations 2.6 and 2.9.

Although the tow aspect ratio, a_t, (defined as tow width divided by tow height) has little effect on the elastic behaviour of the cell, and no effect on the fibre volume fraction, it can be see from Figure 6.13 that a change in aspect ratio from 3 to 4 results in a reduction in failure stress of around 22%. This is a comparable reduction to that observed when the number of fibres (and hence V_{ft} and V_{fc}) is doubled. While no designer would ignore such a change in fibre volume fraction, it is most unlikely that the cross section of the tow is even considered in such an environment. It may be argued that well designed composite components should not be susceptible to transverse failure modes. However, in most applications of textile reinforcements while one set of tows may carry the load along its principal axis, there is a perpendicular set of tows within which cracks may develop and spread to interlaminar regions, such as those observed in [171].

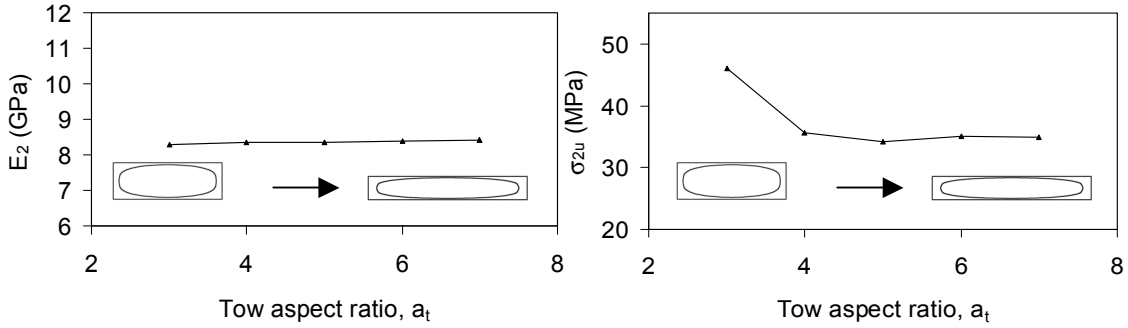

Figure 6.13 Effect of tow aspect ratio on the elastic and failure behaviour of the unit cell.

When the tow shape parameter, n, is changed, V_{ft} changes while V_{fc} remains constant. The volume fraction within the tow increases with increasing n due to the subsequent reduction in tow area. While increasing V_{ft} has already been shown to reduce failure stress, it is still not obvious that the modulus would increase under the same circumstances, although the results presented in Figure 6.14 indicate that this is the case.

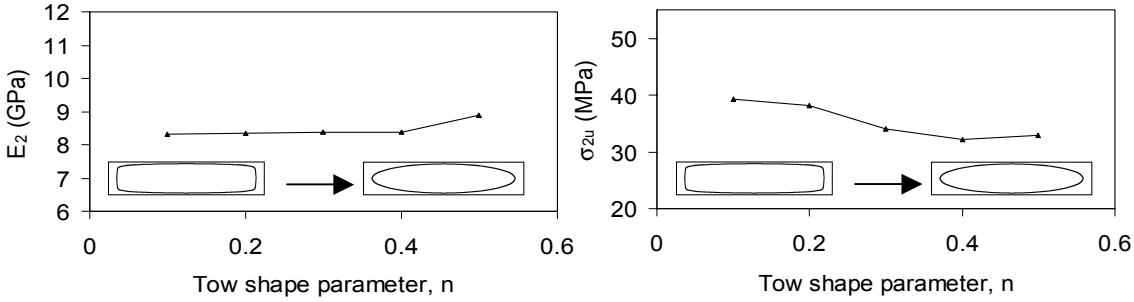

Figure 6.14 Effect of tow shape parameter on the elastic and failure behaviour of the unit cell.

Experimental testing of transverse mechanical behaviour of UD composites has been undertaken by the author and is reported in Chapter 4. Formax UD-468 unidirectional fabric reinforcement (constructed from tows of the same specification as those used to manufacture FGE-106 reinforcement, examined in Section 6.2) was used to construct glass-polyester laminates at three fibre volume fractions, using Norpol 420-100 resin. Results showed an increase in failure stress with fibre volume fraction within the laminate, which contradicts the predictions of micromechanics models for σ_{2u} as shown in Figure 6.15. From the results presented in this chapter, it seems that this phenomenon may be explained by changes in tow geometry which are not considered by more traditional approaches. For example, Robitaille and Gauvin [172] observed that tows became more rectangular with compaction, and hence that at higher fibre volume fractions the value of the tow shape parameter, n, may be inferred to be lower; following the results in Figure 6.14 this could explain an increasing failure stress with V_f. It should be noted that predictions from the FE model agreed more closely with failure stresses observed experimentally than those obtained using micromechanics.

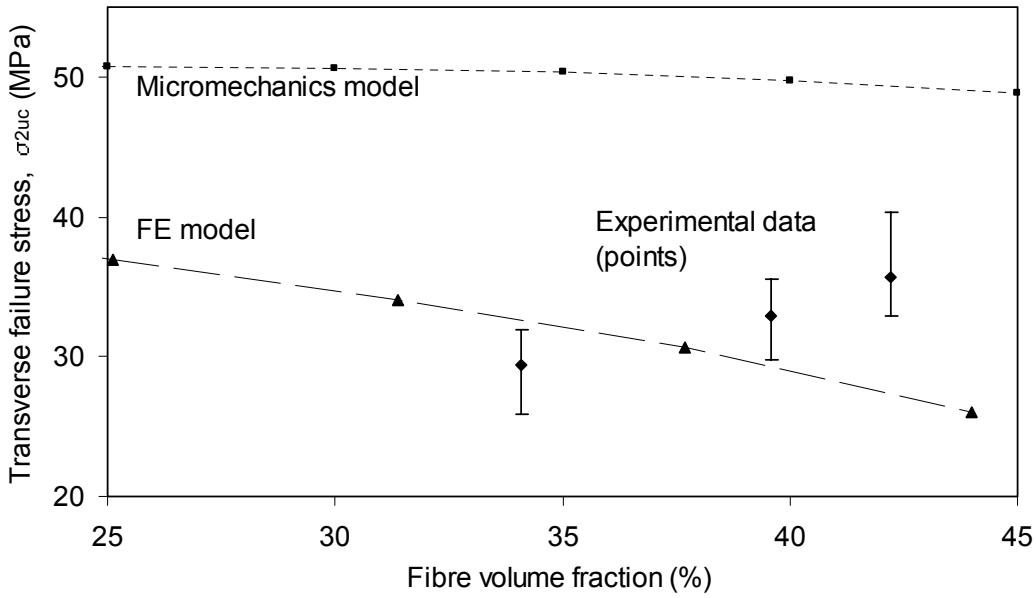

Figure 6.15 Experimental data for laminates manufactured from unidirectional glass fabric compared with micromechanics model which assumes an even distribution of fibres within the laminate & 2D FE of a single tow. Error bars show maximum and minimum values obtained during testing.

6.7 Initial studies of 3D unit cells

An initial attempt at modelling three-dimensional unit cells with solid finite elements has been undertaken. Two cases were produced using a highly idealised model of the textile structure. These cases consisted of two layers of tows forming a representation of a non-crimp fabric (NCF). In the first case the layers of tows were orthogonal, at ±45° to the reference (x) direction, while in the second they were orientated at ±30°. The cuboidal unit cells were orientated such that the sides were parallel to the bisectors of the tow directions, hence the models represented the structure of angle-ply laminates manufactured from a single layer of textile reinforcement. A schematic illustration of the ±30° model is shown in Figure 6.16. By applying displacements to the North face (in the global x direction) and to the East face (in the global y direction) in two separate analysis steps it was possible to determine the behaviour of ±30° and ±60° unit cells using the same model. Simplified boundary conditions were employed to enforce geometric compatibility, extending those described in Section 6.3 into three dimensions.

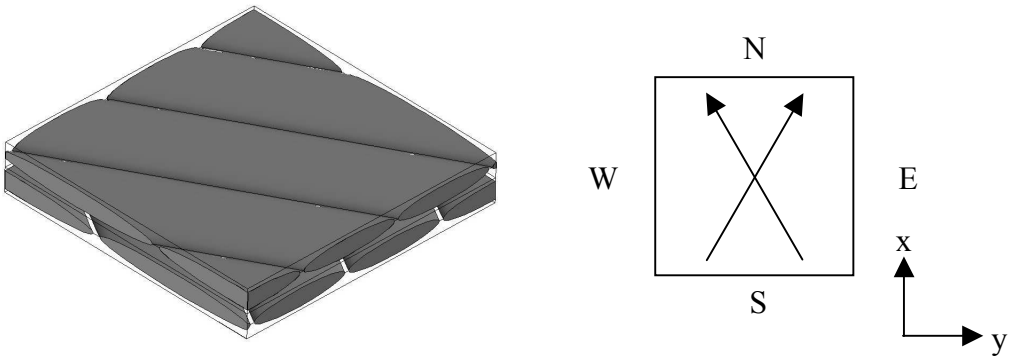

Figure 6.16 (a) Shaded image of 3D unit cell model for a ±30° NCF reinforced composite; (b) Schematic diagram indicating designation of faces used to specify boundary conditions (z direction comes out of the page). Arrows indicate tow directions.

An elliptical tow cross section (n=0.5 and a_t=5 in Equation 6.2) was used, and the presence of stitching was ignored; these simplifications of the true geometry were used to facilitate the mesh generation process. The tows occupied 53.9% of the total cell volume. Mechanical properties of the tow material were calculated in the same way as those for analysis of the 2D cells, reported in Section 6.4. In order to obtain a cell fibre volume fraction, V_{fc}, of 38% (comparable with laminates tested experimentally), a tow fibre volume fraction, V_{ft}, of 70.5% was used, according to Equation 6.8.

$$V_{ft} = \frac{V_{fc}}{V_t} \tag{6.8}$$

where V_{ft} is the fibre volume fraction of the tow, V_{fc} is the target fibre volume fraction of the cell and V_t is the proportion of the cell volume occupied by the tows.

It should be noted that the value of V_{ft} observed in manufactured laminates would be lower than this, since the cross-sectional area of the tows in the models is smaller than that in the true geometry. Properties used for the constituent phases (E-glass and Norpol 420-100 polyester resin) can be found in Table 3.2.

Difficulties were encountered in obtaining a suitably refined mesh to give accurate results while maintaining a small enough number of elements such that it was possible to run the analysis on the computing hardware available. Each mesh consisted of approximately 50,000 four-noded (first order) tetrahedral elements

(Abaqus element designation C3D4). Due to the intricate nature of the geometry, a number of elements were highly skewed or had large aspect ratios. Because of this, the meshes were not considered suitable for accurate evaluation of stresses or failure behaviour; however, since force-displacement results are much less sensitive to mesh quality, these cells were used for evaluation of elastic behaviour. The mesh used for the ±45° model is shown in Figure 6.17(a); the distribution of axial stress, σ_1, is also shown for illustration in Figure 6.17(b), where the upper resin regions have been removed for clarity. Note that in the resin (isotropic) regions, σ_1 is the stress in the global 1 direction, as indicated by the axes, while in the tow (orthotropic) regions, the Abaqus software reports stress in the local material coordinate system, i.e. σ_1 is the stress in the tow axial direction.

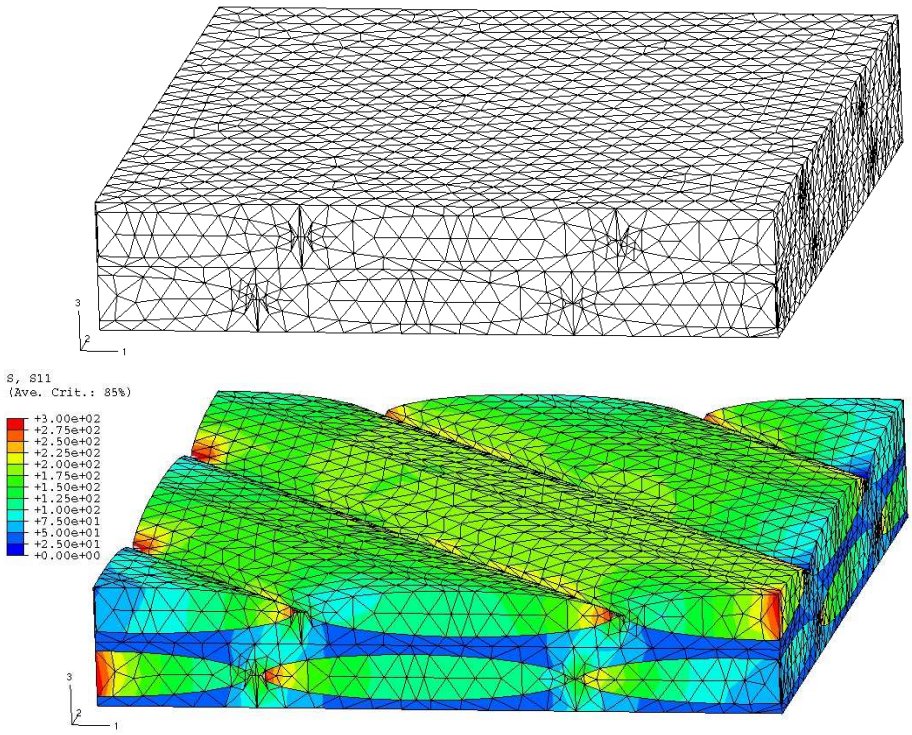

Figure 6.17(a) Mesh used for 3D unit cell model for a ±45° NCF reinforced composite; (b) Predicted stress distribution, σ_1, under application of a displacement boundary condition in the global 1 direction. Note that σ_1 reports stress in the global 1 direction in resin regions, but in the tow regions axial stress (i.e. that in the local 1 direction) is reported. Upper resin regions were removed for clarity.

It can be seen from the stress distribution shown in Figure 6.17(b), that local stress concentrations were apparent in the regions around the intersection of the tow and model edges. It is thought that this is due to the boundary conditions employed, and that these stresses would not be present if periodic boundary conditions were used.

However, the application of periodic boundary conditions requires opposite faces of the mesh to be the same, whereupon specification of the boundary conditions in the Abaqus software requires two lines of input for each matching pair of nodes (*EQUATION option to link degrees of freedom). This process would only be feasible for such geometries if it was automated; development of such a technique is currently in progress at the University of Nottingham.

The effective modulus of these cells was evaluated using an extension (into three dimensions) of the techniques described in Section 6.3, summing reaction forces over a whole face instead of an edge. The bottom face was restrained against movement in the z direction, the South face was restrained against movement in the x direction, the West face was restrained against movement in the y direction, and a displacement in the x direction was applied to the North face. The top and East faces were not constrained to remain plane; this was not expected to have a significant influence on the results of force-displacement calculations, although it is a further simplification of the true problem.

The results from these cases are presented in Figure 6.18, together with data from comparable experimental measurements and from classical laminate theory (CLT). Results of numerical analyses are tabulated in Table 6.5, while those of experimental measurements can be found in Appendix C. FE predictions were observed to be as close or closer to experimental values as those from classical laminate theory, giving confidence in the method; discrepancies between results may be attributable to some of the inherent simplifications used in the models, both for the boundary conditions and the geometric description of the reinforcement.

Table 6.5 Results of Young's modulus obtained using 3D solid FE analysis. Predictions using classical laminate theory (CLT) are also provided for comparison.

Ply angle, ϕ (°)	Unit cell modulus, E_{xc} (GPa)	Laminate modulus, E_x (GPa) (CLT)
30	16.72	16.45
45	11.53	9.40
60	10.14	8.06

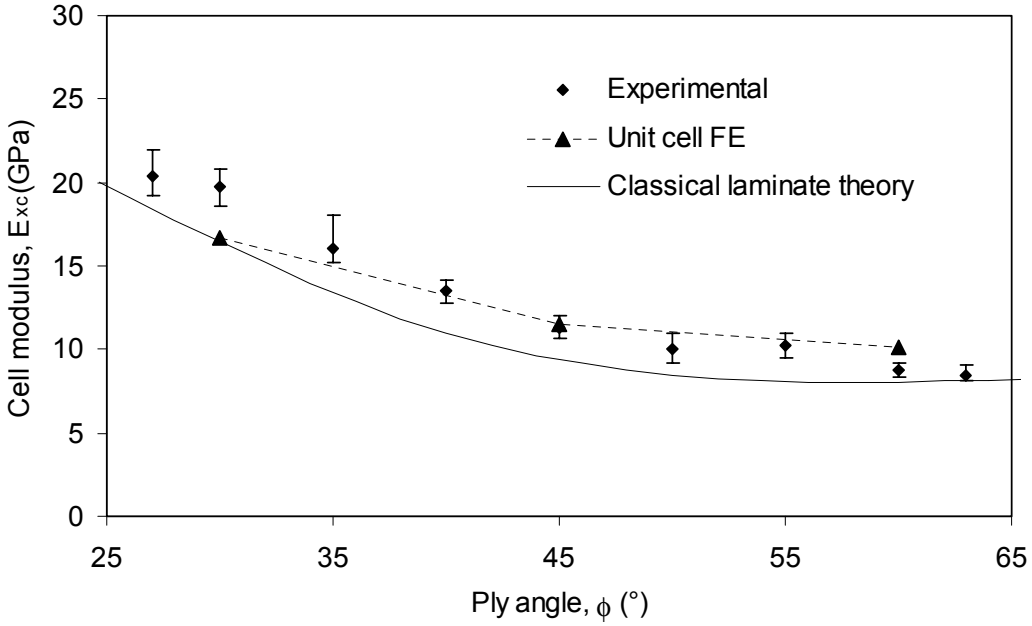

Figure 6.18 Experimental data for laminates manufactured from non-crimp glass fabric compared with results of comparable three-dimensional unit cell FE models and classical laminate theory. Error bars show maximum and minimum values obtained during experimental testing. Ply angle is defined in Figure 3.3.

6.8 Conclusions

In Chapter 5, differences between experimental measurements and analytical models for composite mechanical behaviour (which did not consider the true geometry of the textile reinforcement) were observed. In this chapter, a clear link has been established between the internal structure of textile composites and their mechanical properties. Non-crimp fabric reinforced composite laminates were examined using optical microscopy in order to determine approximate bounds for geometric description of the tows, and a high degree of variability was observed. Two dimensional cross sections were analysed using generalised plane strain finite elements, in order to determine the effects of specific geometric and material parameters on elastic and failure behaviour under transverse loading conditions, since transverse failure stress was one of the properties significantly overestimated by micromechanics. The work presented indicated that the shape of the tows forming the reinforcement may give rise to a 25% change in transverse failure stress (case 18 vs. case 21, Table 6.4). The sensitivity of the results to changes in material properties of the constituent phases was also evaluated. Although a convergence study was performed in order to determine the mesh density required, the evaluation

of the failure criterion at each integration point may induce a higher level of mesh sensitivity than would be observed using a volume averaging approach, such as that employed by Carvelli and Poggi [118]. Further investigation of such a technique is recommended.

Three dimensional solid finite element (FE) models of NCF reinforced angle-ply laminates were also analysed, and predictions of elastic behaviour were shown to agree well with both experimental data and classical laminate theory. While this agreement suggests that the technique is, in essence, reliable, it also indicates that much simpler analysis may prove satisfactory for prediction of elastic behaviour. However, the use of FE analysis removes the need to make assumptions regarding the stress or strain fields within the composite, offering the potential for more accurate failure predictions; behaviour under biaxial loading can also be simulated easily. At present, the main limiting factors preventing straightforward application of this technique to strength prediction are the lack of an automated and reliable method to generate models with appropriate boundary conditions and, more significantly, a method to produce good quality meshes which can be analysed with available computing hardware. While the three dimensional models analysed in this chapter each used approximately 50,000 four-noded tetrahedral finite elements, local stress gradients were not always smooth, indicating that convergence had not occurred for this level of mesh refinement. The same meshes exceeded the available computational resources when they were converted to ten-noded (quadratic) tetrahedral elements in an attempt to improve the solution. Possible solutions to this problem were discussed in Section 2.4.4.

7 DISCUSSION AND CONCLUSIONS

7.1 Introduction

The aim of this chapter is to discuss the findings of the work presented in this thesis as a whole, to highlight the significant conclusions and to make recommendations for future study in the field, based on perceived limitations of the techniques suggested. This chapter will address these objectives in the order stated above.

7.2 Discussion

The work presented in this thesis is concerned with the structural analysis of components manufactured from textile reinforced composites. In order to develop an integrated system facilitating this process, predictive material models have been employed to determine elastic and failure properties of textile composites depending on the fibre volume fraction and the reinforcement architecture after forming. These models have been incorporated into an existing application for predicting fibre reorientation during draping, such that it is possible to generate input files for a commercial finite element package in an automated fashion, enabling structural analysis of components to be performed giving due consideration to the true reinforcement orientations. Experimental validation was performed for each stage of the modelling.

Lamina level predictions

Micromechanics models have been investigated and suitable techniques were selected to determine the properties of unidirectional composites according to their fibre volume fraction. Closed-form analytical models were used such that they could be implemented using simple solution methods. Prediction of principal lamina failure stresses was found to be less straightforward than that of elastic behaviour, with the result that the in-plane shear strength of a lamina was not predicted. Predictions for lamina properties using micromechanics were compared with experimental data obtained by testing unidirectional laminates manufactured using

exactly the same fibre, resin and processing parameters as those used for the manufacture of angle-ply laminates later in the work. Predicted parameters were generally in reasonable or good agreement with measurements; the notable exception to this statement was transverse strength, σ_{2u}, where predictions significantly overestimated the property according to experimental findings. In order to restrict the required mechanical property data to those of the fibre and matrix materials, models for fibre/matrix debonding were not considered since these introduce the requirement for further experimental testing; the models considered were only capable of predicting resin failure under transverse loading. The effects of process-induced residual stresses were also not considered. However, the implementation of the integrated modelling application was structured in such a way that other micromechanics models could be incorporated easily, without causing any significant change to other aspects of the analysis procedure.

Laminate level predictions

In order to evaluate predictive capabilities for laminates, and to determine the effects of reinforcement deformation during draping, angle-ply laminates were manufactured at a range of ply angles by inducing simple shear deformation into textile reinforcement before moulding. One non-crimp fabric (NCF) and one plain weave fabric were used. Large changes in both stiffness and strength of these laminates were observed with changing ply angle in bias tensile tests. Classical laminate theory (CLT) was used to predict the stiffness of such laminates assuming that each layer of fabric could be described as two layers of unidirectional composite. This assumption is approximately true for NCF reinforcements, although the fibre waviness (crimp) present in woven fabrics is not considered using this technique alone. A simple model for fibre waviness was implemented to calculate the effective on-axis Young's modulus for a woven fabric reinforced composite, and extended to calculate the corresponding strength; these properties were used for each of the two layers considered to represent the bi-directional woven reinforcement. Comparisons between CLT and experimental measurements showed good agreement for elastic behaviour, although certain anomalies were observed in the experimental data.

The first of these anomalies was that for both woven and NCF reinforced specimens, stiffness and strength of laminates was lower for ply angles of 25° than for 27°. This contradicts the suggestions of CLT and the cause remains to be investigated; possible reasons may include experimental errors or changing fabric geometry (e.g. tow shape) during shear deformation. The other unusual observation from the experimental results was that the laminates manufactured from woven fabric had both higher stiffness and ultimate strength than those made from NCF reinforcement at the same fibre volume fraction. Both intuition and published models dictate that the presence of fibre waviness is expected to reduce mechanical performance, at least in the fibre direction. The reasons for differences in elastic behaviour could not be explained with the models employed. However, determination of initial failure behaviour using the 0.2% proof stress suggested that the onset of failure in both sets of laminates occurred at similar stress levels; hence the difference between ultimate stresses suggests that the woven fabric reinforced laminates had better post-failure performance, although the reinforcement architecture may not affect initial failure so significantly.

Using the ply stresses determined by CLT, a failure criterion was used to predict the onset of failure in the same laminates. In the case of those specimens manufactured from woven reinforcement, a reduced on-axis strength was calculated using an extension to the model used for on-axis stiffness considering fibre waviness. Predicted values followed approximately the same trend observed in experimental findings and agreement was reasonable, although strength predictions were significantly higher than measured values for ply angles greater than 45°. This was found to be caused by the micromechanics model used for transverse strength, since the substitution of principal strengths measured from the unidirectional laminates resulted in significant improvements in predictions for this range of ply angles.

Component level predictions

For investigation of components, finite element (FE) analysis provides an established method to determine the behaviour of complex structures. The predictions of strength and stiffness of angle-ply laminates obtained using CLT were replicated exactly using layered shell elements within the Abaqus FE package, confirming that

behaviour of this method was in agreement with the experimental validation performed.

At the component level, a knowledge of the fibre orientations over the whole geometry was required. This information was obtained using an existing draping simulation tool based on a modified pin-jointed net approach which accounted for deformation behaviour of specific reinforcements using measured data from in-plane shear tests performed on dry fabrics. Since the source code for this software was available for modification, additional routines were incorporated; some of these were to overcome specific problems associated with obtaining suitable output from the draping simulation, while others involved the implementation of material models and the data export operations required to generate input files for the Abaqus package.

A conical component, based on the geometry of a jet engine nose cone for which tooling was available, was produced using the RTM process. Textile reinforcement was formed to shape by draping it manually over the male tool. Due to processing considerations, it was necessary to use a small amount of continuous filament random mat (CFRM) reinforcement, for which layers were tailored to fit the component shape without in-plane deformation. This component was tested under a diametric pinch loading, and it was observed that the elastic response was not constant as it was rotated about its axis of symmetry. A draping simulation of the component was performed and the aforementioned procedures were used to produce a finite element model using layered shell elements. This model incorporated the layers of CFRM, calculating relative layer thicknesses using a simple compaction model which was shown to give predictions in agreement with layer thicknesses measured using microscopy of specimens cut from the component. The analysis data prepared by this simulation tool were considered to have a significantly higher degree of prediction than that afforded by the available commercial laminate design packages, none of which contains mechanical property models requiring only fibre and matrix properties or compaction models.

The results of FE analysis showed very good agreement with experimental measurements of elastic behaviour. Since component manufacture suffered from a low success rate it was not possible to test parts to failure under different loading conditions. However it was felt that, since predictions which were validated for in-

plane loads on flat laminates also agreed in the elastic regime at the component level, the method proposed forms a valuable contribution to the field of structural analysis of textile composite components, both for elastic and failure behaviour.

Finite element analysis of the repeating unit cell

In order to determine the likely effects of fabric geometry on mechanical behaviour, a parametric study was performed using FE analysis of a cross section through a single tow embedded within resin under generalised plane strain conditions. Significant effects of the cross-sectional geometry of the tow were observed on the transverse failure stress of the cell which had not been reported previously in the literature; such effects could not be represented by the micromechanics models employed at the lamina level and provide some insight into potential reasons for disagreement between models and experiment. Initial studies of three-dimensional unit cell models were also performed, although various technical difficulties were encountered, primarily associated with mesh generation and with the implementation of realistic boundary conditions.

7.3 Major conclusions

In this section, the major conclusions drawn from the work undertaken in the course of this thesis are summarised.

- Experimental testing to failure of laminates manufactured from both NCF and woven fabric reinforcements with in-plane shear deformation showed that the models proposed offered an acceptable means of predicting mechanical behaviour of such materials.
- Implementation of these models in conjunction with an existing model for reinforcement draping has enabled structural analysis of components to be conducted in an automated fashion, giving appropriate consideration to the post-forming reinforcement architecture.
- Mechanical testing of a component was performed which showed that the effects of reinforcement deformation during manufacturing were significant,

and that predictions of elastic behaviour agreed well with experimental measurements.

- It was suggested that a possible cause for differences between experimental and theoretical results was a lack of consideration of the internal geometry of the repeating unit cell of the composite. Simplified FE models were used to investigate the potential effects of tow shape on transverse properties and significant changes in failure stress were observed, although the effect on stiffness was relatively small.
- In order to give full consideration to the effects of fabric geometry, three-dimensional finite element models of NCF unit cells were produced using a simplified geometry, ignoring the presence of stitching. Difficulties were encountered in generating the models and calculated stresses were not considered to be accurate due to issues of mesh quality. Results of Young's modulus in the bias direction calculated using this technique were at least as close to experimental values as those obtained using classical laminate theory.

7.4 Recommendations for further work

While the major conclusions of this work were presented in the preceding section, a number of areas have become apparent where further investigation would be beneficial. These are summarised below.

- Although validation of failure predictions was undertaken for flat laminates under in-plane loading, further validation at component level should be performed. In particular this should consider complex loading conditions. Biaxial tests on laminates made with sheared reinforcement should be performed to validate predicted failure envelopes.
- The micromechanics of the failure process, particularly in states of multiaxial stress, require further investigation to enable accurate prediction of lamina failure using fibre and matrix properties. Consideration should also be given to failure at the fibre/matrix interface.

- Failure under compressive loads has not been examined in this work. This should be addressed and appropriate validation should be performed.
- Consideration should be given to other fibre/matrix materials. The implementation has been performed in such a way that orthotropic fibre properties can be specified for carbon fibres, but validation at the lamina level remains to be performed. Similarly, other material models would be necessary for ductile matrix materials such as thermoplastics.
- Further, more fundamental, studies of the mechanics of textile composites having deformed reinforcement should be performed. The suggested route would be FE analysis of the repeating unit cell, provided that limitations described earlier are overcome. Such studies should investigate the failure behaviour of unit cells under multiaxial loads, as well as completing the parametric study discussed in Chapter 6 to determine the effects of three-dimensional geometric parameters.
- The effects of tailoring reinforcement by the introduction of cuts (darts) to facilitate forming were not considered. Since this practice is often employed in industrial settings, investigation of the effects on mechanical behaviour would be beneficial in order to produce models for such components. Similarly, the practice of using different numbers of layers in different areas, creating steps (known as ply drop-offs) in the reinforcement architecture, should be modelled to make the tools developed more appropriate for use in the composites industry.
- Reinforcement deformation during draping was assumed to occur entirely by in-plane shear, which is frequently suitable for draping of dry textiles by hand. For forming techniques where fibre slip (and fibre straightening in woven textiles) are significant, models should be developed to evaluate the effects on material properties.
- Models for failure by delamination were not incorporated into the work presented. Since this mode of failure is generally considered to be significant in thicker laminates and those subjected to bending loads, predictive models should be implemented and appropriate validation studies should be performed.

- The nose cone component which was tested was observed to exhibit a reduction in stiffness in subsequent tests performed to higher ultimate displacements; this behaviour cannot be described by the models implemented herein. Many published models exist to determine the post-failure behaviour of composites, usually implemented by reducing some or all of the mechanical properties in regions where failure has occurred. The incorporation of such a model, provided that adequate validation was undertaken, would be of benefit. Perhaps most useful would be to employ this model at the unit cell level in order to determine the effect of textile geometry on post-failure performance.
- Using the predictive techniques described, the reinforcement architecture could be optimised for specific applications. Using a geometric model (such as that of Robitaille [84-85]) and unit cell FE, new reinforcements could be designed in a 'virtual environment', enabling reinforcement development with minimum cost.
- In a similar way, optimisation of the reinforcement stack, i.e. layer configurations and orientations, could be performed at the component level. Further investigation into optimisation techniques suitable for such situations is recommended.

REFERENCES

1. 'New Boeing Composite Structure Leads the Way To Lighter, Cheaper Satellites', Boeing Press Release, 2nd October 1996
2. S. Mayer & A.D. Seeds, 'BMW's aluminium light-weight prototype car projects: comparison of aluminium and steel performance', SAE Technical Paper 940154, 1994
3. W. Benjamin & C. Red, 'Advanced composites global outlook for 2003', *Composites Fabrication*, 2003, p.27
4. P.D. Soden, A.S. Kaddour & M.J. Hinton, 'Recommendations for designers and researchers resulting from the world-wide failure exercise', *Composites Science & Technology*, **64**, 2004, pp.589-604
5. NetComposites website, at http://www.netcomposites.com/education.asp , March 2004
6. F.K. Ko, C.M. Pastore & A.A. Head, 'Handbook of industrial braiding', 1989, Atkins and Pearce
7. University of Nottingham website, at http://www.nottingham.ac.uk/~eaxcom/braid.html , March 2004
8. Murata Machinery Company website, at http://www.muratec.net/braider/pro_multibraid.htm , March 2004
9. M. Bannister, 'Challenges for composites into the next millennium – a reinforcement perspective', *Composites: Part A*, **32**, 2001, pp.901-910
10. O.A. Khondker, K.H. Leong, M.K. Bannister, & I. Herszberg, 'The Effect of Architecture on the Impact Properties of Knitted Composites', *Proceedings of the 1st Asian-Australian Conference on Composite Materials (AACCM-1)*, October 1998, Osaka, Japan
11. C.D. Rudd, M.J. Owen & V. Middleton, 'Mechanical properties of weft knit glass fibre/polyester laminates', *Composites Science & Technology*, **39**, 1990, pp.261-277
12. S.D. Pandita & I. Verpoest, 'Tension-tension fatigue behaviour of knitted fabric composites', *Composite Structures*, **64**, 2004, pp.199-209

13. M.R. Piggott, 'The effect of fibre waviness on the mechanical properties of unidirectional fibre composites: a review', *Composites Science & Technology*, **53**, 1995, pp.201-205
14. F.T. Fisher, R.D. Bradshaw & L.C. Brinson, 'Fibre waviness in nanotube-reinforced polymer composites – I: Modulus prediction using effective nanotube properties', *Composites Science & Technology*, **63**, 2003, pp.1689-1703
15. R.D. Bradshaw, F.T. Fisher & L.C. Brinson, 'Fibre waviness in nanotube-reinforced polymer composites – II: Modelling via numerical approximation of the dilute strain concentration tensor', *Composites Science & Technology*, **63**, 2003, pp.1705-1722
16. D.O. Adams & S.J. Bell, 'Compression strength reductions in composite laminates due to multiple-layer waviness', *Composites Science & Technology*, **53**, 1995, pp.207-212
17. D. Liu, N.A. Fleck & M.P.F. Sutcliffe, 'Compressive strength of fibre composites with random fibre waviness', *Journal of the Mechanics and Physics of Solids*, 2004, In press
18. H.M. Hsiao & I.M. Daniel, 'Effect of fibre waviness on stiffness and strength reduction of unidirectional composites under compressive loading', *Composites Science & Technology*, **56**, 1996, pp.581-593
19. B.J. Souter, 'Effects of fibre architecture on formability of textile preforms', Ph.D Thesis, 2001, University of Nottingham
20. Y-Q. Wang & A.S.D. Wang, 'Microstructure/property relationships in three-dimensionally braided fibre composites', *Composites Science & Technology*, **53**, 1995, pp.213-222
21. Fiber Materials Incorporated website, at http://www.fibermaterialsinc.com/2Dws.htm , March 2004
22. 'Occupational Exposure Limits', *Health and Safety Executive Report No. EH40/2000*, 2000, Health and Safety Executive, UK
23. H. Frostling, 'The occupational exposure limit value for styrene – a matter of life or death for the reinforced plastics industry', 2002, Swedish Work Environment Authority
24. N.A.C.M. Correia, 'Analysis of the vacuum infusion moulding process', Ph.D Thesis, 2004, University of Nottingham

25. H.D. Wagner, S. Fischer, I. Roman & G. Marom, 'The effect of fibre content on the simultaneous determination of Young's and shear moduli of unidirectional composites', *Composites*, **12**, 1981, pp.257-259
26. J.C. Halpin & S.W. Tsai, 'Environmental factors in composite design', *United States Air Force Materials Laboratory Technical Report No. AFML-TR-67-423*, USA, 1967
27. J.J. Hermans, 'The elastic properties of fibre reinforced materials when the fibres are aligned', *Proceedings of the Koninklijke Nederlandse Akademie van Wetenschappen*, **B70**, 1967, pp.1-9
28. X.A. Zhong & J. Padovan, 'Influence of geometrical features of unidirectional fibrous lamina on its transverse responses', *Proceedings of the 15th ASCE Engineering Mechanics Conference*, New York, USA, 2002
29. I.M. Daniel & O. Ishai, 'Engineering mechanics of composite materials', 1994, Oxford University Press, pp.73-76
30. J.D. Eshelby, 'The determination of the elastic field of an ellipsoidal inclusion, and related problems', *Proceedings of the Royal Society*, **A241**, 1957, pp.376-396
31. D.F. Adams & D.R. Doner, 'Transverse normal loading of a unidirectional composite', *Journal of Composite Materials*, **1**, 1967, pp.152-164
32. D.F. Adams & D.R. Doner, 'Longitudinal shear loading of a unidirectional composite', *Journal of Composite Materials*, **1**, 1967, pp.4-17
33. C.L. Tucker III & E. Liang, 'Stiffness predictions for unidirectional short-fibre composites: review and evaluation', *Composites Science & Technology*, **59**, 1999, pp.655-671
34. S. Li, 'General unit cells for micromechanical analyses of unidirectional composites', *Composites: Part A*, **32**, 2000, pp.815-826
35. D. Hull & T.W. Clyne, 'An introduction to composite materials' (2nd Ed.), Cambridge University Press, 1996
36. J.A. Kies, 'Maximum strains in the resin of fibre glass composites', *US Naval Research Laboratory Report No. 5752*, USA, 1962
37. T.R. King, D.M. Blackketter, D.E. Walrath & D.F. Adams, 'Micromechanics prediction of the shear strength of carbon fibre/epoxy matrix composites: The influence of the matrix and interfacial strengths', *Journal of Composite Materials*, **26**, 1992, pp.558-573

38. L.E. Asp, L.A.Berglund & R. Talreja, 'Prediction of matrix-initiated transverse failure in polymer composites', *Composites Science & Technology*, **56**, 1996, pp.1089-1097
39. P.D. Soden, M.J. Hinton & A.S. Kaddour, 'Lamina properties, lay-up configurations and loading conditions for a range of fibre-reinforced composite laminates', *Composites Science and Technology*, **58**, 1998, pp.1011-1022
40. R.M. Jones, 'Mechanics of composite materials' (2nd Ed.), Taylor & Francis, 1999, pp.152-153
41. Special issue of journal, *Composites Science & Technology*, **58**, 1998
42. Special issue of journal, *Composites Science & Technology*, **62**, 2002
43. Special issue of journal, *Composites Science & Technology*, **64**, 2004
44. C.F. Jenkins, 'Materials of construction used in aircraft and aircraft engines', Report to the Great Britain Aeronautical Research Committee, 1920
45. P.A. Zinoviev, S.V. Grigoriev, O.V. Lebedeva & L.P. Tairova, 'The strength of multilayered composites under a plane stress state', *Composites Science & Technology*, **58**, 1998, pp.1209-1223
46. E.C. Edge, 'Stress-based Grant-Sanders method for predicting failure of composite laminates', *Composites Science & Technology*, **58**, 1998, pp.1033-1041
47. A. Puck & H. Schürmann, 'Failure analysis of FRP laminates by means of physically based phenomenological models', *Composites Science & Technology*, **58**, 1998, pp.1045-1067
48. P.H. Pettit & M.E. Waddoups, 'A method to predict the nonlinear behaviour of laminated composites', *Journal of Composite Materials*, **3**, 1969, pp.2-19
49. T.A. Bogetti, C.P.R. Hoppel, V.M. Harik, J.F. Newill & B.P. Burns, 'Predicting the nonlinear response and progressive failure of composite laminates', *Composites Science & Technology*, **64**, 2004, pp.329-342
50. L.J. Hart-Smith, 'Predictions of the original and truncated maximum-strain failure models for certain fibrous composite laminates', *Composites Science & Technology*, **58**, 1998, pp.1151-1178
51. L.J. Hart-Smith, 'Predictions of a generalised maximum-shear-stress failure models for certain fibrous composite laminates', *Composites Science & Technology*, **58**, 1998, pp.1179-1208

52. L.J. Hart-Smith, 'Expanding the capabilities of the Ten-Percent Rule for predicting the strength of fibre-polymer composites', *Composites Science & Technology*, **62**, 2002, pp.1515-1544
53. A. Rotem & Z. Hashin, 'Failure modes of angle-ply laminates', *Journal of Composite Materials*, **7**, 1973, pp.448-464
54. A. Rotem, 'Prediction of laminate failure with the Rotem failure criterion', *Composites Science & Technology*, **58**, 1998, pp.1083-1094
55. C.T. Sun & J. Tao, 'Prediction of failure envelopes and stress/strain behaviour of composite laminates', *Composites Science & Technology*, **58**, 1998, pp.1125-1136
56. L.J. Hart-Smith & J.H. Gosse, 'Formulation of fibre-failure criteria for fibre-polymer composites in terms of strain invariants', *Proceedings of the 14th International Conference on Composite Materials*, San Diego, USA, 2003
57. S.W. Tsai, 'Strength characteristics of composite materials', *North American Space Agency (NASA) Contractor Report CR-224*, USA, 1965
58. R. Hill, 'A theory of the yielding and plastic flow of anisotropic materials', *Proceedings of the Royal Society,* **A193**, 1948, p.189-297
59. S.W. Tsai & E.M. Wu, 'A general theory of strength for anisotropic materials', *Journal of Composite Materials*, **5**, 1971, pp.58-80
60. I.I. Gol'denblat & V.A. Kopnov, 'Strength of glass-reinforced plastics in the complex stress state', *Mekhanika Polimerov*, **1**, 1965, p.70; Translated into English and republished in *Polymer Mechanics*, **1**, 1966, p.54
61. S.W. Tsai & H.T. Hahn, 'Introduction to composite materials', Technomic Publishing Co., 1980
62. K.S. Liu & S.W. Tsai, 'A progressive quadratic failure criterion for a laminate', *Composites Science & Technology*, **58**, 1998, pp.1023-1032
63. L.J. Hart-Smith, 'Should fibrous composite failure modes be interacted or superimposed?', *Composites*, **24**, 1993, pp.53-55
64. W.E. Wolfe & T.S. Butalia, 'A strain-energy based failure criterion for non-linear analysis of composite laminates subjected to biaxial loading', *Composites Science & Technology*, **58**, 1998, pp.1107-1124
65. R.G. Cuntze & A. Freund, 'The predictive capability of failure mode concept-based strength criteria for multidirectional laminates', *Composites Science & Technology*, **64**, 2004, pp.343-377

66. P.K. Gotsis, C.C. Chamis & L. Minnetyan, 'Prediction of composite laminate fracture: micromechanics and progressive fracture', *Composites Science & Technology*, **58**, 1998, pp.1137-1149
67. Abaqus/Standard User's Manual, Version 5.8, 1998, Hibbitt, Karlsson & Sorenson Inc., USA
68. M.J. Hinton, A.S. Kaddour & P.J. Soden, 'A comparison of the predictive capabilities of current failure theories for composite laminates, judged against experimental evidence', *Composites Science & Technology*, **62**, 2002, pp.1725-1797
69. M.J. Hinton, A.S. Kaddour & P.J. Soden, 'A further assessment of the predictive capabilities of current failure theories for composite laminates: comparison with experimental evidence', *Composites Science & Technology*, **64**, 2004, pp.549-588
70. M.J. Owen, 'Biaxial failure of GRP – Mechanisms, modes and theories', *Composite Structures*, **2**, 1983, p.21
71. J. Echaabi, F. Trochu & R. Gauvin, 'Review of failure criteria of fibrous composite materials', *Polymer Composites*, **17**, 1996, pp.786-798
72. H. Thom, 'A review of the biaxial strength of fibre-reinforced plastics', *Composites: Part A*, **29A**, 1998, pp.869-886
73. H. Krenchel, 'Theoretical and practical investigations of the elasticity and strength of fibre-reinforced materials', 1964, Copenhagen, Technical University of Denmark, pp.16-21
74. C.D. Rudd, A.C. Long, P. McGeehin, F. Cucinella & L.J. Bulmer, 'Processing and mechanical properties of bi-directional preforms for liquid composite moulding', *Composites Manufacturing*, **6**, 1995, pp.211-219
75. P. Smith, 'Structural preform design for low cost composites processing', Ph.D Thesis, 1998, University of Nottingham
76. Y.C. Roth & N. Himmel, 'Theoretical model and experimental investigation on the effect of stitching on the in-plane stiffness of CFRP', *Proceedings of the 10th European Conference on Composite Materials*, Bruges, Belgium, 2002
77. S.G. Lekhnitskii, 'Anisotropic plates', translated from the 2nd Russian edition by S.W. Tsai & T. Cheron, Gordon and Breach Publishers, 1968
78. F.T. Pierce, 'The geometry of cloth structure', *Journal of the textile institute*, **28**, 1937, pp.T45-T97

79. S.V. Lomov, A.V. Gusakov, G. Huysmans, A. Prodromou & I. Verpoest, 'Textile geometry preprocessor for meso-mechanical models of woven composites', *Composites Science and Technology*, **60**, 2000, pp.2083-2095
80. S.V. Lomov, E.B. Belov, T. Bischoff, S.B. Ghosh, T. Truong Chi & I. Verpoest, 'Carbon composites based on multiaxial multiply stitched preforms. Part I: Geometry of the preform', *Composites: Part A*, **33**, 2002, pp.1171-1183
81. T.M. McBride & J. Chen, 'Unit cell geometry in plain-weave fabrics during shear deformations', *Composites Science and Technology*, **57**, 1997, pp.345-351
82. J. Hofstee, H. de Boer & F. van Keulen, 'Elastic stiffness analysis of a thermo-formed plain-weave fabric composite. Part I: geometry', *Composites Science and Technology*, **60**, 2000, pp.1041-1053
83. J. Hofstee & F. van Keulen, '3-D geometric modelling of a draped woven fabric', *Composite Structures*, **54**, 2001, pp.179-195
84. F. Robitaille, B.R. Clayton, A.C. Long, B.J. Souter & C.D. Rudd, 'Geometric modelling of industrial preforms: woven and braided textiles', *Proceedings of the Institution of Mechanical Engineers*, **213**(L), 1999, pp.69-84
85. F. Robitaille, A.C. Long, I.A. Jones & C.D. Rudd, 'Automatically generated geometric descriptions of textile and composite unit cells', *Composites: Part A*, **34**, 2003, pp.303-312
86. F. Robitaille, B.R. Clayton, A.C. Long, B.J. Souter & C.D. Rudd, 'Geometric modelling of industrial preforms: warp-knitted textiles', *Proceedings of the Institution of Mechanical Engineers*, **214**(L), 2000, pp.71-90
87. M.R. Turner, 'Tow placement studies for liquid composite moulding', Ph.D Thesis, 1998, University of Nottingham
88. E.H. Glaessgen, C.M. Pastore, O.H. Griffin & A. Birger, 'Geometrical and finite element modelling of textile composites', *Composites: Part B*, **27B**, 1996, pp.43-50
89. K. Searles, G. Odegard & M. Kumosa, 'Micro- and mesomechanics of 8-harness satin woven fabric: I – evaluation of elastic behaviour', *Composites: Part A*, **32**, 2001, pp.1627-1655
90. T. Ishikawa & T.W. Chou, 'Elastic behaviour of woven hybrid composites', *Journal of Composite Materials*, **16**, 1982, pp.2-19

91. T. Ishikawa & T.W. Chou, 'Stiffness and strength behaviour of woven fabric composites', *Journal of Materials Science*, **17**, 1982, pp.3211-3220
92. J. Whitcomb, G. Kondagunta & K. Woo, 'Boundary effects in woven composites', *Journal of Composite Materials*, **29**, 1995, pp.507-524
93. T. Ishikawa, M. Matsushima, Y. Hayashi & T.W. Chou, 'Experimental confirmation of the theory of elastic moduli of fabric composites', *Journal of Composite Materials*, **19**, 1985, pp.443-458
94. Y. Dimitrienko, 'Modelling of the mechanical properties of composite materials at high temperatures. Part 3: Textile composites', *Applied Composite Materials*, **5**, 1998, pp.257-272
95. N.K. Naik & P.S. Shembekar, 'Elastic behaviour of woven fabric composites: I – Lamina analysis', *Journal of Composite Materials*, **26**, 1992, pp.2196-2225
96. P.S. Shembekar & N.K. Naik, 'Elastic analysis of woven fabric laminates: Part I – Off-axis loading', *Journal of Composites Technology & Research*, **15**, 1993, pp.23-33
97. V.K. Ganesh & N.K. Naik, 'Failure behaviour of plain weave fabric laminates under in-plane shear loading: effect of fabric geometry', *Composite Structures*, **30**, 1995, pp.179-192
98. N.K. Naik, S.I. Tiwari & R.S. Kumar, 'An analytical model for compressive strength of plain weave fabric composites', *Composites Science and Technology*, **63**, 2003, pp.609-625
99. P. Vandeurzen, J. Ivens & I. Verpoest, 'A three-dimensional micromechanical analysis of woven fabric composites: I. Geometric analysis', *Composites Science and Technology*, **56**, 1996, pp.1303-1315
100. P. Vandeurzen, J. Ivens & I. Verpoest, 'A three-dimensional micromechanical analysis of woven fabric composites: II. Elastic analysis', *Composites Science and Technology*, **56**, 1996, pp.1317-1327
101. P. Vandeurzen, J. Ivens & I. Verpoest, 'Micro-stress analysis of woven fabric composites by multilevel decomposition', *Journal of Composites Materials*, **32**, 1998, pp.623-651
102. P. Vandeurzen, J. Ivens & I. Verpoest, 'An analytical model of the failure process in woven fabric composites', *Proceedings of the 8th European Conference on Composite Materials*, Naples, Italy, 1998

103. J. Hofstee & F. van Keulen, 'Elastic stiffness analysis of a thermo-formed plain-weave fabric composite. Part II: analytical models', *Composites Science and Technology*, **60**, 2000, pp.1249-1261
104. J. Hofstee, H. de Boer & F. van Keulen, 'Elastic stiffness analysis of a thermo-formed plain-weave fabric composite. Part III: experimental verification', *Composites Science and Technology*, **62**, 2002, pp.401-418
105. J. Hofstee & F. van Keulen, 'The effect of simple shear on stiffness and strength of fabric laminates', *Proceedings of the 12th International Conference on Composite Materials*, Paris, France, 1999
106. Z.M. Huang & S. Ramakrishna, 'Modelling inelastic and strength properties of textile laminates: a unified approach', *Composites Science and Technology*, **63**, 2003, pp.445-466
107. D. Bigaud & P. Hamelin, 'Mechanical properties prediction of textile-reinforced composite materials using a multiscale energetic approach', *Composite Structures*, **38**, 1997, pp.361-371
108. P. Tan, L. Tong & G.P. Steven, 'Micromechanics models for the elastic constants and failure strengths of plain weave composites', *Composite Structures*, **47**, 1999, pp.797-804
109. Y. Jiang, A. Tabiei & G.J. Simitses, 'A novel micromechanics-based approach to the derivation of constitutive equations for local/global analysis of a plain-weave fabric composite', *Composites Science and Technology*, **60**, 2000, pp.1825-1833
110. P. Tan, L. Tong & G.P. Steven, 'Modelling for predicting the mechanical properties of textile composites – a review', *Composites: Part A*, **28A**, 1997, pp.903-922
111. B. van den Broucke, F. Tümer, S.V. Lomov, I. Verpoest, P. de Luca & L. Dufort, 'Micro-macro structural analysis of textile composite parts: case study', *Proceedings of the 25th International SAMPE Europe Conference*, Paris, France, 2004
112. O.C. Zienkiewicz, 'The finite element method' (3rd Ed.), McGraw-Hill, 1977
113. K. Woo & J.D. Whitcomb, 'Global/local finite element analysis for textile composites', *Journal of Composite Materials*, **28**, 1994, pp.1305-1321

114. K. Woo & J.D. Whitcomb, 'Three-dimensional failure analysis of plain weave textile composites using a global/local finite element method', *Journal of Composite Materials*, **30**, 1996, pp.984-1003
115. C. Chapman & J.D. Whitcomb, 'Effect of assumed tow architecture on predicted moduli and stresses in plain weave composites', *Journal of Composite Materials*, **29**, 1995, pp.2134-2159
116. Z.N. Feng, H.G. Allen & S.S. Moy, 'Micromechanical analysis of a woven composite', *Proceedings of the 8th European Conference on Composite Materials*, Naples, Italy, 1998
117. V. Carvelli & C. Poggi, 'A homogenisation procedure for the numerical analysis of woven fabric composites', *Composites: Part A*, **32**, 2001, pp.1425-1432
118. V. Carvelli & C. Poggi, 'Two-scale modelling for failure analysis of textile composites', *Proceedings of the 6th International Conference on Textile Composites*, Philadelphia, USA, 2002
119. E. D'Amato, 'Finite element modelling of textile composites', *Composite Structures*, **54**, 2001, pp.467-475
120. P. Rupnowski & M. Kumosa, 'Meso- and micro-stress analyses in an 8HS graphite/polyimide woven composite subjected to biaxial in-plane loads at room temperature', *Composites Science and Technology*, **63**, 2003, pp.785-799
121. D.S. Ivanov, S.V. Lomov, I. Verpoest & A.A. Tashkinov, 'Local elastic properties of a shaped textile composite: homogenisation algorithm', *Proceedings of the 6th International ESAFORM Conference on Material Forming*', Salerno, Italy, 2003
122. H. J. Kim & C.C. Swan, 'Voxel-based meshing and unit-cell analysis of textile composites', *International Journal for Numerical Methods in Engineering*, **56**, 2003, pp.977-1006
123. X. Hu, F. Lin & W. Sun, 'Computer-aided composite unit cell design and modelling', *Proceedings of the 15th Technical Conference of the American Society for Composites*, Virginia Beach, USA, 2000
124. W. Sun, F. Lin & X. Hu, 'Computer-aided design and modelling of composite unit cells', *Composites Science and Technology*, **61**, 2001, pp.289-299

125. D. Durville, 'Finite element modelling of a textile composite unit cell', *Proceedings of the 5th International Conference on Textile Composites*, Leuven, Belgium, 2000
126. B.N. Cox, W.C. Carter & N.A. Fleck, 'A binary model of textile composites – I: Formulation', *Acta Metallurgica et Materiala*, **42**, 1994, pp.3463-3479
127. J. Xu, B.N. Cox, M.A. McGlockton & W.C. Carter, 'A binary model of textile composites – II: The elastic regime', *Acta Metallurgica et Materiala*, **43**, 1995, pp.3511-3524
128. Q. Yang & B.N. Cox, 'Predicting local strains in textile composites using the binary model formulation', *Proceedings of the 14th International Conference on Composite Materials*, San Diego, USA, 2003
129. B.H. Le Page, F.J. Guild, S.L. Ogin & P.A. Smith, 'Finite element simulation of woven fabric composites', *Composites: Part A*, 2004, In press
130. P.S. Shembekar & N.K. Naik, 'Elastic behaviour of woven fabric composites: II – Laminate analysis', *Journal of Composite Materials*, **26**, 1992, pp.2226-2246
131. N.K. Naik & P.S. Shembekar, 'Elastic behaviour of woven fabric composites: III – Laminate design', *Journal of Composite Materials*, **26**, 1992, pp.2522-2541
132. T. Kurashiki, M. Zako & I. Verpoest, 'Damage development of woven fabric composites considering an effect of mismatch of lay-up', *Proceedings of the 10th European Conference on Composite Materials*, Bruges, Belgium, 2002
133. K. Woo & J.D. Whitcomb, 'Effects of fibre tow misalignment on the engineering properties of plain weave textile composites', *Composite Structures*, **37**, 1997, pp.343-355
134. R.E. Robertson, E.S. Hsiue, E.N. Sickafus & G.S.Y. Yeh, 'Fibre rearrangements during the moulding of continuous fibre composites: 1. Flat cloth to a hemisphere', *Polymer Composites*, **2**, 1981, pp.126-131
135. A.C. Long, 'Preform design for liquid moulding processes', Ph.D Thesis, 1994, University of Nottingham
136. P. Boisse, A. Cherouat, J.C. Gelin & H. Sabhi, 'Experimental study and finite element simulation of a glass fibre shaping process', *Polymer Composites*, **16**, 1995, pp.83-95

137. P. Potluri, 'Automated preform manufacture: robotic handling, in-situ measurement of properties and lay-up simulations', *Proceedings of the International Conference for Manufacturing of Advanced Composites*, Belfast, Northern Ireland, 2001
138. J.L. Daniel, A. Cherouat, E. Soccard, S. Maison-Le Poec, F. Lahmar, D. Soulat & P. Boisse, 'Explicit finite element simulations of thermoset and thermoplastic sheet composite forming', *Proceedings of the 13th International Conference on Composite Materials*, Beijing, China, 2001
139. S.W. Hsiao & N. Kikuchi, 'Numerical analysis and optimal design of composite thermoforming process', *Computational Methods in Applied Mechanics and Engineering*, **177**, 1999, pp.1-34
140. W.R. Yu, F. Pourboghrat, K. Chung, M. Zampaloni & T.J. Kang, 'Non-orthogonal constitutive equation for woven fabric reinforced thermoplastic composites', *Composites: Part A*, **33**, 2002, pp.1095-1105
141. T.C. Lim & S. Ramakrishna, 'Modelling of composite sheet forming: a review', *Composites: Part A*, **33**, 2002, pp.515-537
142. C.D. Rudd, A.C. Long, P. McGeehin, F. Cucinella & L.J. Bulmer, 'Processing and mechanical properties of bi-directional preforms for liquid composite moulding', *Composites Manufacturing*, **6**, 1995, pp.211-219
143. P. Smith, C.D. Rudd & A.C. Long, 'The effect of shear deformation on the processing and mechanical properties of aligned reinforcements', *Composites Science and Technology*, **57**, 1997, pp.327-344
144. M. Kuhn, J. Nowacki & N. Himmel, 'Development of an innovative high performance FRP protective toe cap', *Proceedings of the PAM users conference in Europe (EuroPAM)*, Nantes, France, 2000
145. I.A. Jones, 'Finite element modelling and testing of filament wound orthotropic components', Ph.D. Thesis, 1993, University of Nottingham
146. F. Richard & D. Perreux, 'The safety-factor calibration of laminates for long-term applications: behaviour model and reliability method', *Composites Science and Technology*, **61**, 2001, pp.2087-2094
147. O.K. Bergsma, 'Computer aided design of composite shells', *Proceedings of the 13th International Conference on Composite Materials*, Beijing, China, 2001

148. O.K. Bergsma, 'Estimation of fabric properties after forming', *Proceedings of the 13th International Conference on Composite Materials*, Beijing, China, 2001
149. E.A.D. Lamers, 'Shape distortions in fabric reinforced composite products due to processing induced fibre reorientation', Ph.D. Thesis, 2004, University of Twente, The Netherlands
150. H.J. Frissell, 'Engineered materials handbook, Volume 1: Composites', 1987, ASM International, USA
151. C.C. Chamis & J.H. Sinclair, 'Ten-deg off-axis test for shear properties in fibre composites', *Experimental Mechanics*, **17**, 1977, pp.339-346
152. B.W. Chang, D.H. Huang & D.G. Smith, 'A pinned-end fixture for off-axis testing', *Experimental Techniques*, **8**, 1984, pp.28-30
153. M.J. Pindera & C.T. Herakovich, 'Shear characterisation of unidirectional composites with the off-axis tension test', *Experimental Mechanics*, **26**, 1986, pp.103-112
154. C.T. Sun & S.P. Berreth, 'A new end tab design for off-axis tension test of composite materials', *Journal of Composite Materials*, **22**, 1988, pp.766-779
155. C.T. Sun & I. Chung, 'An oblique end-tab design for testing off-axis composite specimens', *Composites*, **24**, 1993, pp.619-623
156. F. Pierron & A. Vautrin, '10° off-axis tensile test: a critical approach', *Composites Science and Technology*, **56**, 1996, pp.483-488
157. F. Pierron, E. Alloba, Y. Surrel & A. Vautrin, 'Whole-field assessment of the effects of boundary conditions on the strain field in off-axis tensile testing of unidirectional composites', *Composites Science and Technology*, **58**, 1998, pp.1939-1947
158. N.J. Pagano & J.C. Halpin, 'Influence of end constraints in the testing of anisotropic bodies', *Journal of Composite Materials*, **2**, 1968, pp.18-31
159. F. Pierron & A. Vautrin, 'Measurement of the in-plane shear strengths of unidirectional composites with the Iosipescu test', *Composites Science and Technology*, **57**, 1997, pp.1653-1660
160. L. Han & M.R. Piggott, 'Tension-compression and Iosipescu tests on laminates', *Composites: Part A*, **33**, 2002, pp.35-42
161. R.J. Young & P.A. Lovell, 'Introduction to polymers', (2nd Ed.), Chapman & Hall, 1991, pp.360-366

162. L.E. Asp, L.A. Berglund & R. Talreja, 'A criterion for crack initiation in glassy polymers subjected to a composite-like stress state', *Composites Science and Technology*, **56**, 1996, pp.1291-1301
163. MatWeb online material data sheet, at http://www.matweb.com/ , March 2004
164. J.J. Crookston, A.C. Long & I.A. Jones, 'Modelling effects of reinforcement deformation during manufacture on elastic properties of textile composites', *Plastics, Rubber and Composites*, **31**, 2002, pp.58-65
165. F. Robitaille & R. Gauvin, 'Compaction of textile reinforcements for composites manufacturing. Part I: Review of experimental results', *Polymer Composites*, **19**, 1998, pp.198-216
166. Z. Cai & T. Gutowski, '3-D deformation behaviour of a lubricated fibre bundle', *Journal of Composite Materials*, **26**, 1992, pp.1207-1237
167. D.H. Lee, G.A. Carnaby, A.J. Carr & P.J. Moss, 'A review of current micromechanical models of the unit fibrous cell', Report C113, 1990, Wool research organisation of New Zealand
168. S. Savci, J.I. Curiskis & M.T. Pailthorpe, 'A study of the deformation of weft-knit preforms for advanced composite structures. Part 2: The resultant composite', *Composites Science and Technology*, **60**, 2000, pp.1943-1951
169. A.C. Long, F. Robitaille, C.D. Rudd & I.A. Jones, 'Modelling strategies for textile composites', *Proceedings of the 14th International Conference on Composite Materials*, San Diego, USA, 2003
170. F. Robitaille, C.C. Wong, A.C. Long & C.D. Rudd, 'Systematic predictive permeability modelling using commercial CFD and dedicated calculation method', *Proceedings of the 14th International Conference on Composite Materials*, San Diego, USA, 2003
171. S.D. Pandita, G. Huysmans, M. Wevers, I. Verpoest, 'Tensile fatigue behaviour of glass plain-weave fabric composites in on- and off-axis directions', *Composites: Part A*, **32**, 2001, pp.1533-1539
172. F. Robitaille & R. Gauvin, 'Compaction of textile reinforcements for composites manufacturing. Part III: Reorganisation of the fibre network', *Polymer Composites*, **20**, 1999, pp.48-62

APPENDIX A PUBLICATIONS ARISING FROM THESIS

J.J. Crookston, B.J. Souter, A.C. Long & I.A. Jones, 'The application of a general fibre architecture model for composite mechanical property prediction', *Proceedings of the 13th International Conference on Composite Materials (ICCM 13)*, 25-29th June 2001, Beijing, China

J.J. Crookston, B.J. Souter, A.C. Long & I.A. Jones, 'The application of a general fibre architecture model for composite mechanical property prediction', *Proceedings of the International Conference on Manufacturing of Advanced Composites (ICMAC)*, 26-27th September 2001, Belfast, Northern Ireland

J.J. Crookston, A.C. Long & I.A. Jones, 'Modelling effects of reinforcement deformation during manufacture on elastic properties of textile composites', *Plastics, Rubber and Composites*, Vol. 31 (2), pp.58-65, 2002, Institute of Materials†

J.J. Crookston, A.C. Long & I.A. Jones, 'The effects of deformation during manufacture on the mechanical performance of textile reinforced polymer composites', *Proceedings of the 10th European Conference on Composite Materials (ECCM 10)*, 3-6th June 2002, Bruges, Belgium

F. Robitaille, A.C. Long, I.A. Jones, J.J. Crookston & C.D. Rudd, 'Automated generation of tow envelopes and inter-tow volumes for composite unit cell modelling', *Proceedings of the 6th International Conference on Textile Composites (TexComp 6)*, Philadelphia, USA, 11-13th Sept 2002, Paper 5-05

A.C. Long, J.J. Crookston, R.G. Gil, I.A. Jones & M.J. Clifford, 'Effects of intra-ply shear during forming on tensile properties of textile composites', *Proceedings of the 6th International Conference on Textile Composites (TexComp 6)*, Philadelphia, USA, 11-13th Sept 2002, Paper 5-08

J.J. Crookston, F. Robitaille, A.C. Long, I.A. Jones, J. Ooi 'A systematic study of the mechanical properties of textile composite unit cells based on geometric modelling', *Proceedings of the 14th International Conference on Composite Materials (ICCM 14)*, 14-18th July 2003, San Diego, USA

† Awarded the Composite Award for published work by the Institute of Materials, Minerals and Mining, 2003

APPENDIX B SUMMARY OF THE FINDINGS OF THE WORLD WIDE FAILURE EXERCISE

In this appendix, the final summary charts indicating the performance of each of the theories in the WWFE are reproduced. This is intended to offer a quick reference for the overall performance of each theory in each area and is not a substitute for reading the detailed conclusion papers [68,69] published as part of the exercise. Note that theory designations carrying the suffix 'B' were slightly revised during part B of the exercise, after the experimental results were provided to participants. Grade A predictions fell within 10% of the measured values, grade B within between 10% and 50%, and grade C fell outside this range.

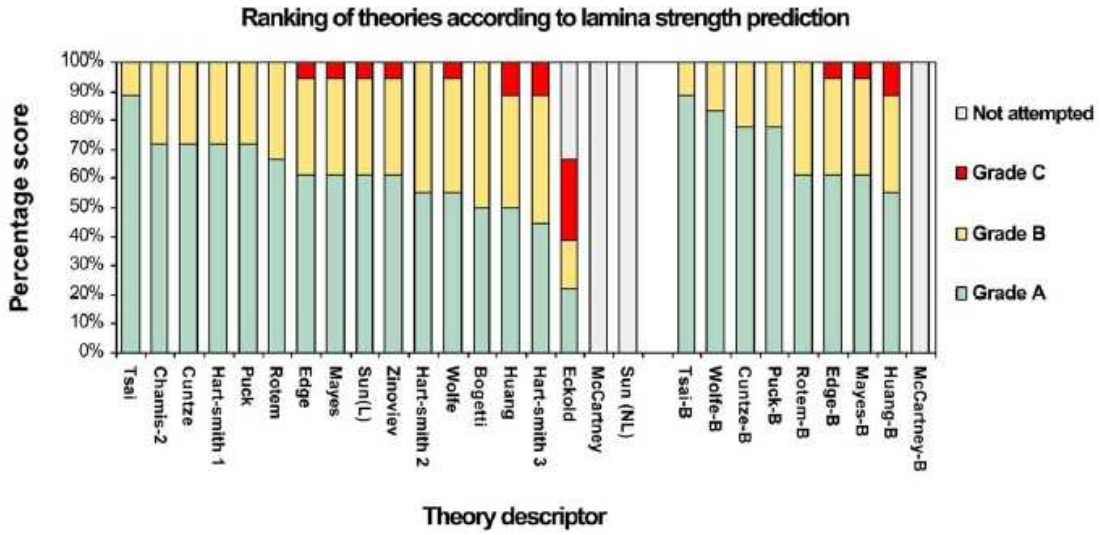

Figure B.1 Ranking the failure theories according to their ability to predict the biaxial failure stresses of unidirectional lamina. Reproduced from [69].

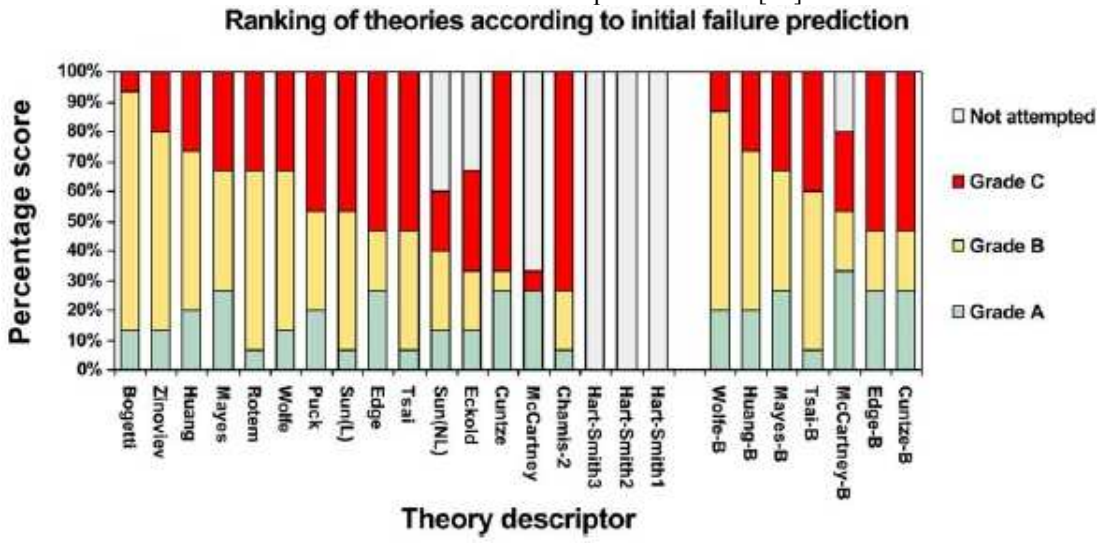

Figure B.2 Ranking the failure theories according to their ability to predict the initial failure characteristics in the multi-directional laminates. Reproduced from [69].

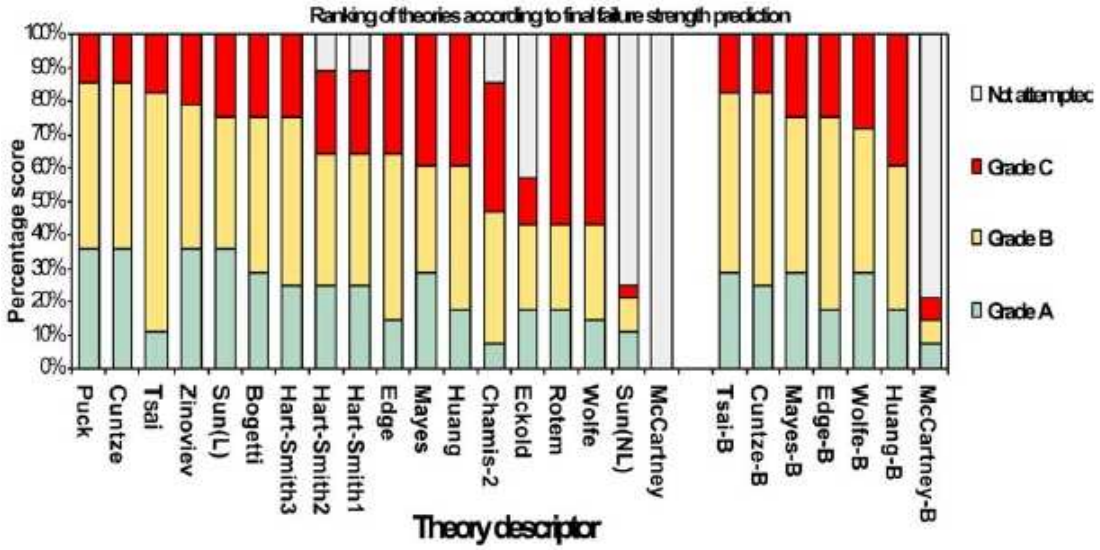

Figure B.3 Ranking the failure theories according to their ability to predict the biaxial failure stresses of multi-directional laminates. Reproduced from [69].

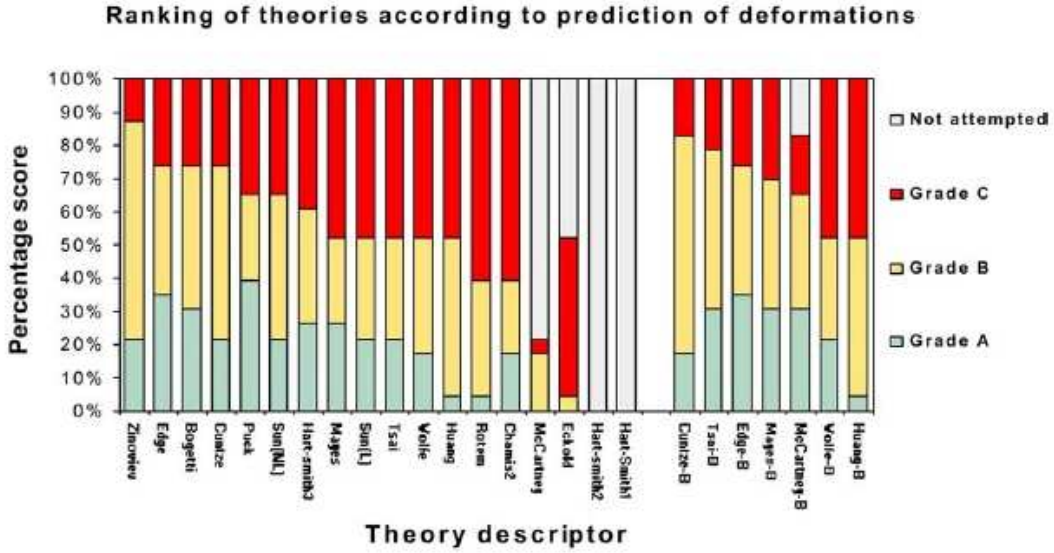

Figure B.4 Ranking the failure theories according to their ability to predict the deformation in the multi-directional laminates. Reproduced from [69].

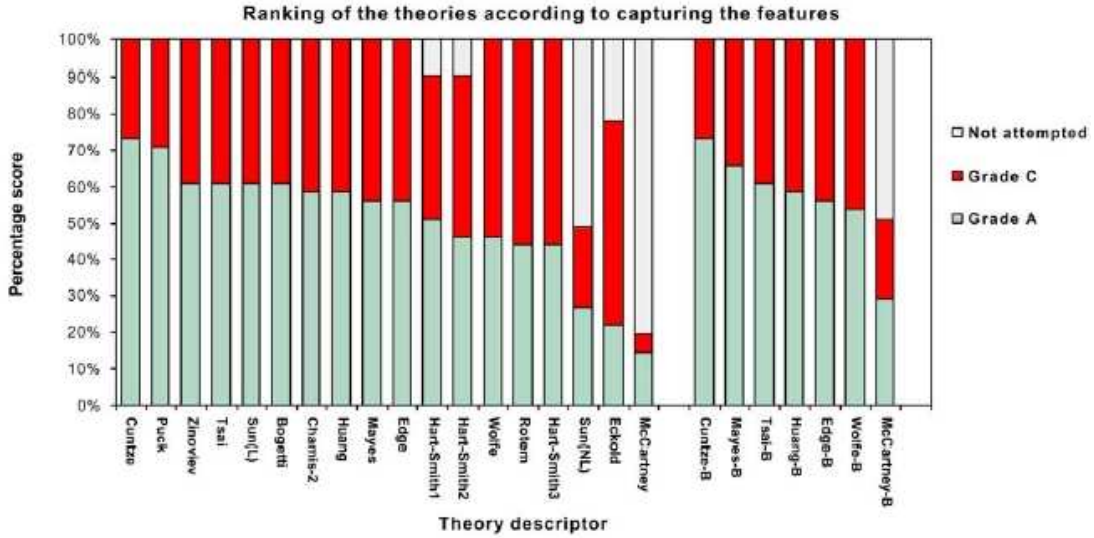

Figure B.5 Ranking the failure theories according to their ability to predict the general features exhibited in the test results. Reproduced from [69].

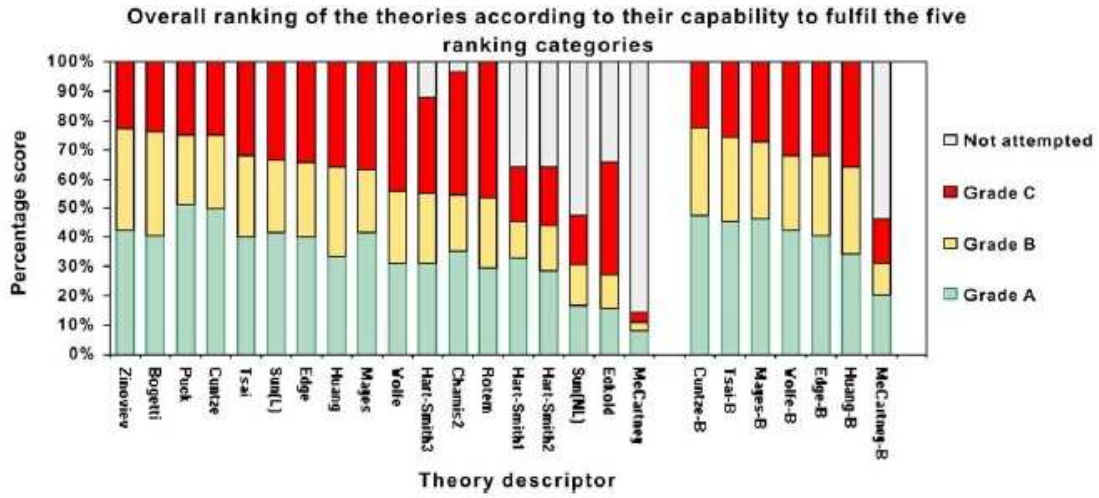

Figure B.6 Overall ranking of the theories according to their capability to fulfil the five ranking categories. Reproduced from [69].

APPENDIX C TABULATED EXPERIMENTAL DATA

Unidirectional laminates

Plaque designation	V_f	E_1 (MPa)	E_2 (MPa)	G_{12} (MPa)	ν_{12}	σ_{1u} (MPa)	σ_{2u} (MPa)	τ_{12u} (MPa)
UD2	34.1	23765	9361	2497	0.275	514	25.9	65.7
		29118	9097	2255	0.303	486	31.6	64.0
		31008	8910	2356	0.314	493	31.9	64.5
		27133	9831	2542	0.325	491	28.1	63.6
		32911		2951	0.348	521		62.6
Average		28787	9300	2520	0.313	501	29.4	64.1
UD3	39.6	31579	10222	3016	0.292	551	35.5	64.8
		32113	10230	3103	0.303	518	34.1	63.1
		39879	10100	2629	0.359	585	32.1	65.6
		31066	10398	2856	0.324	491	29.8	67.0
		34150		2614	0.325	491		63.3
Average		33757	10238	2844	0.321	527	32.9	64.8
UD4	42.2	36183	13782	2767	0.292	532	33.1	65.2
		33870	13845	2910	0.269	599	36.4	64.6
		40448	14122	3007	0.303	576	40.3	63.0
		30348	13364	3024	0.292	590	33.0	65.6
				2641				63.2
Average		35212	13778	2870	0.289	574	35.7	64.3

Non-crimp fabric reinforced angle-ply laminates

Plaque	Ply angle, ϕ (°)	V_f	E_x (MPa)	ν_{xy}	σ_{xu} (MPa)	$\sigma_{x0.2ps}$ (MPa)	ε_x at max stress (%)	$\varepsilon_{x0.2ps}$ (%)
FGE-25	25	36.4	18383	0.550	256	213	1.72	1.36
			19486	0.596	234	214	1.46	1.31
			21811	0.648	231	215	1.31	1.18
			18746	0.639	239	199	1.64	1.26
Average			19607	0.61	240	210	1.53	1.28
FGE-27	27	42.0	22005	0.534	299	220	2.05	1.20
			20252	0.542	295	229	1.91	1.33
			20102	0.539	287	178	1.99	1.09
			19235	0.520	286	182	2.11	1.14
Average			20398	0.53	292	202	2.01	1.19
FGE-30	30	36.8	18622	0.489	278	223	1.89	1.40
			20856	0.559	288	216	1.84	1.23
			20664	0.637	282	182	1.37	1.07
			18774	0.599	241	171	1.70	1.11
Average			19729	0.57	272	198	1.70	1.20
FGE-35	35	40.9	15461	0.544	236	125	3.15	1.02
			15253	0.468	218	126	2.64	0.92
			15356	0.324	216	106	3.14	0.88
			18104	0.616	204	100	2.64	0.74
Average			16043	0.49	218	114	2.89	0.89
FGE-40	40	36.5	12762	0.671	204	95.7	6.19	0.94
			14129	0.635	200	97.2	7.01	0.88
			14189	0.594	190	106	4.41	0.94
			13171		195	98.6	5.73	0.93
Average			13563	0.63	197	99.3	5.84	0.93
FGE-45	45	36.3	10897	0.505	108	82.9	0.99	0.99
			11244	0.560	83.9	58.2	0.72	0.72
			11557	0.526	116	63.0	0.75	0.75
			11207	0.504	77.7	53.5	0.70	0.70
			10720	0.499	111	52.4	0.71	0.71
			11131	0.518	85.6	51.8	0.69	0.69
			12034	0.548	80.7	55.5	0.67	0.67
			11880	0.586	113	53.6	0.68	0.68
Average			11334	0.53	97.0	58.9	0.74	0.74
FGE-40	50	36.5	10695	0.464	53.2	52.1	0.67	0.67
			11022	0.514	54.1	46.3	0.57	0.57
			9359	0.380	53.3	40.5	0.57	0.57
			9179	0.409	53.8	40.5	0.62	0.62
Average			10829	0.49	73.8	44.9	0.61	0.61
FGE-35	55	40.9	10785	0.429	45.2	44.6	0.56	0.56
			9535	0.344	46.9	44.3	0.61	0.61
			10947	0.431	46.5	46.5	0.58	0.58
			9870	0.354	47.9	47.7	0.66	0.66
Average			10284	0.39	46.6	45.8	0.60	0.60

(Table continued overleaf)

Plaque	Ply angle, ϕ (°)	V_f	E_x (MPa)	ν_{xy}	σ_{xu} (MPa)	$\sigma_{x0.2ps}$ (MPa)	ε_x at max stress (%)	$\varepsilon_{x0.2ps}$ (%)
FGE-30	60	36.8	8713	0.207	39.2	n/a†	0.53	n/a†
			8325	0.269	36.9	-	0.50	-
			9169	0.274	37.8	-	0.48	-
			8744	0.359	37.2	-	0.49	-
Average			8738	0.28	37.8	-	0.50	-
FGE-27	63	42.0	9071	0.258	38.5	-	0.49	-
			8228	0.269	39.8	-	0.63	-
			8507	0.255	37.1	-	0.48	-
			8139	0.238	36.9	-	0.66	-
Average			8486	0.26	38.0	-	0.56	-
FGE-25	65	36.4	7191	0.238	28.9	-	0.63	-
			7289	0.220	30.1	-	0.60	-
			7070	0.204	29.7	-	0.45	-
			7209	0.218	29.4	-	0.45	-
Average			7190	0.22	29.5	-	0.53	-

† The intersection between the offset line and the stress-strain curve occurred after failure in specimens where $\phi \geq 60°$; hence the maximum stress value should be used.

Woven fabric reinforced angle-ply laminates

Plaque	Ply angle, ϕ (°)	V_f	E_x (MPa)	ν_{xy}	σ_{xu} (MPa)	$\sigma_{x0.2ps}$ (MPa)	ε_x at max stress (%)	$\varepsilon_{x0.2ps}$ (%)
RT-25	25	37.4	22557	0.423	344	213	2.28	1.36
			21680	0.421	361	210	2.46	1.17
			23144		375	217	2.45	1.14
			21544		352	211	2.36	1.17
			22890		356	225	2.33	1.19
			22389		352	209	2.32	1.13
			23179		341	214	2.12	1.11
Average			22483	0.42	354	214	2.33	1.18
RT-27	27	37.2	24959	0.486	358	215	2.42	1.10
			23623	0.464	346	208	2.39	1.10
			23446	0.453	355	213	2.58	1.13
			24048	0.464	378	235	2.31	1.17
Average			24019	0.47	359	218	2.42	1.13
RT-30	30	42.8	22045	0.442	361	187	2.81	1.04
			24079	0.497	370	183	2.58	0.99
			25133	0.519	377	172	3.23	0.94
			23636	0.475	374	167	3.24	0.93
Average			23723	0.48	371	177	2.96	0.97
RT-40	40	39.1	11401	0.409	159	63.3	6.84	0.77
			11943	0.505	151	64.5	5.65	0.78
			13983	0.494	161	69.0	6.00	0.73
			13467	0.519	156	70.9	5.67	0.73
Average			12699	0.48	157	66.9	6.04	0.75
RT-45	45	37.2	13303	0.410	127	57.6	17.77	0.67
			10798	0.442	105.7	52.4	15.22	0.67
			10238	0.497	104	47.9	17.64	0.64
			10498	0.420	103.4	51.2	12.97	0.66
			10938	0.409	104	49.8	17.73	0.68
			12084	0.452	102.9	51.5	13.84	0.66
			11241	0.442	99.3	49.3	11.71	0.66
			11870	0.464	103	48.8	12.41	0.66
Average			11371	0.44	106.2	51.1	14.91	0.66
RT-40	50	39.1	10083	0.387	49.7	43.0	4.45	0.59
			11167	0.409	49.7	43.7	5.02	0.58
			10002	0.364	50.4	44.1	4.85	0.65
			11261	0.387	50.3	45.4	3.91	0.61
Average			11135	0.42	76.4	44.0	8.89	0.61
RT-30	60	42.8	11373	0.307	33.7	n/a†	0.34	n/a†
			10114	0.254	36.1	-	0.41	-
			12283	0.276	33.1	-	0.31	-
			10802	0.298	33.0	-	0.36	-
Average			11143	0.28	34.0	-	0.36	-

(Table continued overleaf)

Plaque	Ply angle, ϕ (°)	V_f	E_x (MPa)	ν_{xy}	σ_{xu} (MPa)	$\sigma_{x0.2ps}$ (MPa)	ε_x at max stress (%)	$\varepsilon_{x0.2ps}$ (%)
RT-27	63	37.2	9740	0.276	26.1	-	0.28	-
			10553	0.265	29.2	-	0.31	-
			10010	0.276	29.1	-	0.34	-
			9631	0.292	12.9	-	0.13	-
Average			9983	0.28	24.4	-	0.27	-
RT-25	65	37.4	10757	0.265	28.5	-	0.30	-
			10521	0.243	27.2	-	0.29	-
			9700	0.232	27.9	-	0.33	-
			9778		26.6	-	0.30	-
Average			10189	0.25	27.6	-	0.31	-

† The intersection between the offset line and the stress-strain curve occurred after failure in specimens where $\phi \geq 60°$; hence the maximum stress value should be used.

Jet engine nose cone

Orientation	Ultimate displacement during test (mm)	Force at 1mm displacement (N)	Force at ultimate displacement (N)	Force per unit displacement at ultimate displacement (N/mm)
1	1	192	192	192
	2	186	409	204
	3	177	614	205
	4	161	868	217
2	1	229	229	229
	2	221	461	231
	3	198	657	219
	4	203	921	230
3	1	206	206	206
	2	189	431	215
	3	197	667	222
	4	193	936	234
4	1	191	191	191
	2	167	362	181
	3	153	601	200
	4	146	835	209
5	1	207	207	207
	2	184	410	205
	3	178	613	204
	4	150	820	205
6	1	205	205	205
	2	174	415	208
	3	183	650	217
	4	168	880	220

APPENDIX D SYNTAX USED FOR LAYERED SHELL FE ANALYSIS WITH ABAQUS

In order to conduct a finite element analysis using orthotropic layered shell elements a significant amount of data must be specified. In order to ensure that the procedure employed is recorded accurately and described clearly, the following list indicates the data which are required, in addition to the Abaqus keywords and syntax used:

- A geometric mesh consisting of nodes and elements which defines the shell reference surface:

```
*NODE,
1,x1,y1,z1
2,x2,y2,z2
```

where x,y,z are spatial coordinates of nodes 1 and 2

```
*ELEMENT, TYPE=STRI65
e,na,nb,nc,nd,ne,nf
```

where e is the element number and na-nf are the node numbers of the constituent nodes.

- Definition of node/element sets to facilitate application of boundary conditions and definition of material properties:

```
*NODE, NSET=LOADING
na,nb,nc,nd,ne
```

where `LOADING` is the name of the node set and na-ne are the node numbers included.

- Definition of material behaviour:

```
*MATERIAL, NAME=MAT1
*ELASTIC, TYPE=LAMINA
E1,E2,NU12,G12,G13,G23
(optional:)
*FAIL STRESS
S1ut,S1uc,S2ut,S2uc,SS12u,f*
```

This defines the material `MAT1` as a linear elastic material, being of lamina type (orthotropic plane stress) with properties E_1,E_2,ν_{12},G_{12},G_{13},G_{23} as listed. The `FAIL STRESS` option allows incorporation of σ_{1ut}, σ_{1uc}, σ_{2ut}, σ_{2uc}, τ_{12u}, f* which can be used to calculate failure indices for the in-built failure criteria if required. Subscripts t and c denote behaviour in tension or compression

respectively, f* is the coefficient used in the Tsai-Wu criterion, defined in Equation 2.18.

- Definition of material orientations:

```
*ORIENTATION, NAME=ORI1A, SYSTEM=RECTANGULAR,
DEFINITION=COORDINATES
ax,ay,az,bx,by,bz
3,0
```

This defines the orientation `ORI1A`. Two points, a and b, are specified using their vector components x, y and z; point a lies in the lamina 1 direction, while point b is in the lamina 1-2 plane, and not on the 1 or 2 axes. These points are expressed in global coordinates and define a new local axis system (X',Y',Z') as shown in Figure D1a. To satisfy the conventions used within the Abaqus code, a rotation, α, must be specified about one of the local axes, as illustrated in Figure D1b to define the principal material direction. In this case, since the X' axis is parallel to the lamina 1 direction, the principal material direction must be defined along the local X' axis. Hence a rotation of 0° is specified about the local 3-direction (Z' axis) on the final data line for this command.

- Definition of the cross section behaviour of each element:

```
*SHELL SECTION, COMPOSITE, ELSET=ELEM1
1,3,MAT1,ORI1A
1,3,MAT1,ORI1B
1,3,MAT1,ORI1B
1,3,MAT1,ORI1A
```

This assigns layered behaviour to the set of elements `ELEM1`, using the material definition `MAT1`, in four layers, their directions specified by the vectors `ORI1A` and `ORI1B`. Each layer is 1mm thick and has 3 through-thickness integration points.

- Boundary conditions and load cases must be added manually to complete the analysis input file.

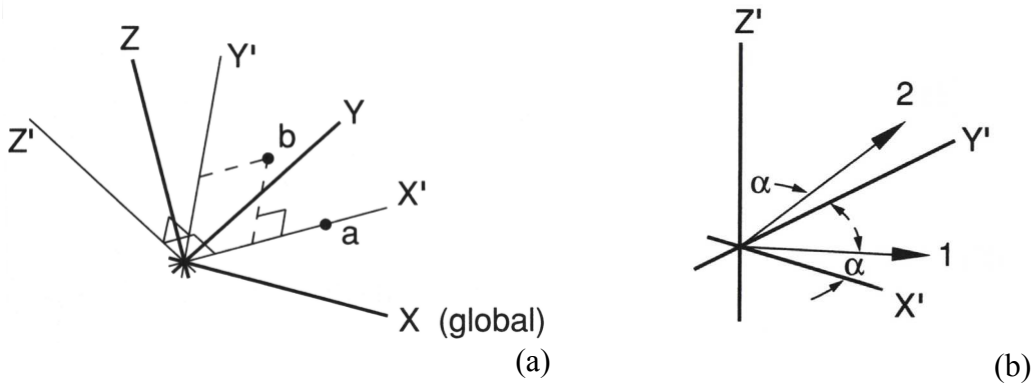

Figure D1 Definition of local axis system (a) and of a local orientation (b) to define the spatial orientation of a lamina with orthotropic mechanical properties within the Abaqus FE system. Reproduced from [67].

APPENDIX E FAILURE CRITERION USER SUBROUTINE FORTRAN CODE LISTING

The following subroutine was incorporated into the FE analyses described in Chapter 6 to evaluate a failure index at each integration point in the model and provide the results for postprocessing. Results are output to the analysis database for graphical postprocessing by using the following option in Abaqus:

```
*OUTPUT VARIABLES
9
```

The results may also be written to the ASCII data file by requesting the output variable UVARM.

```
      SUBROUTINE UVARM(UVAR,DIRECT,T,TIME,DTIME,CMNAME,ORNAME,
     & NUVARM,NOEL,NPT,LAYER,KSPT,KSTEP,KINC,NDI,NSHR,COORD,
     & JMAC,JMATYP,MATLAYO,LACCFLA)
C
      INCLUDE 'ABA_PARAM.INC'
C
      CHARACTER*80 CMNAME,ORNAME
      CHARACTER*8 FLGRAY(15)
      DIMENSION UVAR(NUVARM),DIRECT(3,3),T(3,3),TIME(2)
      DIMENSION ARRAY(15),JARRAY(15),JMAC(*),JMATYP(*),COORD(*)
      INTEGER FM
C
C Error counter:
      JERROR=0
c
c Split criterion into two according to material name defined
c with the *material option
c
      IF (CMNAME.EQ.'RESIN') THEN
c I.e. if this is the resin phase
c Set material flag accordingly:
          UVAR(9)=1
c ---------------------------------------------
c ---------------------------------------------
c Define principal failure stress (MPa) of resin:
c ---------------------------------------------
c ---------------------------------------------
          R_MISES=60
c ---------------------------------------------
c
C Obtain Von Mises stress invariant:
      CALL GETVRM ('SINV',ARRAY,JARRAY,FLGRAY,JRCD,JMAC,JMATYP,
     & MATLAYO,LACCFLA)
      JERROR=JERROR+JRCD
c
c Von Mises Stress is the first value returned (Abaqus 5.8
c documentation, section 24.1.1-5)
      UVAR(1)=ARRAY(1)
c
c Calculate ratio of stress to failure stress
```

```
c
c Find the maximum (and only) failure ratio in the resin (R_MFR)
          R_MFR=UVAR(1)/R_MISES
c Set failure mode variable FM to 9 (flag only)
          FM=9
          UVAR(7)=R_MFR
          UVAR(8)=FM
        ELSE
c I.e. if this is the composite phase
c Set material flag accordingly:
          UVAR(9)=2
c -----------------------------------------------
c -----------------------------------------------
c Define principal failure stresses of composite:
c -----------------------------------------------
c -----------------------------------------------
          R_MDS1=850
          R_MDS2=50
          R_MDS3=50
          R_MSS12=20
          R_MSS13=20
          R_MSS23=50
c -----------------------------------------------
c
C Obtain stress tensor:
      CALL GETVRM ('S',ARRAY,JARRAY,FLGRAY,JRCD,JMAC,JMATYP,MATLAYO,
     & LACCFLA)
      JERROR=JERROR+JRCD
c
c
c Ordering of array: 'Conventions' Abaqus 5.8 section 1.2.2-6
c S11
      UVAR(1)=ARRAY(1)
c S22
      UVAR(2)=ARRAY(2)
c s33
      UVAR(3)=ARRAY(3)
c tau12
      UVAR(4)=ARRAY(4)
c tau13
      UVAR(5)=ARRAY(5)
c tau23
      UVAR(6)=ARRAY(6)
c
c -----------------------------------------------
c Calculate ratios of stress to failure stress
          FRDS1=UVAR(1)/T_MDS1
          FRDS2=UVAR(2)/T_MDS2
          FRDS3=UVAR(3)/T_MDS3
          FRSS12=UVAR(4)/T_MSS12
          FRSS13=UVAR(5)/T_MSS13
          FRSS23=UVAR(6)/T_MSS23
c Find the maximum failure ratio in the tow
          T_MFR=FRDS1
c Failure Mode
          FM=1
          IF(T_MFR.LE.FRDS2)THEN
            T_MFR=FRDS2
            FM=2
          ENDIF
          IF(T_MFR.LE.FRDS3)THEN
```

```
              T_MFR=FRDS3
              FM=3
            ENDIF
            IF(T_MFR.LE.FRSS12)THEN
              T_MFR=FRSS12
              FM=4
            ENDIF
            IF(T_MFR.LE.FRSS13)THEN
              T_MFR=FRSS13
              FM=5
            ENDIF
            IF(T_MFR.LE.FRSS23)THEN
              T_MFR=FRSS23
              FM=6
            ENDIF
            UVAR(7)=T_MFR
            UVAR(8)=FM
       ENDIF
c
C Error handling (sends to .dat file)
       IF(JERROR.NE.0)THEN
           WRITE(6,*) 'REQUEST ERROR IN UVARM FOR ELEMENT NO. ',
      &    NOEL,' INTEGRATION POINT NO. ',NPT
       ENDIF
c
       RETURN
       END
c To summarise, the array of variable UVARM(n) is available for
c plotting in Abaqus/Viewer etc., accessible under the name UVARM1
c UVARM2 etc.
c
c The variables are defined thus:
c UVARM1 = S11
c UVARM2 = S22
c UVARM3 = S33
c UVARM4 = S12
c UVARM5 = S13
c UVARM6 = S23
c UVARM7 = Maximum failure ratio
c UVARM8 = Failure mode (range 1-6, correlating with stress
c          components, or 9 for resin failure by Von Mises)
c UVARM9 = Material flag (1 - resin, 2 - composite)
c
c The resin material must be defined with the name 'RESIN'
```